Catalytic Depolymerization of Lignin

Parker, Heather

Award date:
2016

Awarding institution:
University of Bath

Catalytic Depolymerization of Lignin

Heather Jane Parker

A thesis submitted for the degree of Doctor of Philosophy

Department of Chemistry

University of Bath

November 2015

Contents

Acknowledgements

Firstly I would like to thank Dr Matthew Jones and Dr Chris Chuck for the opportunity to undertake this project. I have truly appreciated their supervision, guidance and advice throughout my PhD. I would also like to thank all members of the Jones and Chuck groups past and present for their support and companionship during my four years at Bath.

Particular thanks are due to Drs Rhodri Owen and Tom Forder for welcoming me into the group, for their invaluable friendship, advice and for being the voices of reason and experience. Thanks also to Sarah Kirk, Paul McKeown and Helena Quilter, George Gregory, Emma Sackville, James Coombs OBrien and everyone else in the 5W SusChemLab for making the last few years so enjoyable!

I am grateful to all of the people who have contributed to the work presented in this thesis, Joshua Spellman for his assistance in designing and building the fuel oxidation equipment, Ursula Potter for the SEM images, Alex Ciupa for assistance with HPLC and especially Tim Woodman and John Lowe for their incredible expertise and unfailing patience in all things NMR.

A huge thank you to the entire team at the Joint BioEnergy Institute in California, particularly Seema Singh and Blake Simmons for giving me the opportunity to work at such an incredible research centre, it was truly enlightening and brilliant fun. Thank you to Gabriella Papa, Anthe George, Jian Sun, Feng Xu and Tanmoy Dutta for their warm welcome, and particularly to Tanmoy for his supervision and guidance on my project.

Thank you to the DTC and EPSRC for their financial support.

To all of my friends, both inside and outside of academia, I must say a massive thank you for being there through thick and thin, keeping me sane through the tough bits and helping me celebrate the good bits! There really are too many to name, but I would like to say special thanks to the members of Cohort ’11, Helen Lomax and Harriet Manning, my wine buddies, Will Mahy, Stephen Wood, James Tyson, Dave Miles and Emily Holt. Thank you also to the Fail Club including Stephanie Griffin, David Gillespie, Dawn Emmerton, Kat Daniels and Matthew Hesse, and the Geordies; Ruth Cooper, Sophie Donkin, Rebecca Molyneux, Fumiyo Welsby and Laraine Mak, for providing many wonderful escapes from the PhD bubble.

Most of all, I would like to say an enormous thank you to my Mum, Dad and sister Fiona. Thank you for your amazing support throughout everything, and for always helping me to believe I could do anything I set my mind to.

Abstract

The valorization of the abundant yet recalcitrant biopolymer lignin *via* selective depolymerization to produce monomeric phenols could greatly improve the process economics of a lignocellulosic biorefinery. Ionic liquid pretreatment has been presented as a potential route to the effective separation of biomass, producing a clean and soluble lignin stream. This could present a significant opportunity for the use of homogenous catalysis for selective lignin depolymerization. Amongst the potential uses for renewable monomeric phenols from lignin could be as antioxidants to increase the oxidative stability of fuels. The aim of this work is to investigate the selective depolymerization of lignin to renewable phenols and also to assess the suitability of these compounds as antioxidants in fuel.

Chapter 1 provides an outline of the research carried out to date in the area of lignin extraction and depolymerization to monomeric phenolic products, with a particular focus on ionic liquid (IL) pretreatment processes and the degradation of model lignin compounds by homogeneous catalysts. An introduction to the use of phenolic antioxidants in the stabilization of biodiesel is also presented.

Chapter 2 reports the systematic study of the activity and selectivity of a range of homogeneous vanadium complexes for the catalytic degradation of phenolic and non-phenolic β-O-4 model lignin compounds. The effects of changing the ligand structure are investigated, in addition to the effect of temperature, catalyst loading and availability of oxygen. Activity and selectivity were found to be highest for catalysts with bulky alkyl-substituted, monophenolate ligands.

Chapter 3 investigates the stability and activity of several of the vanadium catalysts developed in chapter 2 for the degradation of model lignin compounds in a range of ILs. The majority of this work was conducted during a three-month placement in the Biomass Pretreatment team at the Joint BioEnergy Institute in Emeryville, CA, USA. A comparison of catalytic activity and selectivity in the degradation of a β-O-4 model compound in DMSO and the IL [Emim][OAc] was conducted, along with a range of studies in mixtures of the two solvents. Whilst overall activity was lower in the ILs, selectivity for the desired C-O cleavage reaction was dramatically improved. The attempted catalytic degradation of an α-O-4 model lignin compound is also presented, along with preliminary studies of the depolymerization of alkali lignin by homogeneous vanadium catalysts in [Emim][OAc].

Chapter 4 describes the development of a high-throughput accelerated fuel oxidation rig. It also details its subsequent use in the assessment of the antioxidant properties of three renewable phenols, obtainable from lignin, in increasing the oxidative stability of rapeseed methyl ester (RME) biodiesel. The activity of the renewable phenols was compared to that of the commercial antioxidant butylated hydroxytoluene (BHT). Whilst less active than BHT, the renewable phenols were found to be active as antioxidants in RME biodiesel; the trend in activity was observed to be related to the substituents at the 2' and 6' positions. Fuel properties of blends of these renewable phenols are also presented.

Chapter 5 summarizes the findings of the thesis and places them in the context of the thesis aims, whilst chapter 6 presents the experimental and synthetic methodologies employed in the thesis.

Abbreviations and units

Abbreviation/unit	Definition
Å	Angstrom
AA	amino acid
Ad	adamantyl
$[Amim]^+$	1-allyl-3-methylimidazolium
ASTM	American Society for Testing and Materials
BDE	bond dissociation energy
BHA	butylated hydroxyanisole
BHT	butylated hydroxytoluene
$[Bmim]^+$	1-butyl-3-methylimidazolium
BTX	benzene, toluene, xylene
Bu	butyl
Ch	choline
D	diffusion coefficient (in $m^2.s^{-1}$)
DMBQ	2,6-dimethoxy-1,4-benzoquinone
DMF	dimethyl formamide
DMSO	dimethyl sulfoxide
DoE	(United States) Department of Energy
DOSY	diffusion ordered spectroscopy
DSC	differential scanning calorimetry
E_a	activation energy (in $kJ.mol^{-1}$)
$[Emim]^+$	1-ethyl-3-methylimidazolium
Et	ethyl
EtOAc	ethyl acetate
fac	*facial*
FAME	fatty acid methyl ester
FA	formic acid
FTIR	Fourier-transform infrared (spectroscopy)
GC-MS	gas chromatography-mass spectrometry
GEE	guaiacylglycerol β-guaiacyl enol ether
GG	guaiacylglycerol β-guaiacyl ether
$[Gly]^-$	glycinate
GPC	gas permeation chromatography
h	hours
HPLC	high-performance liquid chromatography
HSQC	heteronuclear single quantum coherence (spectroscopy)
Hz	Hertz
IL	ionic liquid
IP	induction period
^{i}Pr	*iso*-propyl
ITSD	internal standard
K	Kelvin
k	Boltzmann constant (in $J.K^{-1}$)
k'	pseudo first-order rate constant
kJ	kiloJoules
LigOH	1-(4-methoxyphenyl)-2-methoxyethanol
$[Lys]^-$	lysinate

m	metres
Me	methyl
MeCN	acetonitrile
mer	*meridonal*
min	minutes
mL	millilitres
$[Mmim]^+$	1,3-dimethylimidazolium
model A	1-(4-ethoxy-3-methoxyphenyl)-2-(2-methoxyphenyl)ethanol
model B	2-phenoxy-1-phenylethanol
model C	guaiacylglycerol-β-guaiacyl ether
model D	1-phenyl-2-(2-methoxyphenoxy)propane-1,3-diol
model E	benzylphenyl ether
mol	moles
nm	nanometres
NMR	nuclear magnetic resonance (spectroscopy)
$[OAc]^-$	acetate
oct	octahedral
OP	oxidation product (2-phenoxy-1-phenylethanone)
Pa	Pascale
PG	propyl gallate
Ph	phenyl
ppm	parts per million
PTFE	polytetrafluoroethylene
PY	pyrogallol
QM	quantum mechanical
R	universal gas constant (in $kJ.mol^{-1}.K^{-1}$)
RI	refractive index (in nD)
RIP	Rancimat induction period
RME	rapeseed methyl ester
rpm	revolutions per minute
RTFO	Renewable Transport Fuel Obligation
s	seconds
$[SCN]^-$	thiocyanate
SEC	size exclusion chromatography
SEM	scanning electron microscopy
T	temperature
TBHQ	*tert*-butyl hydroquinone
^{t}Bu	*tert*-butyl
$[TEA]^+$	triethylammonium
TEMPO	(2,2,6,6-tetramethyl-piperidin-1-yl)oxyl
tet	tetrahedral
THF	tetrahydrofuran
TMDP	2-chloro-4,4,5,5-tetramethyl-1,3,2-dioxaphospholane
VEE	veratrylglycerol β-guaiacyl enol ether
VG	veratrylglycerol β-guaiacyl ether
VOCs	volatile organic compounds
WAT	wax appearance temperature
wt%	weight percent
XRD	X-ray diffraction

α	Kamlet-Taft hydrogen bond acidity
β	Kamlet-Taft hydrogen bond basicity
μw	microwave irradiation
π*	Kamlet-Taft polarizability

Publications and presentations

Fuel additives from the controlled depolymerization of lignin

Parker, H. J.; Jones, M. D.; Chuck, C. J.

Abstr. Pap. Am. Chem. Soc., 2014, *248*, 204-CATL

Renewable fuel additives from depolymerized lignin

Parker, H. J.; Spellman, J. P; Chuck, C. J.; Jones, M. D.

Abstr. Pap. Am. Chem. Soc., 2014, *248,* 391-ENFL

Catalytic deconstruction of model lignin compounds in ionic liquids

Parker, H. J.; Dutta, T.; Singh, S.; Simmons, B. A.; Jones, M. D.; Chuck, C. J.

Abstr. Pap. Am. Chem. Soc., 2015, *249,* 164-CATL

Degradation of β-O-4 model lignin species by vanadium Schiff-base catalysts: Influence of catalyst structure and reaction conditions on activity and selectivity

Parker, H. J.; Chuck, C. J.; Woodman, T.; Jones, M. D.

Catal. Today, 2015*, in press*, doi:10.1016/j.cattod.2015.08.045

1. Introduction

1.1 Lignin as a renewable resource

It is becoming increasingly well accepted that the future of the chemical and energy industries, at least in part, will be dependent on biomass as a renewable feedstock. The development of biomass fuelled power stations and legislated blending of biodiesel into diesel fuels has meant that some biomass utilisation has already been incorporated into the petroleum-dominated energy industry.[1-3] Driving factors for the uptake of biomass-related technologies for energy production have generally included government-led incentives and legislation, however in the long term these technologies will have to be economically competitive.[2, 4, 5]

The production of so-called first generation liquid biofuels for transportation, such as bioethanol and biodiesel, from sugar, starch and vegetable oils has been the source of some controversy due to the potential for competition between fuel and food crops. In contrast, later (second and third) generation biofuels are produced from non-food competitive resources including lignocellulosic material and waste biomass.

Lignocellulosic biomass is comprised of cellulose, hemicellulose and lignin in varying proportions, with typically around 75% celluloses and up to 25% lignin by mass, Figure 1.[6, 7] The lignin and hemicellulose are bound to one another *via* covalent lignin-carbohydrate complexes within the cell wall, providing stability to the plant, Figure 2. The well-defined carbohydrate structure and processability of celluloses has contributed to their use in a wide range of applications including biofuels, paper, adhesives and textiles.[8, 9] In contrast, lignin is a complex, recalcitrant, aromatic biopolymer whose native structure has not been fully characterised as it is inevitably altered on separation from the covalently bonded celluloses. In industries such as paper and pulping, lignin is generally viewed as a contaminant to the more valuable celluloses and much effort, and often energy, is expended in so-called "delignification" of cellulose prior to its processing.[10]

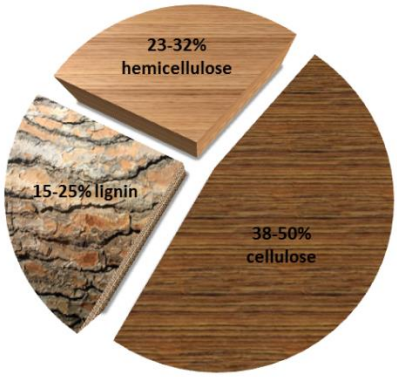

Figure 1: Typical composition of lignocellulosic biomass

The recovered lignin is conventionally burnt for process heat, however, lignin is the largest renewable source of aromatic functionality available and, whilst the percentage by mass of lignin in lignocellulosic biomass is generally between 10-20%, it can account for up to 40% of the energy content. [7, 11] Rather than waste this wealth of chemical potential, it might be more prudent to upgrade lignin to valuable products such as liquid fuels or even platform chemicals, potentially displacing some petroleum-derived aromatics. This could be beneficial not only in an environmental sense, but also economically, by providing an alternative route to high demand chemical building blocks from a source other than oil.[12]

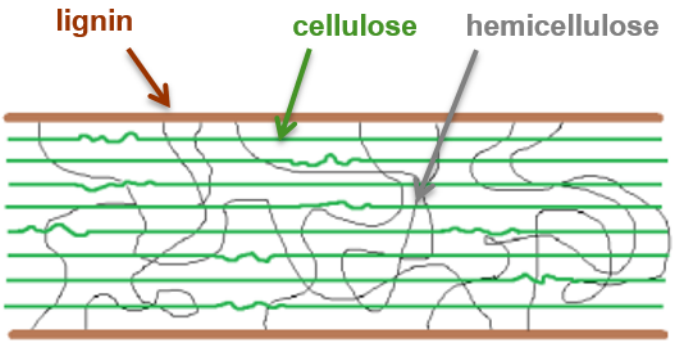

Figure 2: Representative structure of lignocellulosic biomass

1.2 The structure of lignin

Lignin is a 3-dimensional network of interlinked *p*-hydroxyphenylpropane units, called monolignols, Figure 3. In lignin, the monolignols *p*-coumaryl, coniferyl and sinapyl alcohol exist as the phenylpropanoids *p*-hydroxyphenyl (H), guaiacyl (G) and syringyl (S) respectively. The proportions of these monolignols vary between sources, with softwoods containing mainly G, whilst hardwoods contain approximately equal G and S.[13] A variety of different C-O and C-C

linkages are present in lignin, Figure 4; the dominant linkage is the β-O-4, or β-aryl ether bond, Figure 4a.

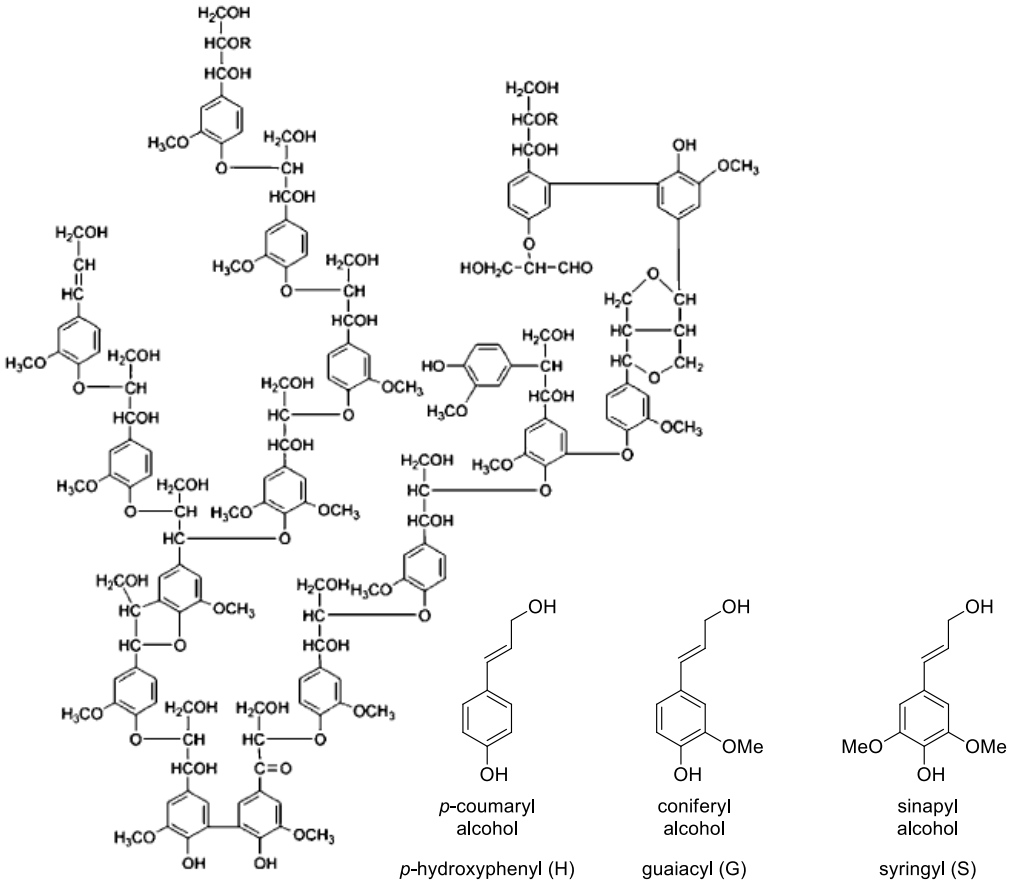

Figure 3: Representative partial structure of lignin as proposed by Adler[14] and the structure of the monolignols

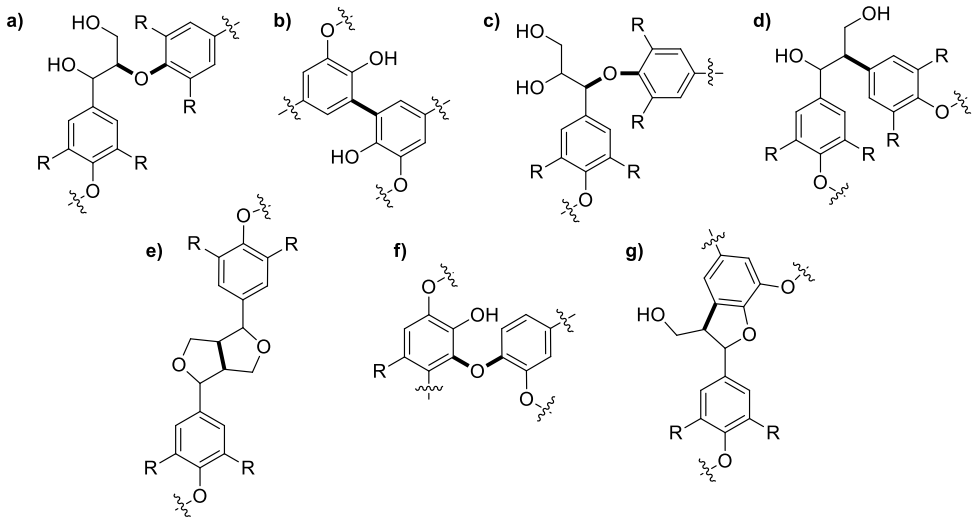

Figure 4: Major linkages in lignin a) β-O-4; b) 5-5; c) α-O-4; d) β-1; e) β-β; f) 4-O-5; g) β-5 [R = H, OCH_3]

1.3 Valorization of lignin

The robust nature of lignin is unsurprising considering its role in nature providing mechanical strength and biological resistance to trees and woody plants, however this resistance to degradation is a significant barrier to lignin valorization which requires breaking down the polymer structure. In 2007 the US Department of Energy (DoE) published a commissioned report on potential targets for value-added chemicals from lignin.[11] These targets fell broadly into three categories; fuels and power (incorporating combustion for process heat, gasification to syngas and pyrolysis to bio-oils), macromolecules (for applications such as carbon fibres) and aromatic chemicals (including phenols and chemical building blocks such as benzene, toluene and xylene (BTX), along with monolignols).

The gasification of lignin to syngas for use as a Fischer-Tropsch feedstock is already a reality, and there has been much research into the breakdown of lignin for use as fuels.[12, 15-18] In the longer term, the DoE report argues that the success of integrated biorefineries will depend on the ability to create higher value products from lignin than fuels. One such method involves the utilisation of lignin's polymeric properties in the production of products such as emulsifiers, adhesives and binders and carbon fibres and resins.[11, 19] The third, and longest-term opportunity identified is that of the production of aromatic chemicals from lignin for use as chemical building blocks.

Within this area, there are two main approaches. The first is the depolymerization of lignin to well-established platform chemicals such as phenol and BTX in order to directly replace their petroleum-derived counterparts within the current infrastructure of the chemical industry.[11]

This approach would require aggressive, unselective C-C and C-O bond rupture and purification of the resulting product stream, as the chemical industry is dependent on reliably uniform raw materials. This method could prove to be inefficient, however, removing all functionality from the lignin before further upgrading to desired chemicals. An alternative, and potentially more efficient, approach would be to selectively depolymerize lignin to its monolignols and utilise the functionality already present. The challenges associated with this approach include the need for highly selective catalysis and also a market and an infrastructure for a new series of more highly functionalised platform chemicals.

1.4 Extraction of lignin

1.4.1 Pretreatment of lignocellulosic biomass

Before depolymerization of lignin can occur, it must first be isolated from the cellulosic fractions of the biomass to which it is bound, Figure 2. This is challenging due to the heterogeneity of the feedstock and its lack of solubility in most organic solvents. The separation is generally achieved by pretreatment of the biomass to selectively extract either the lignin or the carbohydrate fractions and the choice of pretreatment method is dependent on both the source and type of the biomass, and on the desired outcome of the product stream. Traditionally, most pretreatment methods have focussed on the production of a very pure carbohydrate fraction in order to facilitate further upgrading of cellulose for instance *via* enzymatic hydrolysis to produce bioethanol. This can often result in the production of an impure lignin-rich fraction which can cause issues with subsequent upgrading. For this reason, and due to its recalcitrance, lignin is generally viewed as a waste product and is often simply burnt to recover process heat.[20] The development and selection of pretreatment methods which facilitate valorization of all fractions of the biomass is of the utmost importance for the success of the biorefinery model.

There are several well-established methods for biomass pretreatment, which involve varying degrees of degradation or alteration to the native lignin. These can be divided into physical methods, chemical pretreatments, biological processes or solvent fractionation.[21-23] The structure of isolated lignins varies according to the isolation or extraction method, affecting macroscopic properties such as solubility and reactivity.[24-27]

Physical pretreatment involves reducing the particle size of the biomass, generally *via* ball-milling.[25, 28] Whilst some reduction in the degree of polymerization and crystallinity of cellulose is possible during physical pretreatment, this method alone is generally insufficient and does not result in separation of the biomass. For this reason, physical pretreatment is

frequently combined with other pretreatment techniques which require a minimum particle size in order to be effective.[25, 29-31]

Chemical pretreatments can be subdivided into acidic, alkaline and oxidative. Acidic pretreatment can be achieved using either dilute or concentrated acid, resulting in swelling of the biomass and weakening of the lignin-polysaccharide linkages. The Kraft process in the paper and pulping industry is a large source of pretreated lignin and employs strongly alkaline conditions and high temperatures (150-200 °C) in order to extract lignin from the desired celluloses.[10] The use of sodium hydroxide and sodium sulfite during the process results in a lignin stream which is generally soluble in basic aqueous media and also partially fragmented and modified by sulfonation or oxidation. However, the lignin produced from the Kraft process is often not isolated from the so-called "black liquor" following pretreatment, and is integrated into the pulping process as a low-value fuel to supplement the process energy requirements.[11] As a result of this process integration, the supply of commercially available Kraft lignin is potentially limited. Another lignin stream produced by the paper industry is lignosulfonate, produced as a byproduct of sulfite pulping; lignosulfonates are water soluble and have a higher incorporation of sulfur than Kraft lignin. Some fragmentation of lignin can occur during these harsh pretreatment processes, generally due to degradation of β-O-4 C-O linkages, however recondensation *via* the formation of new C-C linkages is also observed in many cases, leading to lignin which can be even more recalcitrant.[32]

Oxidants such as O_2, H_2O_2 and ozone have been employed in the delignification of biomass. Alkaline wet oxidation involves the use of high temperatures (~200 °C) and pressurized O_2 or H_2O_2 to oxidise and solubilize the lignin polymer in order to effect its removal from the biomass.[25] Ozone has been used in a similar manner and has been reported to result in some degradation of the lignin polymer structure, resulting in the production of small oxygenated species such as aliphatic acids, aldehydes and esters.[33-36] The use of oxidants for biomass pretreatment, particularly ozone, can be unselective, resulting in some degradation of the carbohydrates and a loss of aromaticity of the lignin polymer.[25, 36]

Whilst physical and chemical pretreatment techniques often require the use of harsh conditions, such as high temperatures (up to 290 °C), high pressures (up to 5 MPa) and strong acids or bases,[25] biological or solvent fractionation pretreatments are potentially milder methods. Biological pretreatments involve the use of microorganisms, such as white-rot fungi, which contain enzymes capable of degrading the lignin polymer and removing it from the biomass.[25] Whilst not energy-intensive, biological processes are often slow and therefore are

not necessarily useful on a large-scale. Often the microorganisms will also consume some of the celluloses, resulting in a lower glucose yield on hydrolysis of the carbohydrate fraction following pretreatment, and enzymes can be inhibited by compounds present or produced from lignin degradation, reducing their efficiency.[37]

The most common solvent fractionation technique is the organosolv process, producing lignin which is generally less modified than Kraft lignin.[38, 39] After an initial physical pretreatment of the biomass, for instance crushing, solvents such as ethanol or ethanol/water mixtures are used to extract the cellulose, hemicellulose and lignin fractions into separate streams. This method avoids harsh conditions such as high temperatures and pressures and the use of sulfides to produce high purity, low sulfur lignin, however the solvent recovery costs associated with this process tend to be high. Other issues with the use of solvents include their potential flammability and volatility, often resulting in the release of volatile organic compounds (VOCs).

An alternative to traditional solvent fractionation techniques, recent developments in the field of ionic liquids for biomass dissolution and pretreatment could pave the way for a clean, effective and potentially tuneable separation of the carbohydrate and lignin streams.[31, 40-49]

1.4.2 Ionic liquids for biomass pretreatment

Ionic liquids (ILs), generally defined as salts with melting points under 100 °C, have received a great deal of interest as 'green' solvents.[50] Ionic liquids generally consist of a bulky organic cation and either an organic or inorganic anion. The most common cations are highly-substituted ammonium and imidazolium species, whilst anions range from mono-atomic halides to polyatomic species where the charge is delocalised over a larger area, Figure 5.

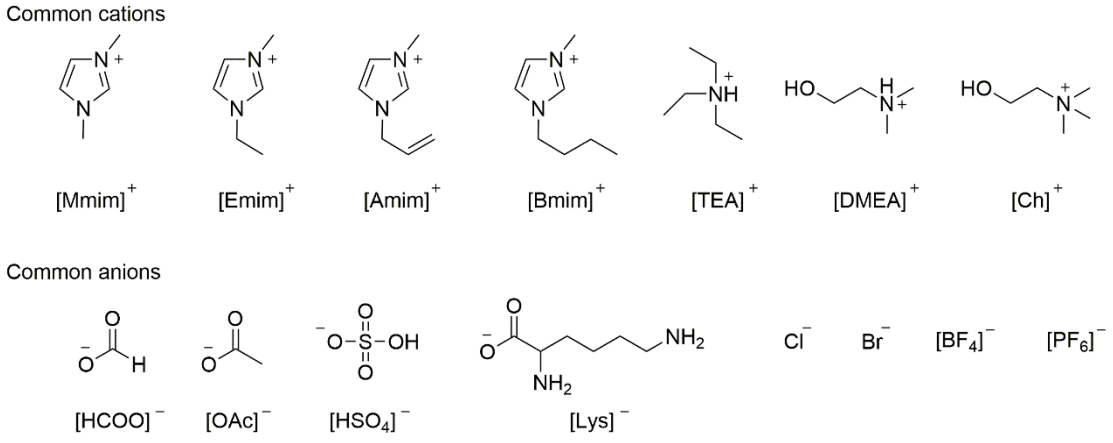

Figure 5: Common ionic liquid cation and anion structures

In general, ionic liquids are thermally stable and non-flammable, having low vapour pressures and exhibiting excellent solubilising properties.[39, 50-53] Whilst ionic liquids cannot universally be described as 'green', there are an almost infinite number of possible combinations of anions and cations and therefore a huge range of ionic liquids which are possible. This variety has led to the description of ILs as "designable" solvents.[39, 50, 52]

Ionic liquids, especially those with imidazolium-based cations, have been shown to have excellent biomass solubilisation properties and have been an area of huge research interest for the dissolution of cellulose and the delignification of biomass for well over a decade.[31, 39, 40, 54-57] Mostly this has focussed on the dissolution and extraction of cellulose, due to its range of well-established applications in the fibre, paper and biofuel industries.[58, 59]

Processing of celluloses is challenging due to its lack of solubility in water and most organic solvents as a result of its crystalline, hydrogen-bonded supramolecular structure. In 2002, however, Swatloski *et al.* demonstrated the efficacy of a range of $[Bmim]^+$-based ILs for the non-derivatising dissolution of cellulose *via* the disruption of the intramolecular hydrogen-bonding network in the polysaccharide.[54] The nature of the anion was found to be strongly influential on the solubilizing properties of the IL, around 25 wt% cellulose could be dissolved in [Bmim]Cl, compared to 5-7 wt% in [Bmim]Br and [Bmim][SCN]. Cellulose was found to be insoluble in $[Bmim][BF_4]$ and $[Bmim][PF_6]$.[54] This trend can be explained be the ability of these anions to disrupt hydrogen-bonding interactions. The small, hard Cl^- anion is far better at disrupting the hydrogen-bonding network in the cellulose than the larger, less coordinating anions, and is therefore better at facilitating cellulose dissolution.

Once solubilised, precipitation of either the whole biomass or selected components can be achieved by the addition of a suitable antisolvent such as water, acetone or ethanol.[39, 54, 60, 61] Regenerated cellulose obtained from the IL pretreatment of biomass has been found to be much more susceptible to enzymatic hydrolysis than untreated cellulose. [29, 45, 54, 57, 62, 63] This has been attributed to two main effects, a significant reduction in cellulose crystallinity and improved access of enzymes to the cellulose polymer by the partial or complete removal of lignin. For example, Lee *et al*. discovered that only 40% lignin removal from wood flour was necessary to effect an increase in cellulose digestibility from 46% for untreated wood flour to >90% for the IL-pretreated substrate.[62]

In 2006 Remsing *et al*. employed ^{13}C and $^{35/37}Cl$ NMR spectroscopy to monitor the interaction of the anions in [Bmim]Cl with the hydrogen-bonding networks in cellobiose (as a model for cellulose) during dissolution by analysing the variation in relaxation rates of the nuclei.[55]

Whilst there was little variation in the relaxation of the ^{13}C nuclei on changing the concentration of cellobiose, the relaxation rates of the $^{35/37}Cl$ nuclei were observed to have a strong dependency on cellobiose concentration, and the anions were observed to interact in a 1:1 manner with the cellobiose hydroxyl protons. In another study, high-throughput screening of a large number of imidazolium-based ionic liquids determined that [Emim][OAc] was the most efficient of those tested for the dissolution of cellulose, whereas [Amim]Cl was the most effective for dissolving full wood chips.[57] [Bmim]Cl has also been employed in the successful dissolution of whole wood chips.[40] During dissolution in the IL, the network of interactions between the lignin and polysaccharides was disrupted, resulting in regenerated cellulose free of lignin and hemicellulose. An interesting visual insight into the dissolution of biomass by [Emim][OAc] was reported by Singh *et al.* in 2009.[61] The autofluorescence of lignin from switchgrass was imaged by confocal fluorescence microscopy and the swelling and dissolution of the structure on contact with the IL was observed. Selective precipitation of the cellulose by the addition of water left the lignin solubilised in the IL-water mixture.

Kamlet-Taft parameters α (hydrogen-bond acidity), β (hydrogen-bond basicity) and π* (polarizability) are frequently used to describe the solubilizing power of different species.[48, 55, 64] Hydrogen-bond basicity, β, is often the most useful parameter when studying the dissolution of lignocellulosic biomass in ionic liquids, as it describes the ability of the IL to disrupt and break the hydrogen bonds within the biomass. The hydrogen-bond basicity of ILs has been found to be most strongly influenced by the nature of the anion.[42, 65]

On investigation of the relationship between β and cellulose solubility for a range of imidazolium-based ionic liquids, it was found that ILs with a $\beta > 0.8$ are generally good at dissolving cellulose, whereas those with $\beta < 0.8$ are poor.[42] For ILs with $\beta \approx 0.8$, other factors such as anion size play more of a role. Hydrogen-bond basicities for a range of imidazolium-based ILs are reported in the 2002 work by Anderson *et al*. and were found to be mainly dependent on the nature of the anion.[65]

Owing to the tuneable nature of ionic liquids, it is possible to select and even design ionic liquids with particular dissolution properties, which can facilitate the effective and selective separation of lignocellulosic biomass into its constituent fractions. For instance Hamada *et al.* exploited the difference in solubility of lignin and cellulose in the ionic liquid *N*-methyl-*N*-(2-methoxyethyl)-pyrrolidin-1-ium 2,6-diaminohexanoate between 60-80 °C to achieve an effective fractionation of lignocellulosic biomass.[43] Ionic liquid pretreatment of biomass could

therefore be employed to obtain a fully solubilized and relatively unaltered lignin stream which could facilitate subsequent lignin processing and upgrading.

Many studies into the mechanisms of lignin dissolution in ILs have been conducted, however it remains comparatively less well understood than the dissolution of cellulose.[27, 39, 47, 56, 57, 66-70] Most ILs reported for lignin dissolution have imidazolium-based cations and highly coordinating anions.[39, 56, 68] ILs containing sulfate or sulfonate groups tend to exhibit very high lignin solubilization abilities, as do those containing halide ions, whilst ILs with large, non-coordinating anions such as $[BF_4]^-$ and $[PF_6]^-$ exhibit very little lignin solubilization ability.[56] This suggests, similarly to cellulose, that the ability of the IL to disrupt hydrogen bonding networks within the lignin polymer facilitates dissolution.[56, 62]

Imidazolium cations have been shown to interact strongly with aromatic species such as benzene *via* associative π-stacking interactions, and these interactions have been used to explain the high solubility of the aromatic lignin polymer in imidazolium-based ionic liquids.[31, 57, 71] The increase in lignin solubility in ILs containing the $[Amim]^+$ cation compared to $[Bmim]^+$ can be attributed to the extension of the π-system in the former.[31] Unfortunately, strong interactions such as these can inhibit the extraction of products from the ionic liquids, as is noted by Varanasi *et al*.[72] Ionic liquids with the highest propensity to dissolve lignin are therefore not always the most effective at extracting it from biomass.[73]

Whilst evidently helpful in lignin solubilisation, aromatic interactions are not required for lignin dissolution, especially when considering feedstocks such as Kraft lignin, where the structure has already been disrupted. Ionic liquids containing the non-aromatic cation cholinium, $[Ch]^+$, have been shown to be effective for the delignification of biomass.[45, 74] A range of [Ch][AA] ILs, where $[AA]^-$ is an amino acid anion, were investigated for the pretreatment of biomass by Liu *et al*. in 2012.[74] These renewably-derived ILs were synthesised *via* straightforward neutralisation reactions of choline hydroxide with amino acids and were all liquids at room temperature. Solubility of lignin in the various [Ch][AA] ILs was found to range from 140-220 mg lignin per gram of IL, and was dependent on a number of factors including alkalinity, which is unsurprising as lignin solubility in alkaline media is well documented,[75-77] and viscosity; lignin dissolution was inhibited in the most viscous ILs. Whilst xylan solubility was also found to depend on these factors and ranged from <1-85 mg per gram of lignin, cellulose was found to be almost entirely insoluble in all of the [Ch][AA] ILs (<5 mg.g^{-1}).[74] The difference in solubility of the biopolymers in these ILs was exploited in the selective extraction of lignin from rice straw by [Ch][Gly]. Following pretreatment by [Ch][Gly]

at 90 °C for 24 h, a 7-fold increase in the glucose yield of cellulose hydrolysis was observed compared to the untreated rice straw, which was attributed to the removal of lignin. Along with their biomass pretreatment abilities, benefits of many cholinium-based ILs include biodegradability and biocompatibility.[74, 78]

Sun *et al.* conducted a study on the effect of the combinations of $[Emim]^+$ and $[Ch]^+$ cations with each of $[OAc]^-$ and $[Lys]^-$ anions on pretreatment efficacy.[45] The highest delignification was observed with the ILs containing $[Lys]^-$, providing further evidence for the critical role of the anion in pretreatment. This can also be related to the Kamlet-Taft parameters, as the hydrogen bond basicities, β, of the $[Lys]^-$ containing ILs are higher than those of the $[OAc]^-$ ILs, indicating higher hydrogen-bond disruption capabilities, Table 1. It was also proposed that the primary amine of the $[Lys]^-$ anion could disrupt the covalent linkages between lignin and hemicellulose *via* amide or hemiaminal formation.

Table 1: Kamlet-Taft parameters α (hydrogen-bond acidity), β (hydrogen-bond basicity) and π* (polarizability) for a range of ionic liquids †measured at 90 °C, ‡extrapolated to 90 °C, N/D not determined

IL	π*	α	β
[Emim][OAc][45]	0.91†	0.51†	1.23†
[Emim][Lys][45]	0.60†	N/D	1.29†
[Ch][Lys][45]	0.64†	N/D	1.31†
[Ch][OAc][45]	0.76†	0.68†	1.22†
[Bmim][OAc][63]	0.89‡	0.57‡	1.18‡

Several theoretical studies have been undertaken in order to further probe the interactions between ILs and lignin. Ji *et al*. modelled the interaction of [Amim]Cl with 1-(4-methoxyphenyl)-2-methoxyethanol (LigOH), a lignin model compound, and determined that the major interaction between the IL and LigOH is *via* hydrogen bonding.[68] It was observed that the interactions between [Amim]Cl and LigOH were stronger than those between two molecules of LigOH, leading to the conclusion that lignin should be soluble in [Amim]Cl. It was also noted that the addition of water to the system resulted in a strong interaction between the anion and the water molecules, which could interfere with the anion-lignin interaction, reducing lignin solubility in the system. This finding goes some way towards explaining the reprecipitation of lignin from IL systems by the addition of water.

Using dispersion-corrected density functional theory, Janesko modelled the interaction between imidazolium chloride ionic liquids with a cellulose model compound and lignin model compound, LigOH.[79] As expected from previous literature,[54] the cellulose model compound was found to interact more strongly with the Cl^- anion than the cation. Janesko also investigated the experimental finding that ILs with large, non-coordinating anions such as $[PF_6]^-$ are unable to solubilise lignin.[79] He reported that models of [Mmim]Cl and [Mmim][PF_6] with LigOH revealed much weaker interactions between [Mmim][PF_6]-LigOH than [Mmim]Cl-LigOH. The lignin model compound LigOH was also found to have significant interaction with the imidazolium cation through both π-stacking and hydrogen-bonding, corroborating previous observations.[31] Sun *et al.* performed quantum mechanical (QM) calculations on the interaction between $[Ch]^+$ and $[Emim]^+$ and a dilignol model compound, containing a hydroxyl group, and found that the major cation-dilignol interactions were a mixture of hydrogen-bonding and electrostatic interactions.[45]

DMSO has been utilized as a co-solvent in ionic liquids to reduce their viscosity and improve ease of processing, however the co-solvent can also affect lignocellulose solubility.[80, 81] A recent study by Radhi *et al.* investigated a number of properties of [Emim][OAc]-DMSO mixtures including viscosity and ^{1}H NMR chemical shifts.[82] As expected, the viscosity was found to decrease with increasing DMSO mole fraction, however the viscosities were slightly higher than expected, indicating non-ideal mixing and suggesting the existence of weak interactions between the DMSO and [Emim][OAc]. Analysis of the ^{1}H NMR spectra of the mixtures revealed changes in the chemical shifts of the protons of both species. The fact that these changes were observed to be relatively small compared to those in [Emim][OAc]-water mixtures[83] provides further evidence for a weak interaction between [Emim][OAc] and DMSO. At mole fractions of DMSO below 0.4, DMSO was found to interact preferentially with the imidazolium cation,[82] whilst at mole fractions above 0.6 it showed preferential association with the acetate anion. This change in preference may explain the increased solubility of cellulose at low mole fractions of DMSO, as the cation-DMSO interaction liberates more anions, allowing further disruption of the cellulose hydrogen-bonding networks. As the anion has also been shown to have a strong influence on the solubility of lignin, it is possible that this effect might also be observed in the dissolution of lignin.

One issue with the use of ILs for biomass processing is that of cost. ILs can be expensive to synthesise and, in order to keep process costs down, recyclability of the ILs is of the utmost importance.[84] Investigations have been carried out into the use of long chain alcohols such as octanol as precipitants in the IL pretreatment of switchgrass.[85] Both [Emim][OAc] and the

precipitant could be reused for pretreatment for at least three cycles. A method for the recovery and reuse of [Emim][OAc] for pretreatment was proposed by Dibble *et al.* whereby a solvent mixture of acetone, alcohol and IL was employed in the precipitation of the biomass, resulting in a reduction in the quantity of solvent required to effect precipitation, a lower energy IL separation process and a high recovery (89%) of the IL.[26] Scale-up of IL pretreatment technologies, including the use of high solid loadings and ability to process mixed feedstocks is also important and both of these have been demonstrated effectively with [Emim][OAc].[86, 87] There have also been recent reports of the development of low-cost ILs which could potentially replace ILs such as [Emim][OAc] for biomass pretreatment.

1.4.3 Depolymerization of lignin in ionic liquids

In addition to the benefits associated with biomass separation, it has been reported that exposure to certain ionic liquids can result in partial depolymerization of the lignin structure.[44, 66, 69, 70, 88] Following pretreatment in the imidazolium-based IL [Emim][OAc] at 120 °C or 160 °C for 6 h, monomeric aromatic products including phenols, guaiacols, syringols and vanillin could be obtained from a range of lignins and biomass feedstocks.[72] The types and amounts of these products could, in some cases, be tuned by adjusting the process conditions such as temperature and biomass loading. At 160 °C and 3% biomass loading, the major monomeric product obtained from the pretreatment of Kraft lignin was guaiacol (around 5 $g.kg^{-1}$ of biomass) and for low-sulfonate the major product was allyl guaiacol (around 2 $g.kg^{-1}$ biomass). Guaiacol and allyl guaiacol were also the major products from the pretreatment of switchgrass, eucalyptus and pine feedstocks (between 0.1-0.6 $g.kg^{-1}$ biomass). It was also noted that the production of vanillin could be increased by lowering the process temperature.

Lignin depolymerization during biomass pretreatment with [Emim][OAc] was investigated in more detail by Sathitsuksanoh *et al.* in 2014.[44] 2D HSQC NMR was used to identify changes in the structure of lignin after pretreatment, a technique which has been extensively employed in the identification and quantification of lignin linkages.[30, 89-91] A decrease in the quantity of β-O-4 linkages was observed on IL pretreatment of wheat straw at 120 °C, indicating depolymerization of the lignin. Analysis by size exclusion chromatography (SEC) corroborated this observation. Separation of lignin and hemicelluloses was implied by the decrease in abundance of p-coumarate and ferrulate units, which are present in lignin-carbohydrate complexes, following pretreatment. There was also a decrease in the dibenzodioxocin linkages, associated with a reduction in branching of the lignin, and an increase in cinnamyl alcohol end groups, which could indicate an increase in the total number of lignin molecules present due to cleavage of β-O-4 linkages. Similar results were obtained for the pretreatment

of miscanthus, and a higher degree of degradation was observed at 160 °C, however pine was found to be substantially more recalcitrant even at 160 °C and only a small amount of depolymerization was observed. This is likely due to the increased abundance of condensed C-C and diphenyl ether linkages in pine compared to wheat straw and miscanthus. Depending on the method of extraction, the researchers reported that depolymerized lignin of various molecular weights could be separated into various streams for subsequent valorization.

As well as affecting the dissolution of lignin, different anion and cation combinations can also have a bearing on the degradation of lignin during IL pretreatment. This effect was systematically assessed by George *et al*. in 2011, where a range of ILs were employed in the pretreatment of organosolv, alkali and alkali low sulfonate lignins.[27] The lignins were mixed with the ILs at a 3% solid loading at 120 °C for 3 h, during which time full dissolution occurred, and the resulting solutions were analysed by SEC. It was found that the anion is more influential than the cation in bringing about degradation of the lignin structure, and that the linkages which were degraded varied from anion to anion. Of the anions investigated, sulfates were found to be the most effective at reducing the molecular weight of the lignin, followed by lactates, acetates, chlorides and phosphates. Whilst the overall molecular weight of the lignins decreased following pretreatment, at least 40% of the lignin was unaffected in each case.

Many studies have attempted to elucidate the mechanisms of the chemical transformations occurring during the ionic liquid pretreatment of lignin. Cleavage of the β-O-4 linkage is amongst the most commonly proposed mechanism of depolymerization. This frequently occurs *via* acid-catalysed hydrolysis or nucleophilic attack, forming a phenol and so-called Hibbert's ketones, Figure 6.[27, 92]

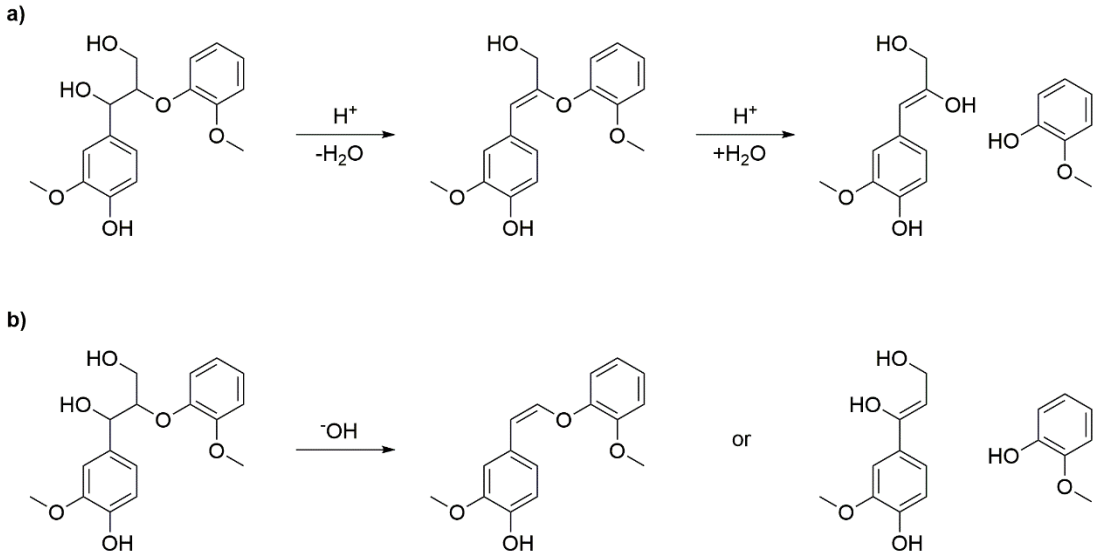

Figure 6: Possible degradation mechanisms of the β-O-4 linkage a) in the presence of acid, b) in the presence of base (or other weak nucleophiles)

Although there has been much interest in the area of catalysis in ionic liquids, to date, there have only been a few reported examples of lignin depolymerization catalysis in ionic liquids.[51, 93] The oxidative degradation of lignin in imidazolium sulfate and sulfonate ILs catalysed by $Mn(NO_3)_2$ was found to produce monomeric aromatic species including syringol, vanillin, syringaldehyde and 2,6-dimethoxy-1,4-benzoquinone (DMBQ).[94] Over 60 % of the lignin could be converted, and the product distribution was dependent on catalyst loading, with high loadings favouring overoxidation of syringaldehyde to produce mainly DMBQ.

Acid-catalyzed degradation of lignin model compounds was observed in the presence of strong Brønsted acids in ILs[95] and also by acidic imidazolium-based ionic liquids themselves.[92, 96] Phenolic and non-phenolic model lignin compounds guaiacylglycerol β-guaiacyl ether (GG) and veratrylglycerol β-guaiacyl ether (VG) respectively, have been used to study the acid-catalyzed degradation of the β-O-4 linkage in ionic liquids, Figure 7. Under acidic conditions, both GG and VG can undergo dehydration to form the enol ethers (GEE and VEE). These enol ether species are not stable under acidic conditions and undergo hydrolysis (which can occur even in the absence of added water due to the initial dehydration reaction).

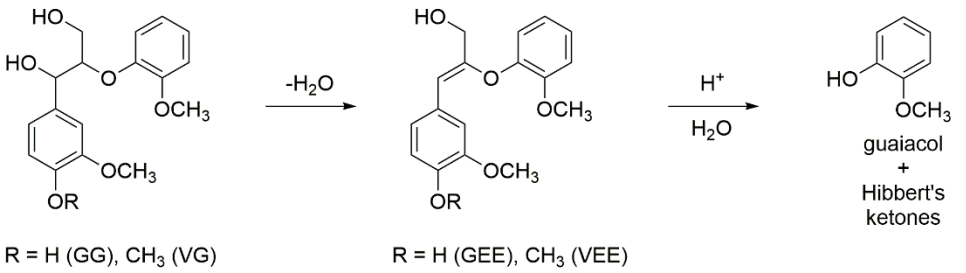

Figure 7: Degradation of phenolic and non-phenolic model lignin compounds guaiacylglycerol β-guaiacyl ether (GG) and veratrylglycerol β-guaiacyl ether (VG)

In terms of metal catalysis, both GG and VG were reportedly cleaved in the presence of catalytic amounts of metal chlorides such as $FeCl_3$, $CuCl_2$ and $AlCl_3$ in the ionic liquid [Bmim]Cl.[97] It was determined, however, that the role of the metal chlorides was simply to facilitate *in situ* generation of HCl, thereby promoting acid-catalyzed hydrolytic cleavage of the ether linkage. The HCl was produced by the hydrolysis of the metal chlorides by water either added to the reaction, or liberated from the dehydration of the model compounds to their respective enol ethers. Degradation of VG was found to be more challenging than GG, possibly due to its lower reactivity and also potentially due to the participation of the GG phenolic hydroxide as a proton donor, assisting in the formation of HCl *in situ*. To the author's knowledge, at the current time there have been no reports of organometallic complexes acting as catalysts for lignin depolymerization in ionic liquids.

1.5 Depolymerization of lignin

As has been discussed, some degradation or depolymerization can occur during the pretreatment of lignin, however, the yields of monomeric species from degradation during pretreatment tend to be low and further breakdown of the isolated lignin is generally necessary in order to obtain significant amounts of valuable monomeric products.[13, 21, 72] Once isolated, there are a number of options for lignin depolymerization including thermal, enzymatic, catalytic and microwave irradiation-assisted degradation and ozonolysis.[13, 22, 35, 36, 98] Due to the complex nature of lignin each of these methods produces a mixture of products including, in most cases, gases, liquid products such as small organic molecules, lignin monomers and oligomers, and solid residues.

Thermal methods such as pyrolysis are amongst the most commonly employed. Pyrolysis involves the thermal decomposition (usually between 400-1000 °C) of biomass in the absence of oxygen and produces mixtures of bio-oils, undesirable solid char and gaseous fractions.[13] The gaseous fraction generally contains H_2, CO, CO_2 and CH_4, which can undergo further upgrading, for example by Fischer Tropsch or related processes, to liquid hydrocarbon fuels.

Bio-oil composition is hugely varied depending on the conditions of pyrolysis but often contains monolignols and small aromatic and aliphatic hydrocarbons.[99-101]

The use of microwave-irradiation in organic synthesis is fairly widespread; the increased heat-transfer efficiency when compared to conventional conductive or convective heating methods can result in dramatic reductions in reaction times and temperatures.[102] Microwave-irradiation has been reported to assist in the degradation of lignin in conjunction with a variety of methods including hydrolysis and catalysis; the efficiency of heating allows for the use of much lower temperatures than those of traditional thermal methods.[98, 103-105] Microwave irradiation has also been employed in the pyrolysis of biomass.[106]

Most other depolymerization techniques attempt to avoid the harsh temperatures and pressures employed by gasification and pyrolysis. One example is enzymatic degradation; certain enzymes, particularly in fungi, have the ability to oxidatively degrade lignin under much milder conditions.[22] Ozonolysis was originally reported as a technique for the delignification of celluloses prior to their processing, however it was noted that some degradation of the lignin was occurring.[34] More recent work has suggested ozonolysis as a technique specifically for oxidative lignin degradation, producing small aromatic and aliphatic organic compounds suitable for blending into fuels.[36]

1.5.1 Catalysis for lignin depolymerization

Catalysis is widely regarded as a key technology required for lignin valorization, enabling a level of control to potentially be applied to the depolymerization process, whilst often simultaneously allowing for the use of milder conditions.[21] As has been mentioned, the production of phenol as a platform chemical from lignin has been identified as a high volume, high value output.[11] The substituted phenolic motif of the monolignols themselves has been recognised as a potential source of antioxidant activity; such compounds are in high demand for applications including food preservation, fuel additives and care products.[107-109] The ability to direct lignin depolymerization using catalysis could provide access to the desired phenolic compounds and monolignols from lignin.

1.5.2 Model lignin compounds

The use of model lignin compounds in the development of catalysts for lignin depolymerization has been widespread.[21] The relative simplicity of these model compounds compared to native lignin renders analysis and therefore mechanistic understanding of the degradation comparatively straightforward. There is a diverse library of model lignin

compounds including monomeric, dimeric, oligomeric and even polymeric species, however they all possess the defining characteristic of a lignin-type linkage, Figure 8. The most abundant linkage in lignin is the β-O-4, or β-aryl ether bond; it is also one of the most susceptible to cleavage.[110-112] Accordingly, the β-O-4 bond is the most highly represented motif in model lignin compounds.[21]

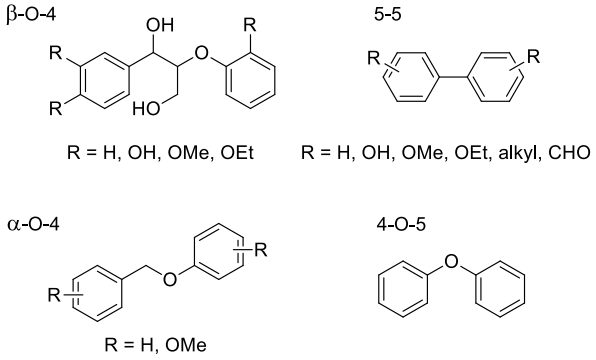

Figure 8: Examples of commonly used model lignin compounds[21]

1.5.3 Heterogeneous catalysis

There are many examples of the use of heterogeneous catalysts for the depolymerization of lignin.[21] However, of the most interest in this report are those which are integrated into processes designed to produce specifically phenolic species. For example, in 2012, Yoshikawa *et al.* described a two-step process for the production of phenols from lignin involving an initial depolymerization step over a silica-alumina catalyst in a butanol/water mixture (Figure 9A).[113] The butanol fraction was then subjected to catalytic cracking using an iron oxide-zirconia catalyst resulting in solid, liquid and gaseous fractions where the liquid fraction contained a high proportion of phenol, cresol and alkyl phenols. An alternative technique was described by Toledano *et al.* in 2013; lignins were ultrafiltered through a range of membranes in order to separate them into fractions of specific molecular weight ranges (Figure 9B).[114] Each of these fractions was then depolymerized over a silica-supported nickel catalyst (Ni SBA15) in the presence of formic acid (FA) and microwave (μw) irradiation. There was a high proportion of residual lignin in all cases, along with gaseous and liquid products. The liquid bio-oils were found to contain monolignols and monolignol-derivatives including syringaldehyde, guaiacol, syringol and vanillin. However, there are issues associated with the use of heterogeneous catalysis for lignin depolymerization such as catalyst fouling or poisoning by lignin itself or impurities in the lignin stream, and also potential over-reduction of the aromatic rings.[21]

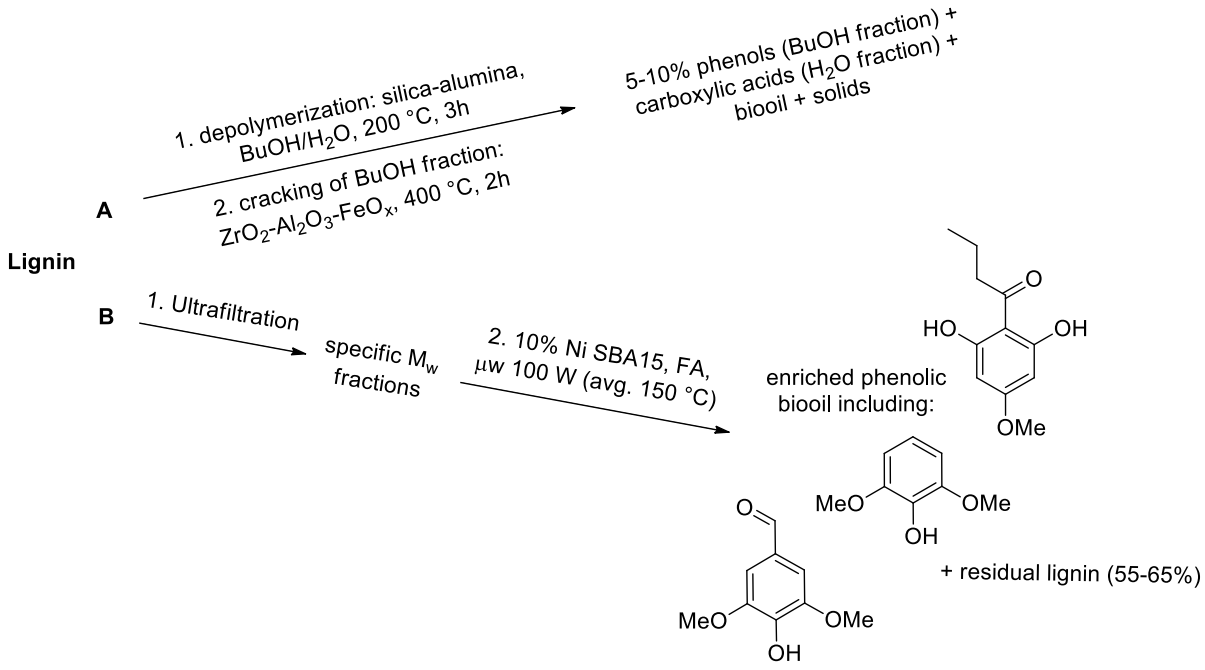

Figure 9: Heterogeneously catalysed methods for the production of phenols from lignin (A: Yoshikawa *et al.*[113]; B: Toledano *et al.*[114]

1.5.4 Homogeneous catalysis

A number of homogeneous catalysts have been proposed for the depolymerization of lignin. They can broadly be divided into reductive and oxidative processes, and the majority to date have only been successfully demonstrated on model lignin compounds. In 2011, Sergeev *et al.* reported the selective hydrogenolysis of the recalcitrant aryl ether (4-O-5) linkage using a nickel-carbene catalyst system and an equivalent of NaO^tBu in the presence of H_2, producing only the desired arene and corresponding alcohol, Figure 10.[110] No competing arene reduction was observed. The catalyst system was also found to selectively cleave the α-O-4 linkage, whilst the β-O-4 bond was cleaved under the reaction conditions in the absence of catalyst and added hydrogen gas but in the presence of an equivalent of NaO^tBu to give guaiacol as a major product along with a range of side products.

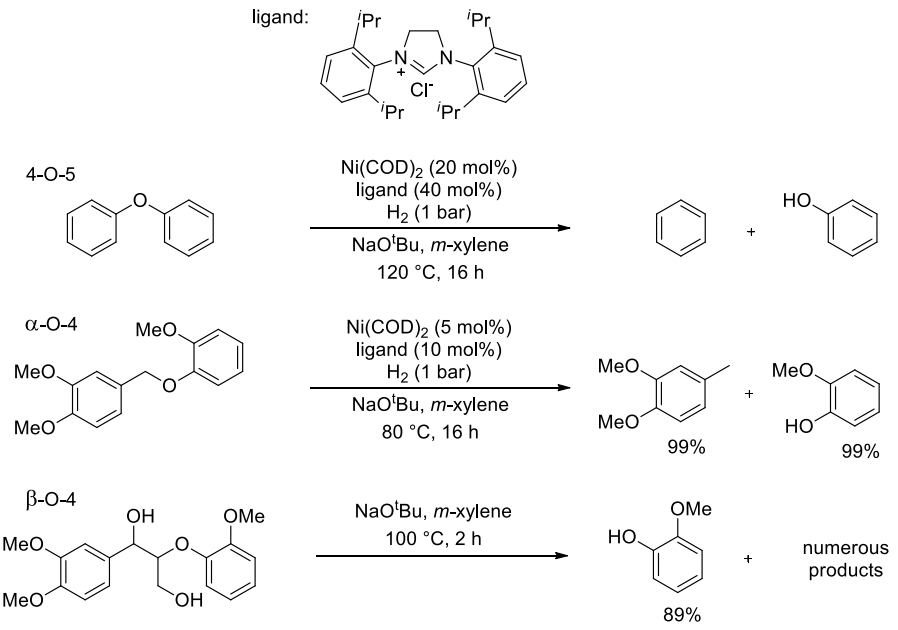

Figure 10: Sergeev *et al.* nickel-catalysed depolymerization of model lignin compounds[110]

There are a handful of examples of ruthenium-catalysed lignin depolymerization catalysts. Several groups have utilised a ruthenium-xantphos complex in the successful degradation of lignin model compounds and even model lignin polymers. Wu *et al*. and Nichols *et al.* reported very similar systems for the cleavage of the β-O-4 in lignin model compounds, Figure 11.[115, 116] Although the conditions are similar, the system reported by Nichols *et al.* effected the conversion of a simple model compound selectively to the C-O cleavage products acetophenone and phenol whilst Wu *et al*. obtained a mixture of oxidation and cleavage products.

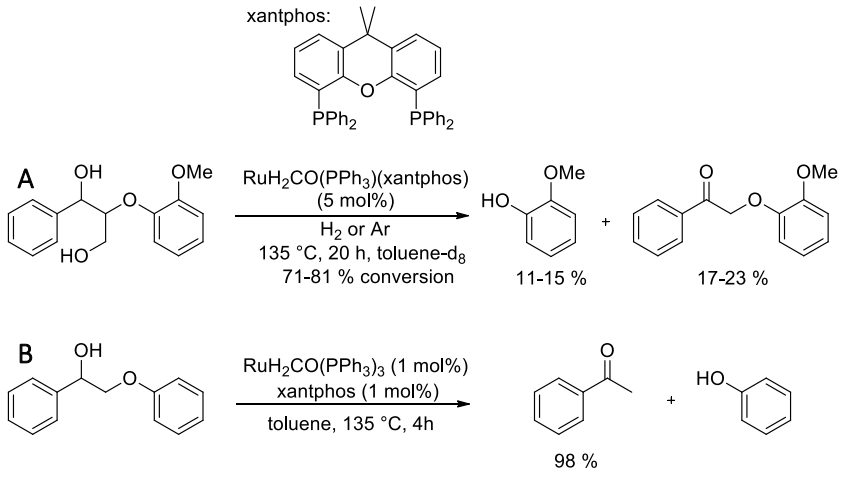

Figure 11: Ruthenium-xantphos catalysed depolymerization of lignin model compounds (A: Wu *et al*.[115]; B: Nichols *et al.*[116])

Catalytic oxidative cleavage of linkages in model lignin compounds has also been reported, the most prevalent examples of which employ vanadium complexes as catalysts. In 2010, both Hanson *et al.* and Son and Toste described the degradation of model lignin compounds by vanadium complexes; the former *via* C-C cleavage and the latter by C-O cleavage.[117, 118] The oxidative C-C cleavage of β-O-4 linkages in several model lignin compounds by a vanadium dipicolinate complex in DMSO-d_6 and pyridine-d_5 was demonstrated by Hanson *et al.*, Figure 12.[117] In the case of the model compound 2-phenoxy-1-phenylethanol, the products included benzoic acid, phenol and formic acid as well as 2-phenoxy-1-phenylethanone. Studies of the reaction revealed higher proportions of the ketone at lower overall conversions, implying that the mechanism for the formation of monomeric products is *via* oxidation to the ketone.

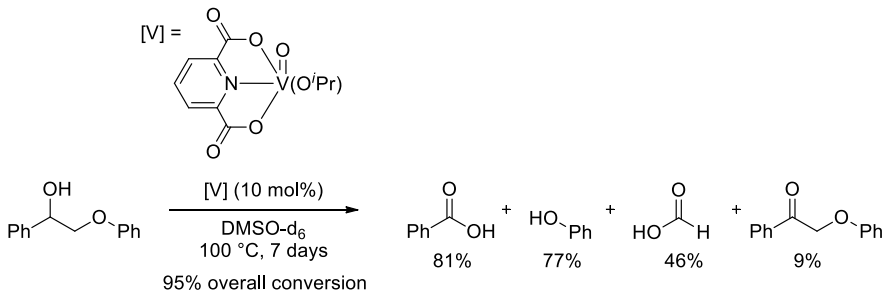

Figure 12: Hanson *et al.* depolymerization of 2-phenoxy-1-phenylethanol using a vanadium-dipicolinate catalyst[117] (conversions determined by ^{1}H NMR spectroscopy and are given as percentages of the theoretical maximum based on the initial amount of substrate)

Son and Toste reported the successful C-O cleavage of the β-O-4 linkage in a dimeric model lignin compound under mild conditions by vanadium Schiff-base complexes, Figure 13.[118] C-O bond cleavage and oxidation reactions were competing and the selectivity was found to be influenced by the ligand structure, Table 2. Whilst catalysts **2**, **3** and **4** effected reasonable to good conversions, oxidation was the dominant reaction. However, catalysts **1a-d** gave not only excellent conversions of 86% to <95% but also high selectivity (61-81%) for C-O bond cleavage. No explicit explanation for this difference in selectivity was provided, however it appears that the oxidation state of the catalyst may have an impact, with the vanadium(V) complexes outperforming vanadium(IV) in terms of C-O cleavage.

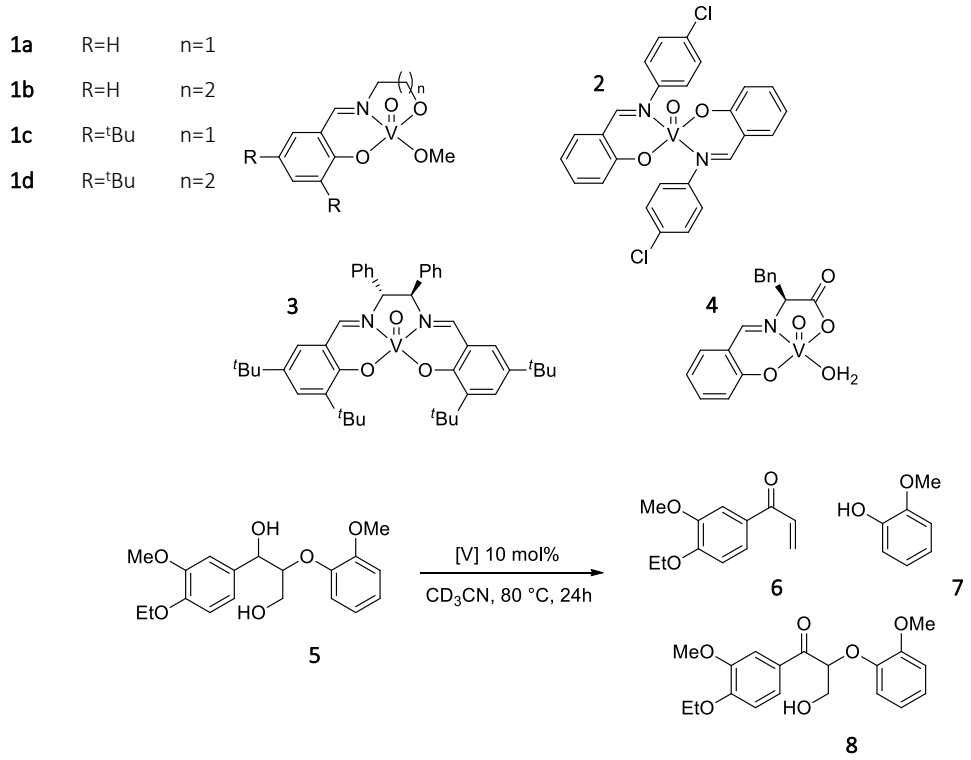

Figure 13: Son *et al*. vanadium Schiff-base catalyzed depolymerization of a model lignin compound[118]

The highest selectivity for C-O cleavage was achieved in the case of catalyst **1d,** Table 2. Within this particular tridentate ligand set, enhanced selectivity for C-O cleavage was observed for the propyl backbone ligands (**1b,d**) over the ethyl analogues (**1a,c**), however no explanation was provided why the bite angle should affect this preference. The higher activity of the *tert*-butyl substituted catalyst **1d** over the unsubstituted **1b** was attributed to the steric bulk of the former complex preventing catalyst deactivation by aggregation.

Table 2: Results of vanadium Schiff-base catalyzed depolymerization of a model lignin compound[118]

Catalyst	V^x	Conversion / %	6 / %	7 / %	8 / %
none	-	0	-	-	-
$VO(O^iPr)_3$	+5	82	5	11	45
1a	+5	>95	61	45	27
1b	+5	86	70	62	8
1c	+5	95	65	50	18
1d	+5	>95	82	57	7
2	+4	86	6	6	59
3	+4	55	3	-	37
4	+4	66	13	14	41

Whilst the overall reaction is formally non-oxidative, significantly higher activities were seen when the depolymerization was attempted in air rather than under anaerobic conditions suggesting that the presence of molecular oxygen greatly increases catalyst turnover. Attempted degradation of **8** by catalyst **1d** did not effect any C-O cleavage to **6** and **7**, Table 2, seemingly ruling out a mechanism whereby the model compound is oxidised to the ketone before cleavage occurs. Model compounds where the benzylic hydroxyl group was substituted for a methoxy group showed greatly decreased activity for depolymerization, implying that the benzylic OH is involved in the mechanism.

The proposed mechanism for C-O cleavage is shown in Figure 14. Ligand exchange of the alkoxide with the free hydroxy group of the model compound is followed by abstraction of the benzylic hydrogen to form a ketyl radical intermediate. Subsequent elimination of the aryloxy radical precedes the formation of the enone *via* hydroxy group elimination and the resulting vanadium(IV) complex is reoxidized to the active vanadium(V) species by the aryloxy radical.

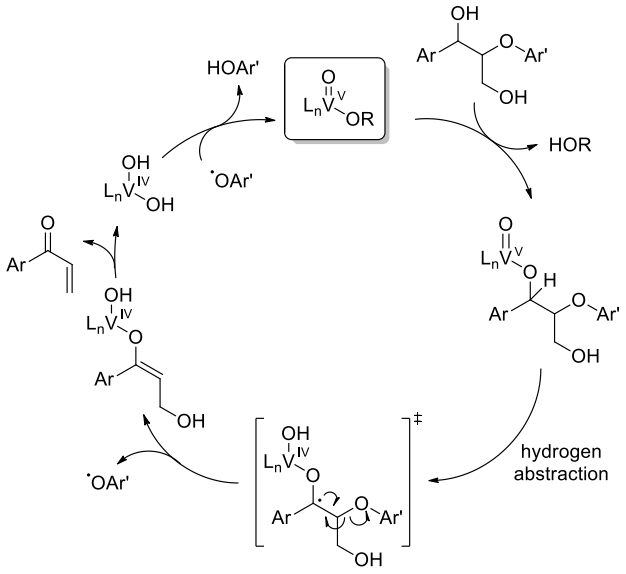

Figure 14: Proposed mechanism for the cleavage of the β-O-4 linkage in a lignin model compound by catalysts 1a-d

Further studies on vanadium catalysed lignin depolymerization have been carried out by both Hanson and Toste, comparing the reactivities of Toste's Schiff-base catalyst, the aforementioned vanadium-dipicolinate species and related vanadium-8-oxyquinolate complex as well as a CuCl/TEMPO system.[111, 119, 120] Hanson's mechanistic studies included deuterium labelling of the benzylic hydrogen in model compound **5** (Figure 13), resulting in dramatically reduced reaction rates when using Toste's catalyst **1d**, thereby confirming the importance of the cleavage of this bond in the mechanism shown in Figure 14.[119]

Further to the cleavage of the β-O-4 linkage in a model compound, Toste also demonstrated the depolymerization of real samples of organosolv lignin extracted from *Miscanthus giganteus* by **1d**, Figure 15.[111] Ethanosolv, dioxasolv and acetosolv lignins were dissolved in either MeCN/THF or EtOAc/THF solvent mixtures (or acetone in the case of acetosolv). After 24 h at 80 °C in the presence of **1d**, the resulting reaction mixtures were dried and analysed by a range of techniques including size exclusion chromatography (SEC) and 2D NMR spectroscopy in order to determine the extent of depolymerization. SEC analysis revealed molecular weight lowering in all cases, however the extent of molecular weight lowering was not as high for the ethanosolv lignin as for the other two. This reduced activity is suspected to be due to the ethylation of many of the free hydroxy groups in lignin during the ethanosolv process, through which the catalyst is suspected to bind, thereby reducing the efficacy of the catalyst in this case. ^{13}C-^{1}H correlation NMR (HSQC) spectra provided further insights into the degradation of the lignins, indicating destruction of the β-O-4 linkages. Finally, GC-MS analysis

was used to identify any volatile products from the degradation; for dioxasolv lignin these included vanillin, syringic acid, syringaldehyde and other related compounds in low yields of less than 1%.

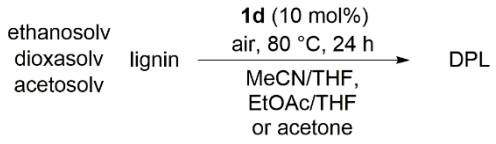

Figure 15: Vanadium-catalysed depolymerization of organosolv lignins derived from *Miscanthus giganteus*[111]

Whilst these results may not appear to be overly impressive at first glance, this is one of very few examples of the successful depolymerization of lignin with a homogeneous metal catalyst. The complex, 3-dimensional structure and potential contaminants such as water and sulfur in real samples of lignin can be very challenging for homogenous catalysis. The successful partial depolymerization of lignin by this catalyst therefore represents a promising step forwards in lignin depolymerization catalysis.

Given the promising reactivity of Son and Toste's vanadium catalyst towards not only model compounds but also real samples of lignin, it was decided to further investigate the catalyst behaviour and attempt to identify other catalysts with similar or even improved activity and selectivity for C-O bond cleavage in lignin.

1.6 Depolymerized lignin as fuel additives

1.6.1 Oxidative stability of biodiesel

One potential higher value application for renewable phenols produced from lignin is as fuel additives. Biodiesel is composed of fatty acid methyl esters (FAMEs), formed from the transesterification of triglycerides, obtained from vegetable, animal or waste oil feedstocks, with methanol. The exact composition of biodiesel depends on the source of the oil, as carbon chain length and degree of unsaturation vary from feedstock to feedstock. Most commonly-used biodiesels from edible vegetable oils, for instance rapeseed and soybean methyl esters, contain mainly C_{16}-C_{18} FAMEs and between zero and three double bonds, Table 3.[121, 122] As the production of biodiesel increases there is a demand for new, more sustainable feedstocks to be employed, such as non-edible jatropha, algae and even yeast oils.[123-126] Common across most of these feedstocks is a significant unsaturated and polyunsaturated FAME content, which renders the biodiesel oxidatively unstable. Standardization of fuel properties and

quality assurance is very important for increased uptake of biodiesel, therefore this oxidative instability must be addressed.

Table 3: Fatty acid profiles of oils commonly used in the production of biodiesel. *16:0, palmitic acid; 16:1, palmitoleic acid; 18:0, stearic acid; 18:1, oleic acid; 18:2, linoleic acid; 18:3, linolenic acid. †from *nannochloropsis salina*; also contains 15 wt% 20:5, eicosapentaenoic acid. ‡from *botryoccus braunii*; also contains 15 wt% 16:3, hexadecatrieneoic acid. ¥from *metschnikowia pulcherrima*.

Source oil	Percentage of the total fatty acids (wt%)					
	16:0*	16:1*	18:0*	18:1*	18:2*	18:3*
Rapeseed (canola)[121]	2-6		4-6	52-65	18-25	10-11
Soybean[121]	10-12		3-5	18-26	49-57	10-11
Palm[127]	45		4	40	9	0.3
Jatropha[123]	15		7	45	31	0.2
Algae†,[124]	38	23	1	12	2	
Algae‡,[125]	21	2	3	3	14	33
Yeast¥,[126]	21	8	4	50	11	7

The Renewable Transport Fuel Obligation (RTFO) Order states that, from April 2013, 5% of all road transport fuel supplied in the UK must be biofuel.[1] This is mainly achieved by the blending of biodiesel into petroleum diesel (petrodiesel). These blends are referred to by the percentage of biodiesel present in the diesel, for instance B5 is a blend of 5% biodiesel and 95% petrodiesel, whilst B50 is a 1:1 volume mixture of the two. Despite the fact that they are miscible at any level, and that it is possible to use neat biodiesel in diesel engines without any modifications, due to the differences in chemical structure between biodiesel and petrodiesel the fuel properties of biodiesel and its blends, and their performance in engines must be taken into account. Comprehensive reviews of the effect of biodiesel on the performance of engines and the resulting emissions were conducted by Lapuerta *et al.* in 2008 and Xue *et al.* in 2011.[128, 129] In terms of engine performance, there is a slight reduction in performance, and corresponding increase in fuel consumption, when using biodiesel rather than petrodiesel. This is largely due to the lower energy density of biodiesel owing to its higher oxygen content.

The addition of biodiesel to petrodiesel has beneficial effects in terms of CO, hydrocarbon and particulate matter emissions. These effects can be attributed to several factors, primarily that

the higher oxygen content of biodiesel favours more complete combustion, but the reduction in particulate matter may also be attributable to the absence of aromatics and sulfur-containing compounds.[129] Biodiesel is also a better lubricant than petrodiesel, and its addition to diesel at low blend levels has helped to provide the lubricity once provided by sulfur-containing compounds, before their levels were restricted.[130] In contrast, NO_x emissions for biodiesel blends were observed to be higher than those of the neat petrodiesel, however the addition of additives such as ethanol can be employed to combat this increase.[129]

In order to ensure that it is suitable for use in diesel engines, biodiesel must conform to certain specifications, such as the EN 14214 in Europe, and ASTM D-6751-03 in the US.[131, 132] These specifications describe the properties of the fuel including maximum and minimum limits for viscosity and density, minimum flash point and cetane number, and also a minimum oxidative stability.

A major barrier to the further uptake of biodiesel into the current fuel market is its oxidative stability. The oxidative stability of biodiesel is lower than that of petrodiesel, in part owing to the presence of olefins, and especially multiple non-conjugated olefins. Biodiesel oxidation leads to a decrease in fuel quality which can cause issues including blocked fuel filters, due to increased viscosity, increased engine wear, as a result of increased viscosity and gum formation, and corrosion of the fuel delivery equipment by the formation of acids.[128, 129, 133-135] The formation of insoluble particulates from biodiesel oxidation can also make the fuel more susceptible to microbial contamination.[134] Although biodiesel is a better lubricant than petrodiesel, the effects of it oxidising within the lubricating oil system can be detrimental to the engine.[136]

1.6.2 Mechanism of biodiesel oxidation

Oxidation which occurs in the presence of air or oxygen, forming peroxides and hydroperoxides, is known as autoxidation and can contribute to the oxidative degradation of biodiesel during storage.[133, 137] There are two main stages in the oxidation process; a radical chain reaction forming hydroperoxide species, and subsequent decomposition of the hydroperoxides.[138]

The chain reaction is initiated by abstraction of a hydrogen to form a radical species, which can then react with molecular oxygen to form hydroperoxides, Figure 16 equations 1-3. Hydrogen abstraction can be instigated in a number of ways, including by the action of light or heat, the presence of metal ions or free radicals. Once initiation has occurred, the chain reaction can propagate to form hydroperoxides. These species then decompose and react

forming a range of secondary oxidation products including alcohols, aldehydes, carboxylic acids and higher molecular weight species such as oligomers.[138-140]

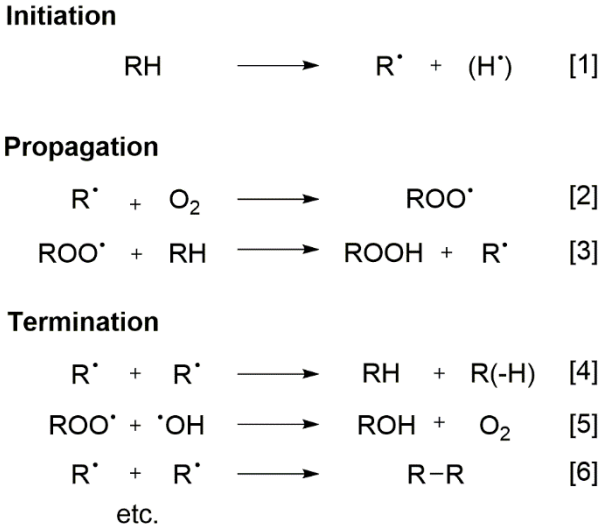

Figure 16: Mechanisms involved in the autoxidation chain reaction[138]

In general, tertiary C-H bonds are more susceptible to oxidative attack than secondary, which are in turn more so than primary C-H bonds. This is due to the increased stability of the formed carbon radicals with increasing substitution. Olefins are more susceptible again, particularly polyunsaturated species such as FAMEs which are methylene-interrupted, rather than conjugated. This is due to the presence of highly reactive allylic or bis-allylic sites where autoxidation can be initiated. The relative stability of FAMEs can be correlated to the number of allylic and bis-allylic sites.[139, 141]

The second phase of the process involves decomposition of the hydroperoxide species formed during the radical chain reaction. There are several potential mechanisms by which this can occur, equations 7-10, Figure 17, and therefore the products of hydroperoxide decomposition vary depending upon the conditions of the reaction. Due to the varying compositions of biodiesels and depending on the conditions of oxidation, a wide range of products can be formed including organic acids, esters and aldehydes, and frequently these products react together to form higher molecular weight species such as oligomers and gums. These higher molecular weight species are often insoluble and can agglomerate to form sediments or deposits which are detrimental to engine performance.[134]

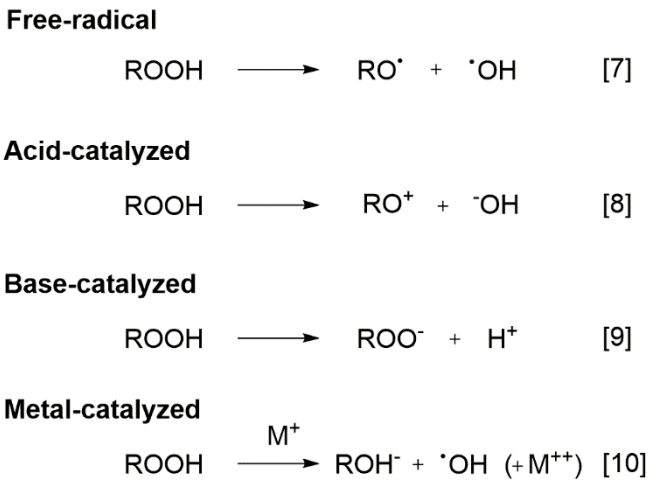

Figure 17: Possible mechanisms for hydroperoxide decomposition[138]

There is commonly an "induction period" which precedes the onset of autoxidation. In very pure hydrocarbons, this can be a result of the time required to build up a sufficient concentration of hydroperoxide to allow propagation of the chain reaction to proceed. However, in less pure samples, for instance in the case of biodiesel fuels, the induction period may be the result of resonance-stabilization of reactive hydroperoxide radicals by impurities.

1.6.3 Measurement of the oxidative stability of biodiesel

Ideally, determination of the oxidative stability of biodiesel is done *in situ* under standard storage conditions. Such studies have been conducted, however as they require long periods of time (months or years) to complete,[142, 143] it is often unfeasible to use these types of tests to measure biodiesel stability.

The oxidative stability of oils such as biodiesel is therefore tested under accelerated oxidative conditions at elevated temperatures and with enhanced oxygen exposure. Whilst these accelerated conditions do not exactly mimic standard storage conditions, they allow for much faster analysis. Increased contact with oxygen has been reported to significantly increase the instability of biodiesel even in long-term non-accelerated tests.[144] There are a range of techniques for monitoring the extent of degradation of the biodiesel, including measurement of insolubles, viscosity, peroxide value or the evolution of volatiles.

The Metrohm Rancimat method is the standard test used to determine the oxidative stability of fats and oils, and is widely used in the analysis of biodiesel, including in the EN 14112 biodiesel specification.[130, 145] The fuel is held at 110 °C and a gas flow of 20 $L.h^{-1}$ of purified air is passed through the sample.[146] Measurement of the degradation of the sample is performed

by passing the exhaust from the oxidation reaction through deionized water. The electrical conductivity of this solution is measured and, as the fuel oxidises and volatile secondary oxidation products are formed, these volatiles dissolve in the water causing a dramatic increase in conductivity. The time between the start of the reaction until this increase in conductivity is called the Rancimat induction period (RIP).

The PetroOXY method for determining the stability of diesel fuels from B0 to B100 is a highly accelerated oxidation method involving subjecting the fuel sample to 700 kPa pressure of oxygen at 140 °C. The pressure is monitored and the induction period is calculated from the time from the start of the experiment to the drop in pressure corresponding to consumption of the oxygen by the oxidation reaction.[130] This method has the advantage of being much faster that the Rancimat test (minutes rather than hours), making it more suitable for commercial testing and development of new additives, however reproducing these conditions is unfeasible in a standard research laboratory. There has also some concern about the correlation between the results of the PetroOXY and Rancimat tests, with the former not an accepted test method within Europe, however there have been recent efforts to rectify this.[130, 147]

An issue with the Rancimat method is that it provides an incomplete analysis of the oxidative stability of the sample as it measures only the latter stages of oxidation, that is, the volatiles produced from the decomposition of the hydroperoxides, and does not take into account the effect of any changes in the biodiesel in the reaction vessel. These changes include increases in viscosity due to the production of non-volatiles such as gums, changes in density, acid value and peroxide value. Long term tests have shown that there is a significant increase in viscosity, peroxide value and Rancimat score over the course of one year under commercial storage conditions.[144] This effect was more pronounced when the biodiesel was stored incorrectly.

In order to gain a more detailed understanding of the oxidative decomposition of biodiesels, a wide range of analytical techniques can be employed. ^{1}H NMR spectroscopy and gas-chromatography-mass spectrometry (GC-MS) allow for detailed analysis of the compositional changes occurring in the fuel during the course of the oxidation, however they require extensive sample preparation which is not conducive to real-time monitoring. Fourier transform infrared (FTIR) spectroscopy has been successfully utilised as an *in vitro* monitoring technique for individual biodiesel oxidation experiments, however it would be prohibitively expensive to use in a high throughput setting.[148]

As has been discussed, the viscosity of fuels is known to increase during oxidation, the formation of higher molecular weight species such as gums by the decomposition of hydroperoxides causes an increase in the viscosity of biodiesel and therefore viscosity can be a useful measure of the extent of oxidation. There has been shown to be a good correlation between viscosity and other parameters such as acid value and peroxide value, however measurement of kinematic viscosity can also be time consuming.[149, 150] The refractive index (RI) of a liquid is known to be related to its viscosity and RI is a simple and fast analytical technique requiring little to no sample preparation, making it suitable for this application.[151] RI has been previously successfully employed as a technique for fast analysis of the oxidation of fuels.[148]

Along with the structure of the biodiesel itself, a number of other factors can contribute to the oxidative instability of biodiesel. Test temperature has been found to be strongly influential in the rate of oxidation.[145, 152-155] Higher temperatures are likely to facilitate both initiation by hydrogen abstraction and also the decomposition of hydroperoxide radicals. Access to light has been found to increase the rate of oxidation of biodiesel, due to the photo-initiation of autoxidation, and the presence of metals has been shown to negatively impact the oxidative stability of biodiesel by catalysing the decomposition of hydroperoxides.[141, 156, 157] Depending on their structure, contaminants present in biodiesel can positively or negatively affect the oxidative stability of biodiesel, either by disrupting the radical chain reaction, or by reacting with hydroperoxides.[133]

1.6.4 Effect of antioxidant addition on the stability of biodiesel

It would possible to extend the storage lifetime of biodiesel by changing the conditions, for instance storing the fuel under an inert atmosphere or in temperature controlled containers, however this is impractical on a large scale. Even if the fuel was stored under ideal conditions, however, in the engine block the fuel is subjected to harsh conditions as unburnt fuel is recirculated to the tank and also accumulates in the sump oil. These conditions are unavoidable and therefore the only way to prevent degradation of the fuel by oxidation is through the use of antioxidants.

The most common antioxidants are chain breakers which prevent the formation of hydroperoxides by acting as radical scavengers. Less common are the hydroperoxide decomposers; these act as reducing agents, resulting in the degradation of the hydroperoxides to alcohols, rather than acids and aldehydes which are associated with many of the detrimental consequences of fuel oxidation.[158] There is little literature on the latter,

however the use of chain breakers as antioxidants in fuels is widespread. There are two main types of chain breaking antioxidants, amine-based and phenolic. Phenolic antioxidants are by far the most widely used in FAME applications.[127, 159-162] Phenolic compounds work as chain breaking antioxidants as they contain a highly labile hydrogen which can be abstracted by peroxy radicals much more easily than from a FAME molecule, thereby preventing oxidation of that species, Figure 18.

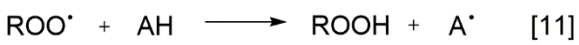

Figure 18: Mechanism of chain-breaking antioxidant formation by antioxidant AH, where A· is a stable radical

The effectiveness of phenolic compounds as antioxidants is dependent on both the lability of the hydrogen and also the stability of the formed phenoxy radical. Phenoxy radicals can participate in resonance with the p-orbitals of the neighbouring aromatic ring system, Figure 19, leading to greater stability. This resonance stabilization can be increased by the presence of certain substituents at the *ortho* and *para* positions. Bulky alkyl substituents such as *tert*-butyl groups can stabilise neighbouring radicals *via* a positive inductive effect, and also potentially by preventing attack of the radical by other species such as oxygen due to their steric hindrance. Hydroxyl moieties and conjugated substituents can also lend greater stabilization to the radical species by also participating in resonance, thereby extending the delocalization of the radical.

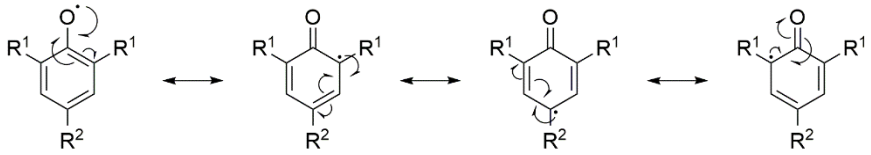

Figure 19: Resonance stabilization of phenoxy radicals

Vitamin E derivatives α, β, γ, and δ-tocopherol are antioxidants naturally occurring in the vegetable and plant oils used in the production of biodiesel, Figure 20. Depending on the production method, varying levels of tocopherols may be present in the biodiesel itself. Distillation of different biodiesels to remove any tocopherols prior to testing has been observed by many researchers to result in a decrease in oxidative stability.[127, 141, 144, 159] Whilst this result indicates that tocopherols are active as antioxidants in biodiesel, comparisons between tocopherols and a range of synthetic antioxidants have shown that the naturally occurring antioxidants are generally less active than their synthetic counterparts.[133, 152, 161]

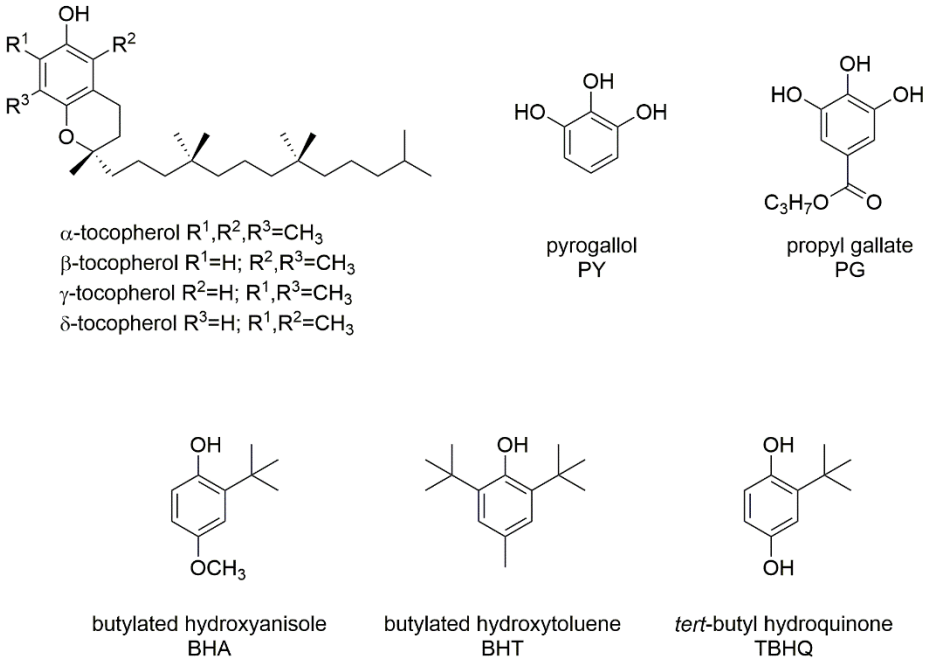

Figure 20: Structures of common naturally-occurring (α,β,γ,δ-tocopherols) and synthetic antioxidants (PY, PG, BHA, BHT, TBHQ)

Bondioli *et al*. reported that synthetic antioxidants pyrogallol (PY) and *tert*-butyl hydroquinone (TBHQ), Figure 20, were significantly more effective than tocopherols at extending the RIP of batches of rapeseed methyl ester (RME) biodiesel.[144] The addition of 400 mg.kg^{-1} of TBHQ to RME increased the RIP from 7.51 h to 36.00 h, and 250 mg.kg^{-1} of PY effected an increase from 7.75 h to 22.42 h. However, the removal of most of the naturally-occurring tocopherols by distillation (from 486 to 152 mg.kg^{-1}) only reduced the RIP of the RME batch from 9.20 h to 4.16 h. Mittelbach *et al*. tested the performance of PY, TBHQ, propyl gallate (PG), butylated hydroxylanisole (BHA), butylated hydroxytoluene (BHT), Figure 20, and a range of tocopherol-based commercial additive mixtures at extending the RIP of a range of oils and biodiesels, reporting the results in terms of a calculated stabilization factor.[159] In rapeseed oil, the stabilization factors of the antioxidants followed the order of TBHQ>PG≈PY≈BHA>>BHT≈tocopherols. Liang *et al*. found that TBHQ and BHT both outperformed α-tocopherol in increasing the stability of palm diesel, with 100 ppm of the natural antioxidant required to increase the RIP above 6 h, whilst only 50 ppm of BHT was required to achieve the same outcome and 50 ppm of TBHQ raised the RIP to almost 9 h.[127]. A linear increase in the RIP was observed on addition of higher loadings of BHT, with a 1000 ppm loading effecting an RIP of 17 h, whilst an RIP in excess of 48 h was observed at a 1000 ppm of TBHQ. In a study into the oxidative stability of jatropha biodiesel, Sarin *et al*. found similarly that TBHQ and BHT were more effective at extending the RIP than α-tocopherol over a range of loadings.

The effectiveness of specific antioxidants also varies depending on the composition of the biodiesel. Mittelbach *et al*. found that TBHQ was significantly more effective in extending the RIP of rapeseed oil than PY and PG, however in used frying oil methyl ester they all behaved similarly, with PY performing slightly better than the other two.[159] Added tocopherol antioxidants were found to be much more effective in used frying oil methyl ester than in the rapeseed oil. In studies of jatropha biodiesel, with an RIP of 4 h in the absence of an antioxidant, the difference in antioxidant effectiveness of TBHQ and BHT was small, with the RIP at an antioxidant loading of 600 ppm increased to 10 h for TBHQ and 9.5 h for BHT.[161]

Several studies have focussed on the derivation of structure-activity relationships for different types of antioxidants. Lien *et al*. in 1999 reported quantitative structure-activity relationship analyses for a range of substituted phenols, flavonoids and vitamin E derivatives by considering parameters such as the energies of the lowest unoccupied molecular orbital of the radical and the highest occupied molecular orbital of the parent compound.[163] Of the commonly investigated antioxidants listed in Figure 20, TBHQ, PY and PG are generally reported as performing the best in biodiesel.[137] This can be attributed to the increased number of hydroxyl groups compared to BHT, BHA and the tocopherols, providing more sites both for free radicals to attack the antioxidant and abstract a hydrogen, but also more resonance structures thereby increasing resonance stabilization.

1.7 Aim of thesis

The primary aim of this thesis is to investigate the potential applicability of homogeneous vanadium Schiff-base complexes as catalysts for the selective depolymerization of lignin to monomeric phenols, potentially as part of an ionic liquid biomass pretreatment process. A secondary aim was to assess the use of renewable phenols produced from lignin depolymerization as antioxidants in fuel. These aims were to be achieved through the following objectives:

i. Assessment of the activity and selectivity of a range of vanadium Schiff-base complexes for the catalytic degradation of model lignin compounds *via* a systematic study of catalyst structure and reaction conditions
ii. Investigation into the stability and activity of the catalysts for the degradation of model lignin compounds in ionic liquids
iii. Development of a high-throughput fuel oxidation rig to test the antioxidant properties of a number of monolignols in biodiesel

2. Vanadium Schiff-base complexes for the catalytic degradation of β-O-4 model lignin species

The selective degradation of lignin to produce value-added monomeric phenolic compounds has the potential to improve the process economics of a lignocellulosic biorefinery concept. The advantages of homogeneous catalysis for lignin depolymerization over traditional thermochemical or heterogeneous catalyzed processes include the potential for mild reaction conditions, high selectivity and the potential for catalyst tunability through alterations to ligand structure. Following on from promising literature precedent of the use of homogeneous vanadium Schiff-base catalysts for the degradation of model lignin compounds, this study aims to conduct a systematic assessment of the effect of the catalyst structure and reaction conditions on the degradation of non-phenolic β-O-4 model lignin compound 2-phenoxy-1-phenylethanol (model B). The effects of ligand substitution, denticity and backbone structure, in addition to variation of the temperature, catalyst loading and availability of oxygen, will be investigated. The degradation of phenolic model compound guaiacylglycerol-β-guaiacyl ether (model C) in the presence of these catalysts will also be discussed.

2.1 Model compound synthesis

As discussed in section 1.5.2, a diverse library of potential model lignin compounds is available. These range in size and complexity from monomeric and dimeric species up to oligomeric and polymeric models and each contains at least one representative lignin linkage, Figure 4.[21] As well as being the most abundant linkage in lignin, the β-O-4 bond is amongst the most susceptible to cleavage and is therefore a prime target in many lignin depolymerization studies.[21, 112] Dimeric β-O-4 species are amongst the most commonly employed,[116-120] and are also the class of model compounds chosen for these studies.

The synthesis of β-O-4 model compound 1-(4-ethoxy-3-methoxyphenyl)-2-(2-methoxyphenyl)ethanol (model A) is shown in Figure 21. The initial step, ethylation of the free hydroxyl group using ethyl iodide, proceeded in high yields to form large, rectangular crystals. Despite the high purity of 1-(4-ethoxy-3-methoxyphenyl)ethanone, the subsequent bromination step, which was originally attempted using copper(II) bromide in a large excess (method 1), proved to be low yielding and resulted in a product contaminated with bromine.

Bromination was also attempted using pyridinium tribromide (method 2). This was much more successful however there was still some contamination by bromine which was almost impossible to remove from the product by solvent washing or recrystallization. This was found to have a detrimental effect on the subsequent steps of the synthesis, which proceeded in low conversions. Purification of the intermediates was impeded by low solubilities of these species in a range of organic solvents including ethanol, methanol, dichloromethane, hexane and toluene.

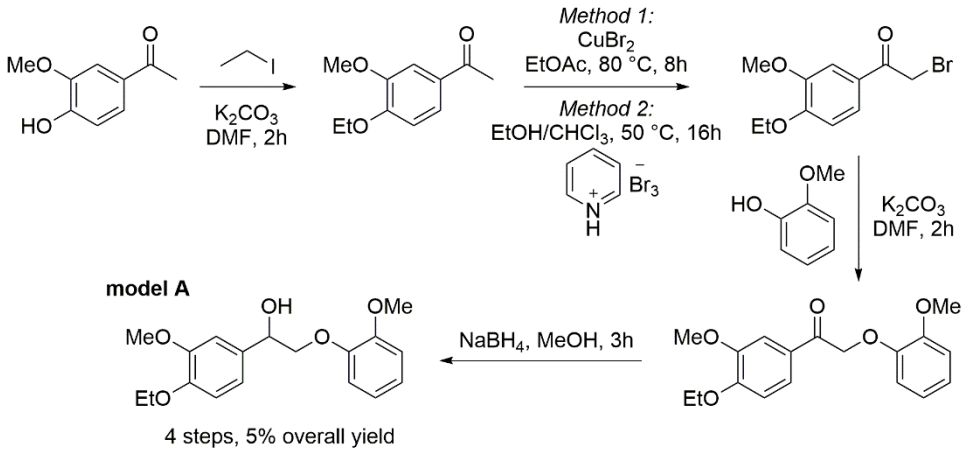

Figure 21: Synthesis of 1-(4-ethoxy-3-methoxyphenyl)-2-(2-methoxyphenyl)ethanol (model A)

A second β-O-4 model compound, 2-phenoxy-1-phenylethanol (model B), was synthesized, Figure 22. Importantly, model B could be produced in two steps from commercially available starting material 2-bromoacetophenone whilst avoiding the bromination reaction. Thus model B was synthesized by condensation of 2-bromoacetophenone with phenol in DMF using KOH as a base to afford 2-phenoxy-1-phenylethanone which was crystallized directly from the reaction mixture. The resulting pure compound was found to be suitable for reduction to 2-phenoxy-1-phenylethanol (model B) using sodium borohydride in methanol. This method was easily conducted on a multi-gram scale resulting in a 75% yield of 2-phenoxy-1-phenylethanol (6 g), over 2 steps.

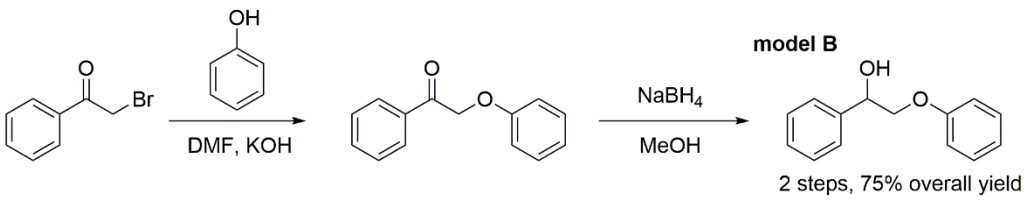

Figure 22: Synthesis of 2-phenoxy-1-phenylethanol (model B)

2.2 Ligand synthesis

With the exception of ligands (**10**)H_2 and (**15**)H_2, which were synthesized by other members of the group,[164, 165] the ligands in Figure 23 were formed *via* condensation of the relevant salicylaldehyde with either one equivalent of amino alcohol [for tridentate ligands (**1**-**7**,**11**-**15**)H_2] or half an equivalent of diamine [for tetradentate ligands (**8**-**10**)H_2]. Ligands (**1**-**7**)H_2 are close analogues of the *tert*-butyl substituted Schiff-base ligand, (**5**)H_2, utilised by Son and Toste,[118] such that the steric and electronic effects of the phenolate substituents on the activity and selectivity of the complexes could be systematically investigated. Whilst the halo-, *tert*-butyl- and un-substituted salicylaldehydes are commercially available, the adamantyl- and trityl-substituted salicylaldehydes are not and were thus synthesised according to literature procedures.[166] Ligands (**8**-**15**)H_2 were synthesised to investigate the influence of the ligand coordination sphere on the behaviour of the vanadium catalysts. Backbone length [(**8**-**9**)H_2 and (**11**-**14**)H_2], backbone rigidity [(**10**-**15**)H_2] and ligand denticity [(**8**-**10**)H_2] were varied, as well as the lability of the second hydroxyl group by the introduction of a second phenolate group [(**8**-**10**)H_2 and (**15**)H_2].

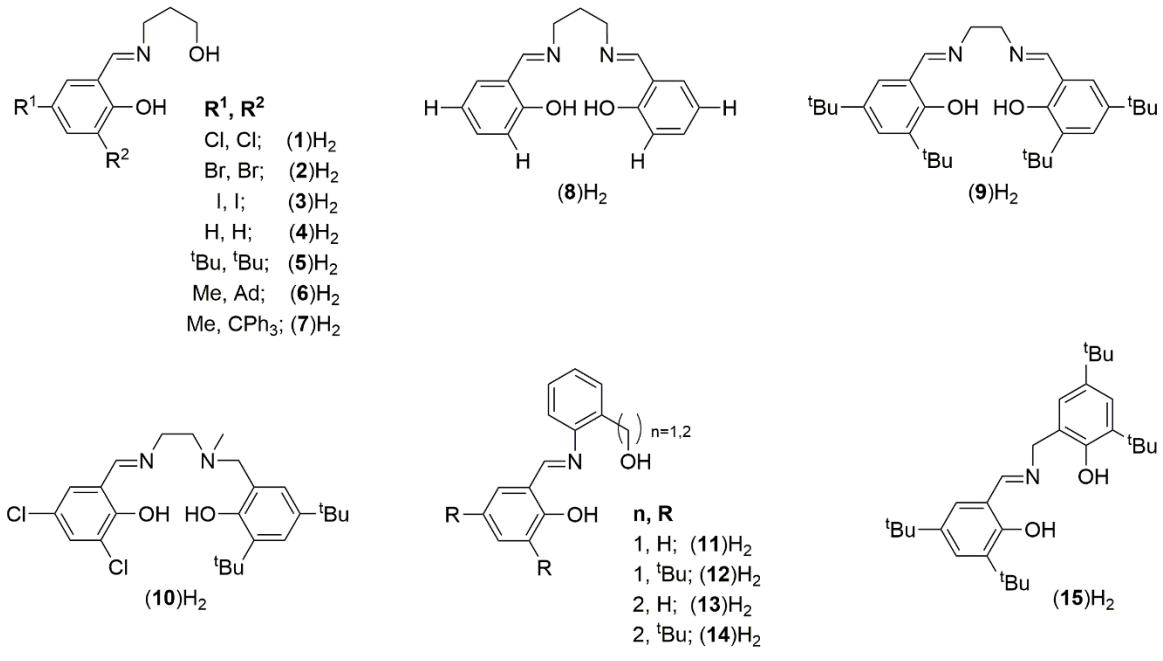

Figure 23: Structures of the Schiff-base ligands employed in this study

2.3 Catalyst synthesis

The catalysts were synthesised under an inert atmosphere *via* complexation of the ligands, (**X**)H_2 (Figure 23), with vanadium(V) oxytriisopropoxide according to the general method in Figure 24. It was theorised that the resulting complexes would be vanadium(V) species of the general form VO(**X**)(O^iPr).

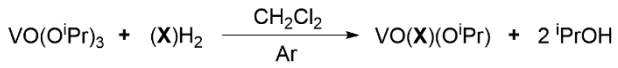

Figure 24: General catalyst synthesis method (X = 1-15)

2.3.1 Tridentate ligand complexes

Complexes VO(**1-7**)(O^iPr) were isolated as red, orange or brown crystalline samples in moderate to good yields. The solution state ^1H NMR spectrum of VO(**1**)(O^iPr) in $CDCl_3$ is consistent with the data provided for similar complexes in the literature.[118] Figure 25 shows the ^1H NMR resonances corresponding to the four O-C$\underline{H}_2$ and N-C$\underline{H}_2$ protons from both VO(**1**)(O^iPr) and (**1**)H_2 (*overlaid). Coordination of the ligand to the metal is evidenced by a downfield chemical shift of these backbone protons from the ligand to the complex, as well as splitting of the multiplet (3.4 ppm, 4H) into four distinct resonances (each 1H). The more defined resonances at around 4.1 and 5.4 ppm display both geminal (J ≈ 3 Hz) and vicinal coupling (J ≈ 11 Hz) indicating that the backbone protons become diastereotopic in the complex and demonstrating that the propyl chain is locked into configuration. ^{51}V NMR spectroscopy of the same complex confirms the presence of only one vanadium species in solution, Figure 26.

^1H and ^{51}V NMR spectra of complexes VO(**2-7**)(O^iPr) were analogous to that of VO(**1**)(O^iPr) and elemental analyses of VO(**1-7**)(O^iPr) were as expected for the general structure VO(**X**)(O^iPr) proposed in Figure 24. The ^{51}V NMR resonances of VO(**1-7**)(O^iPr) were similar to those reported for other vanadium(V) Schiff-base species[118, 167] and the difference in chemical shift between the complexes was small (<15 ppm). As the ^{51}V nucleus is highly sensitive to changes in the local environment,[168] this suggests that there is no change in the direct coordination sphere of the vanadium atoms between these complexes.

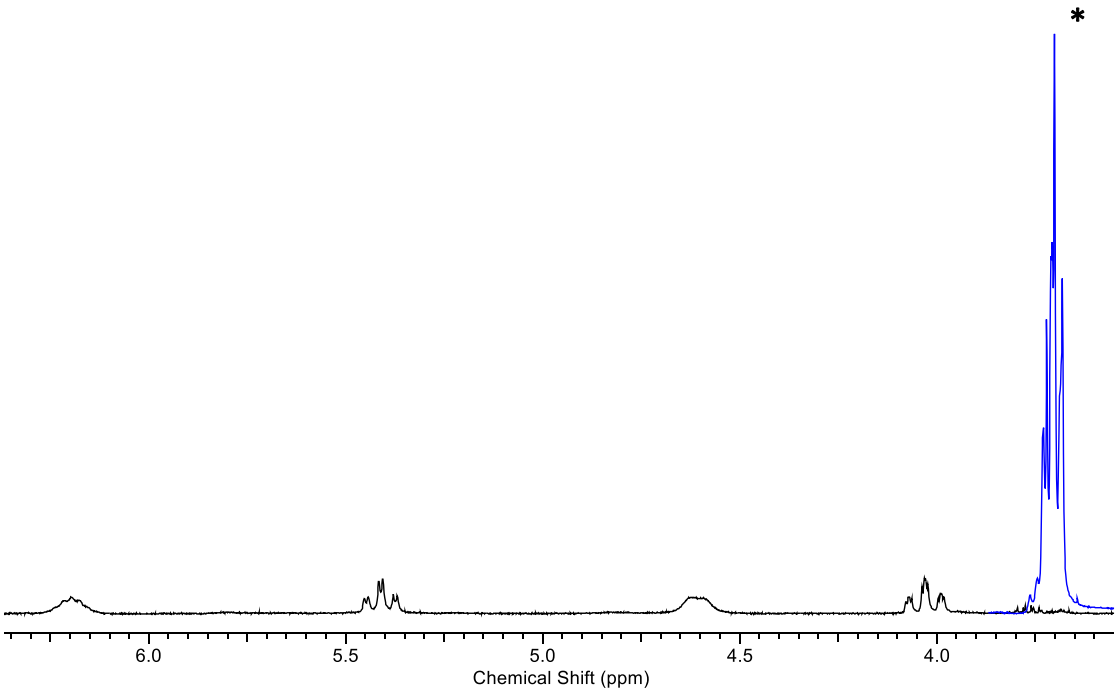

Figure 25: ^{1}H NMR Spectrum of N-C$\underline{H}_2$ and O-C$\underline{H}_2$ resonances in VO(1)(O^{i}Pr), (4 × 1H) [*original CH_2 resonance in (1)H_2 (4H)]

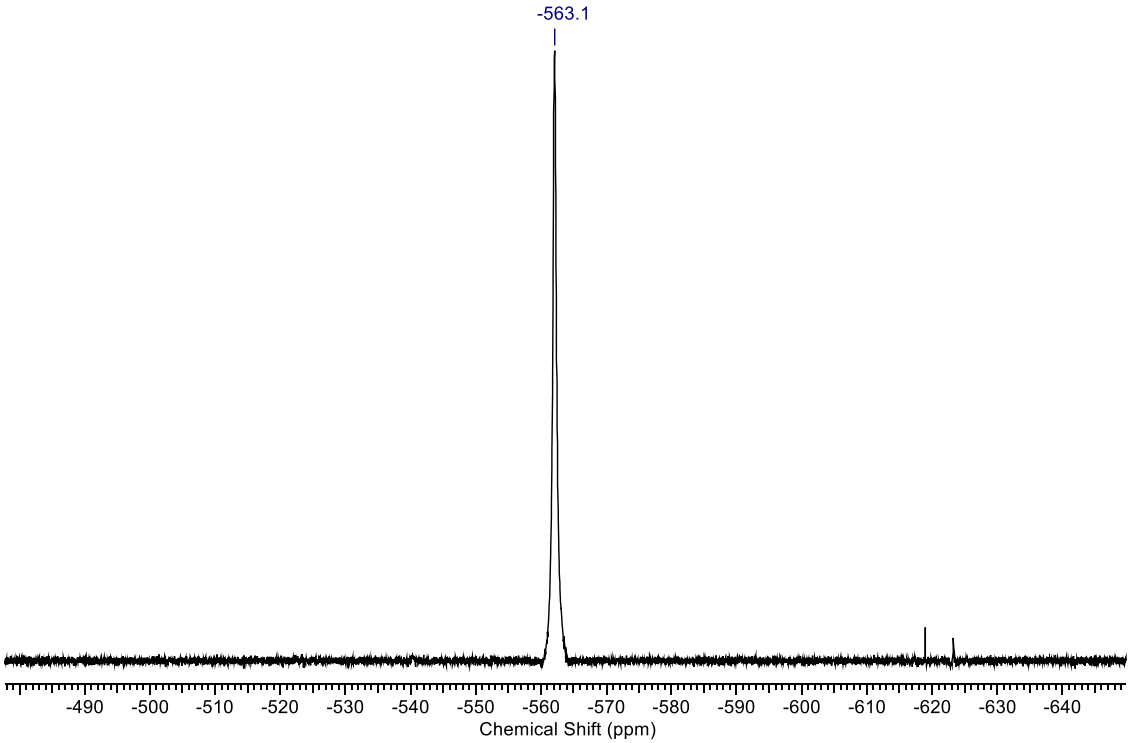

Figure 26: ^{51}V NMR spectrum of VO(1)(O^{i}Pr)

The solid state structures of novel complexes VO(**1-5**)(O^{i}Pr) have been determined by single crystal X-ray diffraction (XRD). Analogous vanadium-methoxy analogues of catalysts VO(**4-5**)(O^{i}Pr) have been previously reported.[118] In the solid state, complexes VO(**1-5**)(O^{i}Pr) are dimeric, with structures analogous to that of VO(**5**)(O^{i}Pr) shown in Figure 27. The two vanadium atoms in each complex are bridged by the aliphatic alcohol, O(2), and all vanadium atoms are in pseudo-octahedral environments, as indicated by N(1)-V(1)-O(1) ≈ 180° and O(3)-V(1)-O(1) ≈ 90°, Table 4. The ligand is bound to vanadium in a 1:1 ratio in a tridentate meridonal arrangement through the $O_{phenolate}$, N_{imine} and $O_{aliphatic}$ atoms. Each species [VO(**1-5**)(O^{i}Pr)] has a centre of inversion and thus the two vanadium atoms in each complex are equivalent to one another. The centrosymmetric nature of the crystal space groups [$P2_1/c$ for VO(**1-3**)(O^{i}Pr) and P-1 for VO(**4-5**)(O^{i}Pr)] explains the consistency of the ^{1}H and ^{51}V NMR spectra and elemental analyses with a monomeric structure. The V-$O_{phenolate}$ [V(1)-O(3)] and V-N_{imine} [V(1)-N(1)] bond lengths average 1.91 Å and 2.12 Å respectively. These are comparable to those of similar vanadium-Schiff base complexes.[169, 170] The average vanadyl bond length [V(1)-O(4)] of 1.60 Å is also typical of vanadium(V) Schiff-base species.[169, 170] Although solid state structures were not obtained for complexes VO(**6**,**7**,**11-15**)(O^{i}Pr) it seems likely that their structures are also analogous, given the consistency of the NMR and elemental analysis data with those obtained for VO(**1-5**)(O^{i}Pr).

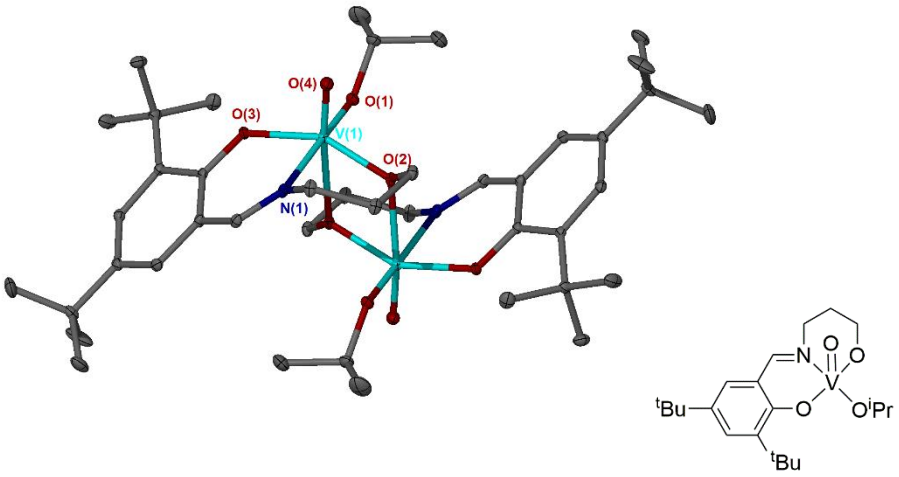

Figure 27: Solid state structure of VO(5)(O^{i}Pr), thermal ellipsoids are shown at the 30% probability level, all hydrogen atoms have been removed for clarity.

Table 4: Selected bond lengths (Å) and angles (°) for complexes VO(1-5)(O^iPr)

	VO(**1**)(O^iPr)	VO(**2**)(O^iPr)	VO(**3**)(O^iPr)	VO(**4**)(O^iPr)	VO(**5**)(O^iPr)
V(1)-O(1)	1.781(2)	1.7815(19)	1.781(2)	1.7905(18)	1.7957(11)
V(1)-O(2)	1.8731(18)	1.8757(19)	1.879(2)	1.8867(18)	1.8870(10)
V(1)-O(3)	1.9193(19)	1.9218(19)	1.925(2)	1.8983(19)	1.9011(10)
V(1)-O(4)	1.596(2)	1.5955(19)	1.595(3)	1.6013(17)	1.5954(11)
V(1)-N(1)	2.192(2)	2.196(2)	2.199(3)	2.178(2)	2.1616(13)
N(1)-V(1)-O(1)	172.96(9)	173.26(9)	173.38(12)	173.97(8)	172.37(5)
O(3)-V(1)-O(1)	93.39(9)	93.68(8)	94.29(11)	93.60(9)	94.73(5)

Although dimeric in the solid state, it was expected that complexes VO(**1-7**)(O^iPr) would dissociate in solution into monomeric, coordinatively unsaturated species. In order to probe this hypothesis the complexes were analysed by diffusion-ordered NMR spectroscopy (DOSY). DOSY separates species in solution according to their diffusion coefficient and can provide quantitative information about the size and molecular weight of small- to medium-sized molecules.[171] The DOSY spectrum of VO(**7**)(O^iPr) in $CDCl_3$ clearly indicates the presence of a single species in solution, Figure 28.

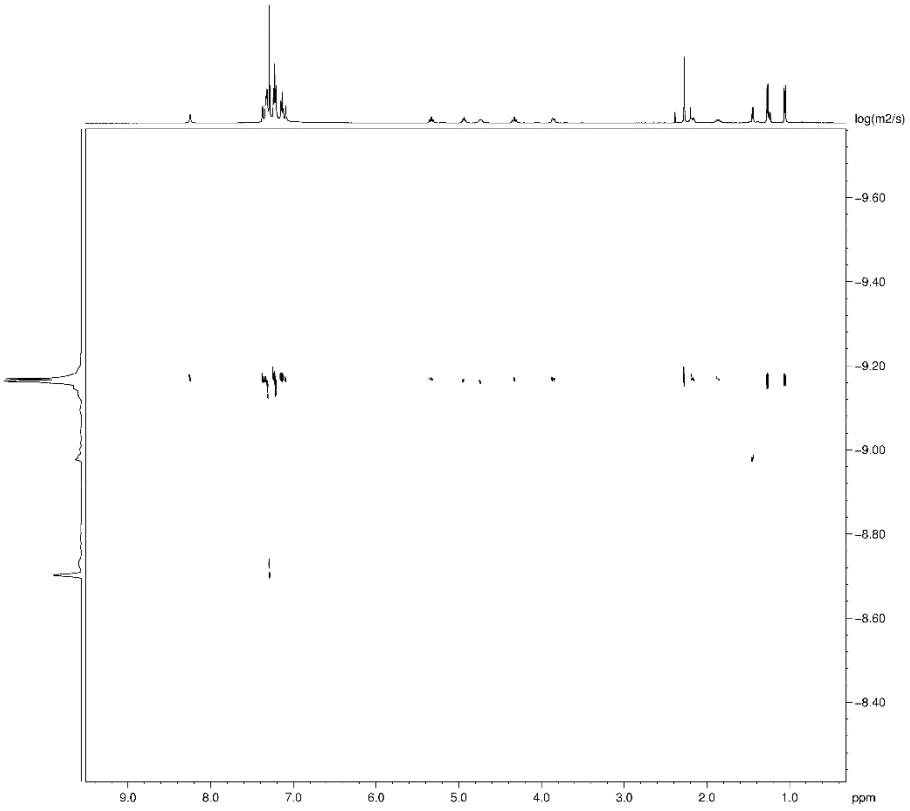

Figure 28: DOSY NMR spectrum of VO(7)(O^{i}Pr) in $CDCl_3$

Measured diffusion coefficients, D, were obtained from the DOSY NMR spectra, Table 5. The diffusion coefficient of a species in solution is inversely related to its hydrodynamic radius, r_H, by the Stokes Einstein equation [**12**], where k is the Boltzmann constant in $J.K^{-1}$, T is the temperature in Kelvin and η is the viscosity coefficient of the liquid.

$$D = \frac{kT}{6\pi\eta r_H} \qquad [12]$$

For the alkyl-substituted complexes an obvious trend was observed, with the diffusion coefficient decreasing as the complex size increases from VO(**4**)(O^{i}Pr) to VO(**7**)(O^{i}Pr). Although the *tert*-butyl (^{t}Bu) and adamantyl (Ad) substituents differ significantly in size, the overall size and molecular weight of complexes VO(**5**)(O^{i}Pr) and VO(**6**)(O^{i}Pr) are roughly comparable, accounting for the similar diffusion coefficients for these two species. The diffusion coefficients for the halide-substituted species VO(**1-3**)(O^{i}Pr) were very similar.

For complexes VO(**5,7**)(O^iPr) the diffusion coefficients (Table 5) were consistent with the dimeric solid state structure persisting in solution.[171] Values for the halide and adamantyl complexes VO(**1-4,6**)(O^iPr) were less definitive, however they were closer to those expected for dimeric species than monomeric, indicating that all the complexes are dimeric in solution in $CDCl_3$.

Table 5: Diffusion coefficients for complexes VO(1-7)(O^iPr) in $CDCl_3$

Complex	R^1, R^2	D / m^2s^{-1}
VO(**1**)(O^iPr)	Cl, Cl	$(8.7 \pm 0.5) \times 10^{-10}$
VO(**2**)(O^iPr)	Br,Br	$(8.4 \pm 0.4) \times 10^{-10}$
VO(**3**)(O^iPr)	I, I	$(8.5 \pm 0.5) \times 10^{-10}$
VO(**4**)(O^iPr)	H, H	$(10.2 \pm 0.5) \times 10^{-10}$
VO(**5**)(O^iPr)	^{t}Bu. ^{t}Bu	$(7.7 \pm 0.4) \times 10^{-10}$
VO(**6**)(O^iPr)	Me, Ad	$(7.8 \pm 0.4) \times 10^{-10}$
VO(**7**)(O^iPr)	Me, CPh_3	$(6.8 \pm 0.3) \times 10^{-10}$

^{1}H and DOSY NMR analysis of VO(**4**)(O^iPr) in d_8-THF produced significantly more complex spectra than their counterparts in $CDCl_3$ (Figures 29-31). It can be inferred from these spectra that in the presence of a more highly coordinating solvent the dimers dissociate into monomeric species. As the model lignin compound (model B) is itself a coordinating species, it was anticipated that in the presence of the model compound the complexes will be present in their monomeric form.

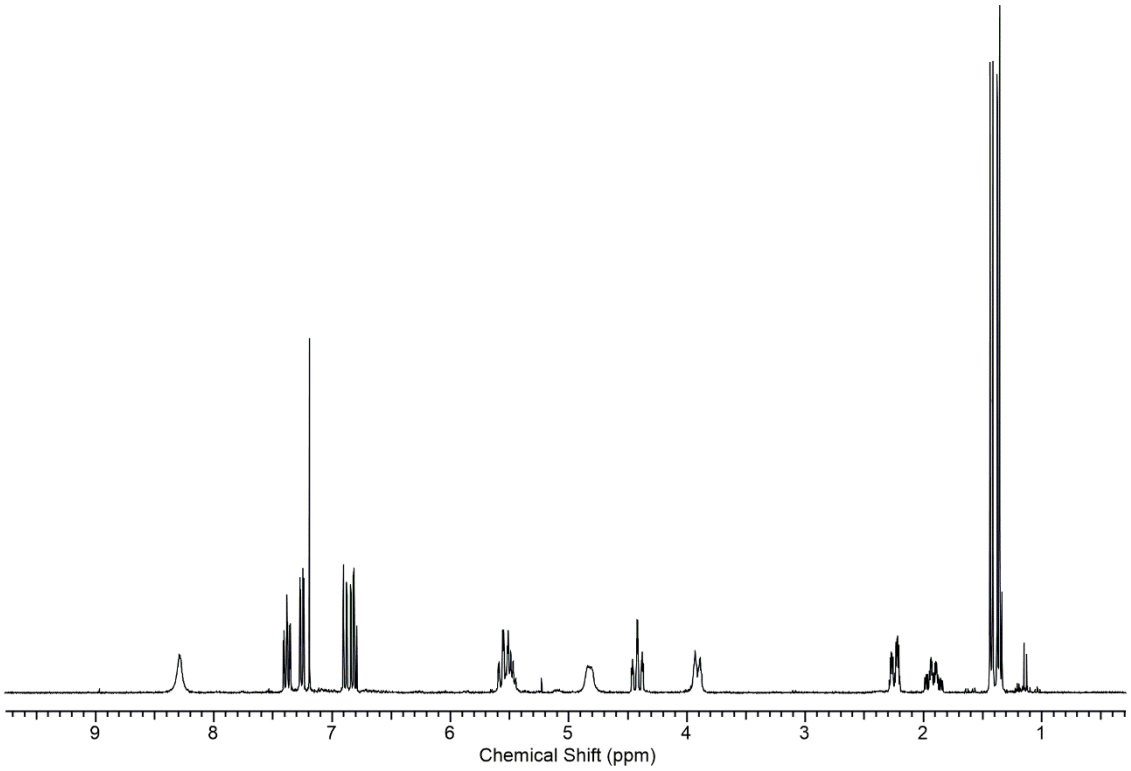

Figure 29: ^{1}H NMR spectrum of VO(4)($O^{i}Pr$) in $CDCl_3$

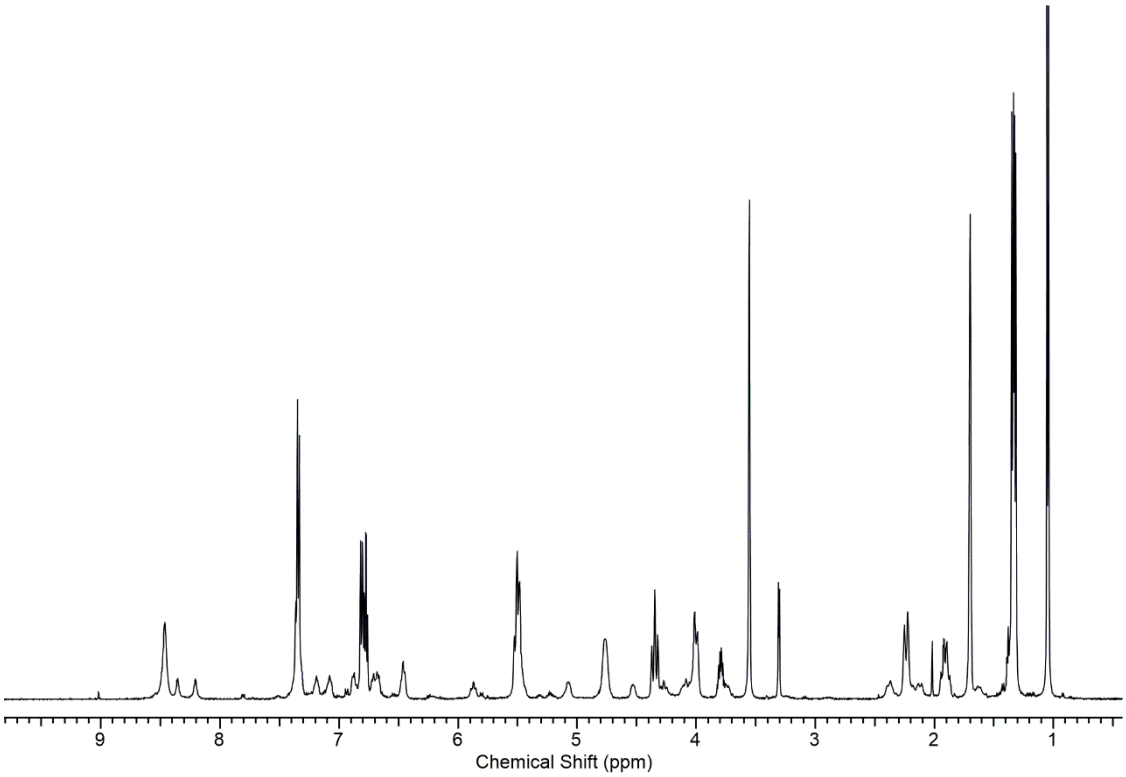

Figure 30: ^{1}H NMR spectrum of VO(4)($O^{i}Pr$) in d_8-THF

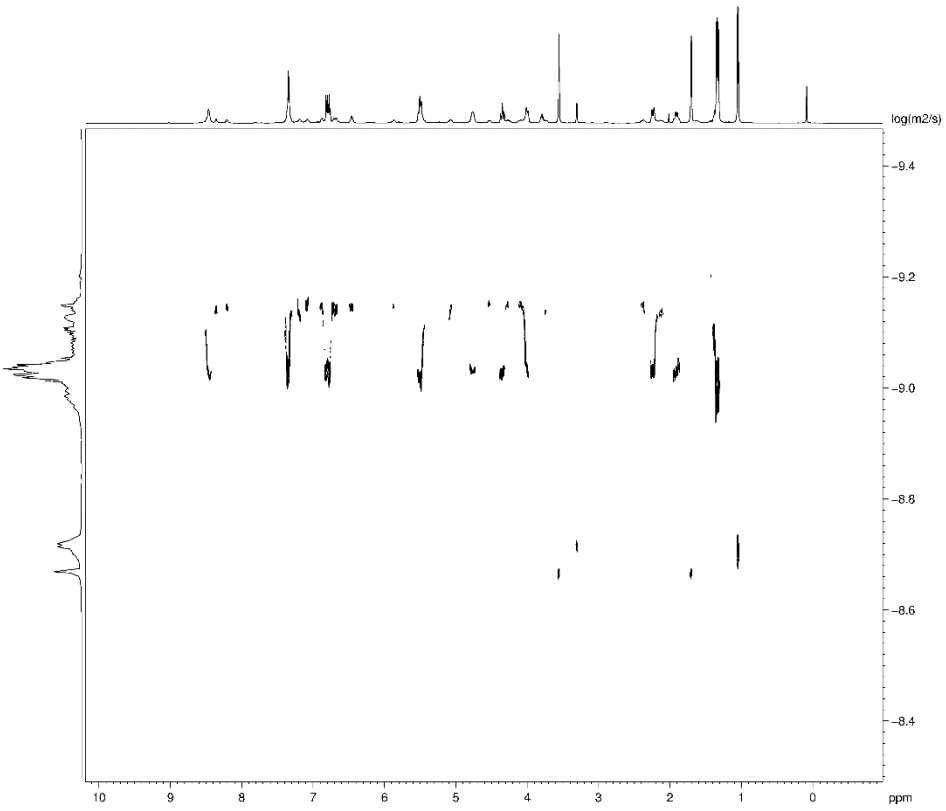

Figure 31: DOSY NMR spectrum of VO(4)(O^{i}Pr) in d_8-THF

2.3.2 Investigation into catalyst-model coordination complexes

Various ratios of catalyst and model B in $CDCl_3$ were analysed by ^1H, ^{51}V and DOSY NMR spectroscopy in order to investigate the coordination of the model compound to the vanadium catalysts. As has already been ascertained, the presence of a coordinating solvent such as THF induces dissociation of dimeric complex VO(**4**)(O^{i}Pr), and it was thus anticipated that the presence of a model lignin compound would have the same effect. The ^1H NMR spectrum of a 1:1 mixture of model compound B and VO(**4**)(O^{i}Pr) is shown in Figure 32. The proposed mechanism of coordination of the model compound to vanadium is *via* ligand exchange with the isopropoxide, Figure 33. The ^1H NMR spectrum indicates that there is not a 100% binding of the model compound to the catalyst as the presence of the unbound, or "free" model compound can be confirmed from its distinctive C<u>H</u>-OH resonance at 5.15 ppm (dd) and the "free" vanadium catalyst VO(**4**)(O^{i}Pr) from the bound isopropoxide C<u>H</u>$_3$ resonances at 1.45 ppm and 1.51 ppm (both doublets). However, there are also new resonances which are not assigned to either of these two species, including a doublet at 1.22

ppm, assigned to free isopropanol that is released on coordination of the model compound *via* ligand exchange with the vanadium isopropoxide group.

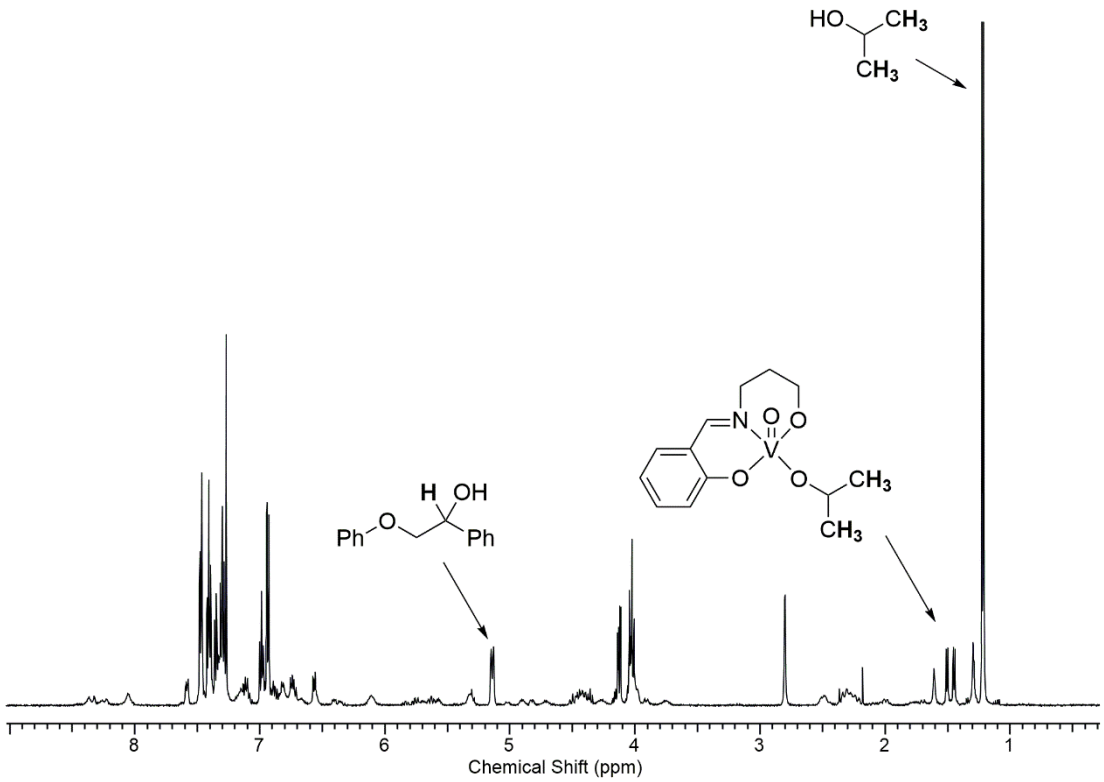

Figure 32: ^{1}H NMR Spectrum of 1:1 mixture of model compound B and VO(4)(O^{i}Pr)

The amount of coordination was calculated from the relative proportions of VO(**4**)(O^{i}Pr) and the coordinated model complex, Figure 33. These can be approximated from the ratio of the integrals of the free isopropanol and VO(**4**)(O^{i}Pr) isopropoxide CH_3 resonances in the ^{1}H NMR spectrum. For the 1:1 mixture of model B and VO(**4**)(O^{i}Pr), around 80% of the vanadium centres were coordinated by the model compound. As the ratio of model B to VO(**4**)(O^{i}Pr) was raised to 2:1 and 3:1, the percentage of vanadium centres coordinated by model B increased to 84% and 88% respectively. This suggests that the equilibrium of the coordination lies towards the coordinated model complex. It would be expected, therefore, that when a large excess of the model compound is present (such as would be the case for a 5-10% catalyst loading, for example), the majority of the vanadium centres will be coordinated by the model.

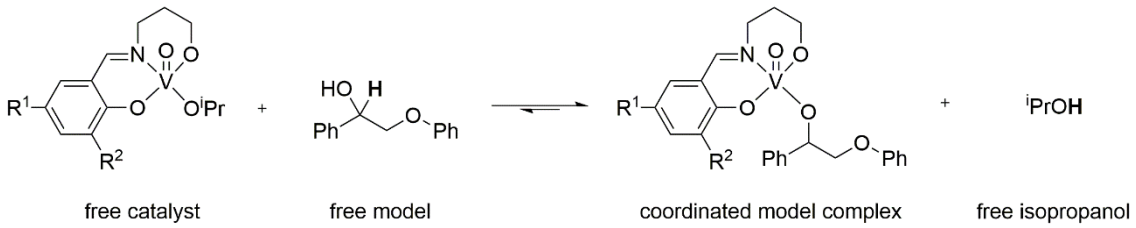

Figure 33: Proposed coordination of model B to vanadium Schiff-base complexes VO(X)(O^{i}Pr)

The DOSY spectrum of a 1:1 mixture of model B and VO(**4**)(O^{i}Pr) provides further evidence for the presence of a single coordinated model complex, Figure 34. Using the characteristic resonances identified in the ^{1}H NMR spectrum in Figure 32, the resonances corresponding to free isopropanol (blue), free model B (green) and free catalyst [VO(**4**)(O^{i}Pr)] (orange) were identified, with diffusion coefficients of 20.1 × 10^{-10}, 11.2 × 10^{-10} and 10.2 × 10^{-10} $m^{2}.s^{-1}$ respectively. Another set of resonances (grey) corresponding to a larger species with diffusion coefficient 8.0 × 10^{-10} $m^{2}.s^{-1}$ was observed to correlate to the resonances in the ^{1}H NMR spectrum which had been tentatively assigned to the coordinated model complex. This set of resonances contains aromatic and aliphatic resonances which are consistent with those expected for this species, and no resonances were observed in the isopropoxide region. The diffusion coefficient suggests that the dimeric structure of the catalyst is retained on complexation of the model compound.

^{51}V NMR spectroscopy has been utilised to provide information about the number and type of vanadium environments, including in the identification of metal binding sites in proteins.[172] As vanadium(V) is diamagnetic and vanadium(IV) is paramagnetic, ^{51}V NMR spectroscopy can also be used to provide some information about oxidation state. The ^{51}V NMR spectra for catalysts VO(**1-7**)(O^{i}Pr) all displayed reasonably sharp, single resonances corresponding to a single vanadium environment, however when equimolar amounts of VO(**4**)(O^{i}Pr) and model compound B were mixed, several new resonances were also observed, Figure 35. In addition to a resonance at -557 ppm, assigned to "free" VO(**4**)(O^{i}Pr), it was initially unclear whether the other resonances were due to different vanadium environments within the same complex or from distinct species.

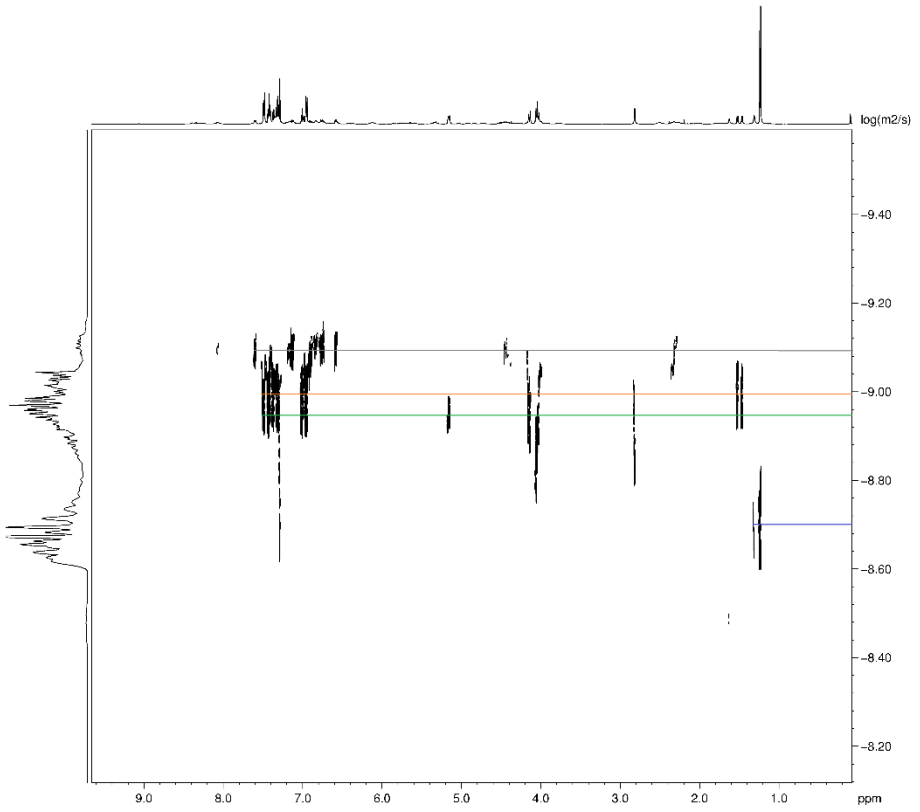

Figure 34: DOSY NMR Spectrum of 1:1 mixture of model compound B and VO(4)(O^{i}Pr)

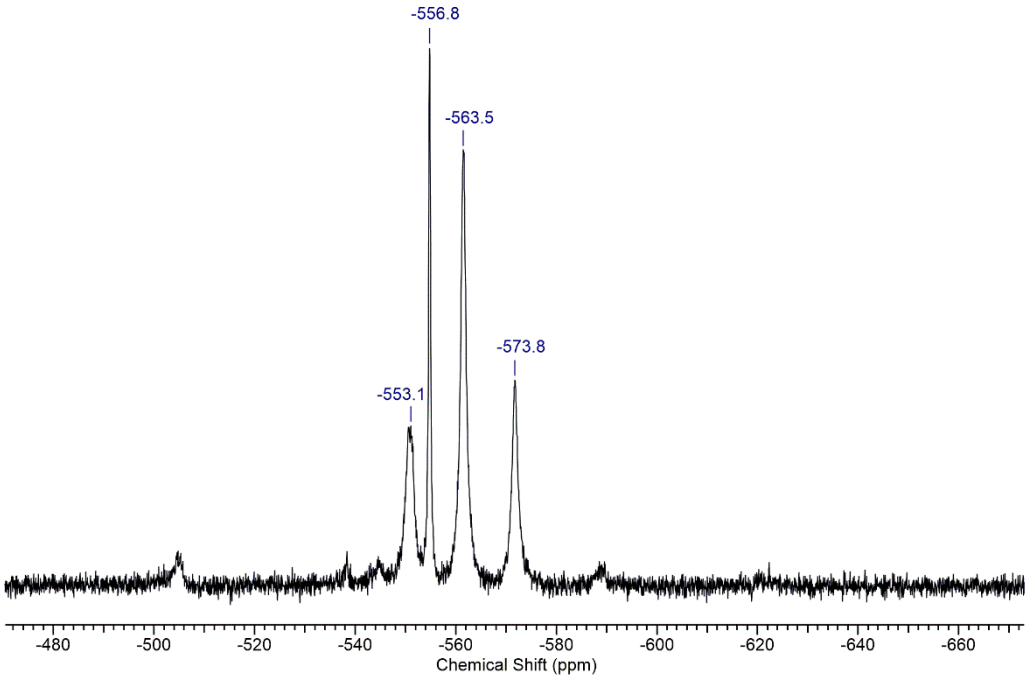

Figure 35: ^{51}V NMR Spectrum of 1:1 mixture of model compound B and VO(4)(O^{i}Pr)

Analysis of the ^{51}V NMR spectra of the 1:1, 2:1 and 3:1 mixtures of model B and VO(**4**)(O^{i}Pr) revealed that the relative integrals of the resonances at -573.8, -563.5 and -553.1 ppm were very similar in all three cases. The ratio of the integrals of these resonances is approximately 1:2:1, and the distances between the peaks are 1349 Hz and 1405 Hz. The peak ratios and the similar distances lead to the tentative hypothesis that a single resonance has been split into a triplet. Coupling of vanadium to nitrogen has been observed previously, however ^{51}V-^{14}N coupling constants were of the order of 50-100 Hz and therefore cannot account for these peaks.[167] As the diffusion coefficient suggests that the dimeric structure of the catalyst is retained on coordination of the model compound, another possible explanation could be vanadium-vanadium coupling, through the bridging oxygen. Whilst the two vanadium atoms in the dimer are usually equivalent, coordination of the model compound to the dimer could break the symmetry, resulting in coupling between the two vanadium atoms. Vanadium-vanadium coupling has been observed in solid state ^{51}V magic angle spinning NMR studies of mixed vanadium oxides, however as ^{51}V is a quadrupolar nucleus, the coupling of two non-equivalent vanadium atoms should result in a multiplet with 15 peaks in the ratio 1:2:3:4:5:6:7:6:5:4:3:2:1.[173] As this pattern is not observed it can be concluded that no vanadium-vanadium coupling is occurring. Assuming that the peaks do not belong to a triplet, and considering the dimeric structure of the complex, the separate resonances could be assigned to the vanadium atoms in the singly and doubly model-coordinated complexes B and C, Figure 36. The two resonances at -573.8 ppm and -553.1 ppm could be assigned to the two inequivalent vanadium atoms in B, whilst the resonance at -563.5 ppm may be assigned to the two equivalent vanadium centres in C. Due to their similar molecular weight, these two complexes would likely diffuse at a similar rate, explaining why they are not observed as separate species by DOSY NMR, Figure 34.

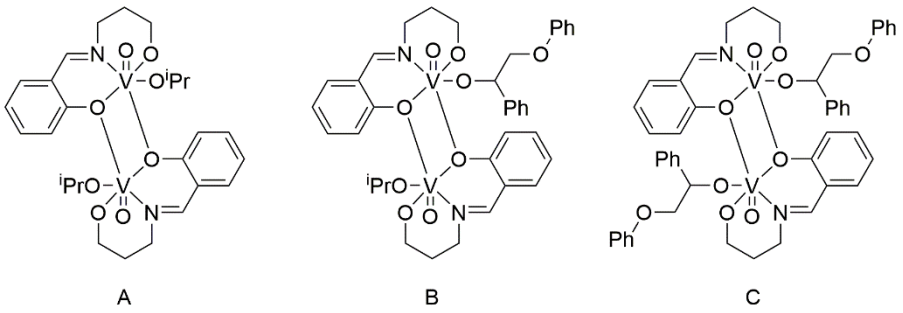

Figure 36: Proposed assignments for resonances in the ^{51}V NMR spectrum of 1:1 mixture of model compound B and VO(4)(O^{i}Pr), Figure 35. A, VO(4)(O^{i}Pr), -556.8 ppm; B, -573.8 ppm and -553.1 ppm; C, -563.5 ppm.

A similar, if more complex, set of spectra were obtained for VO(**6**)(O^{i}Pr). Free isopropanol, catalyst and model compound are clearly visible in the ^{1}H NMR spectrum, along with new resonances which cannot be accounted for by these species alone, Figure 37. Analysis of the ^{51}V NMR spectrum, Figure 38, reveals two species present in solution, that of VO(**6**)(O^{i}Pr), at -556 ppm, and a new, broader resonance at -582 ppm which can be tentatively assigned to the coordinated model complex, Figure 33. This is in contrast to the several new resonances observed for VO(**4**)(O^{i}Pr), and is potentially a result of the increased steric hindrance around the vanadium centres afforded by the bulky adamantyl substitutents preventing the coordination of two model compounds to the dimer.

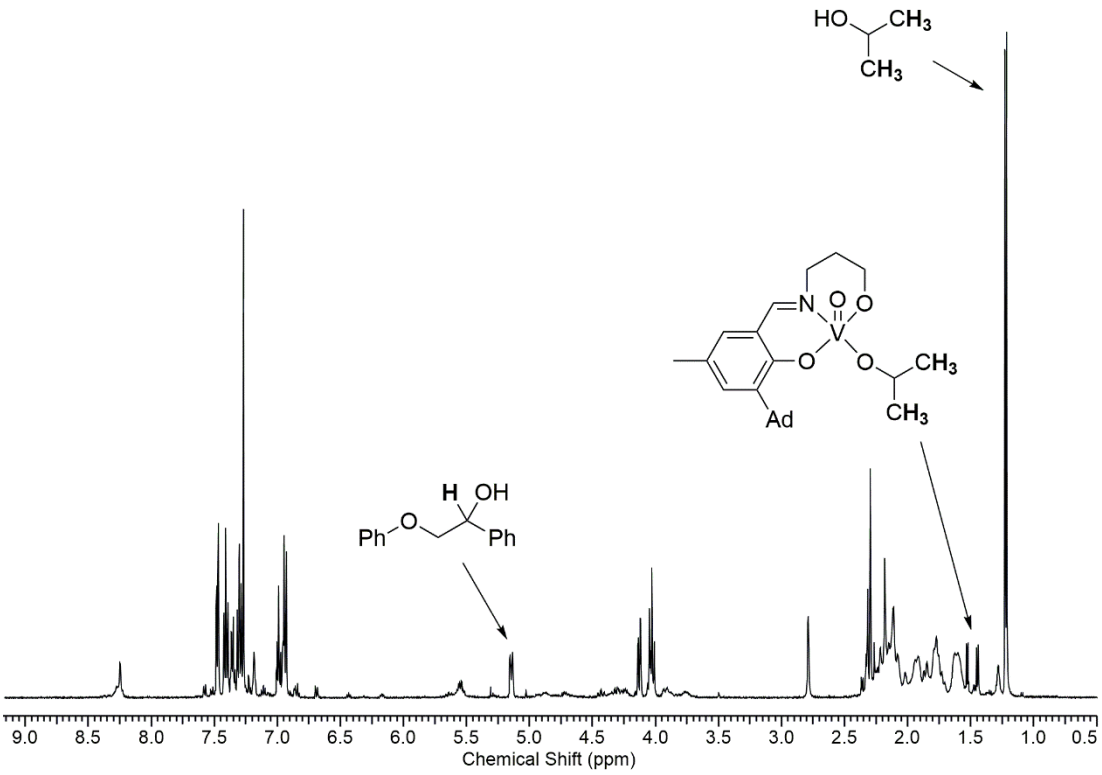

Figure 37: ^{1}H NMR Spectrum of 1:1 mixture of model compound B and VO(6)(O^{i}Pr)

Again, further evidence for the presence of a coordinated model complex is provided by the DOSY spectrum, Figure 39. As for VO(**4**)(O^{i}Pr), resonances corresponding to free isopropanol (blue) and model compound B (green) are visible. Although less clear than the spectrum obtained for VO(**4**)(O^{i}Pr), there is evidently a new species with diffusion coefficient 6.4 × 10^{-10} $m^2.s^{-1}$ (grey), significantly larger than the catalyst (orange, D = 7.8 × 10^{-10} $m^2.s^{-1}$). The diffusion coefficient for the new species is consistent with the dimeric catalyst structure being retained on coordination of the model compound. From these data it can be reasonably concluded that, as suggested in the proposed mechanism, there is only one catalyst-model

coordination mode, and that the model compound binds to the vanadium catalysts through the hydroxyl group, releasing isopropanol.

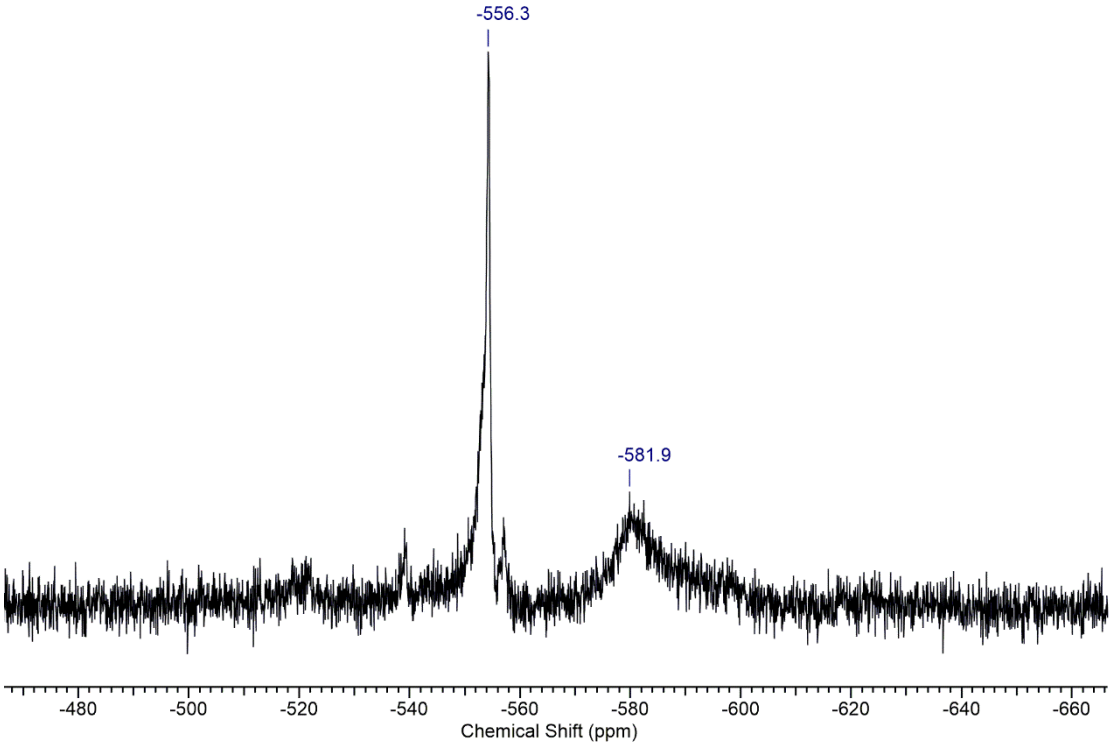

Figure 38: ^{51}V NMR Spectrum of 1:1 mixture of model compound B and VO(6)(O^{i}Pr)

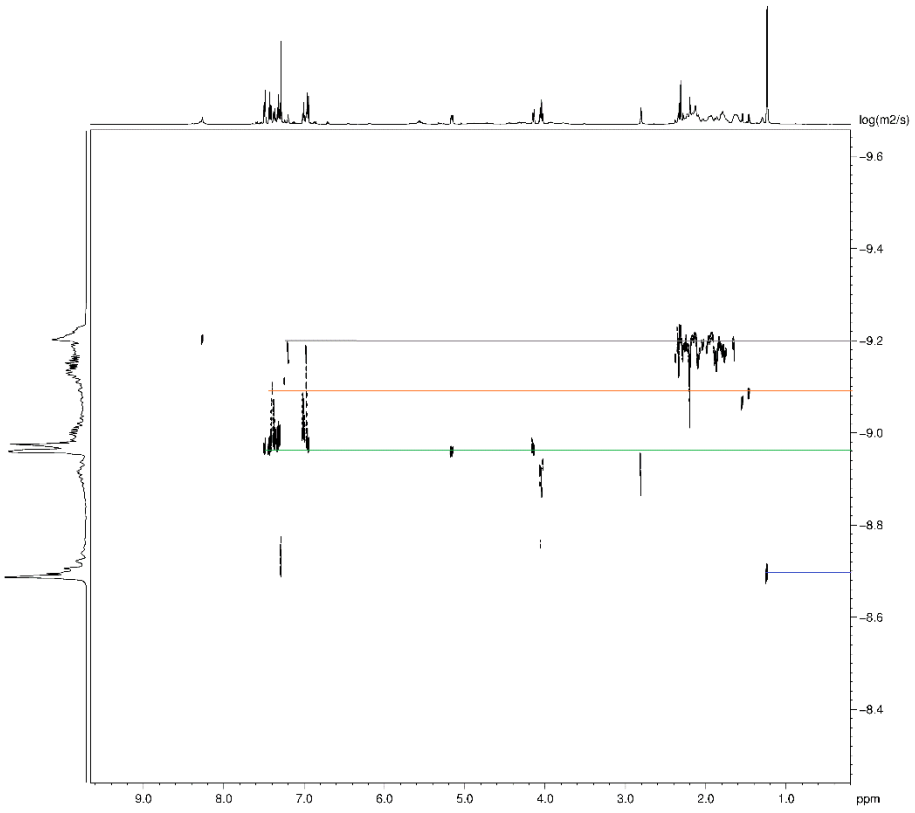

Figure 39: DOSY NMR Spectrum of 1:1 mixture of model compound B and VO(6)(O^{i}Pr)

2.3.3 Catalyst stability

It was observed during these studies that the catalysts were not indefinitely stable in solution, and had a tendency to form precipitates which were unable to be re-solubilized, Figure 40. The bulky, alkyl-substituted catalysts VO(**5-7**)(O^{i}Pr) were notably more stable in solution than the unsubstituted and halo-substituted analogues, VO(**1-4**)(O^{i}Pr). Under an inert atmosphere of argon, complexes VO(**5,7**)(O^{i}Pr) were stable in solution in anhydrous $CDCl_3$ for one week, whilst VO(**6**)(O^{i}Pr) remained in solution for over a month. In contrast, precipitates were observed in VO(**1-4**)(O^{i}Pr) within two days. ^{1}H and ^{51}V NMR spectra of the catalyst solution after precipitation revealed very broad line widths. This could be due to the presence of solid particulates, however another possible explanation is the formation of paramagnetic vanadium(IV) species, Figure 41. The formation of insoluble vanadium(IV) dimers was observed by Son *et al.* during the anaerobic degradation of a model lignin compound by an analogous vanadium Schiff-base catalyst.[118]

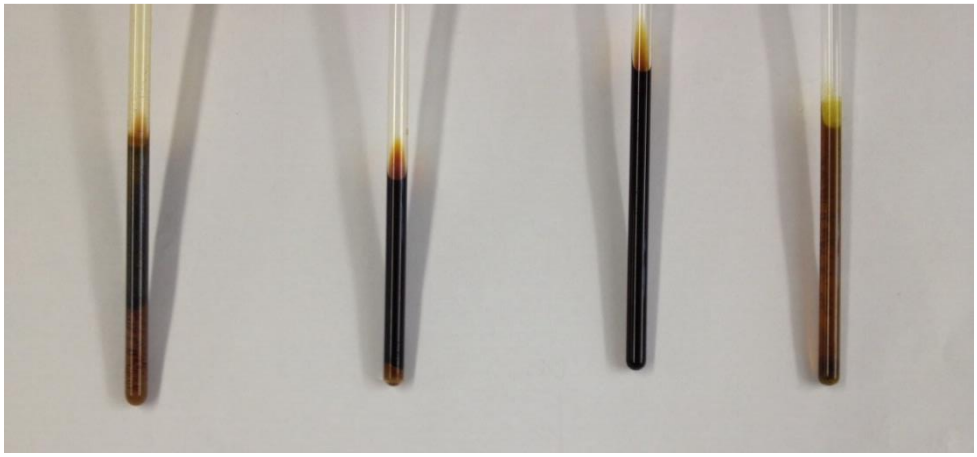

Figure 40: Solutions of catalysts (L-R) VO(1,4,6,7)(O^{i}Pr) after 3 weeks in anhydrous $CDCl_3$ under an atmosphere of argon

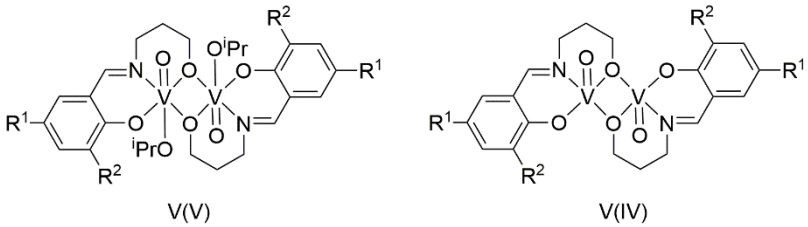

Figure 41: Structures of proposed soluble vanadium(V) and insoluble vanadium (IV) species

2.3.4 Tetradentate ligand complexes

Single crystal XRD analysis of crystals obtained from the complexation of $VO(O^iPr)_3$ with (**8**)H_2, revealed that the solid state structure is an oxy-bridged dimeric species, [VO(**8**)]$_2$O, rather than the expected VO(**9**)(O^iPr), possibly arising from the presence of adventitious oxygen during synthesis, Figure 42. This type of structure was first reported by Adão *et al*. in 2009.[170] The tetradentate ligand is bound in a *cis*-β geometry, where the two $O_{phenolate}$ atoms are *cis* to one another [O(2)-N(1)-N(2) *fac*; O(3)-N(2)-N(1) *mer*].

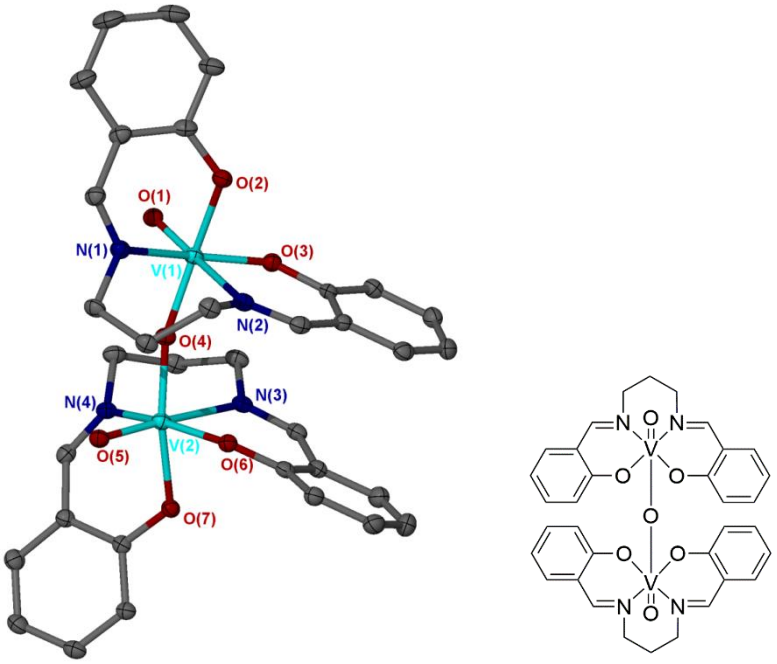

Figure 42: Solid state structure of [VO(8)]$_2$O, thermal ellipsoids are shown at the 30% probability level, all hydrogen atoms have been removed for clarity.

The complex does not have a centre of symmetry and as such the vanadium centres are inequivalent. This inequivalency is small, however, as the vanadyl V=O bond lengths [V(1)-O(1) and V(2)-O(5)] and O-V-O angles [O(2)-V(1)-O(4) and O(4)-V(2)-O(7)] are statistically equivalent and the bridging V-O bond lengths V(1)-O(4) and V(2)-O(4) are similar, Table 6. Both vanadium(V) atoms in the dimer are in pseudo-octahedral environments (O-V-O and O-V-N angles ≈ 180° or 90°). V=O bond lengths are similar to those observed for VO(**1**-**5**)(O^iPr). V-$O_{phenolate}$ bonds *trans* to a bridging V-O bond [V(1)-O(2) and V(2)-O(7)] are significantly longer than those opposite an imine [V(1)-O(3) and V(2)-O(6)], presumably as a result of the trans effect.[170] Elemental analysis was consistent with [VO(**8**)]$_2$O, indicating that this is the structure of the bulk species in the solid state. The ^{1}H NMR spectrum of [VO(**8**)]$_2$O indicted the presence of several species in solution suggesting dissociation of the oxy-bridged dimer, however these were not able to be isolated for further analysis. ^{51}V NMR analysis also indicates the presence of a major and minor species in solution, Figure 43.

Table 6: Selected bond lengths and angles for $[VO(8)]_2O$

Angle	(°)	Bond length	(Å)
V(1)-O(4)-V(2)	163.60(15)	V(1)-O(4)	1.829(2)
O(2)-V(1)-O(4)	164.28(11)	V(2)-O(4)	1.795(2)
O(4)-V(2)-O(7)	164.34(11)	V(1)-O(1)	1.608(2)
O(1)-V(1)-N(2)	172.06(12)	V(2)-O(5)	1.614(2)
O(5)-V(2)-N(3)	171.50(11)	V(1)-O(2)	1.946(2)
O(1)-V(1)-N(1)	93.15(12)	V(1)-O(3)	1.849(2)
O(2)-V(2)-N(2)	81.83(11)	V(2)-O(7)	1.972(2)
O(5)-V(2)-N(4)	92.10(12)	V(2)-O(6)	1.864(2)
O(6)-V(2)-N(3)	84.19(11)		

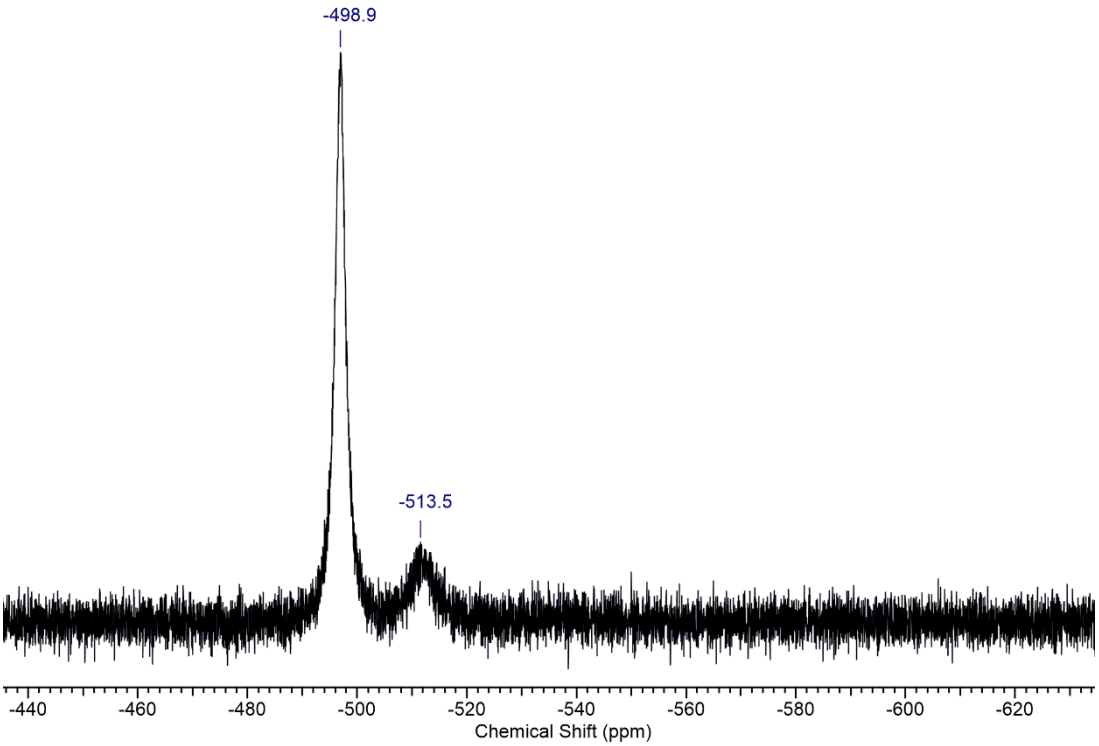

Figure 43: ^{51}V NMR spectrum of $[VO(8)]_2O$

Crystals obtained from the complexation of (**9**)H_2 with $VO(O^iPr)_3$ exhibited an interesting and novel solid state structure containing four non-equivalent oxy-bridged vanadium atoms in a pseudo-linear configuration, [VO(**9**)(VO_2OMe]$_2$O, Figure 44. V(1) and V(4) are in 6-coordinate pseudo-octahedral environments [O(3)-V(1)-N(1) and O(11)-V(4)-N(3) ≈ 180°; O(1)-V(1)-O(2) and O(13)-V(4)-O(11) ≈ 90°] and the ligand is in a planar coordination [O(2)-N(1)-N(2) *mer*; O(3)-N(2)-N(1) *mer*] with the vanadyl and bridging oxygen trans to one another. This is in contrast to the *cis*-β geometry observed for [VO(**8**)]$_2$O, Table 7. V(2) and V(3) are in 4-coordinate pseudo-tetrahedral geometries [O(4)-V(2)-O(7) and O(7)-V(3)-O(10) = 109.8°], with the 4th coordination site occupied by a methoxy ligand. It is suspected that these methoxy groups were introduced during the addition of methanol for recrystallization, and that isopropoxide groups may have originally been present instead.

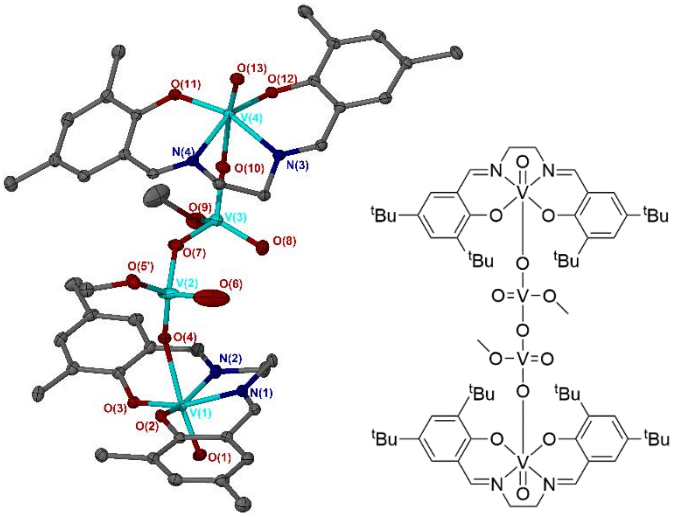

Figure 44: Solid state structure of [VO(9)(VO_2OMe)]$_2$O, thermal ellipsoids are shown at the 30% probability level. The methyl groups of the ^{t}Bu groups and all hydrogen atoms have been removed for clarity.

Despite the two different geometries, all four vanadium atoms are in the +5 oxidation state. The V=O bond lengths are all within the range expected for vanadium(V) Schiff base complexes.[170] There is significant variation in the length of the bridging V-O bonds throughout the complex, although this variation is fairly symmetrical around the central O(7) atom. The V_{tet}-O(-V_{tet}) bridging V-O bond lengths [V(2)-O(7) and V(3)-O(7)] average 1.78 Å, whilst the V_{tet}-O(-V_{oct}) bond lengths [V(2)-O(4) and V(3)-O(10)] are much shorter, averaging 1.65 Å. The V_{oct}-O(-V_{tet}) bonds [V(1)-O(4) and V(4)-O(10)] are significantly longer, at 2.16 Å. Whilst it is

possible that this elongation is a result of the trans effect from the vanadyl groups, it is more likely a result of the poorer orbital overlap in the tetrahedral environment as compared to the octahedral.

Table 7: Selected bond angles and lengths for $[VO(9)(VO_2OMe)]_2O$

Angle	(°)	Bond length	(Å)
O(3)-V(1)-N(1)	160.49(9)	V(1)-O(1)	1.6008(18)
O(11)-V(4)-N(3)	160.98(8)	V(2)-O(6)	1.624(4)
O(1)-V(1)-O(2)	98.76(9)	V(3)-O(8)	1.612(2)
O(13)-V(4)-O(11)	100.17(9)	V(4)-O(13)	1.597(2)
O(4)-V(2)-O(7)	109.78(11)	V(1)-O(4)	2.1431(19)
O(7)-V(3)-O(10)	107.60(10)	V(4)-O(10)	2.1679(19)
O(10)-V(4)-O(13)	172.15(9)	V(2)-O(4)	1.644(2)
O(1)-V(1)-O(4)	173.70(9)	V(3)-O(10)	1.6644(19)
		V(2)-O(7)	1.782(2)
		V(3)-O(7)	1.772(2)

In order to determine whether this unusual structure was representative of the bulk material, elemental analysis was conducted and compared to theoretical values corresponding to the solid state structure $[VO(\mathbf{9})(VO_2OMe)]_2O$, an oxo-bridged dimer structure analogous to $[VO(\mathbf{8})]_2O$, and the originally proposed structure, $VO(\mathbf{9})(O^iPr)$, Table 8. The measured values correspond very closely to those calculated for the solid state structure, confirming that $[VO(\mathbf{9})(VO_2OMe]_2O$ is likely to be the bulk species.

Table 8: Measured and predicted CHN values for $[VO(9)(VO_2OMe)]_2O$, $[VO(9)]_2O$ and $VO(9)(O^iPr)$

	C / %	H / %	N / %
Calculated % for $[VO(\mathbf{9})(VO_2OMe)]_2O$	58.32	7.27	4.12
Calculated % for $[VO(\mathbf{9})]_2O$	67.95	8.20	4.95
Calculated % for $VO(\mathbf{9})(O^iPr)$	67.33	8.39	4.76
Measured %	59.19	7.29	4.15

^{51}V NMR analysis indicates the presence of four vanadium species or environments in solution, Figure 45. As the ^{1}H NMR spectrum of $[VO(\mathbf{9})(VO_2OMe)]_2O$ is consistent with the solid state structure, it is hypothesised that these correspond to the four vanadium environments present in the complex. The two pairs of resonances at -583.9 and -577.6 ppm, and -469.9 and -491.6 ppm are proposed to correspond to the pairs of octahedral vanadium atoms V(1) and V(4) and tetrahedral vanadium atoms V(2) and V(3), however, due to the lack of analogous complexes in the literature, these were unable to be explicitly assigned.

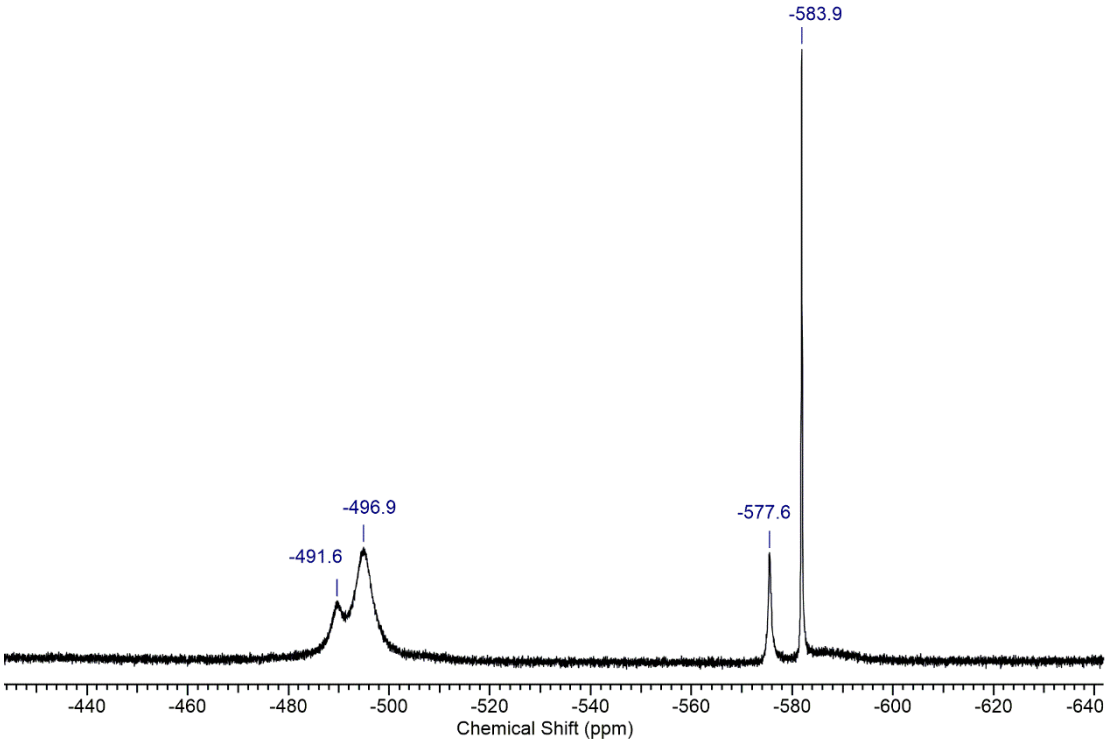

Figure 45: ^{51}V NMR spectrum of $[VO(9)(VO_2OMe)]_2O$

Crystals obtained from the complexation of the salalen ligand (**10**)H_2 with VO(O^iPr)$_3$ revealed an oxy-bridged dimeric solid state structure, [VO(**10**)]$_2$O, Figure 46. This species is analogous to that of [VO(**8**)]$_2$O, with the two vanadium centres in crystallographically equivalent, pseudo-octahedral environments [O(1)-V(1)-N(1), O(3)-V(1)-O(4) ≈ 180° and O(1)-V(1)-N(2) ≈ 90°], Table 9.

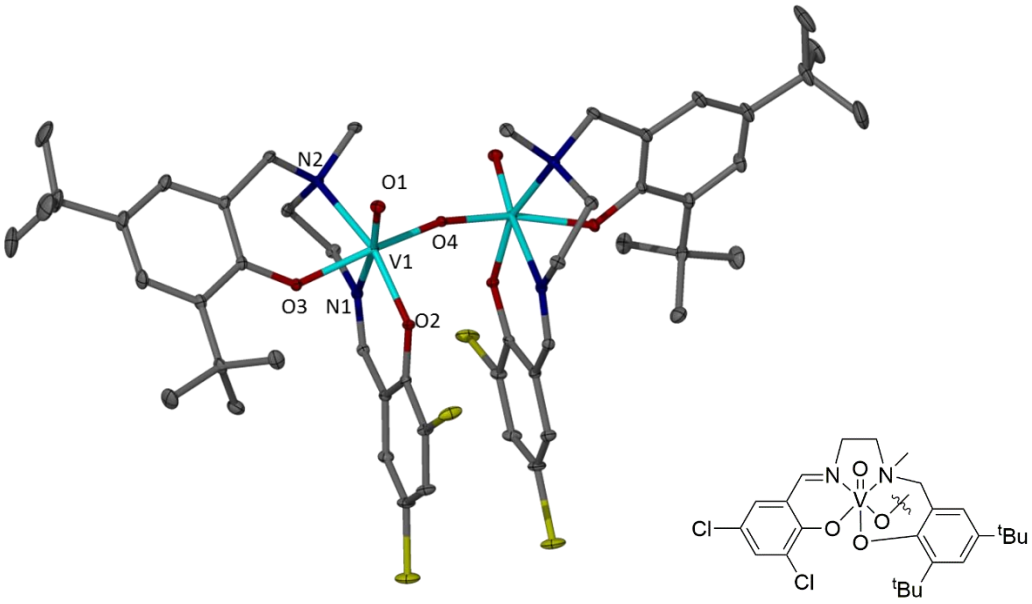

Figure 46: Solid state structure of [VO(10)]$_2$O, thermal ellipsoids are shown at the 30% probability level, all hydrogen atoms have been removed for clarity.

Table 9: Selected bond angles and lengths of [VO(10)]$_2$O

Angle	(°)	Bond length	(Å)
O(1)-V(1)-N(1)	169.97(4)	V(1)-O(1)	1.6081(8)
O(3)-V(1)-O(4)	161.48(3)	V(1)-O(2)	1.8918(7)
O(1)-V(1)-N(2)	92.93(4)	V(1)-O(3)	1.8865(10)
V(1)-O(4)-V(1)*	163.81(6)	V(1)-O(4)	1.8065(7)

The vanadyl bond length V(1)-O(1), Table 9, is comparable to those of the complexes reported above (1.61 Å). Unlike in [VO(**8**)]$_2$O and equivalent complexes in the literature, however, there is no evidence of the trans effect caused by the bridging oxo ligand, as V(1)-O(2) and V(2)-O(3) are almost identical in length.[170] The bridging oxo ligand is relatively linear [V(1)-O(4)-V(1)* = 164.81]. ^{1}H and ^{51}V NMR indicated the presence of a major and minor species in solution,

however elemental analysis confirmed that the bulk structure is that of the structure obtained by XRD. This suggests that the minor species observed by ^{51}V NMR is present either only in trace amounts, or on dissociation in solution.

With these vanadium complexes in hand, depolymerization studies were undertaken in order to investigate and understand the efficacy of these species for the degradation of model lignin compounds. It was anticipated that the range of catalyst structures would provide enough information to allow qualitative structure-activity relationships to be constructed.

2.4 Catalyst screening

Previous work has shown that microwave irradiation assists in the pretreatment of lignin by increasing the heating efficiency and dramatically reducing reaction times, as well as resulting in some degradation of the lignin polymer.[98, 105, 174, 175] Microwave-assisted degradation of lignin model compounds in the presence of heterogenized-Co(salen) and homogeneous vanadium Schiff-base catalysts has also been reported.[103, 104, 176] As the use of microwave irradiation was found to decrease reaction times from the order of a day to a few hours, initial catalyst screening was conducted in a microwave reactor in order to increase efficiency.

Model compound B, 2-phenoxy-1-phenylethanol, is known to degrade to oxidation product (OP) 2-phenoxy-1-phenylethanone, and C-O cleavage products acetophenone and phenol, Figure 47.[117, 118, 176] The GC-MS data obtained during these studies was calibrated using known concentrations of phenol, acetophenone and 2-phenoxy-1-phenylethanone with reference to dodecane as an internal standard, Figure 48.

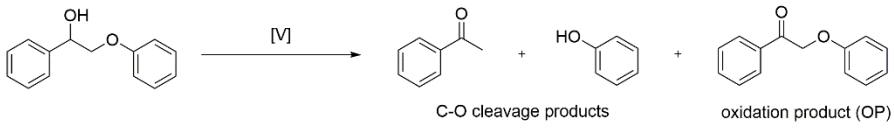

Figure 47: General reaction scheme for the depolymerization of model compound B, 2-phenoxy-1-phenylethanol to C-O cleavage products acetophenone and phenol, and oxidation product 2-phenoxy-1-phenylethanone

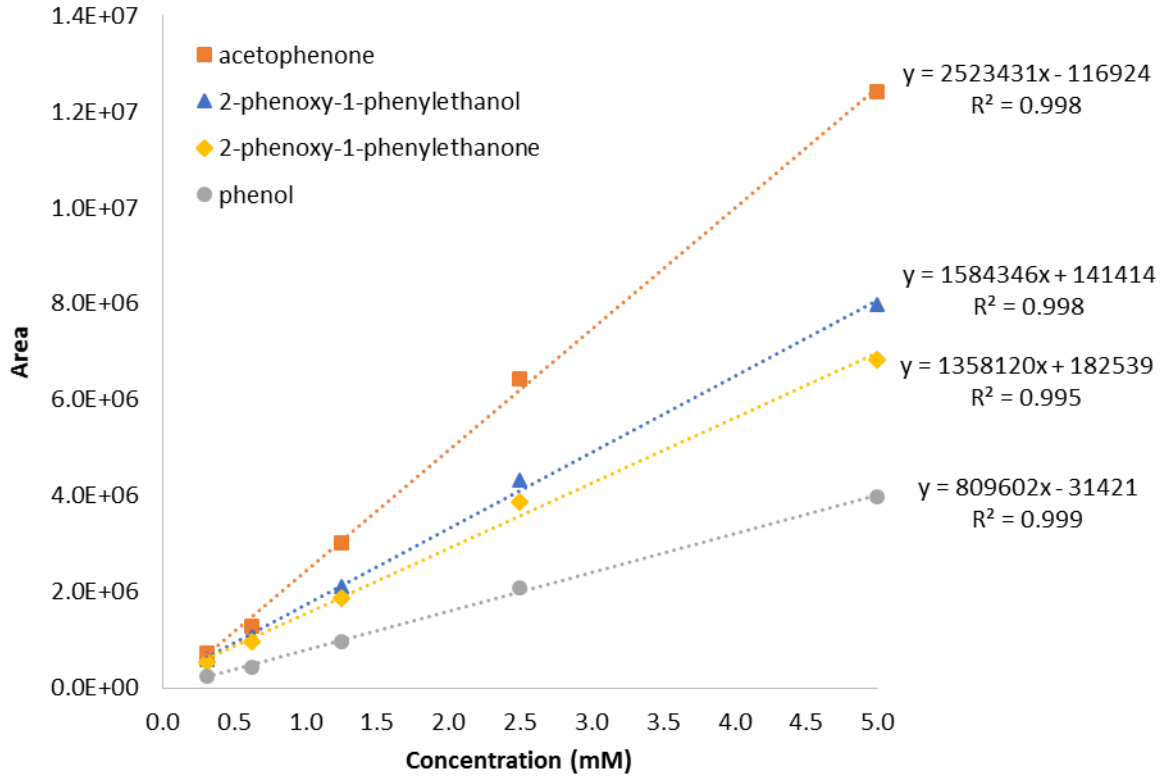

Figure 48: GC-MS Calibration for depolymerization of 2-phenoxy-1-phenylethanol (model B)

Depolymerizations of 2-phenoxy-1-phenylethanol (model B) were conducted on a 5 mL scale (0.09 M model B in acetonitrile, 10 mol% catalyst) in 30 mL sealed microwave vials. The vials were heated to 80 °C for 1 or 4 h in an Anton Parr Monowave 300 Microwave Synthesis Reactor. The crude reaction mixture was then sampled and analysed by GC-MS to determine conversion. This system was used to investigate a range of vanadium complexes as potential lignin depolymerization catalysts, Figure 49. It should be noted that the reaction conditions utilised are adapted from the literature and, as such, they do not necessarily represent optimised conditions for the catalysts being tested, however they do provide a basis for comparison.[118] Of the complexes investigated, ^{t}Bu-substituted tridentate Schiff-base complex VO(**5**)(OMe) effected the highest overall conversion of 55% after 4 h. The proportion of oxidation to C-O cleavage products (calculated from the yields of 2-phenoxy-1-phenylethanone and acetophenone respectively) was approximately 1:1, however when the reaction was run for only 1 h, the proportion was 4:1. This could suggest that initially the rate of oxidation is higher than the rate of C-O cleavage but that, over time, the available oxygen is depleted therefore inhibiting the rate of oxidation. An alternative explanation might be that, contrary to the proposed mechanism, Figure 14, the C-O cleavage mechanism proceeds *via* the oxidation product, however this is unlikely under these reaction conditions given that the

conversion to 2-phenoxy-1-phenylethanone increased steadily over time and this did not appear to be consumed.

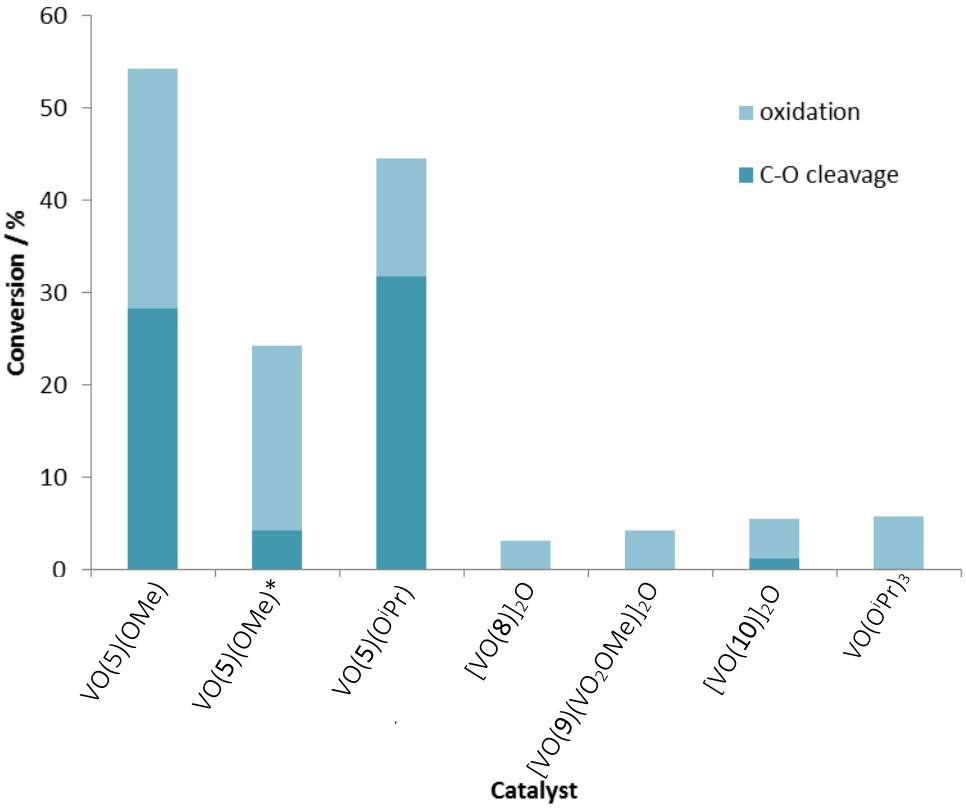

Figure 49: Catalyst screen for the depolymerization of model compound B [conditions: MeCN, 80 °C, µw, 10 mol% catalyst, 4 h (*1 h)]

Replacement of the methoxy ligand with an isopropoxide group, VO(**5**)(O^{i}Pr), resulted in a slight drop in conversion and a shift in the bias of the reaction in favour of C-O cleavage, Figure 49. This is unusual as it has been proposed that the first step in the catalytic cycle is ligand exchange of the substrate for the spectator alkoxide ligand and as such it should not greatly affect the reaction. In the mechanism proposed by Son and Toste, the release of acetophenone by the catalyst species resulted in a vanadium species with two OH ligands.[118] In the modified mechanism shown in Figure 50 it is theorised, due to the high concentration of substrate compared with the concentration of potential alkoxide or hydroxyl groups present in the reaction, that acetophenone production is accompanied by direct coordination of a new substrate molecule. It should also be noted that only half an equivalent of oxygen (with respect to the model compound) is present in the headspace of the microwave vial in these reactions. It is likely, therefore, that as well as potentially restricting the reoxidation of

the catalyst to its active V(v) form, the total possible yield of the OP will be limited under these conditions.

In contrast to the tridentate, monophenolate species, the tetradentate ligand complexes ([VO(**8**,**10**)]$_2$O and [VO(**9**)(VO$_2$OMe)]$_2$O) and VO(O^{i}Pr)$_3$ failed to reach 10% conversion within 4 h and most showed no evidence of C-O cleavage. The low conversion in the case of VO(O^{i}Pr)$_3$ can be explained by the highly moisture sensitive nature of this species. As the reactions are not conducted under inert conditions it is possible that the catalyst is hydrolysed to vanadium pentoxide by the presence of atmospheric moisture. The Schiff-base species are potentially more hydrolytically stable than VO(O^{i}Pr)$_3$ as a result of their less labile multidentate ligands. As for the tetradentate complexes, it is possible that they are too coordinatively saturated to allow successful coordination of the model compound, as they lack a labile isopropoxide group with which the model compound can undergo ligand exchange. Based on these results, the tridentate monophenolate ligand set was subjected to further investigation.

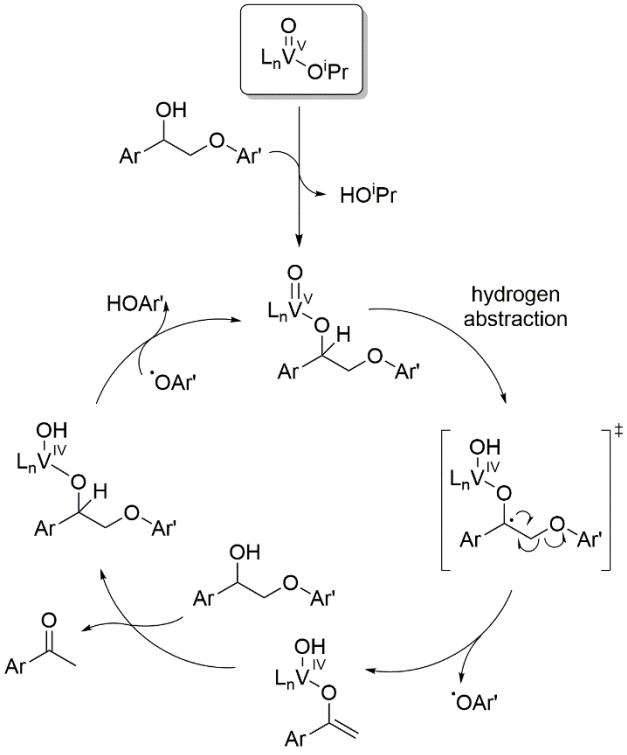

Figure 50: Modified mechanism for C-O bond cleavage by vanadium(V) Schiff-base type catalysts

2.5 NMR Experiments

In order to gain further insights into the action of the better performing tridentate Schiff-base catalysts, a series of degradation tests were conducted and monitored by ^{1}H NMR

spectroscopy, Figure 51. A similar technique has been reported in the literature;[117] the reaction was reported to be slower in DMSO-d_6 than alternatives such as pyridine-d_5, however due to its higher boiling point and in order to avoid overlapping resonances in the ^{1}H NMR spectra, DMSO-d_6 was selected as the solvent for these experiments. Although DMSO-d_6 is not necessarily the optimal solvent for this reaction, it provides a useful basis from which to compare different catalysts and reaction conditions.

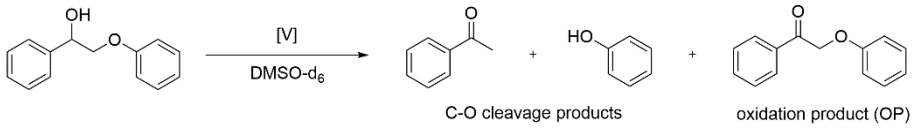

Figure 51: General scheme for the degradation of model compound B in DMSO-d_6; experiments conducted in an NMR tube with hexamethylbenzene as internal standard (conversions determined by ^{1}H NMR spectroscopy)

Degradation of model compound B and yields of products were quantified *via* integration of the ^{1}H NMR spectra with respect to an internal standard (ITSD), hexamethylbenzene (δ 2.13 ppm, s, 18H). There are three resonances in the ^{1}H NMR spectrum of model B which could be used to determine conversion, Figure 52. ^{1}H NMR spectra of a typical reaction are shown in Figure 53. In initial studies, overall conversion was quantified from the CH_2 resonance (δ 4.01 ppm), however it was noted that during the reactions, which were run for up to seven days in uncapped NMR tubes, water accumulated in the samples. This is likely due to the hygroscopic nature of DMSO.[177] The accumulation of water did not appear to have a detrimental effect on the catalysis, however as the reaction progressed the increasingly broad H_2O resonance (δ 3.37 ppm) often overlapped that of the CH_2 resonance, thereby interfering with the integration process.

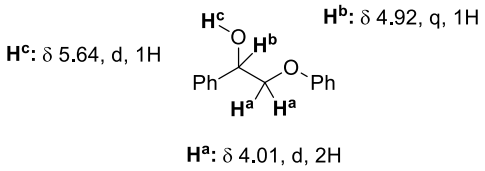

Figure 52: Resonances of interest in the ^{1}H NMR spectrum of model B in DMSO-d_6

The accumulation of water also had an effect on the OH resonance of both 2-phenoxy-1-phenylethanol and also the phenol produced during the reaction. Starting as a defined doublet and sharp singlet respectively, as the proportion of water in the reaction increased they

broadened and lost definition suggesting possible proton exchange with water. As phenol and acetophenone are produced in a 1:1 ratio the amount of C-O cleavage was quantified from the distinctive acetophenone CH_3 resonance (s, 2.57 ppm), whilst benzylic oxidation was quantified *via* the CH_2 resonance in 2-phenoxy-1-phenylethanone (s, 5.57 ppm), Figure 54.

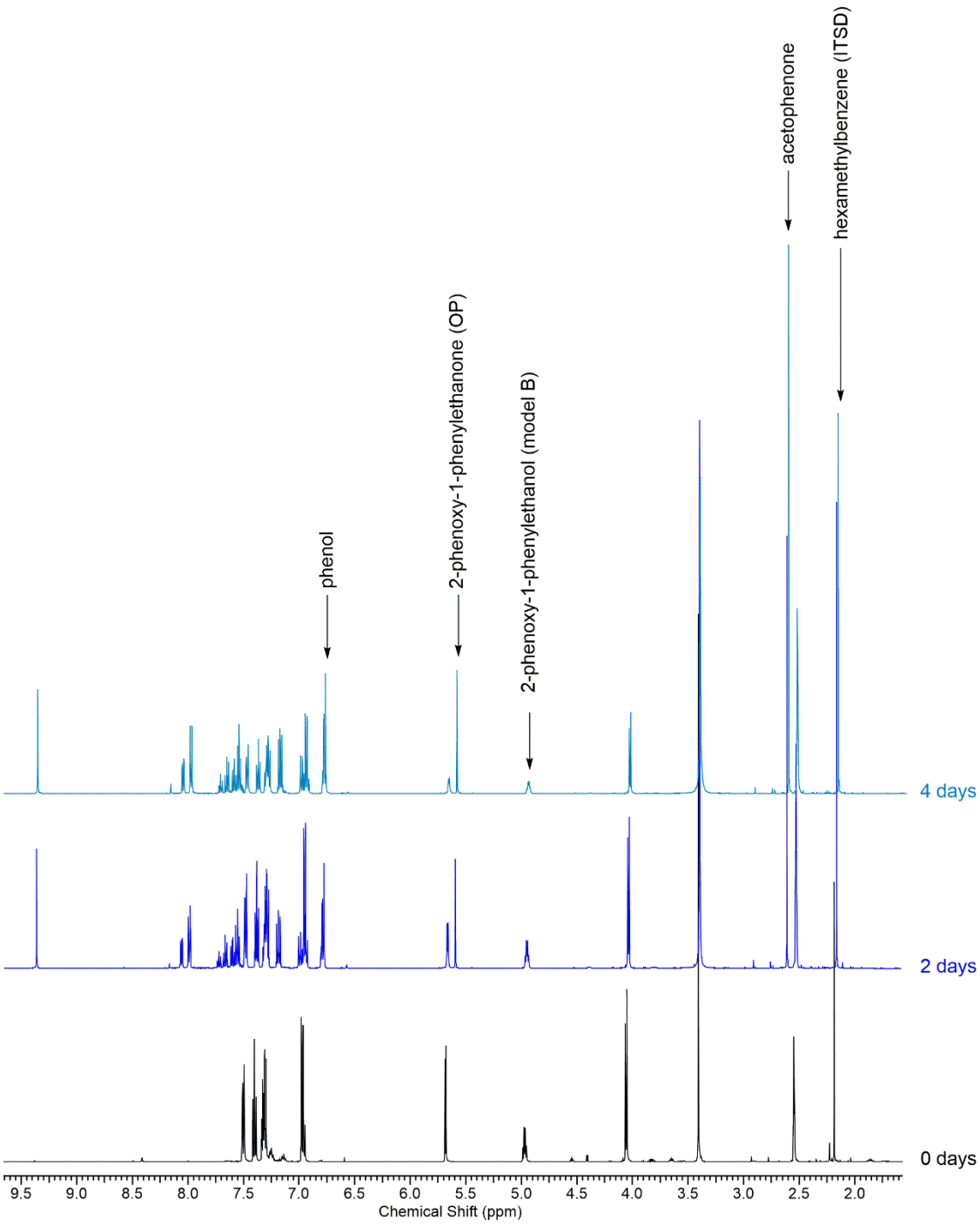

Figure 53: ^{1}H NMR spectra of model B degradation in DMSO-d_6

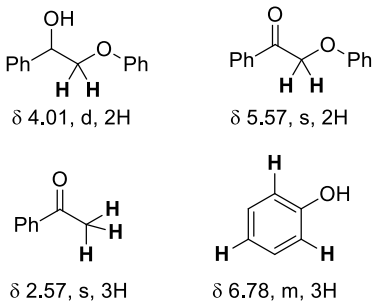

Figure 54: Resonances of protons in DMSO-d_6 used for conversion and yield determination by ^{1}H NMR spectroscopy

2.5.1 Effect of catalyst structure: ligand substitution

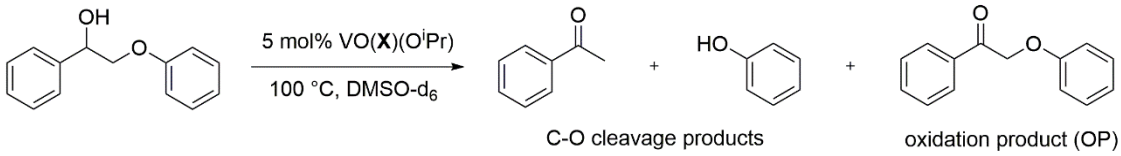

Figure 55: Standard reaction conditions for ^{1}H NMR depolymerization studies. VO(X)(O^{i}Pr); X = 1-7, 11-14

The reaction conditions employed in the ligand investigation studies are outlined in Figure 55. Under these conditions the C-O bond cleavage products acetophenone and phenol were found to be stable and did not undergo further reaction, and no conversion of the model compound was observed in the absence of a catalyst. In agreement with previous studies,[117] the benzylic oxidation product (OP), 2-phenoxy-1-phenylethanone, did not appear to be broken down under these conditions, suggesting that C-O cleavage of the model compound occurs directly from the alcohol rather than *via* the OP.[118] This is in contrast to the C-C cleavage reported by Hanson *et al*. which proceeds *via* oxidation. Increased steric bulk on the phenolate ring has previously been reported to improve catalyst activity, possibly by preventing the aggregation of active catalytic intermediates into inert dimeric species.[118] To gain further insight into this effect, the size of the substituent at the 3' position was systematically increased and pseudo-first order rate constants were calculated for each catalyst.

Under these conditions, the unsubstituted catalyst VO(**4**)(O^{i}Pr) was found to have an observed pseudo first order rate constant, k', of 0.24 days^{-1}. As in the literature, a dramatic increase in activity was observed on addition of *tert*-butyl groups at the 3' and 5' positions, with k' = 0.68 days^{-1} for VO(**5**)(O^{i}Pr). Adamantyl substitution at the 3' position produced no further improvement in rate [VO(**6**)(O^{i}Pr): k' = 0.67 days^{-1}], whilst increasing the size of the substituent further again to a trityl group resulted in a significant decrease in activity back to the level of the unsubstituted catalyst [VO(**7**)(O^{i}Pr): k' = 0.23 days^{-1}]. If the role of steric bulk

in increasing activity is related to the prevention of dimerization, it appears that the *tert*-butyl group is large enough to achieve this. The drop in activity observed with the trityl substituent could be a result of reduced coordination access of the model compound to the catalyst active site.

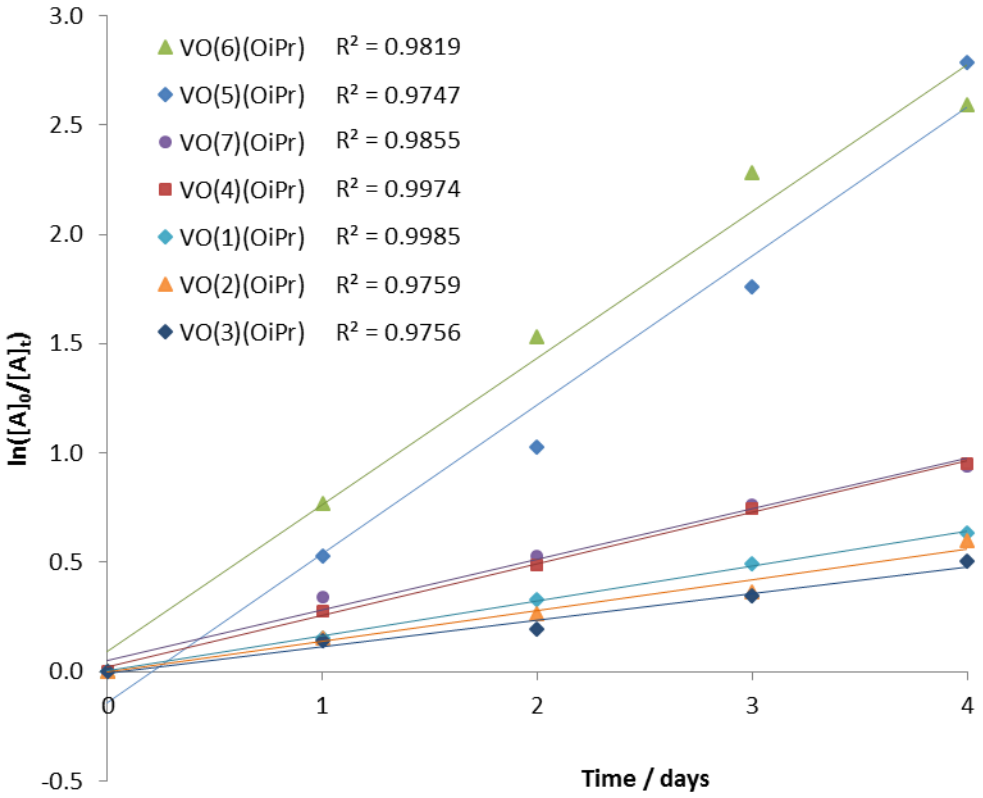

Catalyst	k' (days^{-1})
VO(**1**)(O^{i}Pr)	0.16 ± 0.01
VO(**2**)(O^{i}Pr)	0.14 ± 0.01
VO(**3**)(O^{i}Pr)	0.12 ± 0.01
VO(**4**)(O^{i}Pr)	0.24 ± 0.01
VO(**5**)(O^{i}Pr)	0.68 ± 0.06
VO(**6**)(O^{i}Pr)	0.67 ± 0.05
VO(**7**)(O^{i}Pr)	0.23 ± 0.02

Figure 56: Graph of $\ln([A]_0/[A]_t)$ against time for VO(1-7)(O^{i}Pr) and table of pseudo first order rate constants, k'. Conditions: 5 mol% catalyst, DMSO-d_6, 100 °C. ($[A]_0$ = initial concentration of model compound = 0.15 mol.dm^{-3}, $[A]_t$ = concentration of model compound at time t as determined from ^{1}H NMR spectroscopic analysis.)

In order to probe the electronic effects of the ligand on catalyst performance, a range of halo-substituted catalysts were also subjected to investigation, Figure 56. These species were significantly less active than their bulky alkyl-substituted counterparts and there was a very minor decrease in activity with increasing substituent size going down the group [k' = 0.16, 0.14, 0.12 $days^{-1}$ for VO(**1-3**)(O^iPr) respectively].

Whilst catalytic activity is important, the selectivity of the catalyst for carbon-oxygen bond cleavage over benzylic oxidation is the priority, as breaking the C-O bonds in lignin is more likely to facilitate depolymerization. Catalysts VO(**1-3**)(O^iPr) with electron-withdrawing ligand substituents were found to favour oxidation and demonstrated low selectivity towards C-O bond cleavage, whilst selectivities for the alkyl-substituted species VO(**5-7**)(O^iPr) were significantly higher, Figure 57. The unsubstituted catalyst VO(**4**)(O^iPr) displayed an intermediate selectivity. The major difference between the trends in activity and selectivity was highlighted in the performance of the three bulky alkyl-substituted species. Selectivity of the catalyst appears to be directly related to the size of the substituent, with the ratio of C-O cleavage to oxidation increasing as $H<<{}^tBu<Ad<CPh_3$, from 0.30 for the unsubstituted catalyst up to 1.80 for the bulkiest trityl substituent. This trend in selectivity could be a result of the increased steric hindrance impeding the access of molecular oxygen to the active site of the catalyst.

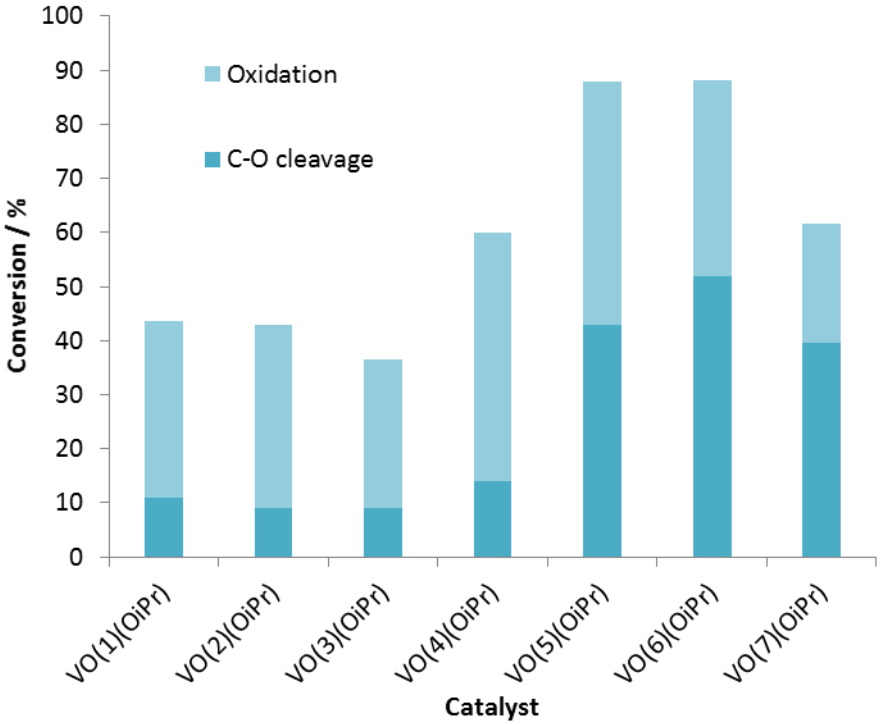

Catalyst	Ratio of C-O cleavage : oxidation products
VO(**1**)(O^{i}Pr)	0.34
VO(**2**)(O^{i}Pr)	0.26
VO(**3**)(O^{i}Pr)	0.33
VO(**4**)(O^{i}Pr)	0.30
VO(**5**)(O^{i}Pr)	0.96
VO(**6**)(O^{i}Pr)	1.43
VO(**7**)(O^{i}Pr)	1.80

Figure 57: Effect of ligand substituents on conversion and selectivity for C-O bond cleavage. Conditions: 5 mol% VO(1-7)(O^{i}Pr), DMSO-d_6, 100 °C, 4 days

2.5.2 Effect of catalyst structure: ligand backbone

In addition to the range of phenolate substituents investigated, the backbone structure of the Schiff-base ligand was also an area of interest for potential tuneability of these catalysts. Thus complexes with alternative backbone structures were synthesized in order to probe the effect

of changing ligand flexibility and O-V-N bite angle on the reaction, Table 10. The most dramatic change was observed on switching the primary hydroxy group for a second phenolate [VO(**15**)(O^iPr)], resulting in an almost complete loss of catalytic activity. This behaviour appears to be similar to that of the tetradentate bisphenolate ligands discussed in section 2.4, suggesting that the presence of at least one labile coordinating group is necessary for this catalytic reaction to proceed effectively. It is not immediately obvious from the proposed mechanism (Figure 50) why this might be the case, however it is possible that, instead of the vanadyl group, abstraction of the hydrogen atom is being facilitated by the ligand alkoxide moiety, Figure 58.

Table 10: Influence of ligand backbone structure on the conversion and ratio of C-O cleavage to oxidation products for the degradation of model B. Conditions: 5 mol% catalyst, DMSO-d_6, 100 °C, 4 days.

Catalyst structure	R	Catalyst	Conversion/ %	Ratio of C-O cleavage : oxidation products
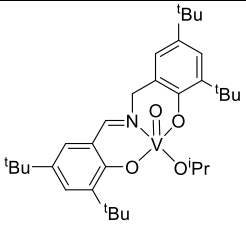	n/a	VO(**15**)(O^iPr)	< 5	-
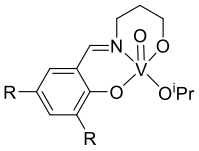	H	VO(**4**)(O^iPr)	64	0.30
	^{t}Bu	VO(**5**)(O^iPr)	94	0.96
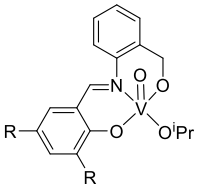	H	VO(**11**)(O^iPr)	16	0.20
	^{t}Bu	VO(**12**)(O^iPr)	31	0.56
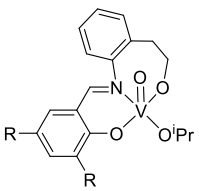	H	VO(**13**)(O^iPr)	27	0.11
	^{t}Bu	VO(**14**)(O^iPr)	37	0.25

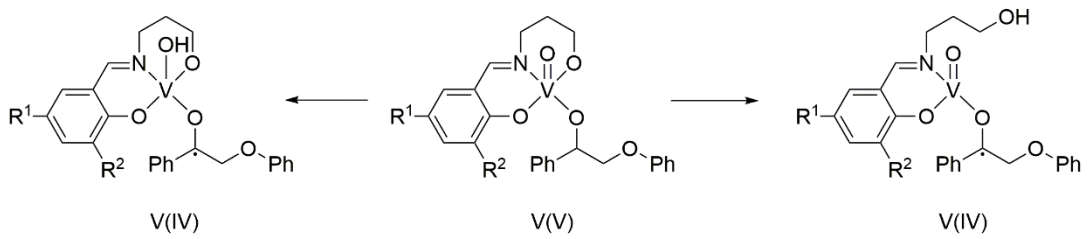

Figure 58: Possible hydrogen abstraction mechanisms

For the monophenolates, addition of an aryl group to the propyl backbone in the case of both the H- and ^{t}Bu-substituted variants was found to severely impact both the catalyst activity, Table 10, and (to a lesser degree) the selectivity [VO(**4,11**)(O^{i}Pr) and VO(**5,12**)(O^{i}Pr)]. In the solid state, the Schiff-base ligands were observed to bind equatorially around the vanadium centre, Figure 27. If this structure is retained in solution it is possible that introduction of an aryl group on the propyl chain causes an increase in ring strain due to the now sp^2 hybridized carbons. If this was the case it might be expected that lengthening the carbon chain could at least partially reverse this effect. Some catalyst activity is regained by lengthening the backbone from propyl to butyl [16%-27% for VO(**11,13**)(O^{i}Pr), and 31%-37% for VO(**12,14**)(O^{i}Pr)], however the catalyst selectivity drops still further (from 0.20 to 0.11 and 0.56 to 0.25 respectively). Son and Toste reported an increase in activity of their catalysts on increasing the backbone length from C_2 to C_3,[118] suggesting that the propyl backbone (forming a 6-membered ring) is the optimum length and flexibility to avoid any unnecessary ring strain.

As previously discussed for catalysts VO(**4**-**5**)(O^{i}Pr), the introduction of the bulky *tert*-butyl substituents on the phenolate ring increased both the conversion and C-O cleavage selectivity of the reaction. This effect was also observed for the other monophenolate variants VO(**11**-**12**)(O^{i}Pr) and VO(**13**-**14**)(O^{i}Pr).

2.5.3 Effect of catalyst loading

Catalyst loadings in the range 0.5-7 mol% were investigated. For complexes VO(**1**-**7**)(O^{i}Pr) conversion of the model lignin compound was found to increase with increasing catalyst loading, however this effect was seen to tail off above 5 mol%, Figure 59. This could be due to insolubility of the catalyst at higher loadings (precipitates were observed at 7 mol% and higher), however it is more likely due to mass transfer limitations resulting from inefficient mixing in the narrow, unstirred reaction vessel. The selectivity was found to be largely unaffected by changes in the catalyst loading.

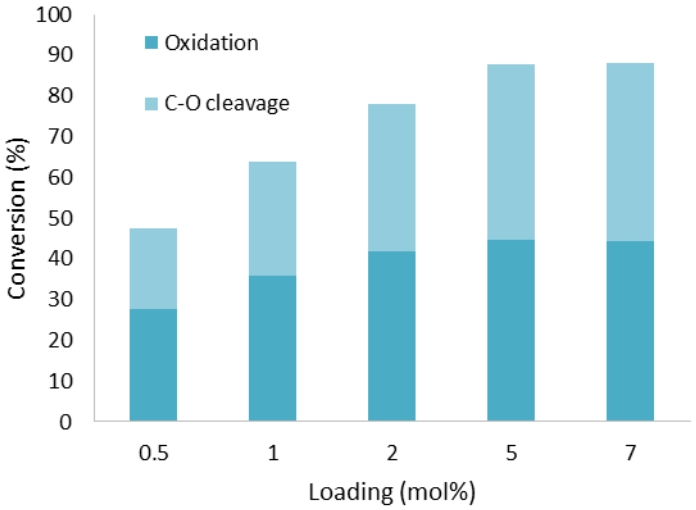

Figure 59: Overall conversion and product distribution for VO(5)(O^{i}Pr)at a range of loadings [conditions: DMSO-d_6, 100 °C, 4 days]

A graph of lnk' against ln[catalyst] was plotted for each catalyst to determine the order of dependence of the catalyst in the rate law, Figure 60. The rate law is given by equation **13**, where k is the rate constant, [catalyst] and [model] are the concentrations of catalyst and model compound, and x is the order of dependence of the rate on the concentration of the catalyst. The reaction was found to be approximately zero order with respect to the catalyst for both VO(**3,7**)(O^{i}Pr), ($x \leq 0.1$), whilst the concentrations of the other catalysts appear to have slightly more effect, with x = 0.16-0.42. However, in all cases the rate is not significantly affected by the catalyst loading, suggesting the reaction is being limited by another factor. A potential explanation is that aspects of the reaction such as the narrow vessel, lack of stirring and low exposed surface area, result in mass transfer limitations such as low oxygen availability and slow transport of the model compound to the catalyst.

$$\text{Rate} = k[\text{catalyst}]^{x}[\text{model}] \qquad [13]$$

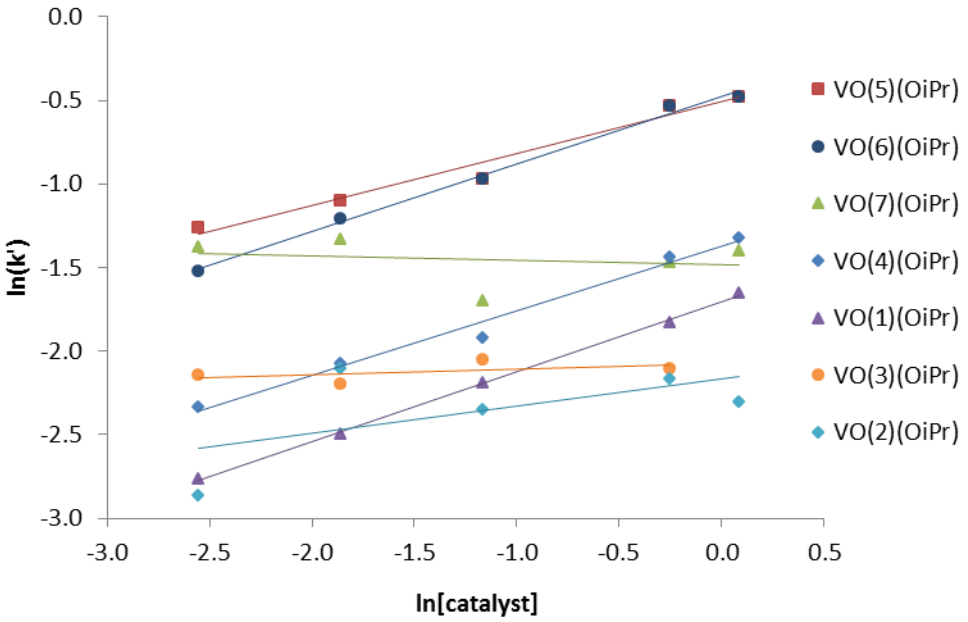

Catalyst	x
VO(**1**)(O^{i}Pr)	0.42 ± 0.01
VO(**2**)(O^{i}Pr)	0.16 ± 0.13
VO(**3**)(O^{i}Pr)	0.03 ± 0.04
VO(**4**)(O^{i}Pr)	0.39 ± 0.03
VO(**5**)(O^{i}Pr)	0.31 ± 0.03
VO(**6**)(O^{i}Pr)	0.40 ± 0.02
VO(**7**)(O^{i}Pr)	-0.03 ± 0.08

Figure 60: Graph of lnk' against ln[catalyst] where the gradient, x, is the order of dependence of the catalyst in the rate law. Conditions: DMSO-d_6, 100 °C

2.5.4 Effect of temperature

The *tert*-butyl and trityl substituted catalysts VO(**5**)(O^{i}Pr) and VO(**7**)(O^{i}Pr) were subjected to further investigation at a range of temperatures (70-120 °C), the results for VO(**5**)(O^{i}Pr) are shown in Figure 61. Whilst it is not especially surprising that catalyst turnover was found to improve with increasing temperature, interestingly the selectivity for C-O bond cleavage over oxidation was also significantly enhanced, increasing from 0.51 at 70 °C to 1.89 at 120 °C. This trend was also observed for VO(**7**)(O^{i}Pr), with a rise in C-O cleavage selectivity from 0.88 to 3.73 over the same temperature range.

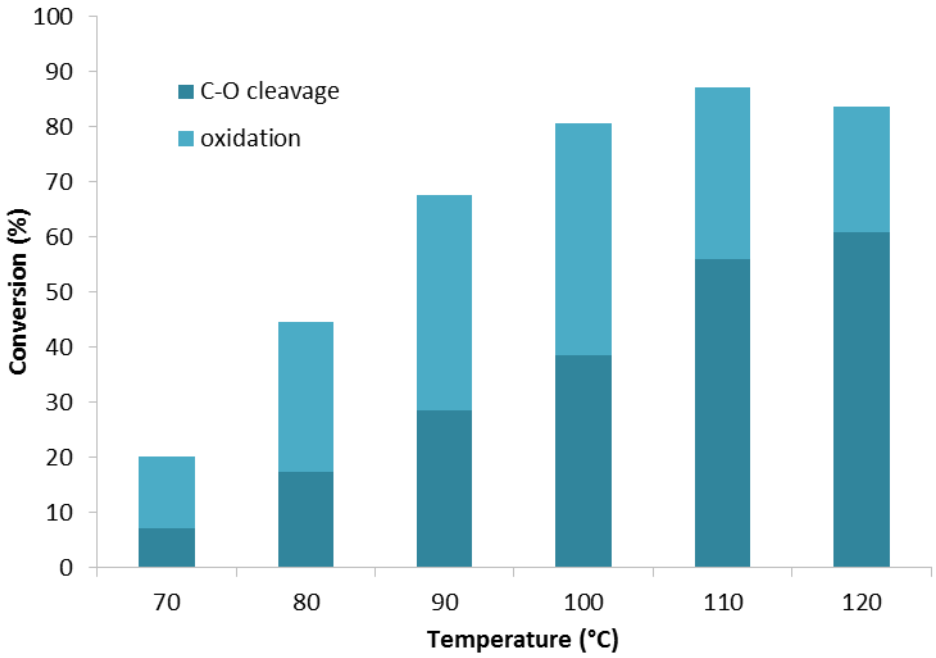

Figure 61: Conversion and selectivity for VO(5)(O^{i}Pr) over a range of temperatures. Conditions: DMSO-d_6, 5 mol% VO(5)(O^{i}Pr)

The Arrhenius equation [**14**] can be rearranged to give [**15**], where k is the rate constant, A is the pre-exponential factor, E_a is the activation energy in kJ.mol^{-1}, R is the universal gas constant (in kJ.mol^{-1}.K^{-1}) and T is the temperature in Kelvin.

$$k = Aexp\left[\frac{-E_a}{RT}\right] \qquad [14]$$

$$\ln k = \ln A - \frac{E_a}{RT} \qquad [15]$$

Rate constants for the two species were measured as a function of temperature and were plotted in a classic Arrhenius form, Figure 62. From this data, two different regimes were observed; below around 400 K, the reaction appears to be limited by the kinetics of the reaction itself, however above this temperature an external influence dominates the kinetics. This is most likely a mass transfer limited regime. Regression analysis of the linear low temperature regime provided values for the activation energy (E_a) for conversion of the β-O-4 model compound; in the case of VO(**5**)(O^{i}Pr) E_a was calculated to be 96 ± 6 kJ.mol^{-1}, whilst for VO(**7**)(O^{i}Pr) the value was found to be 66 ± 8 kJ.mol^{-1}.

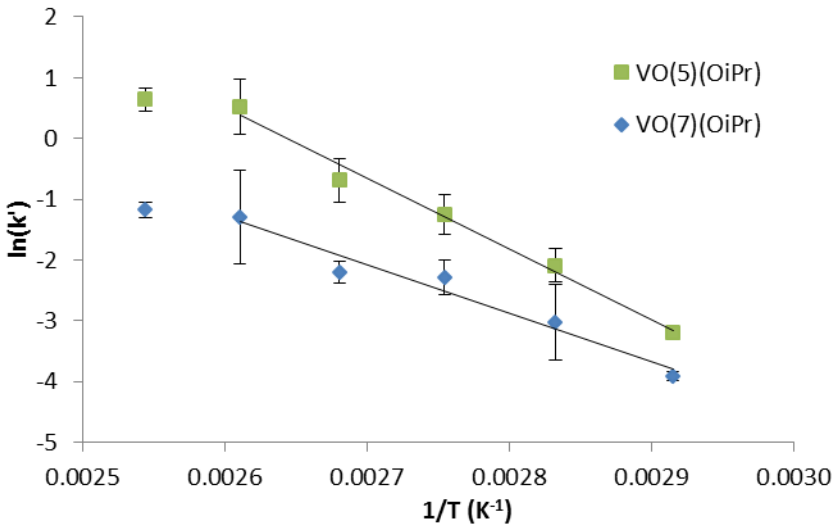

Figure 62: Arrhenius plots for VO(5,7)(O^{i}Pr). Conditions: 5 mol% VO(5,7)(O^{i}Pr), DMSO-d_6, 70-120 °C

2.5.5 Effect of oxygen availability

It had previously been noted that oxygen is not required for catalyst turnover, but that activity was reduced under anaerobic conditions.[118] Degradation of the model compound in the presence of VO(**1**,**7**)(O^{i}Pr) was investigated under "high" and "low" oxygen concentrations (uncapped and capped NMR tubes respectively), Table 11. As expected, a significant reduction in catalytic activity was observed under "low" oxygen conditions in the case of both catalysts. Despite the reduced activity, restricting the availability of oxygen increased the selectivity for C-O bond cleavage (from 0.29 to 0.41 and 1.80 to 2.29 for VO(**1**)(O^{i}Pr) and VO(**7**)(O^{i}Pr) respectively). This improvement in selectivity suggests that the oxidation reaction is limited by the concentration of oxygen even under the "high" oxygen conditions. This is somewhat unsurprising given that the reactions are conducted in narrow, unstirred vessels, however it is important to note that this could have important implications for the activity of the catalysts, as reoxidation of the catalysts to their active V(v) forms is potentially dependent on oxygen concentration.

Table 11: Pseudo first order rate constants, k', and ratio of C-O cleavage to oxidation products for VO(1,7)(O^{i}Pr) under "high" and "low" oxygen conditions. Conditions: DMSO-d_6, 100 °C, 5 mol% VO(1,7)(O^{i}Pr), 4 days, uncapped and capped NMR tubes for high and low oxygen concentrations respectively

Catalyst	[O]	k' (days^{-1})	Ratio of C-O cleavage : oxidation products
VO(**1**)(O^{i}Pr)	"high"	0.19 ± 0.01	0.29
VO(**1**)(O^{i}Pr)	"low"	0.06 ± 0.02	0.41
VO(**7**)(O^{i}Pr)	"high"	0.23 ± 0.02	1.80
VO(**7**)(O^{i}Pr)	"low"	0.10 ± 0.01	2.29

2.5.6 Degradation of a phenolic model lignin compound

To further assess the suitability of these vanadium catalysts for lignin depolymerization, catalyst VO(**6**)(O^{i}Pr) was tested for activity on phenolic β-O-4 model lignin compound guaiacylglycerol-β-guaiacyl ether (model C) under analogous conditions, Figure 63. ^{1}H NMR analysis confirmed complete conversion of the model compound within 24 h and indicated 100% selectivity for C-O bond cleavage, with no evidence of the benzylic oxidation product. No conversion was observed in the absence of a catalyst. The products were confirmed by GC-MS. Comparison of the pseudo first order rate constants, k' for the degradation of non-phenolic model B (k' = 0.67 days^{-1}) and phenolic model C (k' = 10.2 days^{-1}) by VO(**6**)(O^{i}Pr) revealed that the phenolic model is converted around 15 times faster than the non-phenolic species. This faster reaction is likely a result of the lower bond dissociation for phenolic β-O-4 species of 50-60 kcal.mol^{-1} compared to 60-70 kcal.mol^{-1} for non-phenolic.[112]

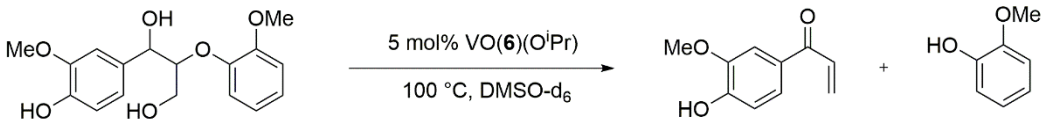

Figure 63: Depolymerization of phenolic β-O-4 model lignin compound guaiacylglycerol-β-guaiacyl ether (model C)

Pseudo first order rate constants, k', for the degradation of model compound C in the presence of complexes VO(**2**,**4**,**6**,**7**)(O^{i}Pr) are shown in Table 12. The trend in catalyst activity was comparable to that observed with the non-phenolic model compound B, with k' increasing as VO(**2**)(O^{i}Pr) < VO(**4**)(O^{i}Pr) < VO(**6**)(O^{i}Pr). As with model B, k' for the trityl-substituted catalyst VO(**7**)(O^{i}Pr) was lower than that of the adamantyl-substituted species, although for model C this effect was even more pronounced. A likely explanation for this

exaggerated effect is that access of the larger, highly-substituted model C to the catalyst active site is more strongly disfavoured by the bulkiest trityl-substituent.

Table 12: Pseudo first order rate constants, k', for the degradation of model C by catalysts VO(2,4,6,7)(O^iPr). Conditions: 5 mol% VO(2,4,6,7)(O^iPr), 100 °C, DMSO-d_6

Catalyst	k' ($days^{-1}$)
VO(**2**)(O^iPr)	1.92 ± 0.06
VO(**4**)(O^iPr)	5.95 ± 0.06
VO(**6**)(O^iPr)	10.17 ± 0.23
VO(**7**)(O^iPr)	3.74 ± 0.08

2.6 Conclusions

Following on from promising literature precedent, a range of homogeneous vanadium(V) Schiff-base catalysts were synthesised and tested for activity in the degradation of β-O-4 model compound 2-phenoxy-1-phenylethanol (model B). The results of these studies have been published in Catalysis Today (doi:10.1016/j.cattod.2015.08.045). Degradation of model B occurred *via* two processes; C-O bond cleavage to form phenol (the desired product) and acetophenone, and benzylic oxidation to form 2-phenoxy-1-phenylethanone (OP). A range of tri- and tetra-dentate ligands (**X**)H_2 were complexed to vanadium and their structures were determined by single crystal XRD and ^{1}H, ^{51}V and DOSY NMR analysis. Complexes with tridentate ligands were found to exist as symmetrical dimers of the general form [VO(**X**)($O^{i}Pr$)]$_2$ bridged through the aliphatic alcohol of the ligand, whilst in general tetradentate ligand complexes were found to exist as oxy-bridged dimers of the form [VO(**X**)]$_2$O. ^{1}H, ^{51}V and DOSY NMR analysis of mixtures of VO(**4**)($O^{i}Pr$) and model B provided further evidence for the proposed mechanism of coordination of the model compound *via* ligand exchange with the vanadium alkoxide ligand.[118]

An initial catalyst screen was conducted in a microwave reactor in order to reduce reaction times and maximise throughput. Further studies were monitored by ^{1}H NMR spectroscopy, allowing kinetic data to be acquired. From these initial studies, tridentate complexes were found to perform dramatically better than their tetradentate counterparts. This is presumed to be related to the coordination of the model compound to the catalyst; the tetradentate complexes exist as oxy-bridged species and are therefore potentially less available for coordination of the model. The tridentate ligand set were therefore taken forward for further investigation.

The steric and electronic effects of ligand substitution and backbone structure on the behaviour of the catalysts was systematically assessed in a series of experiments monitored by ^{1}H NMR spectroscopy. In terms of overall conversion of the model compound, bulky alkyl substituents on the phenolate ring were found to promote higher catalyst activity [VO(**5**,**6**)($O^{i}Pr$)], whilst halo- and un-substituted catalysts VO(**1-4**)($O^{i}Pr$) performed poorly. The bulkiest, trityl-substituted catalyst VO(**7**)($O^{i}Pr$) exhibited lower activity than its alkyl-substituted counterparts, presumably as a result of impeded access of the model compound to the active site of the catalyst due to steric hindrance from the trityl group. Complexes with monophenolate ligands were found to perform dramatically better in terms of model compound conversion than those with bisphenolate ligands. This could be a result of the requirement for the catalyst to have an accessible site for model compound coordination,

which could be hindered by the replacement of a primary hydroxyl ligand with a second, less labile phenolate species.

As degradation of model B can occur by both the desired C-O cleavage reaction to form acetophenone and phenol, and also oxidation to 2-phenoxy-1-phenylethanone (OP), the selectivity of the catalysts is of the utmost importance. Whilst most catalysts were found to promote some amount of conversion of the model compound, many were found only to facilitate oxidation to the OP. It was observed that, by changing the substituents on the tridentate monophenolate catalysts VO(**1**-**7**)(O^{i}Pr), the selectivity for the desired C-O bond cleavage reaction could be tuned. Bulky, alkyl substituents [VO(**5**-**7**)(O^{i}Pr)] were found to favour the C-O reaction, whilst halo-substituted complexes [VO(**1-3**)(O^{i}Pr)] favoured oxidation. Introduction of sp^2 hybridisation to the ligand backbone resulted in a significant loss of both activity and selectivity of the catalysts, possibly due to an increase in rigidity and resulting ring strain.

The availability and transport of oxygen was found to have a significant effect on the catalytic activity. Under conditions of restricted oxygen concentration, the activity was severely reduced and the catalysts were often found to form inactive precipitates. It is proposed that the lack of an available oxidant to reoxidize the vanadium species during the catalytic cycle causes a build-up of inactive vanadium(IV) dimers. Along with an expected increase in reaction rate, at higher temperatures the reaction was found to be more selective for C-O bond cleavage. Arrhenius analysis revealed that the activation energy for degradation of model compound B was around 70-100 kJ.mol^{-1}.

A phenolic model compound was also successfully degraded in the presence of VO(**6**)(O^{i}Pr), achieving complete conversion within 24 h with 100% selectivity for the C-O cleavage products. The trend in catalyst behaviour for the phenolic model compound was analogous to that observed for the non-phenolic model.

2.7 Future work

It was observed during the course of these experiments that the concentration of oxygen in these reactions was a limiting factor, both in the oxidation of the model compound and also potentially in the reoxidation of the catalysts to the active V(v) species. This area warrants further study in order to determine whether or not the catalyst behaviour and trends are the same in the presence of excess oxygen. This is potentially challenging to investigate *in situ* in an NMR tube, although air (or even oxygen) could be bubbled through the system. Failing this, the reactions could be conducted in a stirred vessel with ample surface area in contact with the air. The reactions could then be sampled or transferred to NMR tubes for analysis. These experiments could assist in clarification of the reoxidation mechanism of the vanadium catalysts.

In order to assess the potential applicability of these vanadium complexes in a real-world situation, the next step is to employ them in the degradation of real lignin substrates. The depolymerization of lignin itself presents a range of additional challenges such as limited access of catalysts to the polymer, due to its insolubility and highly branched, 3-dimensional structure, and the presence of potentially reactivity-inhibiting compounds. In promising literature precedent, Chan *et al.* reported that vanadium Schiff-base complexes are capable of lowering the molecular weight of *Miscanthus giganteus*-derived organosolv lignin, and also observed the production of monomeric phenolic degradation products, admittedly in low yields.[111]

The most successful and stable of the complexes tested here should be employed in the attempted degradation of a range of lignins, as the structure of the lignin is dependent on extraction method and is therefore likely to have a profound influence on the efficacy of the catalyst. For instance, the proportion of free hydroxyl groups present in the lignin, which are proposed to be vital for catalyst binding, can vary depending on the extraction process. The extent of molecular weight lowering could be determined by SEC, whilst the proportion of different linkages which are cleaved could be monitored by 2D NMR HSQC analysis.[111] ^{31}P NMR has been utilised in the identification and quantification of phenolic residues in lignin samples following derivatization with a phosphitylating reagent such as 2-chloro-4,4,5,5-tetramethyl-1,3,2-dioxaphospholane (TMDP), and therefore could also be employed here to determine the phenolic content of the lignin both before and after catalytic treatment.[178] The vanadium Schiff base complexes could also be heterogenized onto silica in order to potentially increase their stability and also improve their ease of use and recovery in a large scale process.[179]

3. Catalytic depolymerization of model lignin compounds in ionic liquids and ionic liquid-DMSO mixtures

The majority of the research presented in chapter 3 was carried out during a three month placement as part of the Biomass Pretreatment team at the Joint BioEnergy Institute (JBEI) in Emeryville, CA, USA.

Ionic liquids (ILs) have reportedly been employed in the effective pretreatment of lignocellulosic biomass. Not only does IL pretreatment of biomass produce a carbohydrate fraction which is more susceptible to subsequent enzymatic hydrolysis, it can also result in the production of a solubilized, and even partially degraded, lignin stream. This has implications for the use of homogenous catalysts for lignin depolymerization as the structure of IL-solubilized lignin is potentially much more accessible to these homogeneous species.

As discussed in section 1.5.4, homogeneous organometallic complexes have the potential to be highly selective lignin depolymerization catalysts, however, to date, most examples have only been successfully demonstrated on model lignin compounds. This is due in part to the ease of analysis of model lignin compounds as compared to the lignin polymer itself. More significantly, however, there are complications arising from the difficultly of catalyst access to large parts of the highly interlinked, three-dimensional lignin polymer network, and also catalyst deactivation due to the presence of impurities in the lignin source.[21]

Whilst there is some precedent for metal-catalyzed lignin depolymerization in ILs, only simple metal salts have been employed, either as oxidation catalysts or to promote acid-catalyzed hydrolysis *via* the production of HCl *in situ*.[94, 97] To date, to the author's knowledge, there have been no examples of the use of organometallic complexes in ILs for lignin depolymerization, thus this study represents the first foray into this arena.

In order to assess the suitability of promising homogeneous vanadium catalysts (chapter 2) for depolymerization of IL-solubilized lignin streams, a selection of these species were tested in a range of ionic liquids. The stability of the catalysts in the ionic liquids was assessed, along with their activity and selectivity for the degradation of several model lignin compounds. The influence of reaction conditions such as temperature, addition of water and the effect of DMSO:IL solvent mixtures was also be probed in order to assist in the determination and clarification of the reaction mechanisms. Some preliminary studies on the degradation of real lignin by homogeneous Schiff-base catalysts in [Emim][OAc] will also be presented.

3.1 Choice of catalyst, model compounds and ionic liquids

Structures of the vanadium catalysts used in this study are shown in Figure 64. VO(**2**)(O^{i}Pr) and VO(**6**)(O^{i}Pr) were prepared as in Chapter 2, VO(**16**)(O^{i}Pr) was synthesized according to literature procedure.[117] These species were selected to represent the full scale of reactivity and selectivity for C-O bond cleavage observed in previous investigations in organic solvents, from the highly active and C-O selective VO(**6**)(O^{i}Pr) to the poorly active, C-H selective VO(**2**)(O^{i}Pr) and the C-C selective VO(**16**)(O^{i}Pr), as reported by Hanson *et al*.[117]

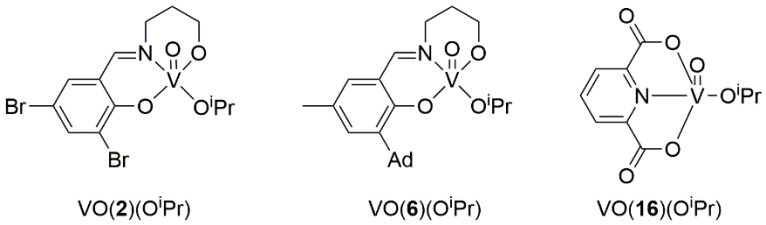

Figure 64: Structures of vanadium complexes used in this study

ILs exhibiting a range of properties, such as acidity and hydrogen bond basicity, were selected for this investigation, Figure 65. As some of the most commonly used and broadly applicable ILs, the imidazolium-based ILs 1-ethyl-3-methylimidazolium acetate, [Emim][OAc] and 1-butyl-3-methylimidazolium acetate, [Bmim][OAc] were the primary choice for initial studies.[44, 72] Reports of acidic IL-catalyzed lignin depolymerization prompted the selection of the acidic IL triethylammonium hydrogen sulfate, [TEA][HSO_4], for investigation.[96] Biocompatible (and potentially bioderived) ILs choline lysinate, [Ch][Lys], and choline acetate, [Ch][OAc], were also tested. Ionic liquids containing the [Lys]$^-$ anion have been shown to be more effective for delignification than their [OAc]$^-$ counterparts.[45] This is most likely due to either the higher hydrogen bond basicity, β, of the [Lys]$^-$ anion compared to [OAc]$^-$ facilitating greater disruption of the hydrogen bond network within the lignin polymer, or possibly due to the reaction of the [Lys]$^-$ primary amine group assisting in the degradation of the lignin-hemicellulose linkages.[45]

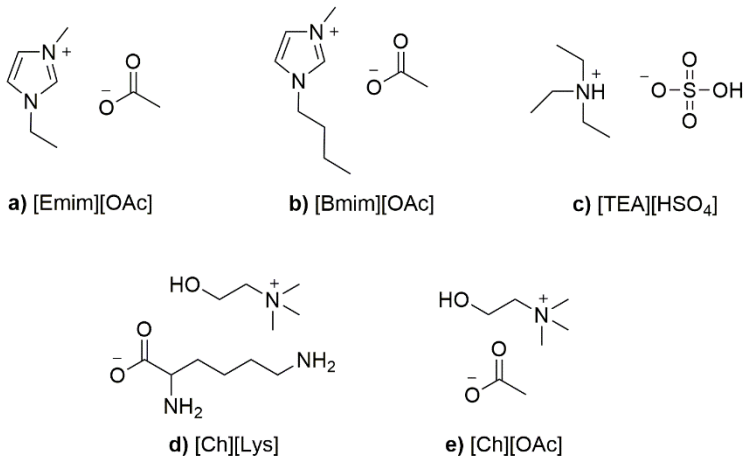

Figure 65: Structures of ionic liquids employed in this study; a) 1-ethyl-3-methylimidazolium acetate, b) 1-butyl-3-methylimidazolium acetate, c) triethylammonium hydrogen sulfate, d) choline lysinate, e) choline acetate

Model compounds representing a number of the most common linkages in lignin were exposed to a selection of different ILs and catalysts. The most common linkage in lignin is the β-aryl-ether or β-O-4. This linkage is also the most susceptible to degradation and therefore forms the basis of most model compound studies.[112] Two different β-O-4 model compounds were employed in this study, 2-phenoxy-1-phenylethanol (model B) and the more highly substituted 1-phenyl-2-(2-methoxyphenoxy)propane-1,3-diol (model D). A model compound containing the α-O-4 linkage (model E) was also subjected to degradation tests in the ionic liquids. The reactions were monitored using high-performance liquid chromatography (HPLC), and yields and conversions are presented as a percentage of the theoretical maximum yield of each species based on the initial amount of substrate.[117, 118]

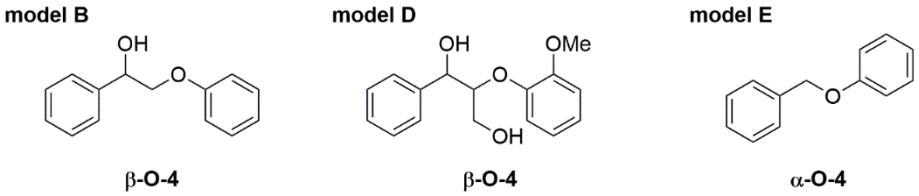

Figure 66: Structures of model lignin compounds B, D and E used in these studies

3.2 Degradation of an unsubstituted β-O-4 model compound

Previous studies have demonstrated that, in DMSO at 100 °C and in the presence of vanadium Schiff-base catalysts such as VO(**1-7**)(OiPr), β-O-4 model compounds such as model B undergo a combination of C-O and C-H bond cleavage forming both phenol and acetophenone (or substituted derivatives thereof) and a benzylic oxidation product (OP) respectively, chapter

2.[180] These two reactions are in competition, and the selectivity is dependent on reaction conditions and catalyst structure. It was anticipated that, if the ILs were simply acting as solvents, the reactivity would be similar in ionic liquids, Figure 68. An HPLC calibration of model compound B, the OP, and C-O cleavage product phenol was run, Figure 68.

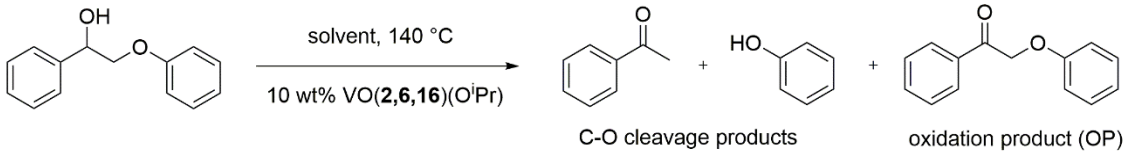

Figure 67: Degradation of β-O-4 model compound B, 2-phenoxy-1-phenylethanol to C-O cleavage products acetophenone and phenol, and oxidation product 2-phenoxy-1-phenylethanone (OP)

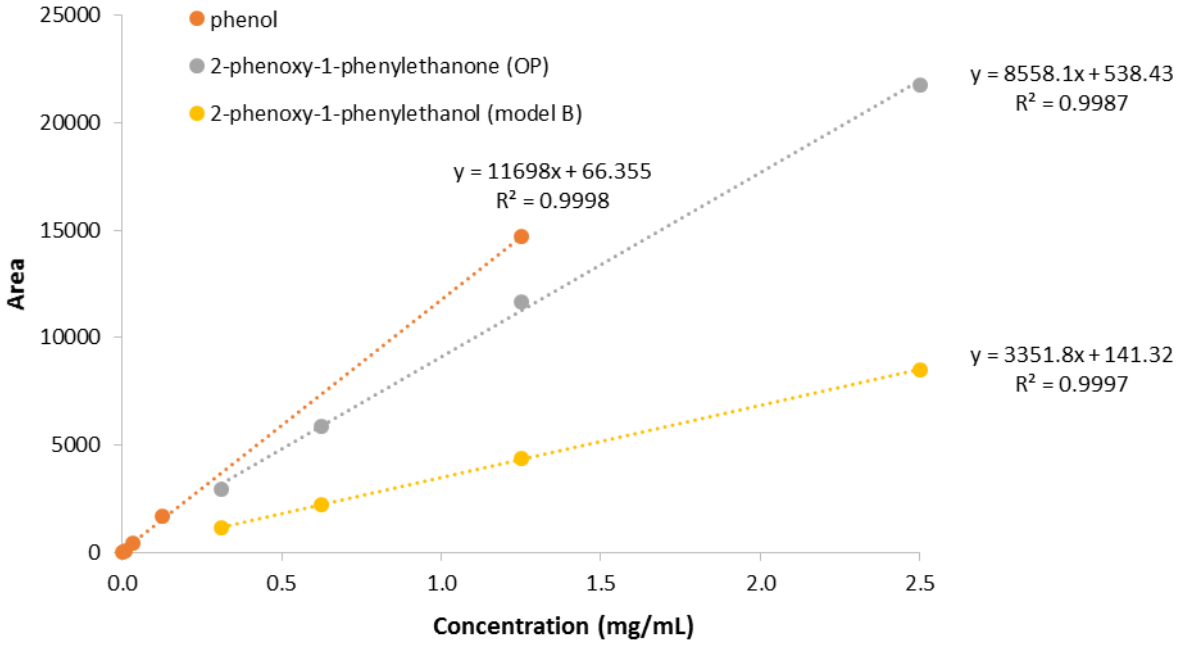

Figure 68: HPLC calibration graph for the degradation of 2-phenoxy-1-phenylethanol (model B) to phenol and oxidation product 2-phenoxy-1-phenylethanone (absorbance at 280 nm)

3.2.1 Effect of ionic liquid structure

Interestingly, in contrast to the mixture of C-O cleavage and oxidation products observed in previous DMSO studies, the reaction of 2-phenoxy-1-phenylethanol in [Emim][OAc] was found to produce exclusively phenol and acetophenone, with no evidence of formation of the OP. It was theorized from this that oxidation was strongly inhibited in the ionic liquid as a result of low oxygen concentration limiting the rate, possibly due to low oxygen solubility in [Emim][OAc]. However, whilst the low solubility of oxygen in a range of ILs has been reported

in the literature, the solubility of oxygen in DMSO is comparable and therefore does not account for this discrepancy.[181, 182] In contrast to previous reactions conducted in DMSO where no conversion of model B was observed in the absence of a catalyst, the background reaction in [Emim][OAc] produced a 7% yield of phenol after 4 h, Figure 69. This supports previous reports of partial lignin depolymerization occurring during pretreatment in [Emim][OAc].[27, 44] In the presence of 10 wt% VO(**6**)(O^{i}Pr) the phenol yield was found to increase significantly to 27%, confirming that this species is an active catalyst for the degradation of the model compound. No directly comparable literature results in DMSO are available, therefore the activity in DMSO and ionic liquids will be investigated later. The fact that VO(**6**)(O^{i}Pr) is active for the degradation of model B in the IL, along with the 100% selectivity for the desired C-O cleavage products, is a promising indicator that the use of homogeneous vanadium catalysts in ionic liquids could be useful in the degradation of lignin.

In the absence of a catalyst, conversion of model B to phenol in [Bmim][OAc] was almost identical to that of [Emim][OAc]. This is somewhat unsurprising considering the similarity between the two ionic liquids; their β (hydrogen-bond basicity) and π* (polarizability) Kamlet-Taft parameters are almost identical, and these have been shown to be related to the interactions between lignin and ILs.[45, 56] However, in the presence of VO(**6**)(O^{i}Pr) the phenol yield was slightly higher in the $[Bmim]^{+}$ analogue, possibly as a result of increased catalyst stability or solubility in the longer-chain solvent. The 100% selectivity for C-O bond cleavage observed in [Emim][OAc] was also retained in [Bmim][OAc].

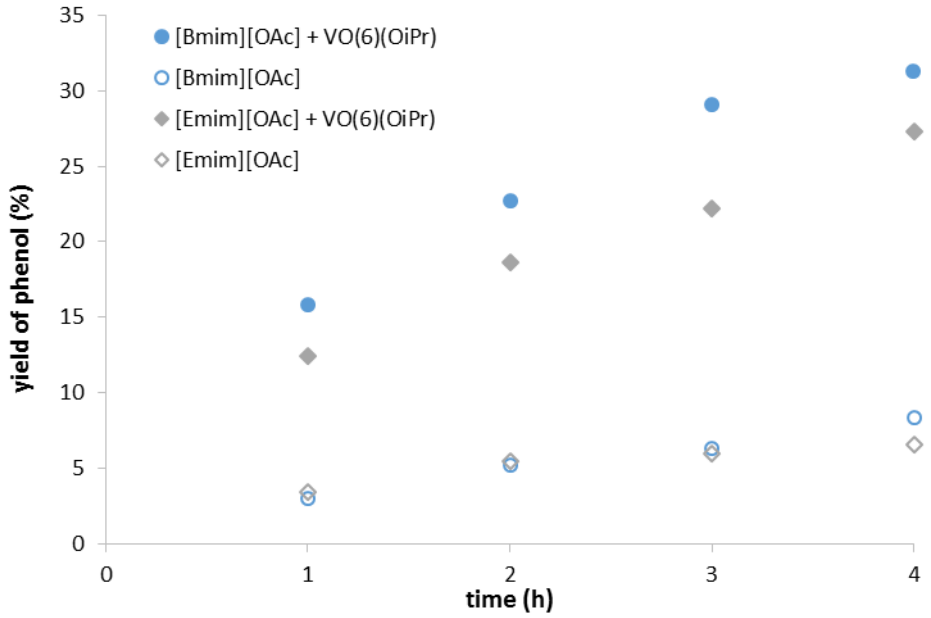

Figure 69: Yield of phenol in the degradation of model compound B in [Emim][OAc] and [Bmim][OAc] Conditions: 140 °C, 0.1 g model B in 1 g IL, 10 wt% VO(6)(O^{i}Pr)

Phenol yields in the acidic IL [TEA][HSO_4] were found to be lower than in the imidazolium-based ILs, Figure 70, although the presence of the catalyst was still found to significantly increase the yield above the background reaction, which is negligible in this IL. The lower activity of VO(**6**)(O^iPr) in [TEA][HSO_4] compared to [Emim][OAc] could be a result of catalyst deactivation by the acidic medium.

The yield of phenol in the bio-derived ionic liquid [Ch][OAc] was comparable to that of [TEA][HSO_4], reaching around 8% after 4 h in the presence of catalyst. Without a catalyst only around 2% phenol was produced, indicating that VO(**6**)(OiPr) is also active in [Ch][OAc]. Exchanging the acetate anion for a lysinate anion resulted in a decrease in the conversion to phenol in both catalyzed and uncatalyzed reactions, with less than 1% phenol produced in 4 h. It is plausible that the lysinate anion is capable of ligating the vanadium, thereby inhibiting coordination of the model compound to the metal centre, which is presumably required for the activity of the catalyst. Although there is no direct evidence for this, the [Ch][Lys]/VO(**6**)(O^iPr) reaction mixture was observed to be a cloudy, orange suspension, in contrast to the dark red-brown homogeneous solution of VO(**6**)(O^iPr) in [Emim][OAc] and [Ch][OAc]. This suggests that there might be degradation of the catalyst in [Ch][Lys] as vanadium(V) Schiff-base complexes are generally brown in colour.[169] No evidence of the OP was observed in the HPLC trace from the reactions in either of the cholinium-based ILs.

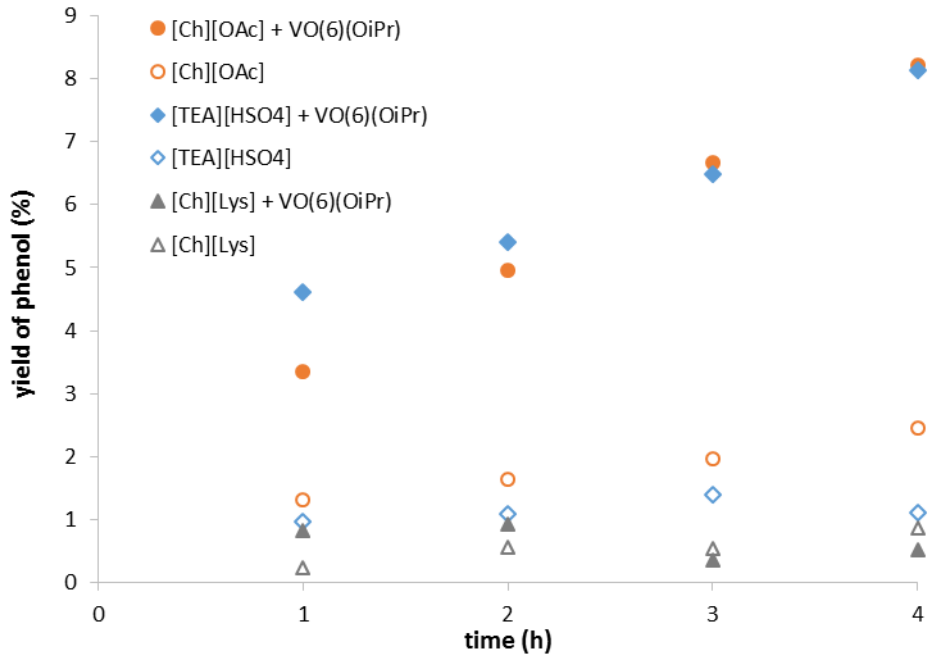

Figure 70: Yield of phenol in the degradation of model compound B in [Ch][OAc], [TEA][HSO_4] and [Ch][Lys]. Conditions: 140 °C, 0.1 g model B in 1 g IL, 10 wt% VO(6)(O^iPr)

3.2.2 .Effect of water

IL-water mixtures have been successfully employed in the pretreatment of lignocellulose, reducing viscosity and potentially improving the economics of the IL pretreatment process by reducing the energy and costs associated with IL recycling, however water can also be utilised as a biomass antisolvent in high concentrations.[46] The presence of a small amount of water has also been shown to be necessary for the cleavage of β-O-4 linkages in some cases, for example by hydrolysis.[97] However, on addition of water (0.3 mL to 1 mL IL) there was a dramatic reduction in conversion and phenol yield in both the catalyzed and uncatalyzed reactions in [Emim][OAc], Figure 71. In the catalyzed reaction, this detrimental effect could be partially due to catalyst deactivation by the water, however the fact that it is also observed in the uncatalyzed reaction suggests another effect is also operating. A plausible explanation could be that the interaction between the water molecules and $[OAc]^-$ anions is stronger than between the anions and the model compound. Ji *et al*. observed a similar effect in theoretical studies of the interaction between a model lignin compound and [Amim]Cl in the presence of water molecules.[68] Such a preferential interaction could prevent degradation of the model compound by the IL. The addition of water to [Emim][OAc] has been shown to decrease its Kamlet-Taft hydrogen bond basicity, β, which could also explain this observation if the uncatalyzed degradation is facilitated by the $[OAc]^-$ interacting with the model compound hydroxyl group.[63]

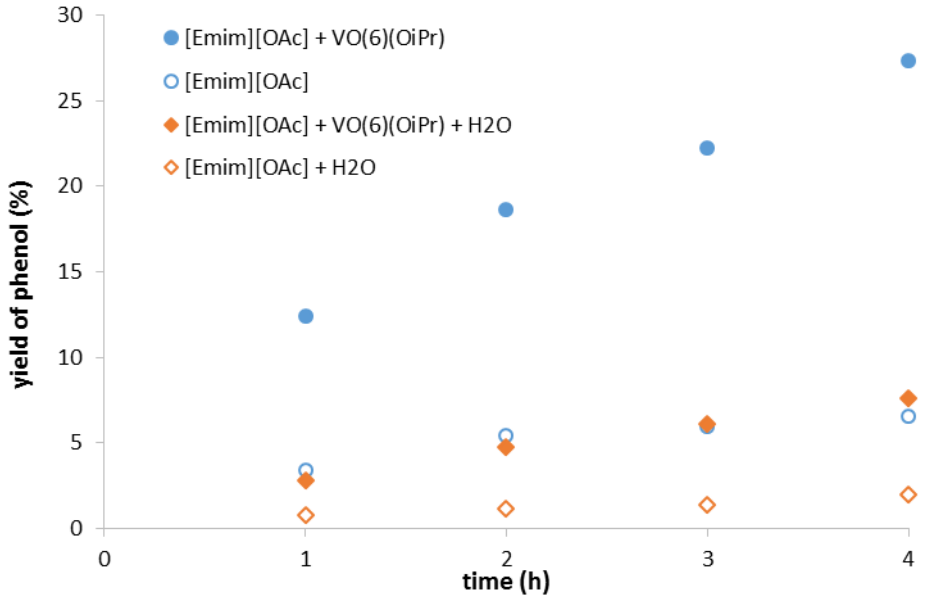

Figure 71: Depolymerization of model compound B in [Emim][OAc], Conditions: 140 °C, 0.3 mL H_2O, 0.1 g model B in 1 g IL, 10 wt% VO(6)(O^iPr)

In [TEA][HSO_4] in the absence of a catalyst, there was no change in the yield of phenol on the addition of water. However, in the presence of the catalyst, the addition of water increased

the yield of phenol from 8% to 17%. This effect has been observed for metal chlorides, whereby the addition of water generated HCl *via* hydrolysis of the catalyst, facilitating acid-catalyzed hydrolytic cleavage.[97] Whilst there are no chlorides present here, it is possible that the presence of water liberates protons from the acidic ionic liquid, promoting acid-mediated degradation.

As in the previous cases there was no evidence of the OP, however in the absence of water the overall conversion of the model compound was around 40-50% in both the catalyzed and uncatalyzed reaction, much higher than can be accounted for by the yield of phenol. HPLC analysis indicated the presence of species other than the expected degradation products. In an attempt to identify these species, a sample was taken for analysis by GC-MS which indicated the presence of a vinyl ether species, Figure 73. This is likely formed *via* a dehydration reaction as has been observed with other similar model compounds.[183]

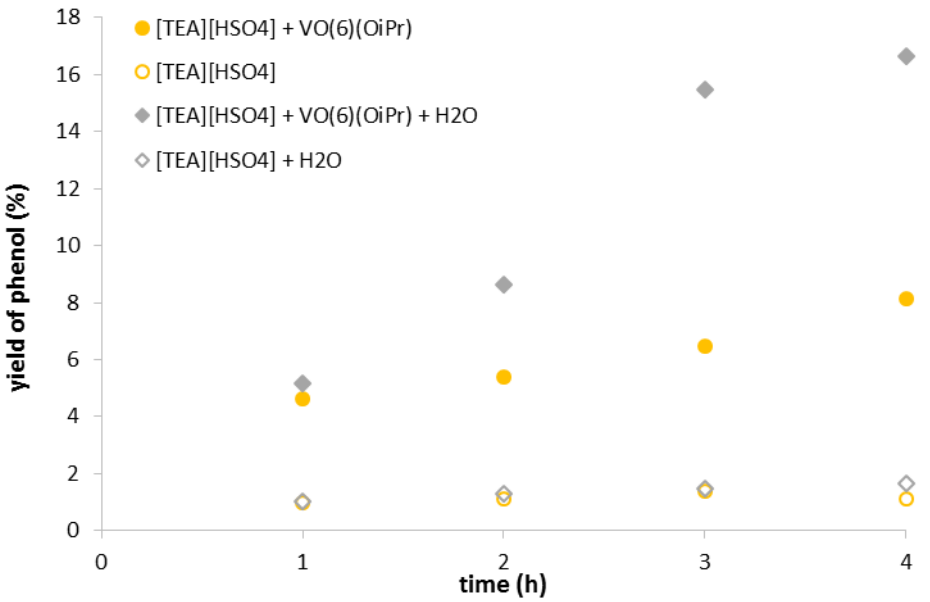

Figure 72: Depolymerization of model compound B in [TEA][HSO_4], Conditions: 140 °C, 0.3 mL H_2O, 0.1 g model B in 1 g IL, 10 wt% VO(6)(O^iPr)

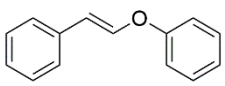

Figure 73: Structure of vinyl ether species produced during the degradation of model B in [TEA][HSO_4] in the presence of water

As the aim of this research is to achieve selective and clean degradation of lignin to phenolic products, the imidazolium-based ionic liquids appear to be the most successful of those tested so far. Given the expertise of the Biomass Pretreatment team at JBEI in the scale-up of IL

pretreatments with a particular focus on the use of [Emim][OAc], this IL was selected for subsequent investigations.[26, 44, 61, 72, 87, 88, 184, 185]

3.2.3 Comparison of performance in [Emim][OAc] and DMSO

As the conditions in this study are not identical to those used previously to investigate these catalysts, analogous reactions were conducted in DMSO in order to provide a more direct comparison, Figure 74. In the absence of a catalyst there was negligible conversion, with only peaks corresponding to the model compound observed and no evidence of phenol production in the HPLC trace. However, on addition of 10 wt% VO(**6**)(O^{i}Pr), the yield of phenol reached almost 70% in 4 h, significantly higher than in any of the ILs. It is obvious, therefore, that the catalyst is inhibited in the presence of all of the ILs, but less so in [Emim][OAc] and [Bmim][OAc] than in [Ch][Lys], [Ch][Lys] and [TEA]HSO_4]. It is also possible that strong ionic or hydrogen-bonding interactions of the ionic liquids with the hydroxyl group of the model compound interfere with catalyst binding. Unlike in the ILs, formation of the OP was also observed in DMSO. The selectivity in DMSO and ILs will be discussed in further detail in section 3.2.5.

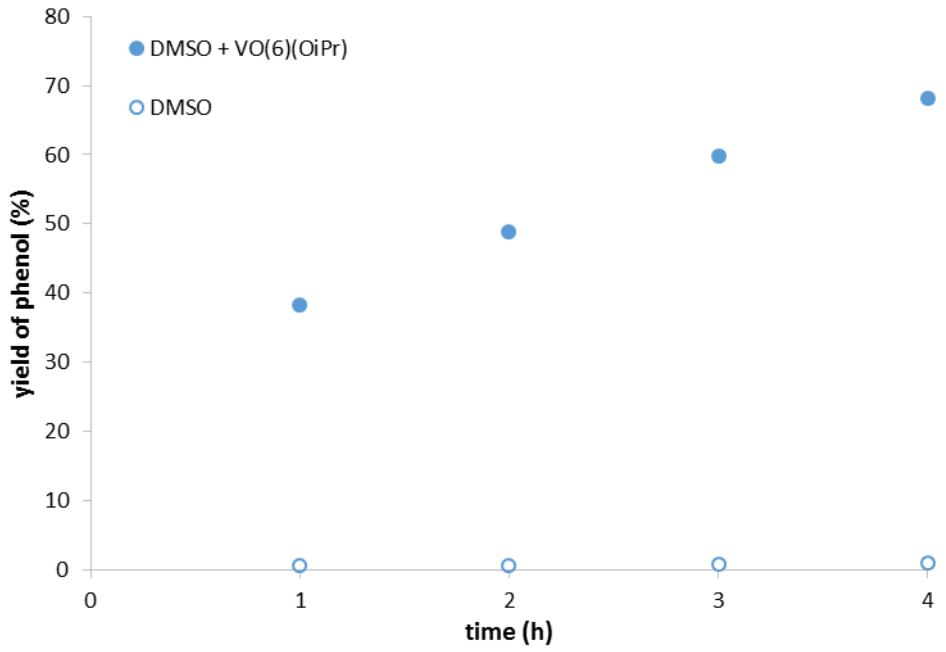

Figure 74: Yield of phenol from the degradation of model B in DMSO. Conditions: 140 °C, 0.1 g model B in 1 g DMSO, 10 wt% VO(6)(O^{i}Pr)

3.2.4 Effect of catalyst structure

In previous studies in organic solvents, vanadium catalysts VO(**2**,**6**,**16**)(O^{i}Pr) displayed markedly different reactivity and selectivity,[117, 118, 180] for example VO(**6**)(O^{i}Pr) promoted much faster degradation of model B than VO(**2**)(O^{i}Pr), Chapter 2. Further evidence for this trend was observed in this study, with VO(**6**)(O^{i}Pr) producing significantly higher phenol yields than either VO(**2**)(O^{i}Pr) or VO(**16**)(O^{i}Pr) in DMSO at 140 °C, Figure 75. It should be noted that this effect is not an artificial result produced by the wt% catalyst loadings, as the molar loadings of VO(**2**)(O^{i}Pr) and VO(**6**)(O^{i}Pr) are almost identical (≈ 5 mol%) and the loading of VO(**16**)(O^{i}Pr) is around 0.5 times higher (7.5 mol%).

In contrast however, in [Emim][OAc], all three catalysts behaved almost identically, Figure 76. A possible explanation could be that the catalysts interact with the ionic liquid in such a way as to form identical species. It is interesting to note that, whilst the two Schiff-base catalysts VO(**2**,**6**)(O^{i}Pr) perform less well in the ionic liquid, the yield of phenol is increased in the case of VO(**16**)(O^{i}Pr) relative to DMSO.

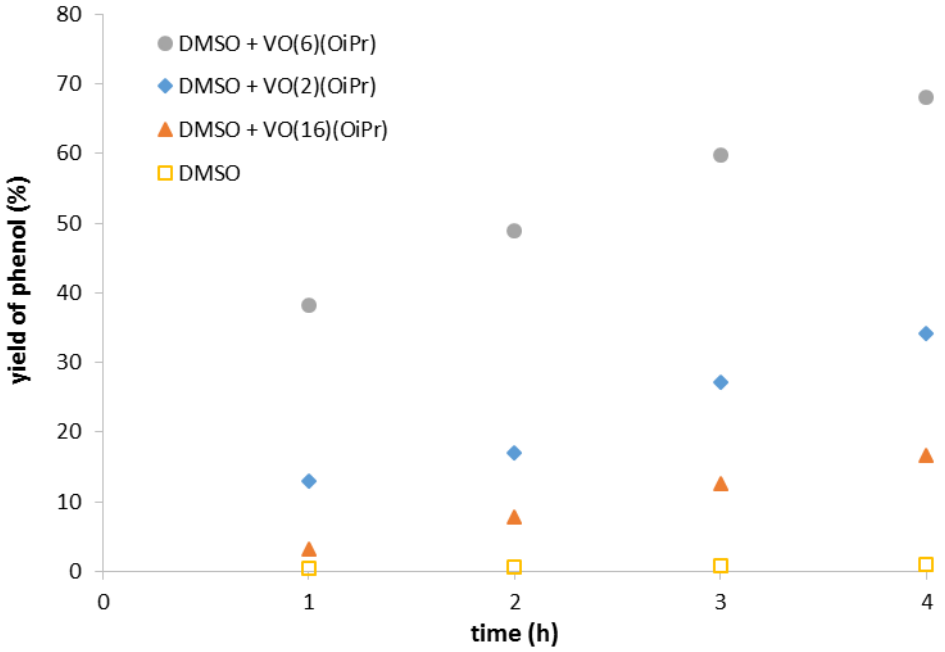

Figure 75: Comparison of vanadium catalysts VO(2,6,16)(O^{i}Pr) in the degradation of model B to phenol in DMSO, . Conditions: 140 °C, 0.1 g model B in 1 g DMSO, 10 wt% VO(2,6,16)(O^{i}Pr)

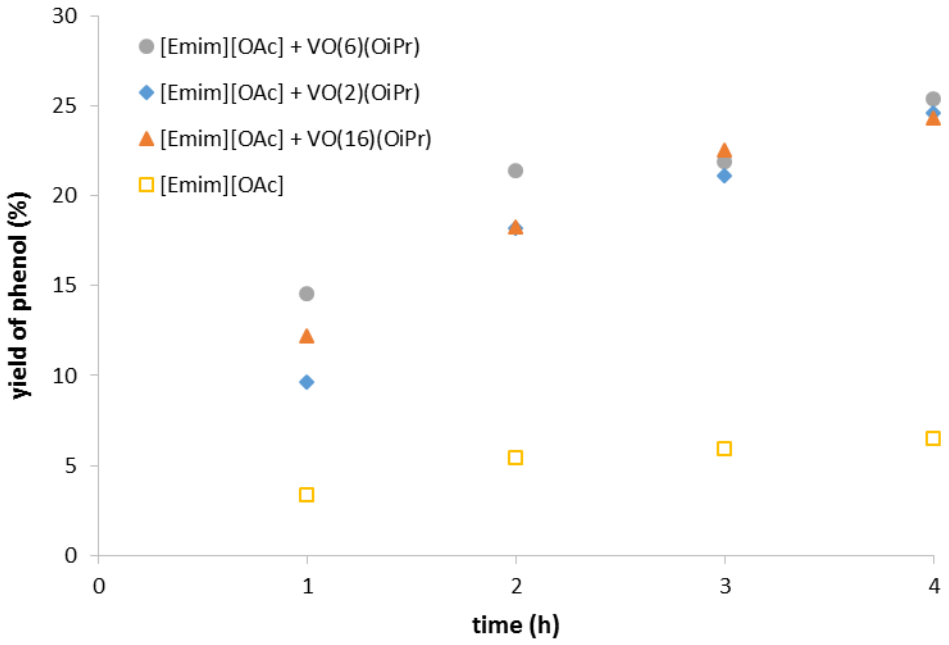

Figure 76: Comparison of vanadium catalysts VO(2,6,16)(O^{i}Pr) in the degradation of model B to phenol in [Emim][OAc]. Conditions: 140 °C, 0.1 g model B in 1 g IL, 10 wt% VO(2,6,16)(O^{i}Pr)

Selectivity for C-O bond cleavage in [Emim][OAc] was >99% for all three catalysts, whilst selectivity in DMSO ranged from 43% for VO(**16**)(O^{i}Pr) and 48% for VO(**2**)(O^{i}Pr) up to 74% for VO(**6**)(O^{i}Pr) [140 °C, 4 h, 10 wt% catalyst]. It was noted that the selectivity for C-O bond cleavage increased during the course of the reaction in DMSO, Table 13. In the presence of VO(**6**)(O^{i}Pr), almost complete conversion of the model compound was observed after only 2 h, Figure 77a. The pseudo first order rate constant, k', for the conversion of model compound under these conditions was calculated to be 1.75 ± 0.27 h^{-1}. Interestingly, the yield of phenol continues to increase even after complete consumption of the model compound and the yield of OP reaches a distinct maximum before starting to reduce. This suggests that, contrary to what has previously been observed, the OP is undergoing further degradation *via* C-O bond cleavage to form phenol.[118] It is likely that this is a result of the higher temperature of these reactions (140 °C) as compared to those employed in the literature (80-100 °C). At this higher temperature, the activation barrier to degradation of the OP is now reachable and it is therefore converted into phenol under these conditions. The transformation of OP into phenol under the reaction conditions explains the increase in selectivity seen over the course of the reaction.

Table 13: Selectivity for phenol (%) during the course of the degradation of model B in DMSO. Conditions: 140 °C, 0.1 g model B in 1 g DMSO, 10 wt% VO(2,6,16)(O^{i}Pr)

Catalyst	Selectivity for phenol (%)	
	1 h	4 h
VO(**2**)(O^{i}Pr)	48	74
VO(**6**)(O^{i}Pr)	31	48
VO(**16**)(O^{i}Pr)	20	43

As was observed in Chapter 2, the rate of conversion of the model compound in the presence of VO(**2**)(O^{i}Pr) was significantly slower than for VO(**6**)(O^{i}Pr), with k' = 0.26 ± 0.02 h^{-1}, Figure 77b. Similarly to with VO(**6**)(O^{i}Pr), the OP appeared to reach a maximum conversion (in this case at around 3 h) before levelling off. It is expected that the yield of OP would begin to decrease again longer time periods as the OP is converted into phenol. Conversion of model B by VO(**16**)(O^{i}Pr) in DMSO was slower again (k' = 0.10 ± 0.01 h^{-1}), Figure 77c.

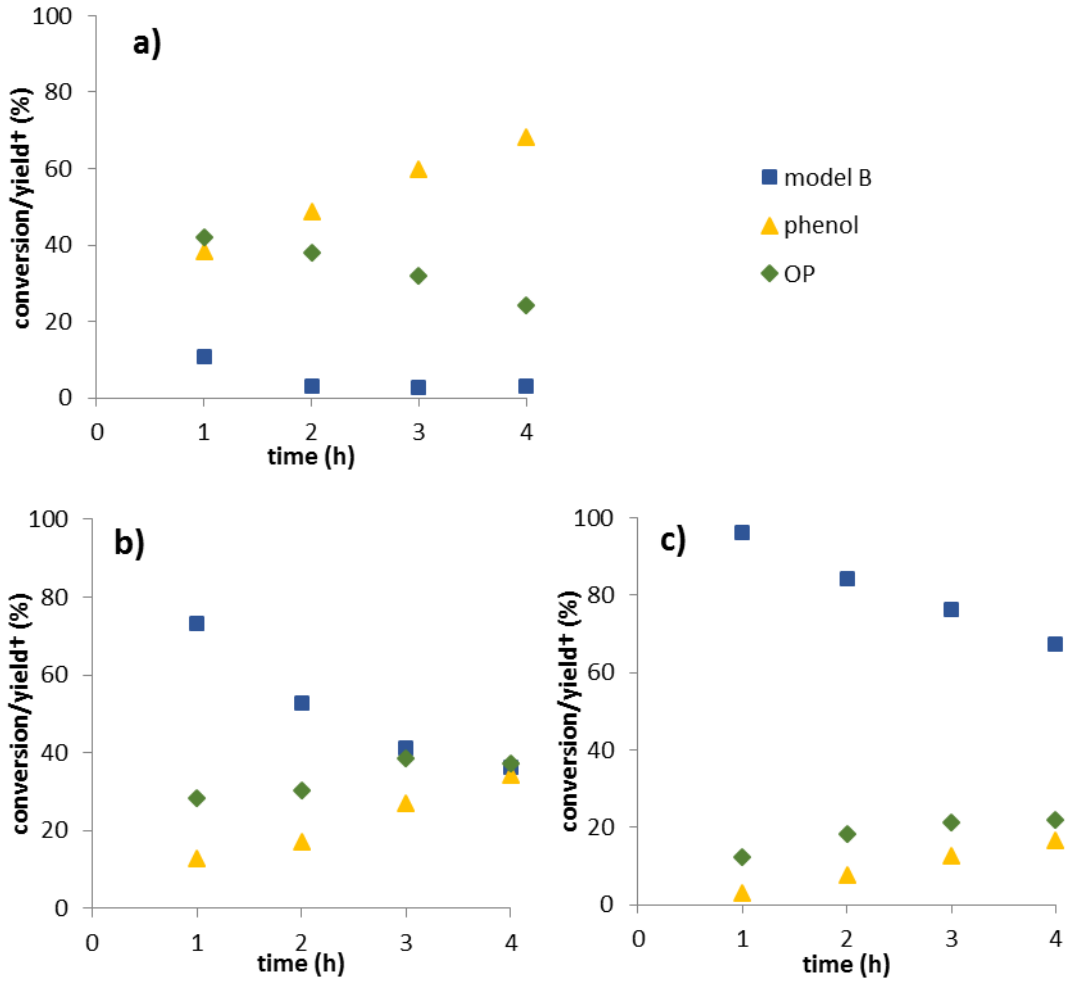

Figure 77: Degradation of model compound B to phenol and OP. †Conversion of model B, yield of phenol/OP Conditions: 140 °C, 0.1 g model B in 1 g DMSO, 10 wt% VO(X)(O^{i}Pr) a) VO(6)(O^{i}Pr), b) VO(2)(O^{i}Pr), c) VO(16)(O^{i}Pr)

3.2.5 Mixtures of DMSO and [Emim][OAc]

It was hypothesized that it might be possible to achieve both the increased C-O selectivity observed in the [Emim][OAc] reactions and the high reactivity in DMSO by employing a mixture of the two solvents. As far as the author is aware, to date there are no examples of lignin model compound degradation in IL:DMSO mixtures. Degradation of model B was attempted in a 1:1 mixture of [Emim][OAc]:DMSO, Figure 78. The rate of production of phenol in this mixture was observed to be the same as in neat [Emim][OAc] for both the catalyzed and uncatalyzed reaction. In the former case, this indicates that the catalyst is similarly inhibited in the 50% IL solution as in the neat IL, however the benefit of the background reaction in the IL is still observed in the 1:1 mixture, with a yield of 9% phenol. Despite the inhibition of the activity of the catalyst in the 1:1 solvent mixture, the selectivity of the reaction was retained, with 100% selectivity for the C-O cleavage products and no evidence of the OP or any other product forming. This promising result led to the investigation of whether it was possible to use the IL as a co-catalyst in the DMSO reactions at a lower loading to improve the selectivity of the reaction without inhibiting the catalyst.

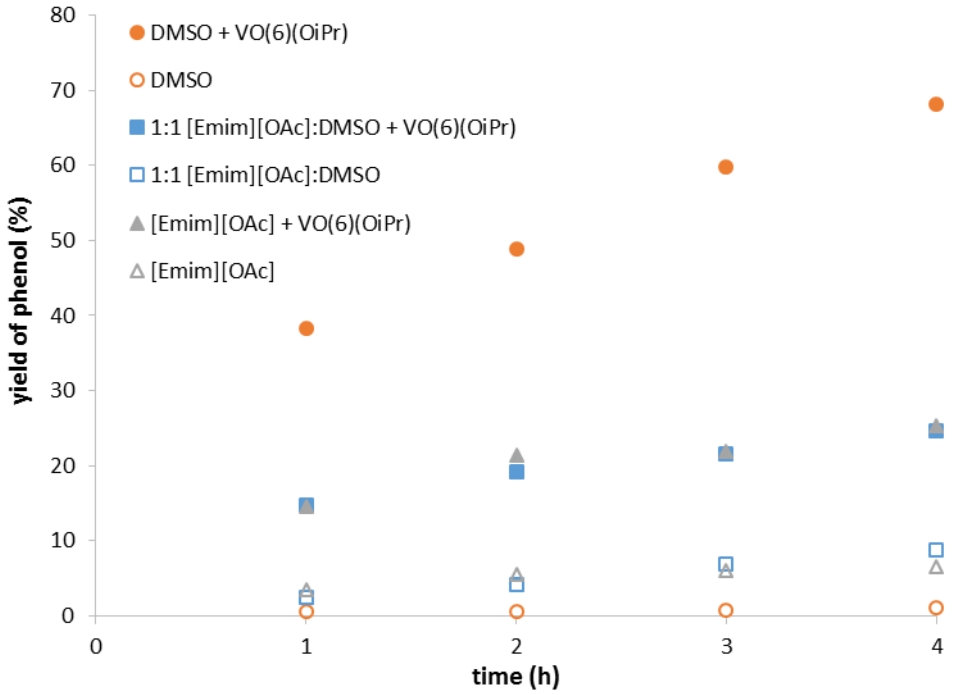

Figure 78: Comparison of phenol production from the degradation of model B in DMSO, [Emim][OAc] and a 1:1 mixture of DMSO and [Emim][OAc]. Conditions: 140 °C, 0.1 g model B in 1 g solvent, 10 wt% VO(6)(O^{i}Pr)

The pseudo first order rate constant, k', for the conversion of model compound B by VO(**6**)(O^{i}Pr) was calculated for reactions in a range of different [Emim][OAc] to DMSO ratios from 0-100 wt% [Emim][OAc], Figure 79. In neat DMSO, k' was calculated to be 3.79 ± 1.10 h^{-1}. Despite the relatively large error in this value it is immediately evident that the catalytic

activity is dramatically inhibited by the presence of even 1 wt% of the IL (k' for 1 wt% [Emim][OAc] = 0.96 ± 0.09 h^{-1}). This reduction in activity becomes even more pronounced as the weight percentage of [Emim][OAc] increases, to a minimum of 0.06 ± 0.01 h^{-1} in neat [Emim][OAc], suggesting increasing deactivation of the catalyst at higher [Emim][OAc] loadings. Above 10 wt% [Emim][OAc] most of the activity has been lost. The catalyst is present at around 2.5 times the molar loading of [Emim][OAc] at this weight percentage thus precluding the formation of a 1:1 catalyst to IL complex.

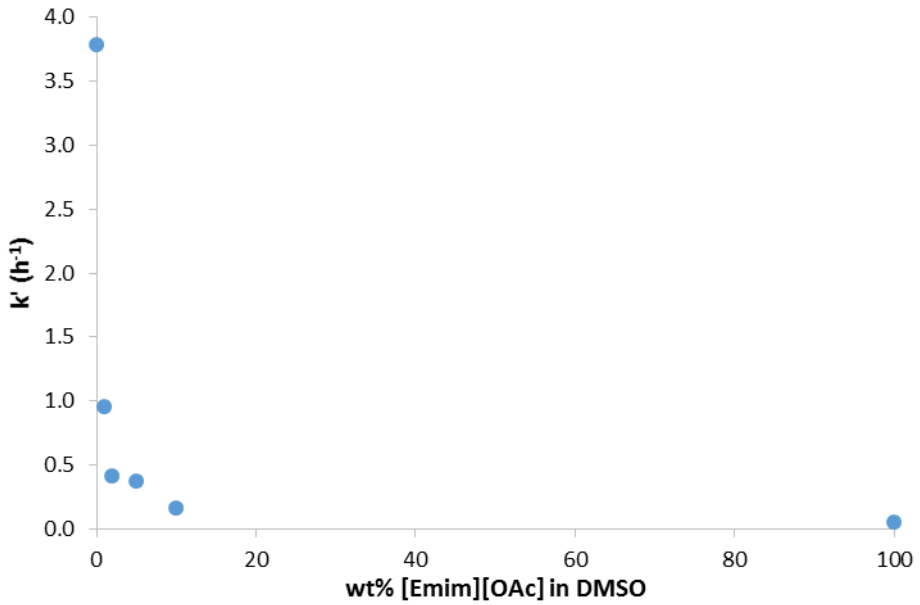

Figure 79: Graph of pseudo first order rate constant, k', for the conversion of model compound B against wt% of [Emim][OAc] in DMSO. Conditions: 140 °C, 4 h, 0.1 g model B in 1 g solvent, 10 wt% VO(6)(O^iPr)

The opposite trend was observed for the selectivities, with the selectivity for phenol increasing at larger weight percentages of [Emim][OAc]. This trend is most evident at short reaction times, for example after 1 h the selectivity in neat DMSO was 47%, rising to 70% in 1 wt% [Emim][OAc] and 96% at only 5 wt% [Emim][OAc], Figure 80.

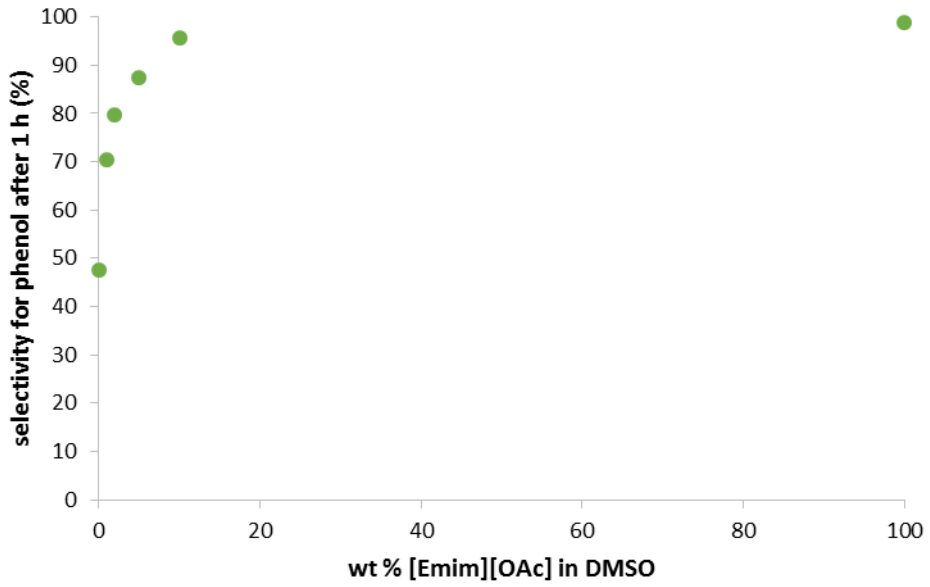

Figure 80: Graph of selectivity for phenol against wt% [Emim][OAc] in DMSO for the conversion of model compound B. Conditions: 140 °C, 1 h, 0.1 g model B in 1 g solvent, 10 wt% VO(6)(O^{i}Pr)

More detailed analysis of the product distribution during the degradation of model B in the solvent mixtures at 140 °C again indicates further conversion of the OP during the reaction, Figure 81. Along with the fact that the production of phenol from model compound B does not follow a pseudo first order plot, it can be inferred that phenol is produced from both direct C-O bond cleavage of model B and indirectly from C-O bond cleavage of the OP, following oxidation of the model compound, Figure 82. The relative rates of these two reactions is determined by the conditions. In neat DMSO and 2 wt% [Emim][OAc] at 140 °C, formation of OP from the degradation of model B appears to be faster than the subsequent conversion of OP to phenol, leading to an initial increase in yield of OP until model B has been consumed. However, in neat [Emim][OAc], no OP is observed, suggesting that the degradation of OP is much faster than its formation and any OP which is formed is instantly converted to phenol.

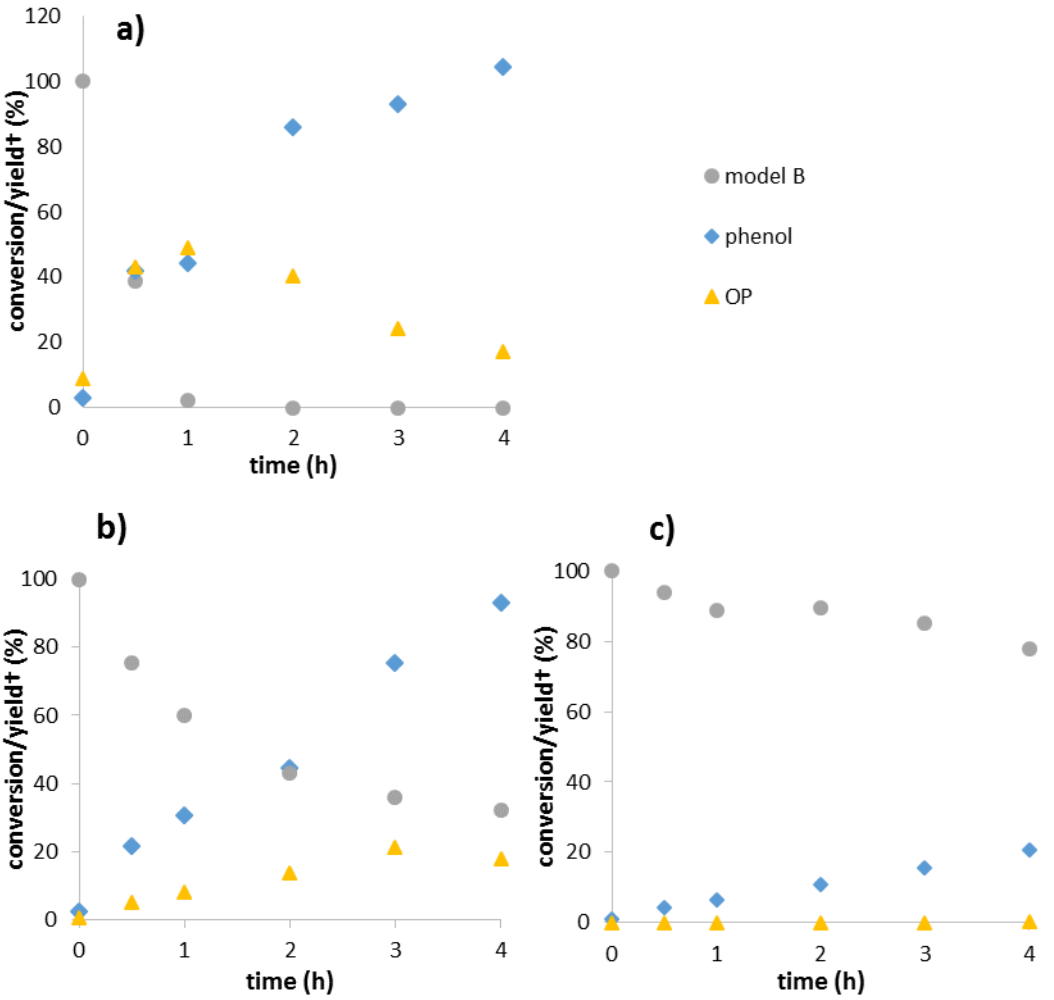

Figure 81: Degradation of model B in various weight percentages of [Emim][OAc] in DMSO a) neat DMSO (0 wt% [Emim][OAc]), b) 2 wt% [Emim][OAc]; c) 100 wt% [Emim][OAc]. †Conversion of model B, yield of phenol/OP Conditions: 140 °C, 0.1 g model B in 1 g solvent, 10 wt% VO(6)(O^{i}Pr)

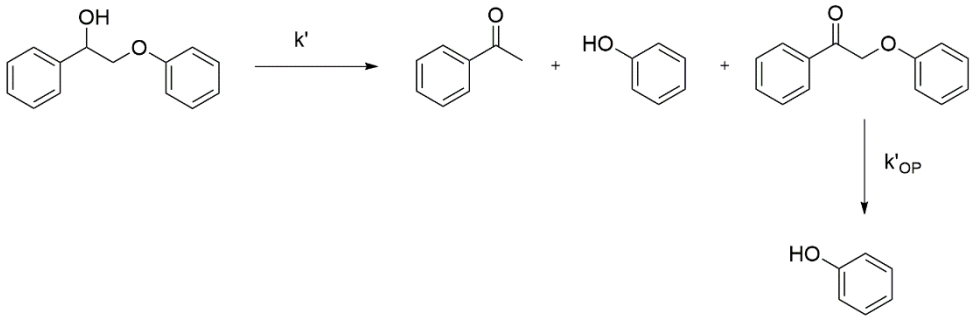

Figure 82: Production of phenol via both direct and indirect C-O bond cleavage

In order to provide further evidence for this hypothesis, the degradation of 2-phenoxy-1-phenylethanone was investigated in the solvent mixtures, Figure 83. Whilst in previous

experiments in DMSO at 100 °C there had been no evidence of any degradation of 2-phenoxy-1-phenylethanol, at 140 °C it was observed to undergo cleavage to form phenol both in the presence and absence of a catalyst, Table 14. The other product or products of this reaction were unable to be identified by GC-MS analysis, however it is possible that degradation occurs *via* further oxidation to benzoic acid and formic acid, along with phenol. This has been observed previously by Hanson *et al.*[117]

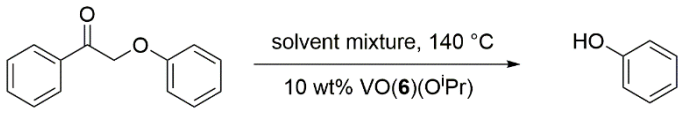

Figure 83: Degradation of 2-phenoxy-1-phenylethanone to phenol

By comparing the pseudo first order rate constants k' and k'_{OP} (for the degradation of model B and the OP 2-phenoxy-1-phenylethanone respectively), the trend of selectivity in the solvent mixtures can now be explained. In neat DMSO (0 wt% [Emim][OAc]), the model compound is converted very quickly (k' = 3.79 ± 1.10 h^{-1}) to a mixture of phenol, acetophenone and the OP. Degradation of the OP to produce more phenol occurs at a much slower rate (k'_{OP} = 0.24 ± 0.03 h^{-1}), resulting in the yield of OP reaching a maximum at around 1 h, Figure 81a. In 100 wt% [Emim][OAc], conversion of the model compound occurs much more slowly (k' = 0.06 ± 0.01 h^{-1}), but subsequent conversion of the OP occurs much faster (k'_{OP} = 1.33 ± 0.25 h^{-1}), explaining why no OP is observed in [Emim][OAc], Figure 81b. In 2 wt% [Emim][OAc] the two rates are far more similar and both phenol and OP appear to be produced simultaneously, Figure 81c.

Table 14: Pseudo first order rate constants, k'_{OP}, for the conversion of 2-phenoxy-1-phenylethanone. Conditions: 140 °C, 0.1 g 2-phenoxy-1-phenylethanone in 1 g solvent, 10 wt% VO(6)(OiPr)

wt% [Emim][OAc] in DMSO	k'_{OP} (h^{-1})	
	No catalyst	VO(6)(O^{i}Pr)
0	0.34 ± 0.05	0.24 ± 0.03
2	0.12 ± 0.03	0.76 ± 0.07
100	1.50 ± 0.25	1.33 ± 0.25

3.2.6 Alternative catalysts

In order to assess whether there might be a cheaper, simpler alternative to the vanadium Schiff-base complexes, several commercially available metal complexes, $Co(OAc)_2$, $CuCl_2$ and $CrCl_2$, were also tested for their activity towards C-O bond cleavage of the simple β-O-4 model compound in both [Emim][OAc] and DMSO, Table 15. Phenol yields were low (<8%) in all cases and no OP was observed. Conversely to the vanadium catalysts, phenol yields were slightly higher in [Emim][OAc] than in DMSO, however this can be attributed to the background reaction in the IL. The poor performance of these simple metal catalysts compared to the vanadium Schiff-base species justifies further research into organometallic complexes for lignin depolymerization in ionic liquids.

Table 15: Yield of phenol from the degradation of model B by a range of non-vanadium catalysts. Conditions: 140 °C, 0.1 g model B in 1 g solvent, 10 wt% catalyst

Catalyst	Solvent	Yield of phenol (%)
$Co(acac)_2$	[Emim][OAc]	5
$Co(acac)_2$	DMSO	3
$CrCl_2$	[Emim][OAc]	7
$CrCl_2$	DMSO	0
$CuCl_2$	[Emim][OAc]	2
$CuCl_2$	DMSO	1

3.3 Degradation of a substituted β-O-4 model compound

β-O-4 model compound 1-phenyl-2-(2-methoxyphenoxy)propane-1,3-diol (model D) was expected to degrade to a number of products including C-O cleavage product guaiacol, Figure 84.[118] The reaction was monitored by HPLC *via* conversion of model compound and yield of guaiacol, which were calibrated across relevant concentration ranges as previously, Figure 85.

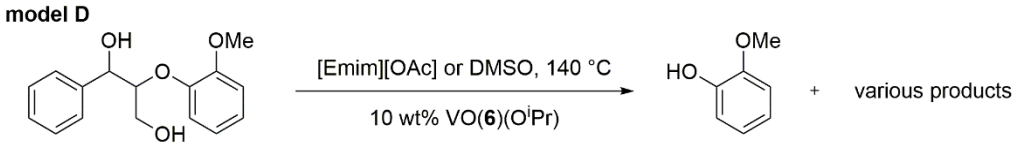

Figure 84: Degradation of substituted β-O-4 model compound 1-phenyl-2-(2-methoxyphenoxy)propane-1,3-diol (model D) to guaiacol

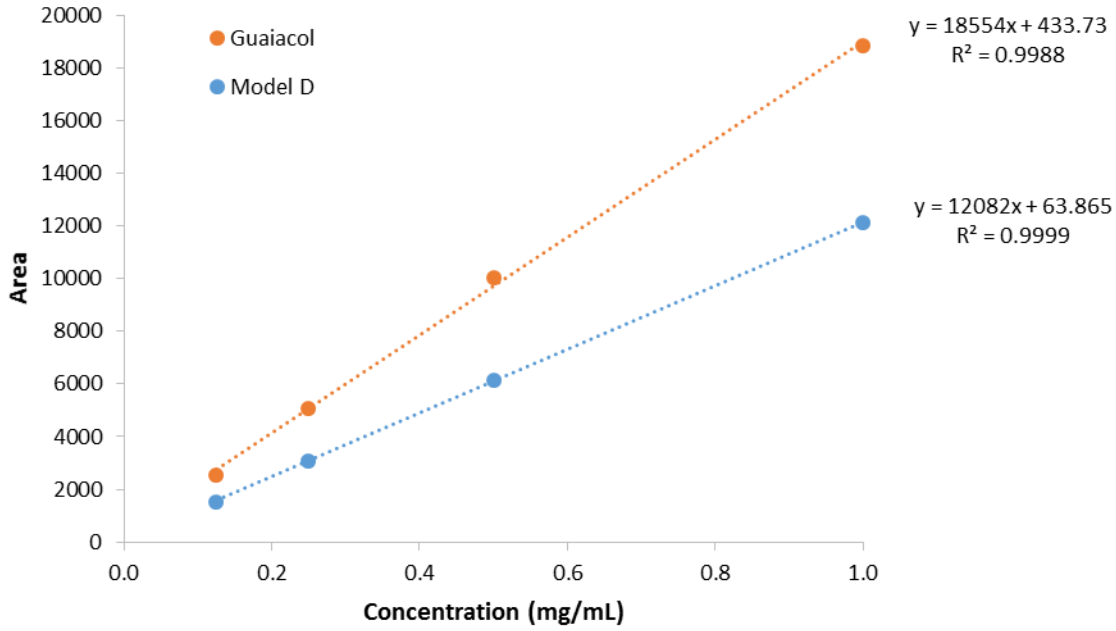

Figure 85: HPLC calibration for β-O-4 model compound 1-phenyl-2-(2-methoxyphenoxy)propane-1,3-diol (model D) and degradation product guaiacol (absorbance at 280 nm)

The presence of a primary hydroxyl group on the β-carbon was found to influence the reactivity of the model compound; in contrast to the unsubstituted model compound B, the degradation of model D proceeded even in the absence of a catalyst in DMSO, Table 16. This could be a result of the lower bond dissociation enthalpy for substituted β-O-4 compounds compared to their unsubstituted analogues.[112] Selectivity for guaiacol production was low in both [Emim][OAc] and DMSO. GC-MS analysis was not sufficient to be able to identify the other products.

Table 16: Degradation of β-O-4 model compound D in [Emim][OAc] and DMSO. Conditions: 140 °C, 4 h, 0.1 g model D in 1 g solvent, 10 wt% VO(6)(O^iPr).

Solvent	Catalyst	Conversion of model D (%)	Yield of guaiacol (%)
[Emim][OAc]	None	0	0
[Emim][OAc]	VO(**6**)(O^iPr)	23	7
DMSO	None	38	8
DMSO	VO(**6**)(O^iPr)	100	13

3.4 Degradation of an α-O-4 model lignin compound

The degradation of benzylphenyl ether, a model lignin compound containing the α-O-4 linkage, was also investigated, Figure 86. Benzylphenyl ether (model E) and expected degradation product phenol, were calibrated as previously, Figure 87.

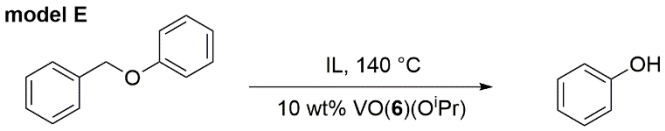

Figure 86: Degradation of α-O-4 model lignin compound E

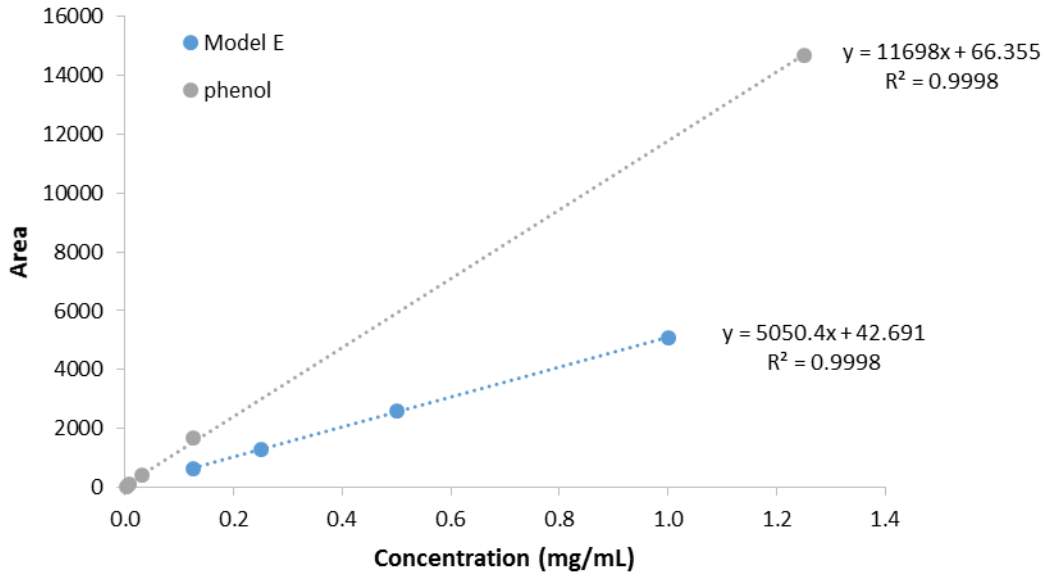

Figure 87: HPLC calibration for α-O-4 model compound benzylphenyl ether (model E), and expected degradation product phenol (absorbance at 280 nm)

Whilst a phenol yield of around 3% was observed in the degradation of model compound E in [Emim][OAc], there was no improvement in this yield on addition of 10 wt% VO(**6**)(O^{i}Pr), Figure 88. There was also no catalytic activity observed in [Ch][Lys], with <1% phenol observed either in the presence or absence of VO(**6**)(O^{i}Pr). The lack of activity of VO(**6**)(O^{i}Pr) in the degradation of the α-O-4 model provides further evidence to support the proposed mechanism of catalyst action, whereby the β-O-4 model compound coordinates to the vanadium centre through the hydroxyl moiety. In the absence of this group, for instance in the case of the α-O-4 linkage, no catalytic degradation can occur.

The slightly lower phenol yields from the background reaction in [Emim][OAc] for model E compared to model B also suggests that the mechanism of IL degradation of lignin model compounds might also be facilitated by the presence of the hydroxyl group, as α-O-4 linkages have similar C-O bond dissociation energies (BDEs) to β-O-4 linkages (around 60-70 kcal.mol^{-1}).[112]

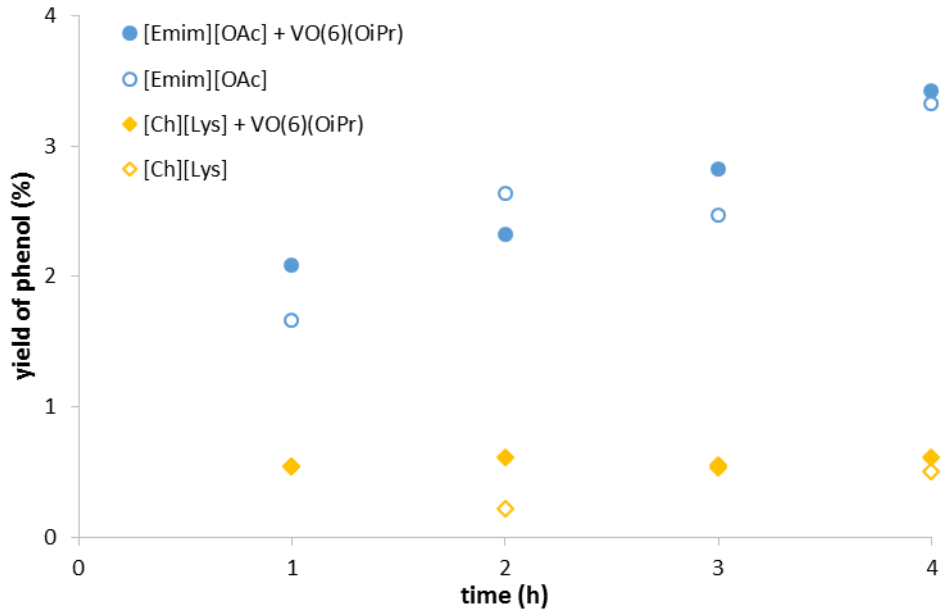

Figure 88: Degradation of α-O-4 model compound E, benzylphenyl ether, in [Emim][OAc] and [Ch][Lys]. Conditions: 140 °C, 0.1 g model E in 1 g IL, 10 wt% VO(6)(O^{i}Pr)

3.5 Degradation of alkali lignin

The pretreatment of lignocellulosic biomass or lignin feedstocks with ionic liquids has been well documented in the literature, with partial depolymerization of lignin occurring in some cases.[27, 44-46, 66, 72, 88, 185] As has been found in this work, homogeneous vanadium Schiff-base catalysts are capable of breaking down the common β-O-4 linkage in lignin model compounds. There are few examples in the literature of successful lignin depolymerization using homogeneous catalysts, mainly due to the recalcitrance and insolubility of the substrate and the likely presence of inhibiting compounds in the lignin source. The IL pretreatment method described by Varanasi *et al*. was therefore employed and adapted with a view to investigating the efficacy of these vanadium catalysts on real lignin substrates, Figure 89.[72] Alkali lignin and [Emim][OAc] were added to a pressure tube (10 wt% lignin in IL), forming a heterogeneous mixture which was then heated to 140 °C for either 1 or 4 h. After pretreatment the lignin was fully solubilized and the homogeneous solution was cooled to room temperature. The solution

was diluted with water and acidified to effect precipitation of the lignin. Following centrifugation the precipitated lignin was collected, thoroughly washed, and dried before analysis by size exclusion chromatography (SEC) and scanning electron microscopy (SEM). The supernatant was extracted by the addition of ethyl acetate and the extract was concentrated and analyzed by GC-MS.

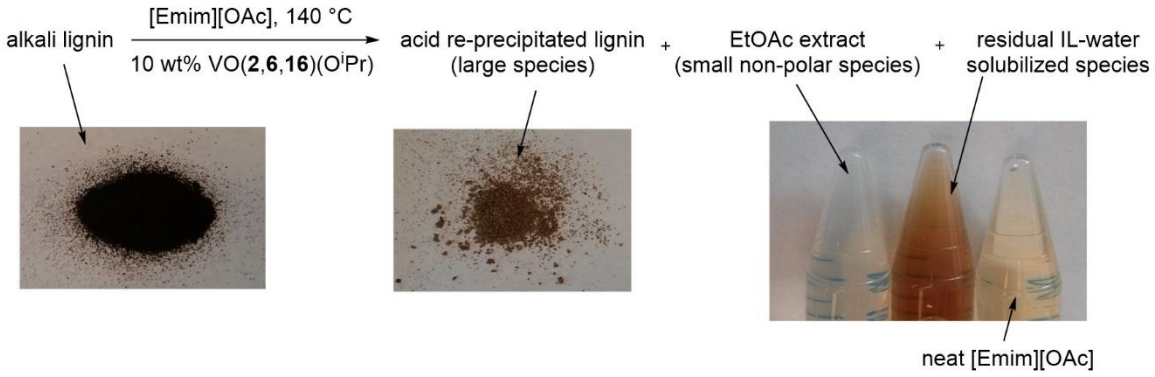

Figure 89: General method for the IL pretreatment of alkali lignin

Gravimetric analysis revealed that around 50-65% of the lignin was recovered by acid precipitation in each case, Figure 90. Whilst it appears that the highest percentage of lignin was converted in the absence of a catalyst, this could be a result of the fact that some or all of the 10 wt% catalyst is precipitated out with the residual lignin, artificially raising the other values. SEC analysis of the residual lignin indicated that, whilst there appeared to be a structural change in the lignin following pretreatment, that there was little noticeable effect of the catalyst, Figure 91. It is possibly that the catalyst is having an effect, but that the change in molecular weight is too small to be identified by SEC analysis. This effect has been observed previously.[27] GC-MS analysis was attempted in order to identify smaller species such as small oligomers and monomers which may have been cleaved from the lignin. Unfortunately, very little solid was recovered from the EtOAc extraction and no compounds were able to be identified by GC-MS. It is likely that many of the oligomeric and small polar compounds are more soluble in the residual IL-water mixture than in the organic solvent. As can be seen in Figure 89, the brown colour of the IL-water mixture compared with the neat [Emim][OAc] suggests the presence of depolymerized lignin species. The recovery of these compounds from the IL is an ongoing problem which has yet to be overcome.[72]

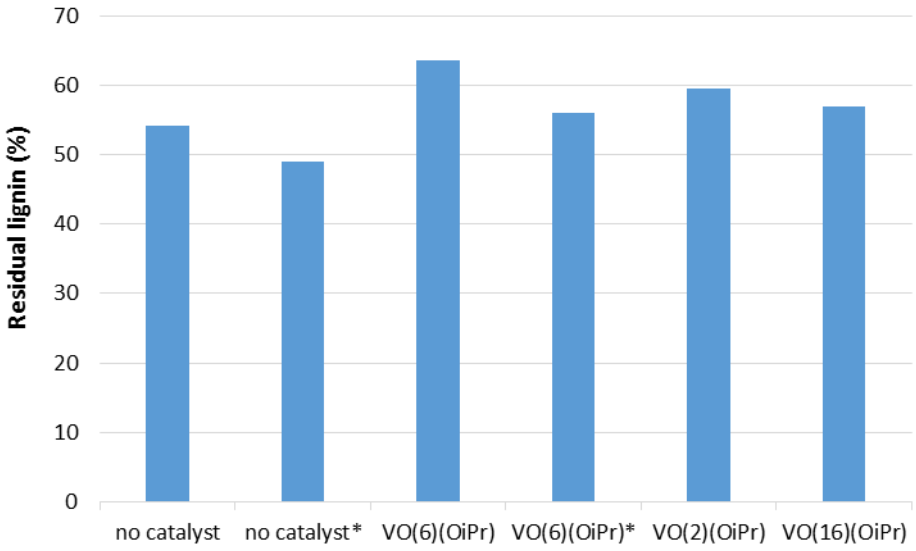

Figure 90: Residual lignin recovered after IL pretreatment. Conditions: [Emim][OAc], 140 °C, 1 h (*4 h), 0.1 g lignin in 1 g IL, 10 wt% VO(2,6,16)(O^{i}Pr)

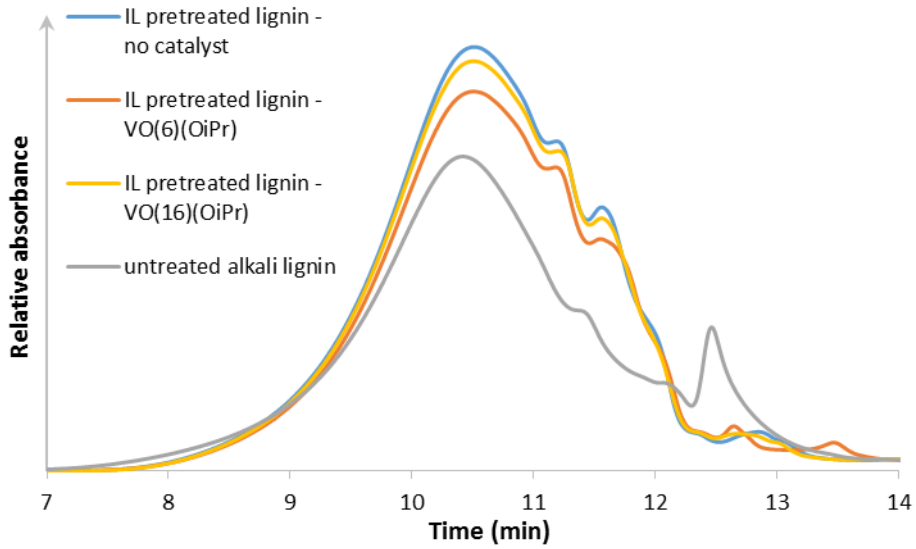

Figure 91: SEC analysis of re-precipitated lignin. Pretreatment conditions: [Emim][OAc], 140 °C, 4 h, 0.1 g lignin in 1 g IL, 10 wt% VO(6,16)(O^{i}Pr)

The morphology of samples of untreated and IL pretreated alkali lignin were compared using scanning electron microscopy (SEM). SEM analysis of the lignin before degradation revealed discrete particles which are approximately 100 µm in diameter, Figure 92. Several of these are damaged and the porous nature of these particles are clearly seen, Figure 93. It is clear from the micrographs that treatment with the IL is having a major effect on the morphology of the particles, with significantly smaller diameter particles being observed after treatment, Figure

94 [no catalyst] and Figure 95 [with 10 wt% VO(**2**,**6**)(O^iPr)]. It is important to note that the micrographs of lignin pretreated with and without the catalysts are to all intents and purposes similar. However, the reduction in particle size, and subsequent increase in exposed surface area, on IL pretreatment is important as this will increase the amount of lignin exposed to the catalyst for potential degradation.

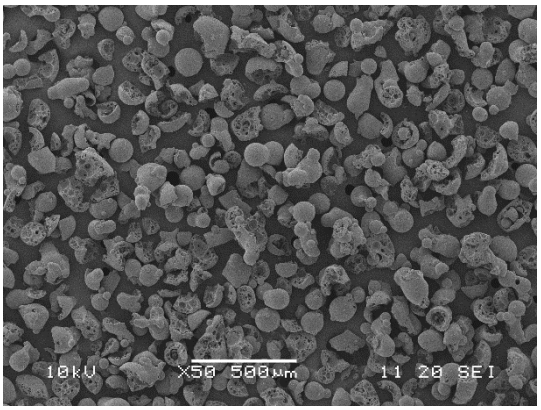

Figure 92: SEM micrograph of untreated alkali lignin

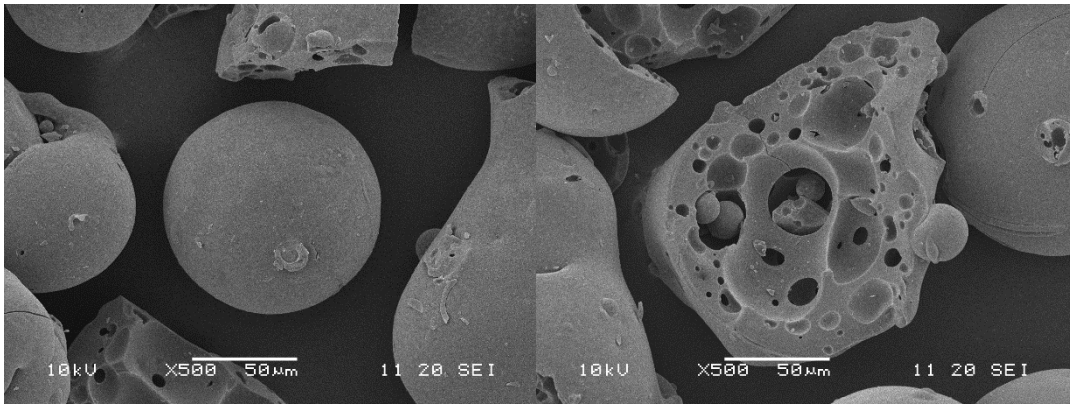

Figure 93: SEM micrographs of untreated alkali lignin particles. Left: undamaged, right: damaged

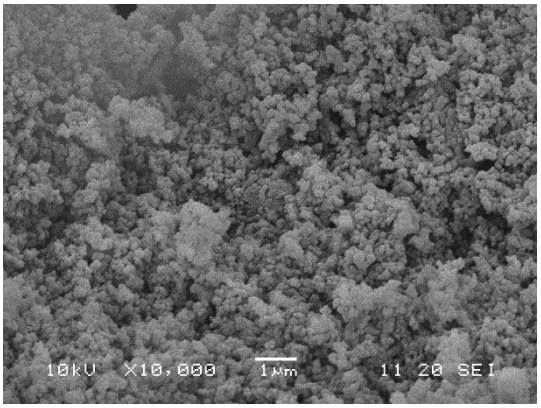

Figure 94: SEM micrograph of IL pretreated alkali lignin. Pretreatment conditions: [Emim][OAc], 140 °C, 4 h, 0.1 g lignin in 1 g IL, no catalyst

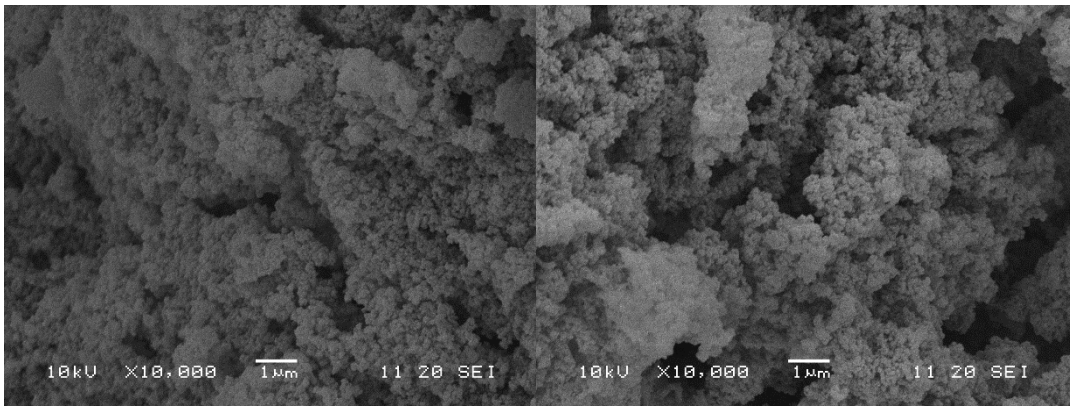

Figure 95: SEM micrograph of IL pretreated alkali lignin in the presence of VO(2)(O^iPr), left, and VO(6)(O^iPr), right. Pretreatment conditions: [Emim][OAc], 140 °C, 1 h, 0.1 g lignin in 1 g IL, 10 wt% VO(2,6)(O^iPr)

3.6 Conclusions

Ionic liquids, particularly imidazolium-based species, have been shown to be effective for the pretreatment of biomass and can be used to produce a clean, solubilized lignin stream.[56, 61, 73] This could facilitate lignin valorization to value-added monomeric phenolic products by allowing homogeneous catalysts improved access to the lignin polymer structure. There is also some precedent for degradation of the lignin polymer by certain ILs, including [Emim][OAc].[44, 72]

Homogeneous vanadium Schiff-base catalysts VO(**2**,**6**)(O^{i}Pr), and vanadium-dipicolinate complex VO(**16**)(O^{i}Pr), previously tested in organic solvents such as DMSO, were found to be active for the degradation of β-O-4 model lignin compounds to phenol and acetophenone in a range of ILs including [Emim][OAc]. Some degradation of the model compounds was observed in the absence of a catalyst, supporting the previous observations of partial lignin depolymerization by [Emim][OAc] itself.[44, 72]

The activity of VO(**2**,**6**,**16**)(O^{i}Pr) was compared in both [Emim][OAc] and DMSO. In DMSO, the activity of the catalysts was dramatically different, with the phenol yield increasing significantly from VO(**16**)(O^{i}Pr) < VO(**2**)(O^{i}Pr) < VO(**6**)(O^{i}Pr). In [Emim][OAc], however, the catalysts behaved almost identically, leading to the hypothesis that the active catalytic species in this case is the same for all three complexes, formed by an interaction of the complexes with the IL.

When compared directly with their activity in DMSO it was noted that the activity of VO(**2**,**6**)(O^{i}Pr) in [Emim][OAc] was significantly lower, suggesting that the active catalyst formed in the IL was less active than that in the DMSO. Conversely, the activity of VO(**16**)(O^{i}Pr) was improved in [Emim][OAc] relative to in DMSO.

Unlike in DMSO, no evidence of formation of the benzylic oxidation product (OP) was observed in any of the reactions in [Emim][OAc], and the reaction was initially suspected to be 100% selective for C-O bond cleavage over oxidation. A series of kinetic studies in [Emim][OAc] and DMSO:[Emim][OAc] solvent mixtures revealed that the OP was in fact produced, but that it underwent subsequent degradation under the reaction conditions, forming phenol. This degradation was much faster in [Emim][OAc] than in DMSO, and occurred even in the absence of a catalyst.

Several cheaper, commercially available metal catalysts were found to be inactive for the degradation of β-O-4 model lignin compounds in DMSO and [Emim][OAc], thereby justifying

further research into more complex species such as VO(**2**,**6**,**16**)(O^iPr) for lignin degradation in ILs. However, there are several issues such as catalyst stability, catalyst and IL recyclability, and product recovery, which require further investigation.

Whilst successful in the degradation of the common lignin β-O-4 linkage, VO(**6**)(O^iPr) did not appear to assist in cleavage of the α-O-4 linkage. This is likely due to the lack of hydroxyl group required for coordination to the catalyst, and suggests that this catalyst would also be incapable of catalyzing the degradation of other lignin linkages.

Preliminary studies into the effect of homogeneous Schiff-base catalysts on the IL pretreatment of lignin were not conclusive, however the increased surface area of the pretreated lignin suggests that this might be a more viable substrate for subsequent catalytic degradation than other available lignin streams.

3.7 Future work

As has been mentioned, further analysis of catalyst stability in a range of ionic liquids (and potentially IL:DMSO mixtures), catalyst and IL recyclability, and the ease of product recovery from the IL would all be necessary in order to determine whether or not this might be a viable technique for the selective depolymerization of lignin in a biorefinery situation. IL cost is also a major factor, and the use of renewable, even lignin derived ILs should be considered.[74, 186, 187]

Catalytic degradation of a range of IL pretreated lignins should be attempted, and the lignins analysed by a range of techniques including SEC for evidence of molecular weight lowering, HSQC NMR to determine the proportion of different linkages which are cleaved during the process, and GC-MS in order to identify any monomeric or small oligomeric products. ^{31}P NMR of phosphitylated lignins could also be employed to monitor the proportion of phenolic groups before and after catalytic treatment.

4. Depolymerized lignin compounds as fuel additives

As the production of biodiesel increases and the chemical structures of biodiesels diversify due to the use of new feedstocks, it is becoming increasingly important to ensure that the quality of the fuel is controlled. A major issue with the use of biodiesel over conventional petroleum diesel is its inherently lower oxidative stability. Oxidation of biodiesel has a negative impact on the performance of the fuel as the associated increase in properties such as acid value and kinematic viscosity can lead to detrimental effects such as corrosion within the engine and particulate formation resulting in filter clogging. The addition of phenolic antioxidants can mitigate the oxidation of biodiesel. The naturally occurring antioxidant α-tocopherol is present in all biodiesels, however its presence alone is frequently not enough to impart sufficient oxidative stability to the fuel.[127] The commercial antioxidant BHT, Figure 96a is widely used in the fuel and food industries, though it is derived from petroleum sources.[188] The total global market for all fuel additives, including antioxidants, was estimated at $6.2 bn in 2015.[189]

The activity of phenolic antioxidants has been found to be dependent on both the lability of the phenoxy proton, and also the ability of *ortho* and *para* substituents on the aromatic ring to stabilise a phenoxy radical. Depolymerization of the abundant, aromatic biopolymer lignin to produce renewable phenols has been widely researched.[21, 190] Monomeric phenols available from the depolymerization of lignin include guaiacol, eugenol and syringol, Figure 96b-d.[36, 72] These species contain *ortho* and *para* substituents which could potentially assist in the stabilisation of phenoxy radicals. In order to assess their suitability as antioxidants, a high-throughput method for accelerated fuel oxidation tests was developed and used to screen the candidate antioxidant species in Figure 96 at a range of loadings in biodiesel.

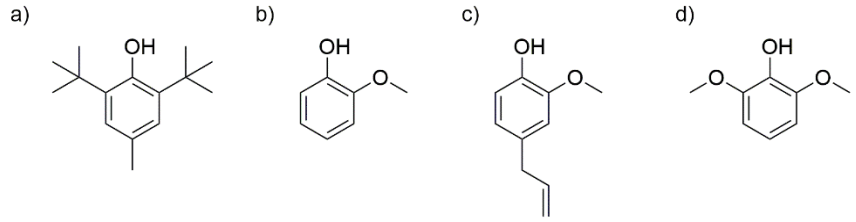

Figure 96: Structures of candidate antioxidant species used in this study; a) non-renewable commercial antioxidant butylated hydroxytoluene, (BHT); renewable monolignols b) guaiacol, c) eugenol, d) syringol

4.1 Development of a high-throughput fuel oxidation rig

In order to investigate the oxidative stability of a range of fuels in a high-throughput manner, a ten port accelerated oxidation rig was designed and built in collaboration with Joshua Spellman, Figure 97. Accelerated fuel oxidation tests, such as the Rancimat and PetroOXY tests have been widely employed in the analysis of the oxidative stability of biodiesel as real-time studies over the course of months or years are often unfeasible.[133, 154, 191] A schematic of one port is shown in Figure 98. Rapeseed methyl ester (RME) biodiesel donated by BP was employed as the fuel in these experiments. Its FAME profile, determined by GC-MS is approximately 50% 18:2, 28% 18:1, 11% 16:1 and 8% 18:3, with trace amounts of other FAME species being present. The fuel samples were held at an elevated temperature and a controlled airflow was passed through the samples. The exhaust from the samples was passed through a condenser to recapture lost volatiles. Although the samples were not stirred, the high airflow through the samples provided sufficient agitation. The sample vessel and air inlet were designed such that the fuel was not in contact with metal, which could catalyse the oxidation. The air was supplied through PTFE tubing and delivered into the fuel through a pipette tip, rather than a metal needle. Originally, thermally resistant plastic tips were used, however these were not stable enough under the conditions and often bent during the experiments, restricting airflow to the sample and severely influencing the results. These were therefore replaced with custom-made glass tips which were found to provide a constant and reliable flow through all ten samples across a number of experiments. Approximately 0.1 mL samples were taken from each of the ten ports at various intervals during the oxidation, and allowed to cool before being analysed by refractive index.

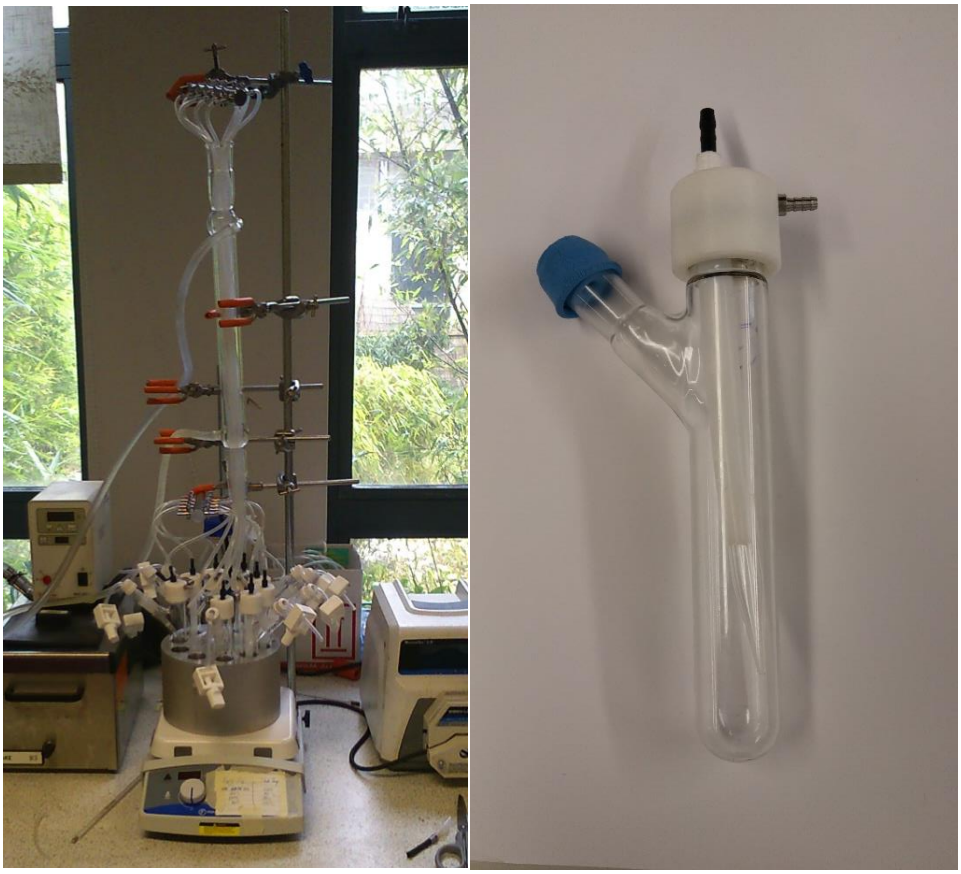

Figure 97: High throughput fuel oxidation rig (L) and close up of one of the sample ports (R)

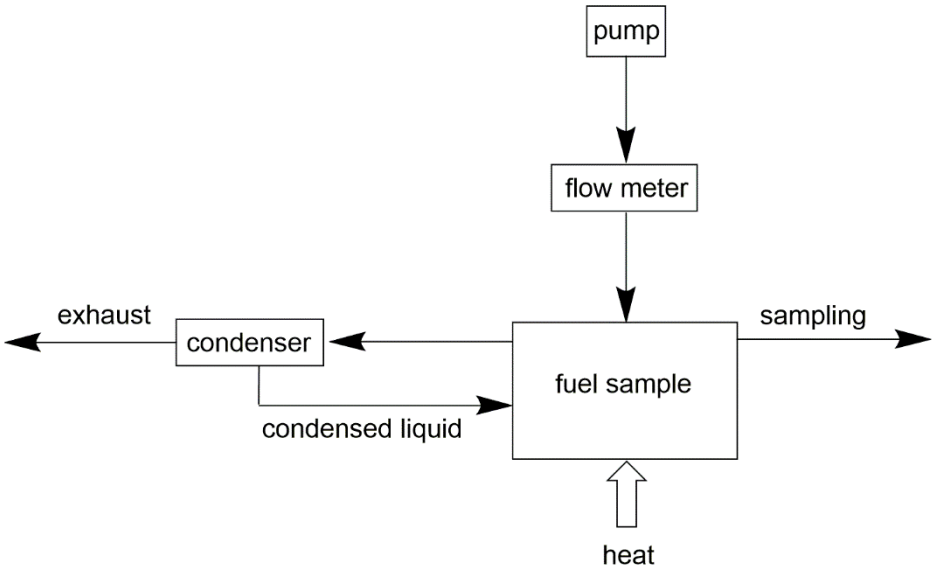

Figure 98: Schematic of one of the ports in the high-throughput fuel oxidation rig utilised in this study

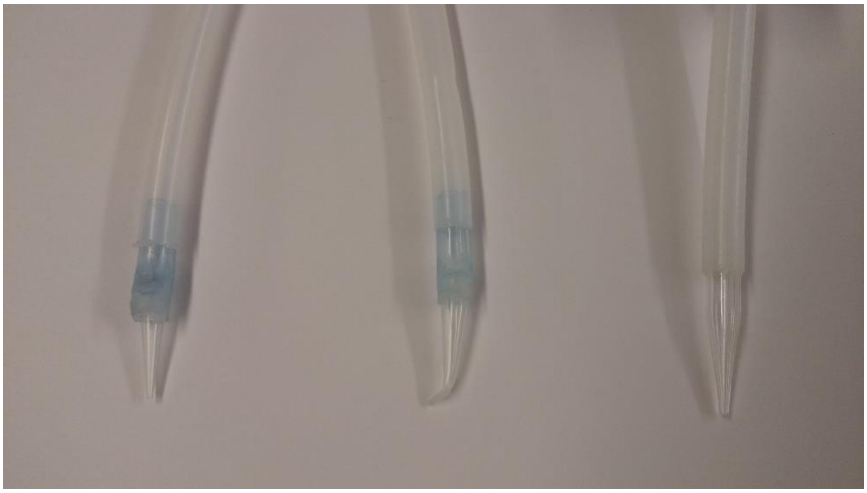

Figure 99: (From L-R) Original plastic tip (before experiment), bent plastic tip (after experiment), glass tip (after several experiments)

4.1.1 Temperature calibration

The ambient temperature of the laboratory was noted to vary significantly during the course of the experiments. As RI is strongly dependent on the temperature of the sample, the RI of each fuel blend was calibrated over a range of temperatures and the values as presented have been corrected to compensate for the ambient temperature difference. A calibration graph for selected species is shown in Figure 100. The gradient values, x, are statistically equivalent, demonstrating that the addition of the antioxidant species has no discernible effect on the RI of the fuel over the relevant temperature range. All RI values presented in subsequent graphs have been adjusted to account for any fluctuations in the ambient temperature of the laboratory.

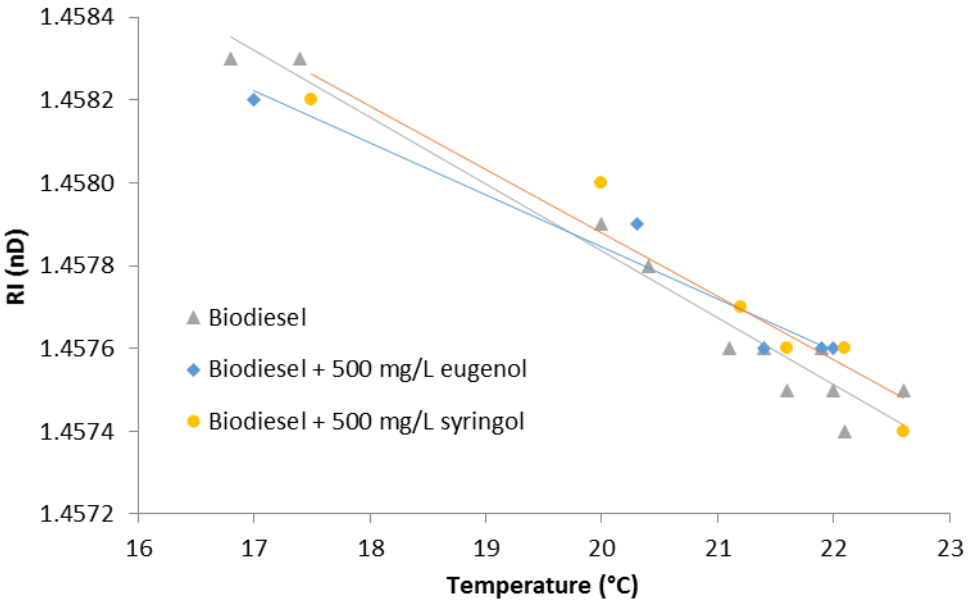

Fuel	x (nD/°C)
Biodiesel	$-1.6 \times 10^{-4} \pm 0.1 \times 10^{-4}$
Biodiesel + 500 mg/L eugenol	$-1.3 \times 10^{-4} \pm 0.2 \times 10^{-4}$
Biodiesel + 500 mg/L syringol	$-1.5 \times 10^{-4} \pm 0.2 \times 10^{-4}$

Figure 100: Calibration graph of refractive index of RME biodiesel over a range of temperatures, with a table of x values

4.1.2 Internal experimental error

To minimize the errors associated with fluctuations in the temperature and airflow, each "experiment" comprised internal repeats of 5 neat fuel samples and 5 samples containing the antioxidant. The variation across 5 samples of neat biodiesel under experimental conditions is shown in Figure 101. The values are presented as a change in refractive index from the initial value, ΔRI. The variation in ΔRI between the samples increased over time to a maximum of approximately 0.001 nD. The standard deviation across the 5 samples was calculated for each data point and is represented by the error bars on subsequent graphs.

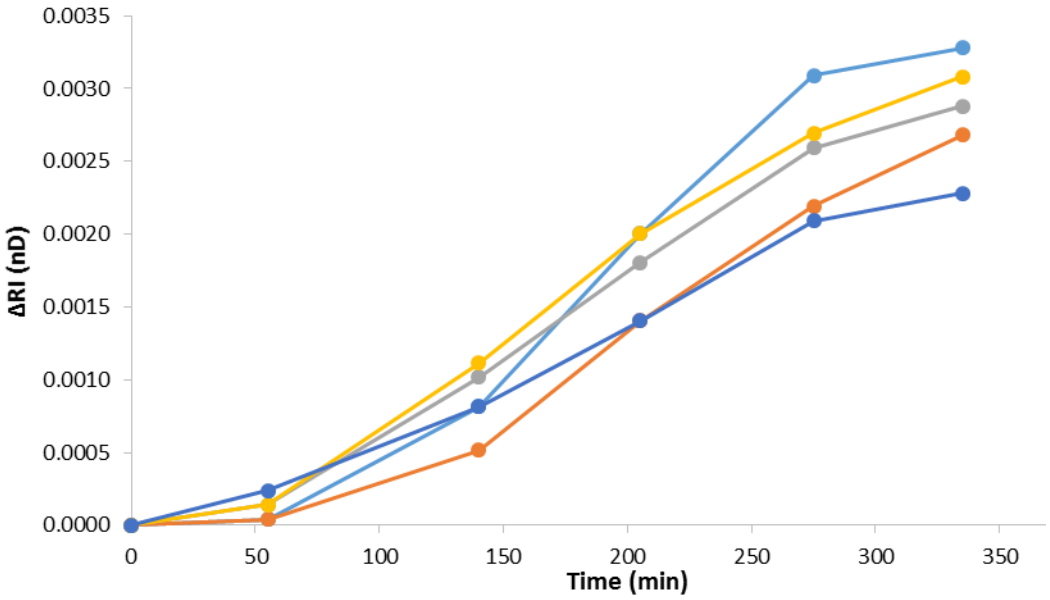

Figure 101: Internal repeats of biodiesel oxidation. Conditions: 110 °C, 0.65 mL.min^{-1} airflow per sample

4.1.3 External experimental error

The external error of the system was assessed by comparing the results of 5 different neat biodiesel oxidation experiments, Figure 102. The error bars denoting the standard deviation in the internal repeats from each experiment show good reproducibility across these 5 external repeats. The median result (grey) was therefore taken as the comparative standard for further experiments.

It should be noted at this stage that there is little to no observable induction period (IP) for this biodiesel under these conditions. It is likely that the IP is too short to be detected by this method suggesting that oxidation occurs very efficiently under these conditions, and possibly that a very low level of naturally occurring α-tocopherol is present in this biodiesel.

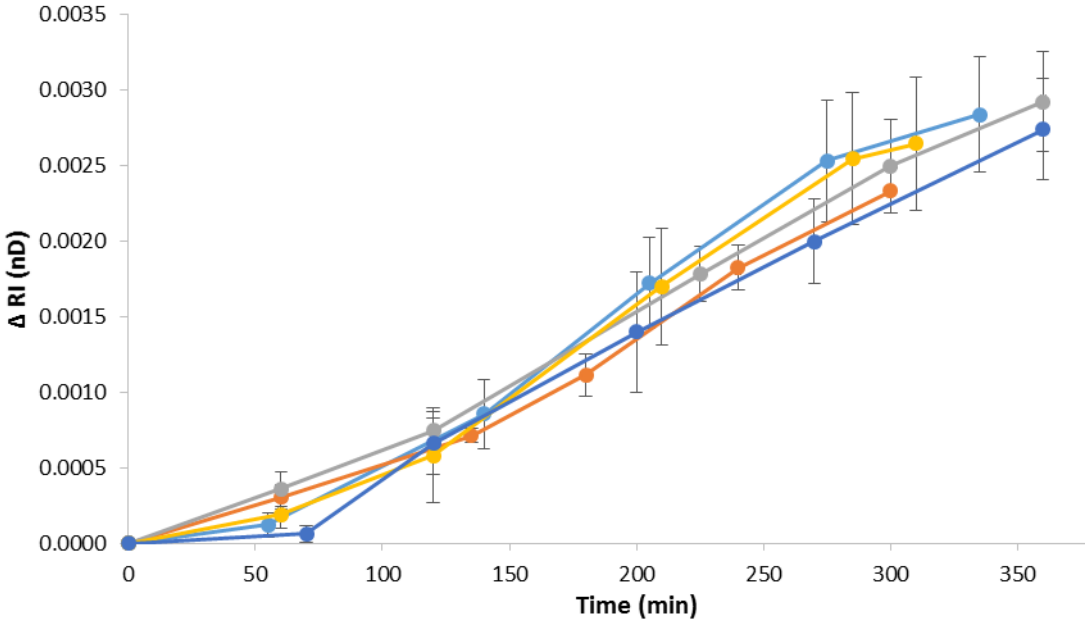

Figure 102: External repeats from 5 different biodiesel oxidation experiments. Conditions: 110 °C, 0.65 mL.min^{-1} airflow per sample. Error bars represent the standard deviation over 5 internal repeats.

4.2 Investigation of the oxidative stability of biodiesel

4.2.1 Effect of antioxidant structure

In order to investigate the influence of structure on the behaviour of these antioxidants, the four substituted phenols were compared under equivalent conditions, Figure 103. Standard concentrations of synthetic antioxidants in biodiesel are usually within the range of 200-1000 ppm and many previous investigations have focussed on this loading window.[133, 137, 142]

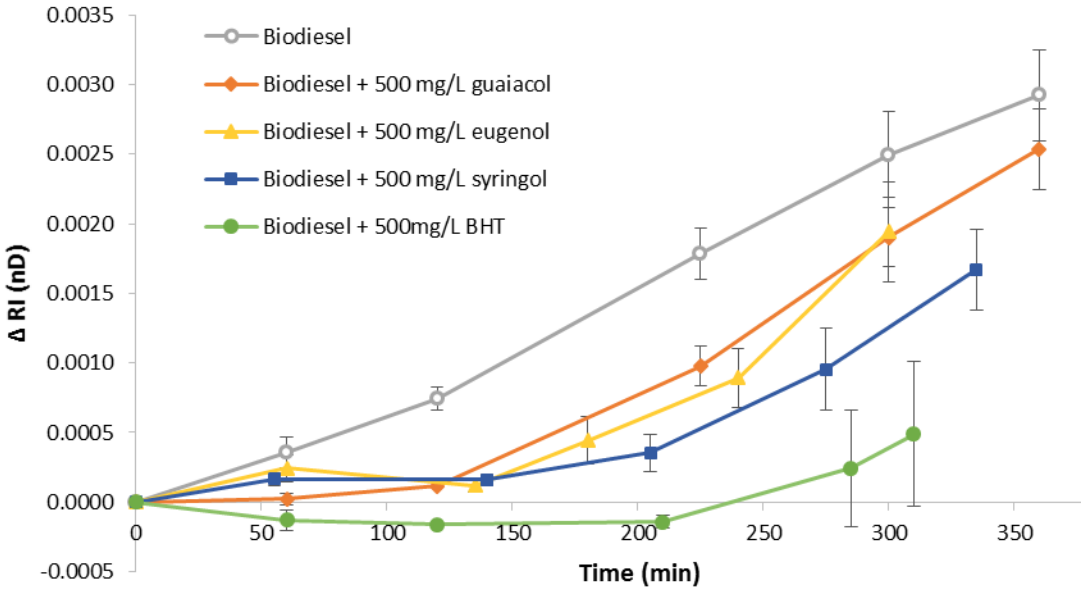

Figure 103: Effect of antioxidant structure on the oxidation of RME biodiesel. Conditions: 110 °C, 0.65 mL.min^{-1} airflow per sample

At the 500 mg.L^{-1} antioxidant loading, all of the phenols increase the oxidative stability of the RME biodiesel under the conditions tested. Di-methoxy substituted phenol, syringol, inhibited the oxidation more than mono-methoxy substituted phenols guaiacol and eugenol, which slowed the oxidation by a similar rate to one another. The di-*tert*-butyl substituted commercial antioxidant BHT performed the best of the four, exhibiting a clear induction period of around 200 min. Considering their molar loadings, this effect is even more pronounced, as BHT is present at the lowest molar loading (2 mmol.L^{-1}), whilst eugenol and syringol are present at 3 mmol.L^{-1} and guaiacol is the most concentrated at 4 mmol.L^{-1}.

As phenolic species work as radical scavenging antioxidants,[137] this trend of antioxidant activity can be explained by comparing the ability of the four species to stabilise a phenoxy radical. Bulky *ortho*-substituents are known to increase phenoxy radical stability by providing steric hindrance around the radical centre and inhibiting further reaction, whilst certain *ortho*- and *para*-substituents are capable of providing extra stability *via* electron donation to radicals formed by resonance stabilisation at the 2', 4' and 6' positions, Figure 104.[163, 192] The trend in antioxidant activity of guaiacol ≈ eugenol < syringol < BHT is likely to be a dual effect, resulting from both the increase in steric bulk around the radical centre (large R^1, R^2) and also the stabilisation of resonance structures by increasing electron donation from *ortho*- and *para*-substituents (R^1, R^2, R^3). Guaiacol and eugenol have only a single *ortho*-methoxy substituent and therefore the lowest amount of steric bulk around the phenoxy position. The slightly increased performance of eugenol over guaiacol might be explained by a stabilising inductive effect from the *para*-alkyl substituent (R_3). The significant improvement in activity of syringol compared to guaiacol suggests that protection of the phenoxy radical by increased steric bulk is more important for the activity of the antioxidant than additional stabilisation by substituents at the *para*-position. The fact that the most hindered di-*tert*-butyl substituted phenol, BHT, performed dramatically better even than syringol appears to support this theory, although it is possible that there is also an increased inductive radical-stabilising effect from the alkyl substituents as compared to the alkoxides.

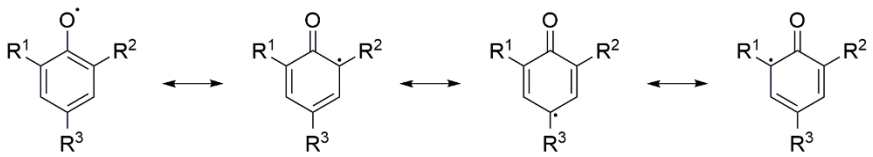

Figure 104: Resonance stabilization of phenoxy radicals

4.2.2 Effect of antioxidant loading

It was expected that the activity of the antioxidants would be dependent on concentration. This was confirmed by comparison of the four antioxidants across a range of loadings, Figure 105, as all of the phenols exhibit increasing activity at higher loadings. For guaiacol and eugenol, this effect is relatively small, and increasing the loading to 1000 mg.L^{-1} does not improve the oxidative stability of the fuel to the same degree as only 500 mg.L^{-1} of the commercial antioxidant BHT. Syringol, which was found to be more effective antioxidant than eugenol and guaiacol at 500 mg.L^{-1}, is not soluble in the biodiesel at 1000 mg.L^{-1}. However, addition of 500 mg.L^{-1} syringol appears to be as effective at increasing the stability of the RME biodiesel as either eugenol or guaiacol at 1000 mg.L^{-1}, demonstrating that syringol is a significantly better antioxidant than the other two renewable phenols.

It should be noted that the effect of all four antioxidants at 50 mg.L^{-1} is very similar. This could be a result of the harsh nature of this oxidation technique. At this fast rate of oxidation, the antioxidants appear to act the same at this loading, however if the oxidation was slowed it is possible that a difference in performance would be observed. Alternatively, this similarity in performance could imply that a minimum amount of the antioxidant is required in order for it to be effective. If there is insufficient antioxidant present to react with the generated peroxide species, the relative activity of the antioxidant becomes irrelevant as the excess peroxide species are able to propagate the chain reaction.

At equivalent loadings, BHT outperformed the three renewable phenols. However, in an attempt to move towards renewable antioxidants, and in turn displacing a larger proportion of fossil-derived fuel components, it might be feasible to replace BHT with a large amount of a renewable component, that while less active, would still perform as an antioxidant at the higher loading. Ideally, the most active of these renewable antioxidants would be used, however the lack of solubility of syringol at high loadings would prohibit this. From these preliminary findings, eugenol appears to have a slightly improved performance over guaiacol, however the proportion of eugenol available from lignin depolymerization is much smaller than that of guaiacol.[72] The effects of blending high levels of these antioxidants, and specifically guaiacol, into biodiesel was therefore further investigated.

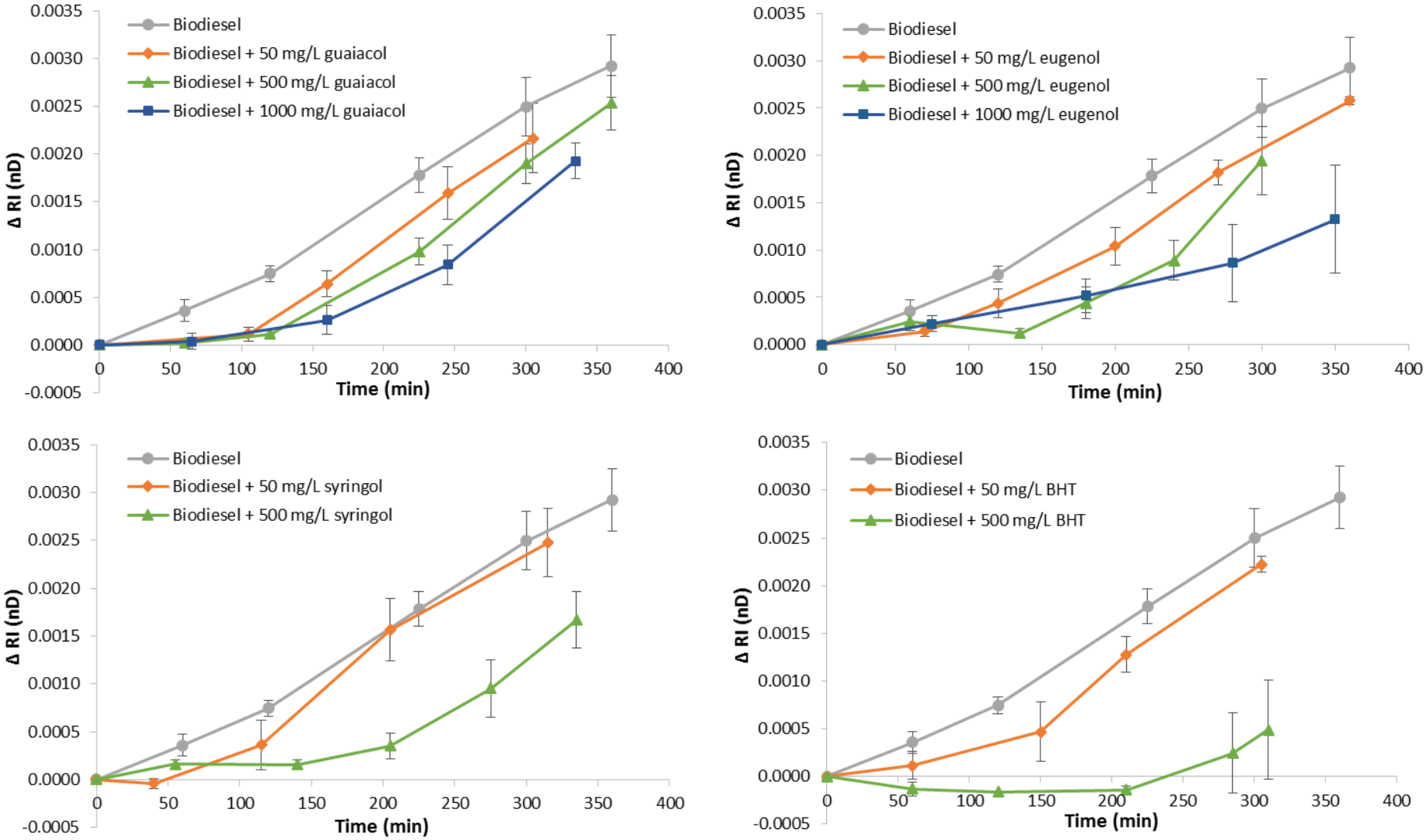

Figure 105: Effect of antioxidant loading on oxidation of RME biodiesel. Conditions 110 °C, 0.65 mL.min^{-1} airflow per sample

4.3 Fuel properties

A key requirement of any fuel additive is that it does not change the fuel properties of the blend significantly. The antioxidant activity of the renewable phenols guaiacol, eugenol and syringol is significantly lower than that of the commercial and non-renewable antioxidant BHT, however it is hypothesised that these species could be utilised at higher loadings than conventional antioxidants in order to increase both the stability of the fuel and potentially its percentage of renewable components (for example in biodiesel/petrodiesel blends). In order to provide a preliminary assessment as to whether it would be possible to blend these renewable phenols with biodiesel at higher concentrations without negatively affecting the quality and performance of the fuel, several key fuel properties of the blends were assessed.

4.3.1 Maximum blend level

The blend level of the renewable phenols in RME biodiesel was investigated, in order to determine the maximum amount which could feasibly be introduced into the fuel, Table 17. As has already been noted, the maximum loading of syringol in RME biodiesel was found to be less than 1000 mg.L^{-1}, above which the solid phenol was insoluble. The two liquid phenols could be blended at significantly higher levels; eugenol was miscible to at least 1000 mg.L^{-1} and guaiacol was fully miscible with RME biodiesel at any concentration.

Table 17: Blend level of renewable antioxidants guaiacol, eugenol and syringol in RME biodiesel. ✓ miscible, ✖ immiscible/not soluble †not determined

Antioxidant	Blend level			
	50 mg.L^{-1}	500 mg.L^{-1}	1000 mg.L^{-1}	1:1 (v/v)
Guaiacol	✓	✓	✓	✓
Eugenol	✓	✓	✓	N/D†
Syringol	✓	✓	✖	✖

4.3.2 Cloud point

The cold temperature properties of biodiesel are important, as fuels can encounter low temperature conditions in cold weather or by coming into contact with cold surfaces such as heat exchangers. On cooling, the FAME molecules in biodiesel begin to freeze, forming waxes which give the biodiesel a cloudy appearance. The various compounds present in biodiesel have a range of melting points, and therefore a single melting point of biodiesel cannot be determined. The cloud point, or wax appearance temperature (WAT), of a liquid mixture is

the temperature at which crystallization begins to occur and is frequently used as an indication of the cold temperature properties of a fuel. Measurement of the WAT of complex mixtures such as fuels presents a challenge, as it can be difficult to determine the exact temperature of the onset of crystallisation. Previous ASTM methods used in the determination of the WAT of petroleum liquids have involved visual inspection of the samples (ASTM D3117, D2500).[193] These methods are therefore subject to the judgement of the inspector and, as such, are often difficult to reproduce reliably.

Differential scanning calorimetry (DSC) has been used in the determination of the WAT of various petroleum liquids (ASTM D4419-96).[193-195] DSC is a type of thermal analysis in which the heat required to change the temperature of a sample is monitored as a function of temperature. This is done in reference to a sample of known heat capacity. Measurement of the WAT by DSC involves cooling a sample of fuel until a change in the heat flow is detected. A rise in the heat flow, which corresponds to an exothermic process, indicates a phase transition, in this case from liquid to solid. The accuracy and resolution of DSC for determination of the WAT can be dependent on the rate of cooling, with a slower cooling rate potentially providing increased accuracy. Primarily, the cloud points of the biodiesel blends used in these experiments were investigated by DSC. Following literature precedent, a cooling rate of 2 °C was selected.[194, 195]

The DSC thermograms of neat RME biodiesel, biodiesel + 500 mg.L^{-1} syringol, biodiesel + 500 mg.L^{-1} guaiacol, and biodiesel + 1000 mg.L^{-1} eugenol are very similar, indicating that the presence of the renewable phenols at these loadings has very little effect on the cloud point of the fuel, which was found to be -14 °C, Figure 106. A 1:1 mixture of RME biodiesel and guaiacol, however, was found to have a significantly depressed cloud point of -24 °C compared to the neat biodiesel, Figure 107. It can be deduced from these results that a small amount of added phenol is not sufficient to disrupt the stacking of the hydrocarbon chains, and therefore has little effect on the cloud point of the blends. However, above a certain blend level the phenol is able to significantly disrupt the associative forces between the FAME molecules as the sample cools, thereby causing a reduction in the cloud point.

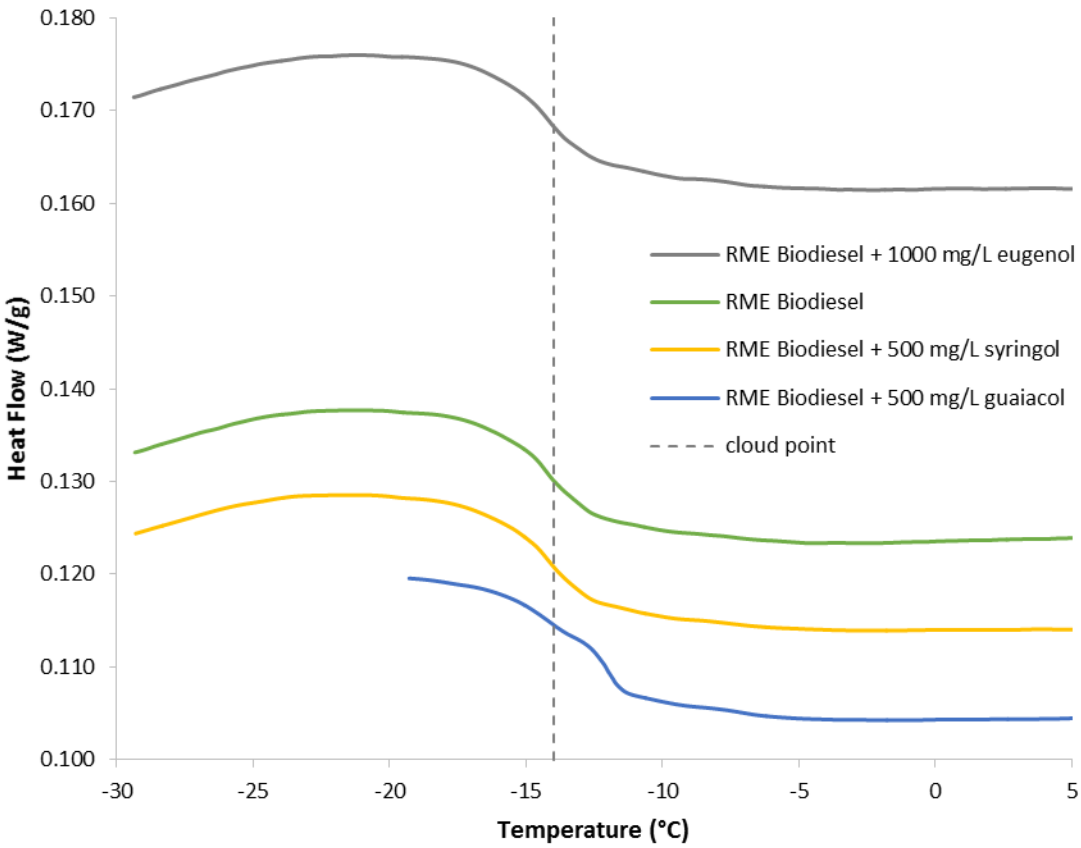

Figure 106: DSC thermograms indicating the cloud point (-14 °C) of neat RME biodiesel and RME biodiesel containing renewable antioxidants

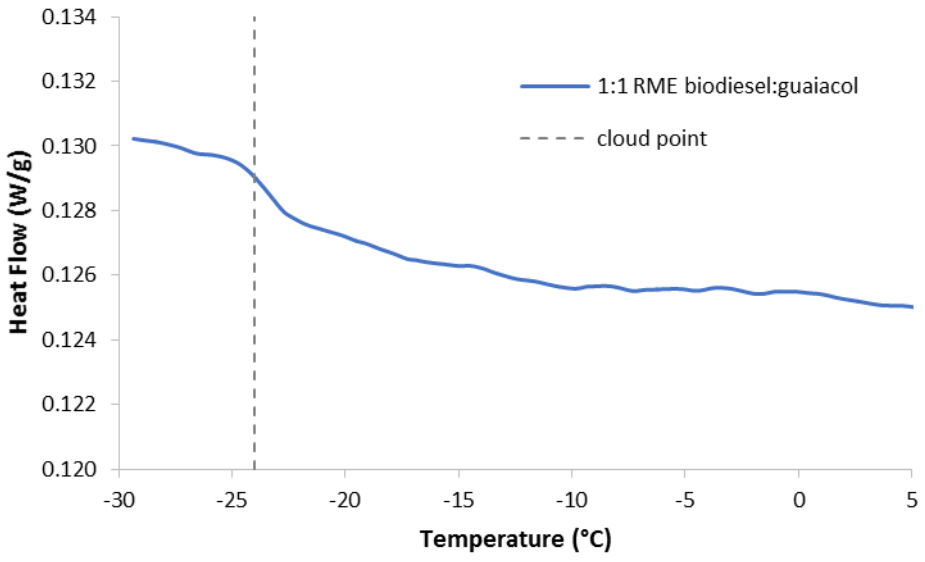

Figure 107: DSC thermogram indicating the cloud point (-24 °C) of a 1:1 mixture of RME biodiesel and guaiacol

4.3.3 Kinematic viscosity

Kinematic viscosity is a vital fuel parameter as it can be indicative of the presence of higher molecular weight species which can form insoluble particulates. Both viscous fuel and the presence of particulates can cause issues in the fuel delivery system, leading to high pressure drops across filters as well as filter-clogging. The kinematic viscosity of RME biodiesel with and without the presence of added antioxidants was therefore measured, Figure 108. The viscosities of blends with 500 mg.L^{-1} syringol (RME-S500), 1000 mg.L^{-1} eugenol (RME-E1000) and 10000 mg.L^{-1} guaiacol (RME-G10000) were found to be statistically indistinguishable from that of the neat biodiesel and therefore well with the EN14124 specifications. As guaiacol was found to be fully miscible with RME biodiesel, the viscosity of a 1:1 mixture of the two was also determined. Whilst there was a significant reduction in the viscosity of this mixture compared with that of the unadulterated biodiesel, the fuel blend still fell within the specified boundaries.

These results appear to corroborate the theory presented for the trend in cloud points of these fuel blends. The interaction between the FAME molecules and the phenol is weak enough that at relatively low levels of antioxidant addition, there is no significant disruption of the intermolecular forces between the FAME molecules and the viscosity remains unchanged. However higher concentrations of the phenol are able to effect a reduction in the viscosity of the fuel by preventing the efficient stacking of the FAME chains.

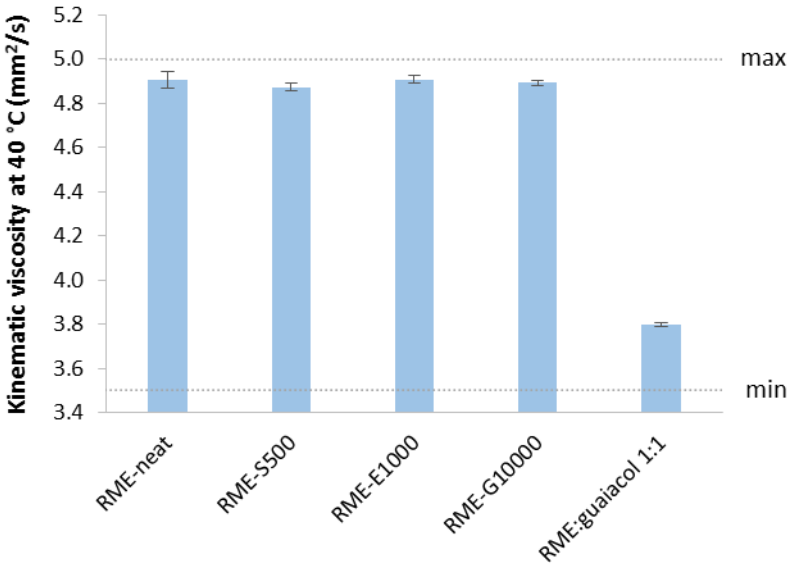

Figure 108: Kinematic viscosities of RME biodiesel (RME-neat) and a range of biodiesel-antioxidant blends; 500 mg.L^{-1} syringol (RME-S500), 1000 mg.L^{-1} eugenol (RME-E1000), 10000 mg.L^{-1} guaiacol (RME-G10000) and a 1:1 (v/v) mixture of RME biodiesel and guaiacol (RME:guaiacol 1:1). "max" and "min" denote the maximum and minimum limits as outlined in the EN14214 specifications

4.3.4 Flash point

The flash point of a fuel is a measure of its tendency to form a flammable mixture with air. In compression engines the fuel is compressed until reaching the autoignition temperature where combustion occurs. Therefore for diesel-type fuels a minimum flash point is mandated for safety reasons. The flash point of diesel, for example, must be higher than 55 °C (EN 590). The flash point of a mixture is related to its lowest flash point components, as long as they are present above approximately 5%. This is due to the ability of these components to create a combustible vapour above the fuel. The flash points of all three renewable antioxidant species and BHT are well in excess of the minimum flash point mandated in the EN590 specifications for diesel and would therefore the flash point of any blends would be that of the neat diesel.

Table 18: Flash points of phenolic antioxidants and the EN590 standard for diesel. †closed cup

	Flash point† (°C)
Guaiacol	82
Eugenol	112
Syringol	140
BHT	127
EN590	>55

These fuel properties are by no means exhaustive, however, the fact that relatively high concentrations of these antioxidants have little effect on the cloud point, viscosity and flash point of the fuels is a promising indicator that they have the potential to be employed as additives at these concentrations.

4.4 Conclusions

An accelerated oxidation rig was developed for the high-throughput screening of candidate antioxidant species in biodiesel. Refractive index was employed as a quick and effective method of monitoring biodiesel oxidation. The external and internal experimental errors of the oxidation rig were investigated in preliminary tests with RME biodiesel and the results demonstrated good reliability and reproducibility.

The accelerated oxidation rig was then used to assess the antioxidant activity of renewable phenols guaiacol, eugenol and syringol, which can be obtained from the depolymerization of lignin, in RME biodiesel. Their activity was compared to that of commercial antioxidant BHT. At a loading of 500 $mg.L^{-1}$, all three renewable phenols were successful in increasing the stability of the RME biodiesel, however they were significantly less active than BHT at the same loading. The trend in activity of guaiacol < eugenol < syringol < BHT was explained by the increase in the ability of the species to stabilise a phenoxy radical, due to increasing substitution and steric hindrance around the radical centre. The activity of the antioxidants was observed to be dependent on loading, with increased fuel stabilisation at higher concentrations of the phenols.

Although the renewable phenols were less active than BHT at equivalent loadings, it was hypothesised that they could be blended at higher loadings into biodiesel in order to effect the required oxidative stability, without significantly affecting the fuel properties. The maximum blend level, viscosity, cloud point and flash point of blends of the phenols in RME biodiesel were therefore investigated. Liquid phenols eugenol and guaiacol could be blended at much higher levels than the solid syringol, which was insoluble at 1000 $mg.L^{-1}$. Guaiacol was fully miscible with RME biodiesel. The cloud point and viscosity of RME biodiesel with up to 1000 $mg.L^{-1}$ of the phenols were almost identical to that of the neat fuel, whilst a 1:1 mixture of biodiesel and guaiacol displayed 10 °C reduction in cloud point and a 20% reduction in viscosity compared to the neat fuel, however these values were still within the range mandated in the EN 14214 specifications.

4.5 Future work

Whilst further investigation would be necessary in order to determine the suitability of these compounds as replacements for current antioxidants in fuel, these preliminary investigations are promising. As the effectiveness of antioxidants has been found to be dependent on the fuel structure, the renewable phenols should be tested for activity in a variety of biodiesels and also in non-renewable fuels such as diesel and kerosene.

Rather than using a single, isolated monolignol, the effect of unisolated depolymerized lignin product mixtures as antioxidants could be investigated. Previous studies have shown that depolymerized lignin from ozonoylsis can be blended into a range of fuels at reasonably high loadings without significantly altering the fuel properties.[36] A similar approach could be applied here and the oxidative stability of resulting fuel blends could be investigated in accelerated oxidation tests as described in this study. The use of mixtures of depolymerized lignin products in this way could dramatically reduce process costs by removing the need for selective separation procedures.

5. Conclusion

The selective depolymerization of the recalcitrant aromatic biopolymer lignin to produce value-added products such as renewable monomeric phenols is desirable in order to improve the economics of a lignocellulosic biorefinery concept. The use of homogeneous catalysis is a potential route to the selective depolymerization of lignin under mild conditions.

To this end, a range of homogeneous vanadium Schiff-base complexes have been synthesized, characterized and tested for their activity in the catalytic degradation of non-phenolic β-O-4 model lignin compound 2-phenoxy-1-phenylethanol (model B). The degradation of model B occurs *via* both C-O bond cleavage to form acetophenone and phenol, and benzylic oxidation producing 2-phenoxy-1-phenylethanone (the oxidation product, OP). The former process is the desired degradation pathway, as cleavage of the β-O-4 linkage in the lignin polymer would lead to depolymerization and molecular weight lowering, whereas benzylic oxidation would not.

Initially, catalysts were tested for overall activity in conversion of the model compound. In general, complexes with tridentate monophenolate ligands with an aliphatic backbone [VO(**1-7**)(O^iPr)] were found to be more effective catalysts than those with tetradentate and tridentate bis-phenolate ligands, [[VO(**8,10**)]$_2$O, [VO(**9**)(VO_2OMe)]$_2$O, VO(**15**)(O^iPr)] and aromatic backbones [VO(**11-14**)(O^iPr)]. For the tridentate monophenolate complexes, catalytic activity was found to be promoted by the presence of bulky alkyl substituents at the 3' position of the phenolate ring, with adamantyl-substituted catalyst VO(**6**)(O^iPr) effecting the fastest conversion of the model compound. The activity of the bulkiest, trityl-substituted catalyst VO(**7**)(O^iPr) was lower than that of VO(**6**)(O^iPr), possibly as a result of impeded access of the model compound to the catalyst active site. Halo-substituted complexes VO(**1-3**)(O^iPr) were found to be poor catalysts for the conversion of model B.

The selectivity of the catalysts for C-O bond cleavage over benzylic oxidation in the degradation of model B was also assessed. In a similar trend to the catalytic activity, selectivity was poor for the halo-substituted and unsubstituted species and significantly higher for alkyl-substituted species. Selectivity for C-O cleavage increased as the size of the substituent at the 3' position was increased from ^{t}Bu < Ad < CPh_3. Selectivity also increased at higher temperatures and lower oxygen concentrations, although the latter resulted in a significant loss of activity. It is proposed that the presence of oxygen improves catalyst turnover by assisting in reoxidation of the catalyst to the active species.

Catalytic degradation of phenolic β-O-4 model compound guaiacylglycerol-β-guaiacyl ether (model C) by VO(**2,4,6,7**)(O^{i}Pr) was around 15-25 times faster than for non-phenolic model B and produced exclusively C-O cleavage products with no evidence of benzylic oxidation. The trend in catalyst activity was analogous to that observed for the non-phenolic model.

Complexes VO(**2,6,16**)(O^{i}Pr) were also assessed for their activity in the degradation of non-phenolic model B in ionic liquids (ILs), in order to determine whether they could potentially be employed as part of an IL-based biomass pretreatment process to effect the depolymerization of lignin. Catalytic degradation of model B by VO(**6**)(O^{i}Pr) was observed in several ILs, with the best performance observed in imidazolium-based ILs [Emim][OAc] and [Bmim][OAc]. However, the activity of VO(**6**)(O^{i}Pr) was significantly lower in the ILs than in DMSO, and it was concluded that deactivation of the catalyst occurs on contact with the ILs. No evidence of benzylic oxidation to form the OP was observed in the ILs, suggesting 100% selectivity for the C-O cleavage reaction.

At 100 °C in DMSO no degradation of the OP had been observed, however at 140 °C there was evidence that conversion of the OP to phenol was occurring. Further investigation through a series of kinetic studies in mixtures of [Emim][OAc] and DMSO revealed that the apparent 100% selectivity of the reaction in [Emim][OAc] was likely a result of the fast conversion of OP to phenol.

VO(**6**)(O^{i}Pr) was unable to effect the catalytic degradation of α-O-4 model lignin compound benzylphenyl ether (model E), corroborating the hypothesis that catalytic activity is dependent on binding of the model compound to vanadium through the hydroxyl group of the β-O-4 linkage, which is absent in the α-O-4 linkage.

Catalysts VO(**2,6**)(O^{i}Pr) were employed in the IL pretreatment of alkali lignin with [Emim][OAc]. Whilst SEM images indicated that IL treatment of the lignin dramatically altered its structure, breaking apart the particles and increasing the exposed surface area, there was no evidence of any additional degradation due to the catalysts. However, it is anticipated that the partially degraded, IL-solubilized lignin could be a suitable substrate for subsequent conversion by homogeneous catalysts.

The monolignols guaiacol, eugenol and syringol and commercial antioxidant BHT were tested for antioxidant activity in RME biodiesel in a series of accelerated oxidation experiments. All three renewable phenols were found to increase the oxidative stability of the biodiesel at a range of loadings, although they were outperformed by BHT. It was hypothesised, however,

that the renewable phenols could be blended at higher loadings in order to achieve the same effect as the non-renewable BHT, without significantly altering the fuel properties. Initial measurements of properties including cloud point and viscosity of blends of the renewable antioxidants in RME biodiesel were promising, indicating only minimal effect of the phenols on these fuel properties at loadings of 1000 $mg.L^{-1}$. Surprisingly, the viscosity and cloud point of a 1:1 mixture of guaiacol and RME biodiesel still fell within the EN 14214 specifications for biodiesel.

These studies, based on model compounds, indicate the potential of homogeneous catalysis for the selective depolymerization of lignin to monomeric phenols, possibly within an IL-based biorefinery setup, and the possible utility of these renewable phenolic compounds as value-added products such as fuel additives. The next step would be to conduct further studies on real lignin substrates in order to gain a better understanding of the potential applicability of these processes in a scaled-up biorefinery-type situation, particularly focussing on assessment of catalyst stability, catalyst and IL recyclability and separation processes.

6. Experimental

6.1 Materials and methods

Materials. [TEA][HSO_4] was synthesised by Feng Xu, and 1-phenyl-2-(2-methoxyphenoxy)propane-1,3-diol (model D) by Tanmoy Dutta at JBEI, Emeryville, CA, USA. Alkali (Kraft) lignin was purchased from Sigma Aldrich (average M_w ~10,000, impurities: 4% sulfur). Rapeseed methyl ester biodiesel was supplied by BP. Unless preparative details are provided, all other reagents were purchased from Sigma Aldrich, TCI Chemicals, Fluka, Lancaster, Acros Organics or Alfa Aesar and used without additional purification.

Microwave Reactor. Microwave experiments were carried out in an Anton Parr Monowave 300 Microwave Synthesis Reactor.

Elemental Analysis. Elemental compositions were obtained by Mr Stephen Boyer at the Microanalysis Service, London Metropolitan University, UK.

NMR Spectroscopy. NMR spectra were obtained on one of Bruker Advance 300, 400 or 500 MHz spectrometers at 298 K in $(CD_3)_2SO$, CD_3OD or $CDCl_3$ as solvent. Chemical shifts are reported in parts per million (ppm) relative to the residual solvent peak and coupling constants are reported in Hertz (Hz).

Electrospray Ionisation-Mass Spectrometry. ESI-MS analysis was recorded on a Bruker Daltonic micrOTOF electrospray time-of-flight (ESI-TOF) mass spectrometer coupled to an Agilent 1200 LC system as an autosampler. 10 µL of sample was injected into a 30:70 flow of water:acetonitrile at 0.3 $mL.min^{-1}$ into the mass spectrometer.

Gas Chromatography-Mass Spectrometry. GC-MS analysis was carried out using an Agilent 7890A Gas Chromatograph equipped with a capillary column (30 m × 0.320 mm internal diameter) coated with HP-5 [(5% phenyl) methylpolysiloxane] stationary phase (0.25 µm film thickness) and a He mobile phase (flow rate: 1.2 $mL.min^{-1}$) coupled with an Agilent 5975C inert MSD with Triple Axis Detector.

X-Ray Crystallography. All data were collected on a Nonius kappa CCD diffractometer by Dr Matthew Jones with MoKα radiation (λ = 0.71073 Å). T = 150(2) K throughout and all structures were solved by direct methods and refined on F^2 data using the SHELXL-97 suite of programs.[196] Hydrogen atoms were included in idealised positions and refined using the riding model.

High-Performance Liquid Chromatography. Samples were analyzed on either an Agilent 1200 or Agilent 1260 High Pressure Liquid Chromatography (HPLC) instrument equipped with a UV detector (λ = 280 nm) and an Agilent ZORBAX Eclipse XDB-C18 column (5 µm particle size, 4.6 × 250 mm) or a Thermo Scientific BetaSil C18 column (5 µm particle size, 4.6 × 250 mm) respectively. 10 or 50 µL samples (for the Eclipse XDB and BetaSil columns respectively) were injected on to the column and were chromatographed using 5% acetic acid (A) and acetonitrile (B) as the mobile phase (0.5 $mL.min^{-1}$) using the following gradient: 0-2.5 min, hold at 25% B; 2.5-6.0 min, linear gradient from 25%-75% B; 6.0-12.0 min, hold at 75% B; 12.0-15.0 min, linear gradient from 75%-90% B; 15.0-17.0 min, hold at 90% B; 17.0-20.0 min, linear gradient from 75%-25% B. The oven temperature was held at 30 °C.

Size Exclusion Chromatography. Lignin solutions (1 $mg.mL^{-1}$) were prepared in analytical-grade dimethyl sulfoxide. Samples were analysed on an Agilent 1200 series binary LC system (G1312B) equipped with DA (G1315D) detector. Separation was achieved with a Mixed-D column (5 mm particle size, 7.5 mm × 300 mm, linear molecular mass range of 200 to 400, 000 u, Polymer Laboratories) at 80 °C using a mobile phase of NMP at a flow rate of 0.5 $mL.min^{-1}$. Absorbance of materials eluting from the column was detected at 300 nm (UV-A).[27]

Scanning Electron Microscopy. SEM was carried out on a JEOL 6480LV at 5 - 25 kV by Ursula Potter at the University of Bath, UK.

Refractive index. Refractive index measurements were recorded on a Krüss DR301-95 Digital Handheld Refractometer. The temperature of each measurement was also noted.

Kinematic viscosity. Kinematic viscosities were measured with calibrated Canon-Fenske Routine Viscometers No. 150 and 200, in accordance with standard test methods set out in ASTM D445 and ISO 3104 at 40 °C.

Cloud Point. Cloud points were measured using a TA-Q20 Differential Scanning Calorimeter with a cooling unit. Samples were placed in a Tzero aluminium pan and equilibrated at 20 °C for 2 min before cooling at a rate of 2 $°C.min^{-1}$ to -30 °C.

6.2 Experimental procedures

6.2.1 Chapter 2 experimental procedures

Microwave-assisted model lignin compound depolymerization studies. 2-Phenoxy-1-phenylethanol (0.1 g, 0.46 mmol), catalyst (10 mol%) and MeCN (5 mL, containing 1 $mg.L^{-1}$ dodecane as internal standard) were added to a 30 mL glass microwave vial which was sealed

and heated to 80 °C for 1 or 4 h with stirring. The crude reaction mixture was sampled directly for GC-MS analysis.

^{1}H NMR model lignin compound depolymerization studies. 2-Phenoxy-1-phenylethanol (33 mg, 0.15 mmol), catalyst (0.5-7 mol%) and hexamethylbenzene (internal standard, 2 mg, 0.01 mmol) were dissolved in 1 mL DMSO-d_6 in an NMR tube (uncapped) and heated (70-120 °C) for 4 days.

Phenolic β-O-4 model lignin compound depolymerization studies. Guaiacylglycerol-beta-guaiacyl ether (10 mg, 0.031 mmol), 5 mol% catalyst and hexamethylbenzene (internal standard, 2 mg, 0.01 mmol) were dissolved in 1 mL DMSO-d_6 in an NMR tube and heated to 100 °C. The reactions were monitored by ^{1}H NMR spectroscopy.

6.2.2 Chapter 3 experimental procedures

Non-phenolic model lignin compound depolymerization studies. A glass vial was charged with 0.1 g model compound (or oxidation product), 1 g solvent (or solvent mixture) and 0.01 g catalyst and heated to the desired temperature with stirring. Reactions were sampled every hour (~10 mg accurately weighed). Samples were dissolved in 1 mL acetonitrile, filtered or centrifuged at 10,000 rpm for 5 min to remove any particulate matter, and the resulting solution analyzed by HPLC.

Alkali lignin depolymerization studies. Alkali lignin (0.1 g), [Emim][OAc] (1 g) and catalyst (0.01 g) were added to a pressure tube, sealed and heated to 140 °C for 1 or 4 h. The resulting mixture was cooled to room temperature, diluted with water (~10mL) and acidified to pH 1-2 by addition of ~6M HCl (aq.). The mixture was centrifuged at 8000 rpm for 15 min, and the supernatant removed and retained for subsequent extraction by ethyl acetate. The residual lignin solids were then washed thoroughly with water until the washings were neutral and dried in a lyophilizer for 3 days.

6.2.3 Chapter 4 experimental procedures

Fuel Oxidation Experiments. 10 × 24 mL samples of fuel were held at 110 °C without stirring. A total airflow of 6.5 L.min^{-1} (ca. 0.65 L.min^{-1} per sample) was passed through the samples. During the course of the oxidation, 0.1 mL samples were taken for analysis by refractive index.

6.3 Model compound synthesis

6.3.1 Model compound A synthesis

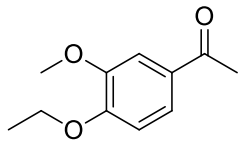

1-(4-Ethoxy-3-methoxyphenyl)ethanone. To a solution of acetovanillone (10 g, 60 mmol, 1 eq.) in DMF (100 mL) was added K_2CO_3 (9.6 g, 69 mmol, 1.15 eq.) and iodoethane (7.24 mL, 90 mmol, 1.5 eq.) and the reaction was stirred at 25 °C for 2 h. The reaction mixture was then poured into hot water (200 mL) and left to cool. The resulting crystals were washed with hexane and dried (54% yield). ^{1}H NMR ($CDCl_3$, 250 MHz): δ 1.51 (t, *J*=7.0 Hz, 3H, CH_2-C<u>H</u>$_3$), 2.57 (s, 3H, C(O)-C<u>H</u>$_3$), 3.94 (s, 3H, O-C<u>H</u>$_3$), 4.18 (q, *J*=7.0 Hz, 2H, C<u>H</u>$_2$), 6.88 (d, *J*=8.2 Hz, 1H, Ar-<u>H</u>), 7.48-7.62 (m, 2H, Ar-<u>H</u>).

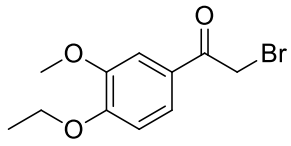

2-Bromo-1-(4-ethoxy-3-methoxyphenyl)ethanone. *Method 1:* To solution of 1-(4-ethoxy-3-methoxyphenyl)ethanone (3.5 g, 18 mmol) in EtOAc (60 mL) at 80 °C was added $CuBr_2$ (8 g, 36 mmol). The reaction was stirred overnight at reflux and then cooled to ambient temperature. The reaction mixture was poured into warm water, filtered and extracted into EtOAc (3 × 30 mL), washed with brine (1 × 30 mL), dried over $MgSO_4$ and the solvent removed *in vacuo*. *Method 2:* To a solution of 1-(4-ethoxy-3-methoxyphenyl)ethanone (5.5 g, 28 mmol, 1 eq.) in 1:1 EtOH/$CHCl_3$ (250 mL) over molecular sieves was added pyridinium tribromide (27 g, 85 mmol, 3 eq.). The reaction mixture was heated to 50 °C and stirred for 16 h, after which time the mixture was cooled to room temperature and filtered through celite. The filtrate was concentrated *in vacuo*, redissolved in EtOAc (50 mL) and washed with water (2 × 30 mL) and brine (1 × 30 mL). The organic layer was dried over $MgSO_4$ and concentrated to give a brown oil which was recrystallized from EtOAc/hexane. ^{1}H NMR ($CDCl_3$, 250 MHz): δ 1.51 (t, *J*=7.0 Hz, 3H, C<u>H</u>$_3$), 3.94 (s, 3H, O-C<u>H</u>$_3$), 4.19 (q, *J*=7.0 Hz, 2H, O-C<u>H</u>$_2$), 4.41 (s, 2H, CH_2-Br), 6.90 (d, *J*=8.2 Hz, 1H, Ar-<u>H</u>), 7.47-7.67 (m, 2H, Ar-<u>H</u>). ^{13}C{^{1}H} NMR ($CDCl_3$, 75 MHz): δ 14.6, 30.5, 56.1, 64.6, 110.9, 111.0, 123.9, 126.8, 149.4, 153.5, 190.1.

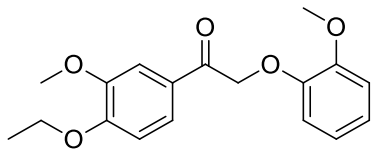

1-(4-ethoxy-3-methoxyphenyl)-2-(2-methoxyphenyl)ethanone. To a solution of 2-bromo-1-(4-ethoxy-3-methoxyphenyl)ethanone (5 g, 18.7 mmol) and guaiacol (2.06 mL, 18.7 mmol) in dimethylformamide (60 mL) was added K_2CO_3 (2.9 g, 21 mmol). The reaction was stirred for 2 h at room temperature then poured into hot water and allowed to recrystallize. The mixture was filtered and the product was subsequently washed through the filter with acetone, dried over $MgSO_4$ and the solvent was removed *in vacuo*. ^{1}H NMR ($CDCl_3$, 300 MHz): δ 1.44 (t, *J*=7.0 Hz, 3H, C<u>H</u>$_3$), 3.82 (s, 3H, O-C<u>H</u>$_3$), 3.86 (s, 3H, O-C<u>H</u>$_3$), 4.11 (q, *J*=6.9 Hz, 2H, O-C<u>H</u>$_2$), 5.24 (s, 2H, C<u>H</u>$_2$-C=O), 6.71-7.02 (m, 5H, Ar-<u>H</u>), 7.51-7.63 (m, 2H, Ar-<u>H</u>). ^{13}C{^{1}H} NMR ($CDCl_3$, 75 MHz): δ 14.6, 55.9, 56.1, 64.6, 71.9, 110.6, 111.0, 112.1, 114.6, 120.8, 122.3, 122.7, 127.6, 147.6, 149.3, 149.7, 153.3, 193.3.

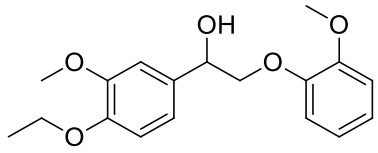

1-(4-ethoxy-3-methoxyphenyl)-2-(2-methoxyphenyl)ethanol (model A). 1-(4-Ethoxy-3-methoxyphenyl)-2-(2-methoxyphenyl)ethanone (5.7 g, 18 mmol) was dissolved in MeOH (150 mL) and $NaBH_4$ (1.4 g, 36 mmol) was added portionwise to minimise the exotherm. The reaction was stirred for 3 h. The solvent was removed *in vacuo* and the residue redissolved in EtOAc (30 mL) before quenching with aqueous NH_4Cl (50 mL). The product was extracted into EtOAc (2 × 30 mL), washed with brine (1 × 30 mL), dried over $MgSO_4$ and the solvent removed *in vacuo* to afford the product. ^{1}H NMR ($CDCl_3$, 250 MHz): δ 1.39 (3H, t, *J*=7.0 Hz, CH_2-C<u>H</u>$_3$), 3.81 (3H, s, O-C<u>H</u>$_3$), 3.82 (3H, s, O-C<u>H</u>$_3$), 3.8-3.9, 4.0-4.1 (2H, m, C<u>H</u>$_2$-CH), 4.03 (2H, q, *J*=7.0 Hz, C<u>H</u>$_2$-CH_3), 4.98 (1H, dd, *J*=9.5, 2.8 Hz, C<u>H</u>-OH), 6.7-7.0 (6H, m, Ar-<u>H</u>), 7.3-7.4 (1H, m, Ar-<u>H</u>). ^{13}C{^{1}H} NMR ($CDCl_3$, 75 MHz): δ 14.8, 55.9, 55.9, 64.4, 72.1, 76.4, 109.6, 112.0, 112.5, 116.0, 118.6, 121.1, 122.5, 132.0, 148.0, 149.4, 150.0.

6.3.2 Model compound B synthesis

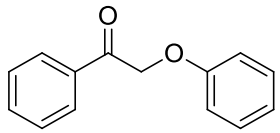

2-Phenoxy-1-phenylethanone. To a solution of 2-bromo-1-phenylethanone (9 g, 45 mmol) in dimethylformamide (150 mL) was added phenol (5 g, 53 mmol) and K_2CO_3 (7.3 g, 53 mmol). The solution was stirred overnight and a colour change from yellow to orange was observed. The reaction mixture was then poured into warm water and left to recrystallize. The crystals were filtered and redissolved in toluene; this solution was dried over $MgSO_4$, filtered and the solvent removed in vacuo to give the product as a cream solid in 83 % yield. ^{1}H NMR ($CDCl_3$, 300 MHz): δ 5.29 (s, 2H, C<u>H</u>$_2$), 6.92-7.06 (m, 3H, Ar-<u>H</u>), 7.28-7.35 (m, 2H, Ar-<u>H</u>), 7.48-7.56 (m, 2H, Ar-<u>H</u>), 7.60-7.68 (m, 1H, Ar-<u>H</u>), 7.98-8.08 (m, 2H, Ar-<u>H</u>). ^{13}C{^{1}H} NMR ($CDCl_3$, 75 MHz): δ 70.8, 114.8, 121.7, 128.2, 128.9, 129.6, 133.9, 158.0, 194.6. ESI-MS: m/z calcd for $[C_{14}H_{12}O_2Na]^+$: 235.0735; found: 235.0792.

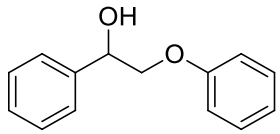

2-Phenoxy-1-phenylethanol (model B). To a solution of 2-phenoxy-1-phenylethanone (7 g, 33 mmol) in methanol (200 mL) was added $NaBH_4$ (2.5 g, 66 mmol) portion wise. The reaction was stirred for 3 h, after which time the solvent was removed in vacuo. The residue was redissolved in ethyl acetate (50 mL) and the reaction was quenched by the addition of aqueous HCl (50 mL). The resulting solution was filtered to remove insoluble salts and the product was extracted into ethyl acetate (3 × 20 mL), washed with brine (1 × 30 mL), dried over $MgSO_4$ and the solvent removed *in vacuo* to afford a waxy, cream solid in 91 % yield. ^{1}H NMR ($CDCl_3$, 300 MHz): δ 4.02 (dd, J=9.8, 9.0 Hz, 1H, C<u>H</u>$_2$), 4.13 (dd, J=9.8, 3.4 Hz, 1H, C<u>H</u>$_2$), 5.15 (dd, J=8.9, 3.2 Hz, 1H, C<u>H</u>), 6.91-7.02 (m, 3H, Ar-<u>H</u>), 7.27-7.51 (m, 7H, Ar-<u>H</u>). ^{13}C{^{1}H} NMR ($CDCl_3$, 75 MHz): δ 72.6, 73.3, 114.6, 126.3, 128.3, 128.6, 129.6, 144.5, 158.4. ESI-MS: m/z calcd for $[C_{14}H_{14}O_2Na]^+$: 237.0891; found: 237.0894. Elemental Analysis: Anal. Calcd for $C_{14}H_{14}O_2$: C, 78.48; H, 6.59. Found: C, 78.31; H, 6.49.

6.4 Ligand synthesis

6.4.1 Bulky salicylaldehyde synthesis[166]

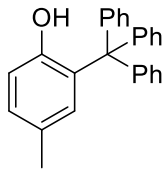

2-Trityl-4-methylphenol. *p*-Cresol (25 g, 0.2 mmol) was heated to 100 °C under a flow of argon. Sodium metal (1.1 g, 0.05 mmol) was added slowly with vigorous stirring to form a cresolate melt. To this was added triphenylchloromethane (10.0 g, 0.036 mmol) and the mixture was heated at 140 °C for 3 h. The reaction mixture was cooled to room temperature and subsequently treated with 7% aq. NaOH (100 mL) and ether (100 mL). The organic layer was separated, washed with 7% aq. NaOH (5 × 50 mL), water (100 mL), and brine (50 mL), dried over $MgSO_4$ and the solvent removed *in vacuo*. The resulting solid was recrystallized from hot diethyl ether to afford the product as a creamy solid in 46% yield. ^{1}H NMR: (400 MHz, $CDCl_3$) δ 2.19 (s, 3H, C<u>H</u>$_3$), 4.33 (s, 1H, O<u>H</u>), 6.74 (d, *J*=8.0 Hz, 1H, Ar-<u>H</u>), 6.86 (d, *J*=2.3 Hz, 1H, Ar-<u>H</u>), 7.04 (dd, *J*=8.0, 2.3 Hz, 1H, Ar-<u>H</u>), 7.16-7.34 (m, 15H, Ar-<u>H</u>). ^{13}C{^{1}H} NMR: (100 MHz, $CDCl_3$) δ 20.9, 62.6, 117.9, 126.7, 127.9, 129.2, 129.4, 130.9, 131.0, 132.8, 144.2, 152.2.

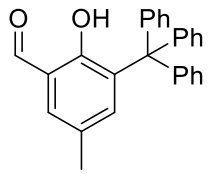

3-Trityl-5-methylsalicylaldehyde. 2-Trityl-4-methylphenol (3.5 g, 0.01 mol), hexamethylenetetramine (2.80 g, 0.02 mol) and trifluoroacetic acid (10 mL) were stirred together for 4 h at 120 °C. The mixture was cooled to 80 °C, 33% aq. H_2SO_4 (15 mL) was added and the reaction was heated for a further 2 h at 130 °C. After cooling to room temperature, ethyl acetate (20 mL) and water (30 mL) were added. The organic layer was separated and the water layer extracted with ethyl acetate (3 × 20 mL). The combined organic extracts were washed with water (50 mL) and brine (30 mL) and dried over $MgSO_4$. The solvent was removed *in vacuo* and the residue was washed with diethyl ether to yield the product as a pale yellow powder in 49% yield. ^{1}H NMR: (400 MHz, $CDCl_3$) δ 2.26 (s, 3H, C<u>H</u>$_3$), 7.10-7.25 (m, 15H, Ar-<u>H</u>), 7.27-7.30 (m, 1H, Ar-<u>H</u>), 7.36 (d, *J*=2.0 Hz, 1H, Ar-<u>H</u>), 9.80 (s, 1H, C<u>H</u>O), 11.11 (d, *J*=0.5 Hz, 1H,

O<u>H</u>). $^{13}C\{^{1}H\}$ NMR: (100 MHz, $CDCl_3$) δ 20.7, 62.9, 120.6, 125.7, 127.2, 127.8, 128.0, 128.2, 129.4, 130.8, 130.9, 132.7, 135.4, 138.8, 144.8, 158.5, 196.5.

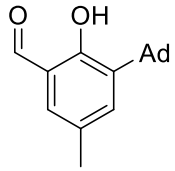

3-(1-Adamantyl)-5-methylsalicylaldehyde. 2-(1-Adamantyl)-4-methylphenol (1.0 g, 4.1 mmol), hexamethylenetetramine (1.16 g, 8.3 mmol) and trifluoroacetic acid (7 mL) were stirred together for 4 h at 120 °C. The mixture was cooled to 80 °C, 33% aq. H_2SO_4 (70 mL) was added and the reaction was heated for a further hour at 130 °C. After cooling to room temperature, ethyl acetate (20 mL) and water (30 mL) were added. The organic layer was separated and the water layer extracted with ethyl acetate (3 × 20 mL). The combined organic extracts were washed with water (50 mL) and brine (30 mL) and dried over $MgSO_4$. The solvent was removed *in vacuo* and the residue was washed with diethyl ether to yield the product as a pale yellow powder in 66% yield. ^{1}H NMR: (400 MHz, $CDCl_3$) δ 1.74-1.82 (m, 6H, Ad-<u>H</u>), 2.05-2.10 (m, 3H, Ad-<u>H</u>), 2.11-2.18 (m, 6H, Ad-<u>H</u>), 2.31 (s, 3H, C<u>H</u>$_3$), 7.13-7.19 (m, 1H, Ar-<u>H</u>), 7.27 (d, *J*=2.3 Hz, 1H, Ar-<u>H</u>), 9.81 (s, 1H, O<u>H</u>), 11.64 (s, 1H, C<u>H</u>O). $^{13}C\{^{1}H\}$ NMR: ($CDCl_3$, 75 MHz): δ 20.6, 28.9, 37.0, 40.1, 120.3, 128.2, 131.3, 135.5, 159.4, 197.2.

6.4.2 General ligand synthesis procedure[1]

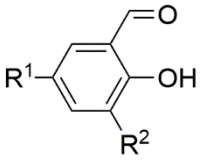

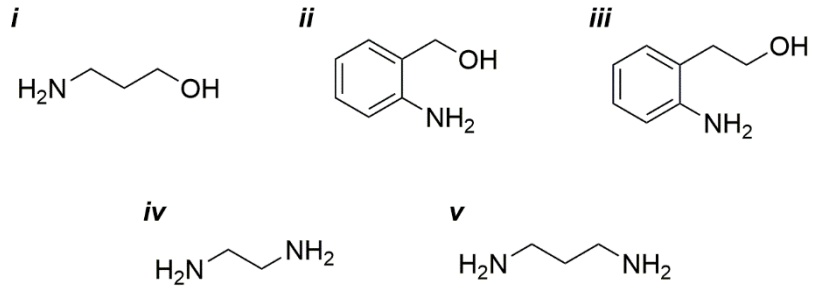

Figure 109: Aldehydes, amino alcohols and diamines used in ligand synthesis

Table 19: Aldehydes, amino alcohols and diamines used in ligand synthesis

Ligand	Aldehyde R^1, R^2	Amino alcohol or diamine
(**1**)H_2	Cl, Cl	*i*
(**2**)H_2	Br, Br	*i*
(**3**)H_2	I, I	*i*
(**4**)H_2	H, H	*i*
(**5**)H_2	^{t}Bu, ^{t}Bu	*i*
(**6**)H_2	Me, Ad	*i*
(**7**)H_2	Me, CPh_3	*i*
(**8**)H_2	H, H	*v*
(**9**)H_2	^{t}Bu, ^{t}Bu	*iv*
(**11**)H_2	H, H	*ii*
(**12**)H_2	^{t}Bu, ^{t}Bu	*ii*
(**13**)H_2	H, H	*iii*
(**14**)H_2	^{t}Bu, ^{t}Bu	*iii*

Tridentate ligand synthesis (1-7,11-14**)H_2.** To a solution of aldehyde (1 g) in MeOH (70 mL) was added Na_2SO_4 (8 eq.) and the relevant amino alcohol (1 eq.). The reaction was heated to reflux and stirred overnight. The mixture was cooled to room temperature, filtered and concentrated *in vacuo* to afford the product.

Tetradentate ligand synthesis (8-9**)H_2.** To a solution of the aldehyde (1 g) in methanol (100 mL) was added the diamine (0.5 eq.) and the reaction was stirred at room temperature for 30 minutes until a precipitate had formed. The product was filtered, washed with methanol and dried.

6.4.3 Ligand data

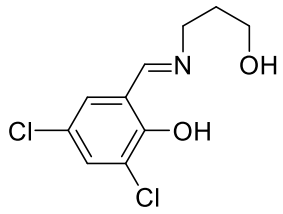

(1)H₂. ^{1}H NMR: ($CDCl_3$, 300 MHz): δ 1.96 (quin, *J*=6.3 Hz, 2H, C<u>H</u>$_2$), 3.78 (t, *J*=6.0 Hz, 2H, C<u>H</u>$_2$-OH), 3.77 (t, *J*=5.7 Hz, 2H, N-C<u>H</u>$_2$), 7.11 (d, *J*=2.6 Hz, 1H, Ar-<u>H</u>), 7.40 (d, *J*=2.6 Hz, 1H, Ar-<u>H</u>), 8.22 (s, 1H, N=C<u>H</u>). ^{13}C{^{1}H} NMR: ($CDCl_3$, 75 MHz): δ 32.7, 53.9, 59.6, 118.4, 121.3, 123.9, 129.1, 132.8, 159.9, 163.9. ESI-MS: m/z calcd for $[C_{10}H_{12}Cl_2NO_2]^+$: 248.0245; found: 248.0237.

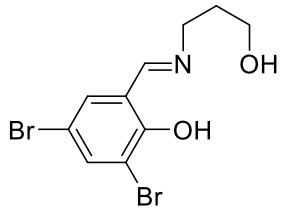

(2)H₂. ^{1}H NMR: ($CDCl_3$, 300 MHz): δ 1.98 (quin, J=6.3 Hz, 2H, C<u>H</u>$_2$), 3.75-3.82 (m, 4H, C<u>H</u>$_2$-OH, N-C<u>H</u>$_2$), 7.32 (d, J=2.3 Hz, 1H, Ar-<u>H</u>), 7.71 (d, J=2.3 Hz, 1H, Ar-<u>H</u>), 8.23 (s, 1H, N=CH). ^{13}C{^{1}H} NMR: ($CDCl_3$, 75 MHz): δ 32.7, 53.7, 59.5, 108.0, 113.9, 118.8, 132.9, 138.3, 161.0, 163.8. ESI-MS: m/z calcd for $[C_{10}H_{12}Br_2NO_2]^+$: 337.9209; found: 337.9527.

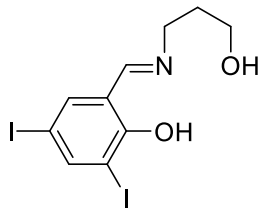

(3)H₂ ^{1}H NMR: ($CDCl_3$, 300 MHz): δ 1.98 (quin, *J*=6.4 Hz, 2H, C<u>H</u>$_2$), 3.75-3.80 (m, 4H, C<u>H</u>$_2$-OH, N-C<u>H</u>$_2$), 7.49 (d, *J*=2.3 Hz, 1H, Ar-<u>H</u>), 8.05 (d, *J*=2.3 Hz, 1H, Ar-<u>H</u>), 8.13 (t, *J*=1.0 Hz, 1H, N=C<u>H</u>). ^{13}C{^{1}H} NMR: ($CDCl_3$, 75 MHz): δ 32.7, 53.5, 59.6, 90.1, 118.8, 140.0, 149.1, 163.5. ESI-MS: m/z calcd for $[C_{10}H_{12}I_2NO_2]^+$: 431.8957; found: 431.8967.

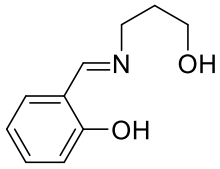

(4)H₂. ^{1}H NMR: ($CDCl_3$, 300 MHz): δ 2.01 (quin, *J*=6.4 Hz, 2H, C<u>H</u>$_2$), 3.77 (t, *J*=6.7 Hz, 2H, C<u>H</u>$_2$), 3.81 (t, *J*=6.2 Hz, 2H, C<u>H</u>$_2$), 6.92 (t, *J*=7.5 Hz, 1H, Ar-<u>H</u>), 7.00 (d, *J*=8.3 Hz, 1H, Ar-<u>H</u>), 7.29 (dd, *J*=7.7, 1.4 Hz, 1H, Ar-<u>H</u>), 7.32-7.38 (m, 1H, Ar-<u>H</u>), 8.42 (s, 1H, N=C<u>H</u>). ^{13}C{^{1}H} NMR: ($CDCl_3$, 75 MHz): δ 33.5, 55.8, 60.2, 117.1, 118.5, 131.3, 132.3, 161.4, 165.3. ESI-MS: m/z calcd for $[C_{10}H_{14}NO_2]^+$: 180.1025; found: 180.1025.

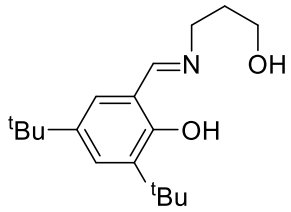

(5)H₂. ^{1}H NMR: ($CDCl_3$, 250 MHz): δ 1.32 (s, 9H, C(C<u>H</u>$_3$)$_3$), 1.45 (s, 9H, C(C<u>H</u>$_3$)$_3$), 1.98 (quin, *J*=6.3 Hz, 2H, C<u>H</u>$_2$), 3.72 (td, *J*=6.6, 1.3 Hz, 2H, N-C<u>H</u>$_2$), 3.79 (t, *J*=6.3 Hz, 2H, C<u>H</u>$_2$-OH), 7.10 (d, *J*=2.5 Hz, 1H, Ar-<u>H</u>), 7.39 (d, *J*=2.5 Hz, 1H, Ar-<u>H</u>), 8.40 (t, *J*=1.3 Hz, 1H, N=C<u>H</u>), 13.82 (br. s, 1H, Ar-O<u>H</u>). ^{13}C{^{1}H} NMR: ($CDCl_3$, 75 MHz): δ 29.4, 31.5, 33.5, 34.2, 35.1, 55.9, 60.3, 117.8, 125.8, 126.9, 136.7, 140.0, 158.2, 166.4. ESI-MS: m/z calcd for $[C_{18}H_{28}NO_2]^-$: 290.2120; found: 290.2121.

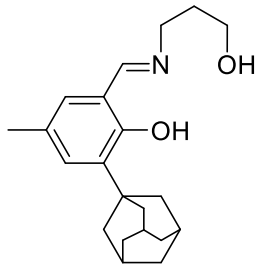

(6)H₂. ^{1}H NMR: (CD_3OD, 300 MHz): δ 1.85-1.91 (m, 6H, Ad-<u>H</u>), 1.99 (quin, *J*=6.7 Hz, 2H, C<u>H</u>$_2$), 2.09-2.16 (m, 3H, Ad-<u>H</u>), 2.22-2.27 (m, 6H, Ad-<u>H</u>), 2.32 (s, 3H, C<u>H</u>$_3$), 3.75 (t, *J*=6.4 Hz, 4H, C<u>H</u>$_2$-OH, N-C<u>H</u>$_2$), 7.02 (d, *J*=1.3 Hz, 1H, Ar-<u>H</u>), 7.11 (d, *J*=1.8 Hz, 1H, Ar-<u>H</u>), 8.46 (s, 1H, N=C<u>H</u>). ^{13}C{^{1}H} NMR: (CD_3OD, 75 MHz): δ 20.9, 30.7, 35.0, 38.1, 38.4, 41.6, 56.9, 60.5, 120.0, 128.0, 130.7, 131.3, 138.4, 159.7, 167.9. ESI-MS: m/z calcd for $[C_{21}H_{29}NO_2Na]^+$: 350.2096; found: 350.2089.

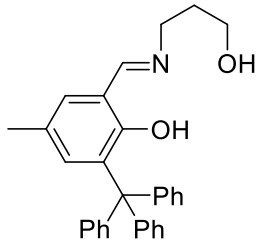

(7)H₂. ^{1}H NMR: (DMSO-d_6, 400 MHz): δ 1.71 (quin, *J*=6.6 Hz, 2H, C$\underline{H}_2$), 2.21 (s, 3H, C$\underline{H}_3$), 3.42 (t, *J*=6.3 Hz, 4H, C$\underline{H}_2$-OH, N-C$\underline{H}_2$), 7.06 (d, *J*=2.0 Hz, 1H, Ar-$\underline{H}$), 7.13-7.21 (m, 9H, Ar-$\underline{H}$), 7.23 (d, *J*=1.8 Hz, 1H, Ar-$\underline{H}$), 7.28 (t, *J*=7.3 Hz, 6H, Ar-$\underline{H}$), 8.50 (s, 1H, N=C$\underline{H}$). ^{13}C{^{1}H} NMR: (CDCl3, 75 MHz): δ 20.8, 21.5, 33.3, 55.8, 60.3, 63.2, 118.6, 125.3, 125.5, 126.1, 127.2, 128.3, 129.1, 130.7, 131.1, 134.4, 134.5, 145.6, 158.0. ESI-MS: m/z calcd for $[C_{30}H_{29}NO_2Na]^+$: 458.2096; found: 458.2102.

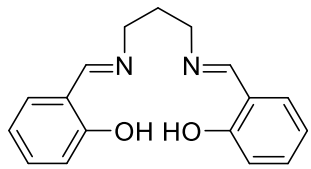

(8)H₂. ^{1}H NMR: ($CDCl_3$, 300 MHz): δ 2.05 (quin, J=6.4 Hz, 2H, N-CH_2-C$\underline{H}_2$), 3.65 (td, J=6.8, 1.1 Hz, 4H, N-C$\underline{H}_2$), 6.77-6.94 (m, 4H, Ar-$\underline{H}$) 7.14-7.29 (m, 4H, Ar-$\underline{H}$), 8.30 (t, J=1.1 Hz, 2H, N=C$\underline{H}$), 13.39 (br. s, 2H, O$\underline{H}$). ^{13}C{^{1}H} NMR: ($CDCl_3$, 75 MHz): δ 31.7, 56.8, 117.0, 118.7, 118.8, 131.3, 132.3, 161.1, 165.5. ESI-MS: m/z calcd for $[C_{17}H_{17}N_2O_2]^-$: 281.1290; found: 281.1281. Elemental Analysis: Anal. Calcd for $C_{17}H_{18}N_2O_2$: C, 72.32; H, 6.43; N, 9.92. Found: C, 71.9; H, 6.60; N, 10.0.

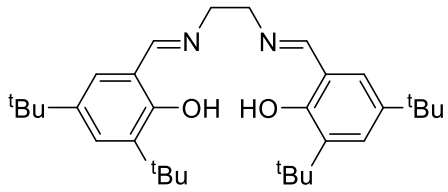

(9)H₂. ^{1}H NMR: ($CDCl_3$, 300 MHz): δ 1.29 (s, 18H, C$\underline{H}_3$), 1.44 (s, 18H, C$\underline{H}_3$), 3.94 (s, 4H, C$\underline{H}_2$), 7.07-7.13 (m, 2H, Ar-$\underline{H}$), 7.38 (d, *J*=2.6 Hz, 2H, Ar-$\underline{H}$), 8.41 (br. s, 2H, N=C$\underline{H}$). ESI-MS: m/z calcd for $[C_{32}H_{48}N_2NaO_2]^+$: 515.3608; found: 515.364.

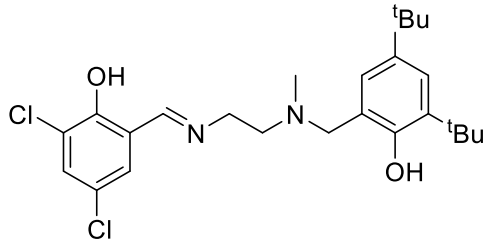

(10**)H₂.** ^{1}H NMR ($CDCl_3$, 300 MHz): δ 1.29 (s, 9H, C(C<u>H</u>$_3$)$_3$), 1.35 (s, 9H, C(C<u>H</u>$_3$)$_3$), 2.39 (br. s, 3H, N-C<u>H</u>$_3$), 2.80-2.92 (m, 2H, N-C<u>H</u>$_2$), 3.74 (br. s, 2H. Ar-C<u>H</u>$_2$), 3.78-3.90 (m, 2H, C=N-C<u>H</u>$_2$), 6.80-6.85 (m, 1H, Ar-<u>H</u>), 7.17 (d, *J*=2.6 Hz, 1H, Ar-<u>H</u>), 7.19-7.24 (m, 1H, Ar-<u>H</u>), 7.42 (d, *J*=2.3 Hz, 1H, Ar-<u>H</u>), 8.30 (br. s, 1H, N=C<u>H</u>).

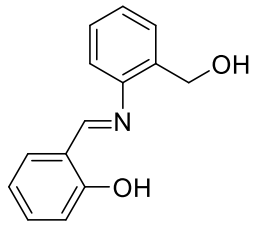

(11**)H₂.** ^{1}H NMR: ($CDCl_3$, 300 MHz): δ 4.87 (s, 2H, C<u>H</u>$_2$), 6.97 (td, *J*=7.6, 0.9 Hz, 1H, Ar-<u>H</u>), 7.05 (d, *J*=7.9 Hz, 1H, Ar-<u>H</u>), 7.15 (dd, *J*=7.7, 1.1 Hz, 1H, Ar-<u>H</u>), 7.32 (td, *J*=7.6, 0.9 Hz, 1H, Ar-<u>H</u>), 7.36-7.45 (m, 3H, Ar-<u>H</u>), 7.53 (dd, *J*=7.3, 0.9 Hz, 1H, Ar-<u>H</u>), 8.62 (s, 1H, N=C<u>H</u>), 13.11 (br. s, 1H, O<u>H</u>). ^{13}C{^{1}H} NMR: ($CDCl_3$, 75 MHz): δ 61.9, 117.3, 118.1, 119.2, 127.1, 128.4, 128.9, 132.4, 133.5, 134.5, 161.1, 163.2. ESI-MS: m/z calcd for $[C_{14}H_{14}NO_2]^+$: 228.1025; found: 228.1019.

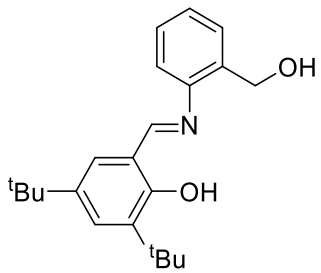

(12**)H₂.** ^{1}H NMR: ($CDCl_3$, 300 MHz): δ 1.26 (s, 9H, C(C<u>H</u>$_3$)), 1.41 (s, 9H, C(C<u>H</u>$_3$)$_3$), 4.80 (s, 2H, C<u>H</u>$_2$), 7.05 (dd, *J*=7.7, 1.1 Hz, 1H, Ar-<u>H</u>), 7.17 (d, *J*=2.5 Hz, 1H, Ar-<u>H</u>), 7.21 (td, *J*=7.5, 1.0 Hz, 1H, Ar-<u>H</u>), 7.29 (td, *J*=7.5, 1.4 Hz, 1H, Ar-<u>H</u>), 7.41 (d, *J*=2.5 Hz, 1H, Ar-<u>H</u>), 7.44 (dd, *J*=7.6, 0.9 Hz, 1H, Ar-<u>H</u>), 8.54 (s, 1H, N=C<u>H</u>). ^{13}C{^{1}H} NMR: ($CDCl_3$, 75 MHz): δ 29.3, 29.5, 31.4, 31.5, 61.9, 116.0, 118.3, 126.8, 127.0, 127.9, 128.1, 128.4, 128.8, 129.2, 129.4, 131.9, 134.5, 140.8, 147.0, 158.2, 164.6. ESI-MS: m/z calcd for $[C_{22}H_{30}NO_2]^+$: 340.2277; found: 340.2287.

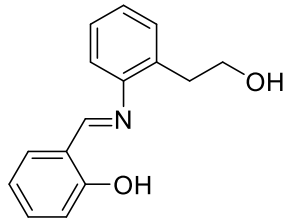

(13)H₂. ^{1}H NMR: ($CDCl_3$, 300 MHz): δ 3.03 (t, *J*=6.8 Hz, 2H, C<u>H</u>$_2$), 3.82 (t, *J*=6.8 Hz, 2H, C<u>H</u>$_2$-OH), 6.91-6.98 (m, 1H, Ar-<u>H</u>), 6.99-7.02 (m, 1H, Ar-<u>H</u>), 7.09-7.14 (m, 1H, Ar-<u>H</u>), 7.21-7.26 (m, 1H, Ar-<u>H</u>), 7.27-7.33 (m, 2H, Ar-<u>H</u>), 7.35-7.42 (m, 2H, Ar-<u>H</u>), 8.57 (s, 1H, N=C<u>H</u>). ^{13}C{^{1}H} NMR: ($CDCl_3$, 75 MHz): δ 35.5, 62.7, 117.2, 118.2, 119.2, 127.1, 127.9, 130.8, 132.3, 133.3, 161.0, 162.8. ESI-MS: m/z calcd for $[C_{15}H_{16}NO_2]^+$: 242.1181; found: 242.1166.

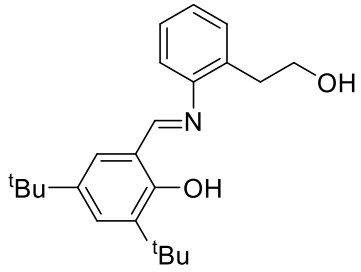

(14)H₂. ^{1}H NMR: ($CDCl_3$, 300 MHz): δ 1.33 (s, 9H, C(C<u>H</u>$_3$)), 1.48 (s, 9H, C(C<u>H</u>$_3$)), 3.07 (t, *J*=6.7 Hz, 2H, C<u>H</u>$_2$), 3.86 (t, *J*=6.7 Hz, 2H, C<u>H</u>$_2$-OH), 7.10-7.16 (m, 1H, Ar-<u>H</u>), 7.21-7.25 (m, 2H, Ar-<u>H</u>), 7.28-7.36 (m, 2H, Ar-<u>H</u>), 7.48 (d, *J*=2.0 Hz, 1H, Ar-<u>H</u>), 8.60 (s, 1H, N=C<u>H</u>). ^{13}C{^{1}H} NMR: ($CDCl_3$, 75 MHz): δ 29.4, 31.4, 62.8, 118.3, 118.5, 126.6, 126.8, 127.9, 128.2, 130.6, 132.3, 137.0, 140.7, 147.9, 158.2, 164.1. ESI-MS: m/z calcd for $[C_{23}H_{32}NO_2]^+$: 354.2433; found: 354.2435.

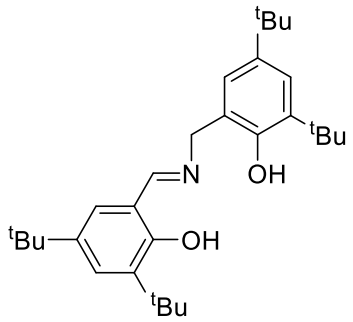

(15)H₂.[164] ^{1}H NMR ($CDCl_3$, 300 MHz): δ 1.22-1.24 (m, 18H, C(C<u>H</u>$_3$)$_3$), 1.36 (s, 9H, C(C<u>H</u>$_3$)$_3$), 1.37 (s, 9H, C(C<u>H</u>$_3$)$_3$), 4.74 (s, 2H, N-C<u>H</u>$_2$), 6.99 (d, *J*=2.3 Hz, 1H, Ar-<u>H</u>), 7.03 (d, *J*=2.6 Hz, 1H, Ar-<u>H</u>), 7.22 (d, *J*=2.3 Hz, 1H, Ar-<u>H</u>), 7.32 (d, *J*=2.3 Hz, 1H, Ar-<u>H</u>), 8.42 (s, 1H, N=C<u>H</u>). ^{13}C{^{1}H} NMR ($CDCl_3$,

75 MHz): δ 29.3, 29.4, 29.7, 29.9, 31.3, 31.5, 31.6, 34.2, 34.3, 34.8, 35.1, 61.3, 117.9, 123.8, 124.2, 126.4, 127.5, 136.0, 136.8, 140.5, 142.6, 151.0, 157.6, 159.1, 167.8.

6.5 Catalyst synthesis

6.5.1 General catalyst synthesis procedure

Catalyst syntheses were conducted using glove box and Schlenk line techniques under an atmosphere of argon. In a glove box, equimolar amounts of the ligand (**X**)H_2 and $VO(O^iPr)_3$ were dissolved separately in anhydrous dichloromethane. The ligand solution was added dropwise to the metal solution and the reaction mixture was stirred for 0.5 h. The solvent was removed *in vacuo* and recrystallization was attempted from methanol, hexane, toluene or dichloromethane.

6.5.2 Catalyst data

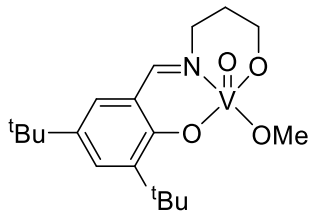

VO(5)(OMe) Synthesized from $VO(OEt)_3$ in MeOH. Recrystallized from methanol. ^{1}H NMR ($CDCl_3$, 300 MHz): 1.33 (s, 9H, C(C$\underline{H}_3$)$_3$), 1.49 (s, 9H, C(C$\underline{H}_3$)$_3$), 1.90-2.03 (m, 1H, C$\underline{H}_2$), 2.28 (d, *J*=15.4 Hz, 1H, C$\underline{H}_2$), 3.96 (d, *J*=13.2 Hz, 1H, C$\underline{H}_2$), 4.43 (t, *J*=12.4 Hz, 1H, C$\underline{H}_2$), 4.82-4.94 (m, 1H, C$\underline{H}_2$), 4.99 (s, 3H, O-C$\underline{H}_3$), 5.56 (t, *J*=12.1 Hz, 1H, C$\underline{H}_2$), 7.18 (d, *J*=2.3 Hz, 1H, Ar-$\underline{H}$), 7.57 (d, *J*=2.3 Hz, 1H, Ar-$\underline{H}$), 8.35 (br. s, 1H, N=C$\underline{H}$). ^{13}C{^{1}H} NMR ($CDCl_3$, 75 MHz): δ 29.6, 31.4, 32.6, 34.3, 35.3, 36.2, 127.2, 129.9, 141.3, 164.0. ^{51}V NMR ($CDCl_3$, 105 MHz): δ -544.8, -584.2.

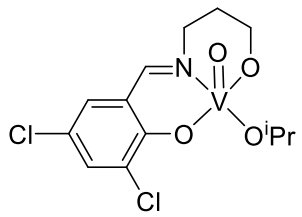

VO(1)(O^{i}Pr). Recrystallized from dichloromethane. ^{1}H NMR ($CDCl_3$, 300 MHz): 1.46 (d, *J*=6.0 Hz, 3H, CH-C$\underline{H}_3$), 1.55 (d, *J*=6.4 Hz, 3H, CH-C$\underline{H}_3$), 1.93-2.11 (m, 1H, C$\underline{H}_2$), 2.32-2.43 (m, 1H, C$\underline{H}_2$), 3.95-4.10 (m, 1H, C$\underline{H}_2$), 4.55 (t, *J*=12.2 Hz, 1H, C$\underline{H}_2$), 4.92 (d, *J*=7.9 Hz, 1H, C$\underline{H}_2$), 5.65 (t, *J*=11.1 Hz, 1H, C$\underline{H}_2$), 5.83 (spt, *J*=6.8 Hz, 1H, C$\underline{H}$-CH$_3$), 7.22 (d, *J*=2.6 Hz, 1H, Ar-$\underline{H}$), 7.54 (d, *J*=2.3 Hz, 1H, Ar-$\underline{H}$), 8.31 (br. s., 1H, N=C$\underline{H}$). ^{13}C{^{1}H} NMR: ($CDCl_3$, 75 MHz): δ 24.0, 32.6, 63.6, 80.4, 130.3, 134.2, 162.1. ^{51}V NMR ($CDCl_3$, 105 MHz): δ -563.1. Elemental Analysis: Anal. Calcd for $C_{13}H_{16}Cl_2NO_4V$: C, 41.96; H, 4.33; N, 3.76. Found: C, 41.83; H, 4.46; N, 3.84.

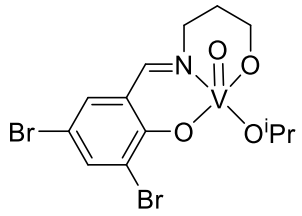

VO(2)(O^{i}Pr). Recrystallized from dichloromethane. ^{1}H NMR (CDCl3, 300 MHz): δ 1.39 (d, J=6.0 Hz, 3H, CH-C$\underline{H}_3$), 1.48 (d, *J*=6.0 Hz, 3H, CH-C$\underline{H}_3$), 1.86-2.04 (m, 1H, C$\underline{H}_2$), 2.22-2.35 (m, 1H, C$\underline{H}_2$), 3.94 (d, *J*=12.4 Hz, 1H, C$\underline{H}_2$), 4.47 (t, *J*=12.2 Hz, 1H, C$\underline{H}_2$), 4.84 (d, *J*=9.0 Hz, 1H, C$\underline{H}_2$), 5.56 (td, *J*=11.2, 2.8 Hz, 1H, C$\underline{H}_2$), 5.75-5.88 (m, 1H, C$\underline{H}$-CH$_3$), 7.32 (d, *J*=2.3 Hz, 1H, Ar-$\underline{H}$), 7.76 (d, *J*=2.3 Hz, 1H, Ar-$\underline{H}$), 8.20 (br. s., 1H, N=C$\underline{H}$). ^{13}C{^{1}H} NMR: ($CDCl_3$, 75 MHz): δ 24.2, 32.6, 63.5, 80.5, 109.3, 134.1, 139.7, 162.0. ^{51}V NMR ($CDCl_3$, 105 MHz): δ -563.2. Elemental Analysis: Anal. Calcd for $C_{13}H_{16}Br_2NO_4V$: C, 33.87; H, 3.50; N, 3.04. Found: C, 33.72; H, 3.40; N, 2.98.

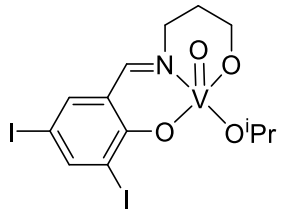

VO(3)(O^{i}Pr). Recrystallized from toluene. ^{1}H NMR ($CDCl_3$, 500 MHz): δ 1.50 (d, *J*=6.0 Hz, 3H, CH-C$\underline{H}_3$), 1.58 (d, *J*=6.0 Hz, 3H, CH-C$\underline{H}_3$), 2.03 (q, *J*=12.3 Hz, 1H, C$\underline{H}_2$), 2.35 (d, *J*=12.9 Hz, 1H,

C$\underline{H}_2$), 4.00 (d, *J*=12.0 Hz, 1H, C$\underline{H}_2$), 4.52 (t, *J*=12.6 Hz, 1H, C$\underline{H}_2$), 4.90 (d, *J*=9.8 Hz, 1H, C$\underline{H}_2$), 5.61 (t, *J*=10.6 Hz, 1H, C$\underline{H}_2$), 5.90-6.03 (m, 1H, C$\underline{H}$-CH_3), 7.58 (br. s, 1H, Ar-$\underline{H}$), 8.20 (br. s, 2H, Ar-H, N=C$\underline{H}$). $^{13}C\{^1H\}$ NMR: ($CDCl_3$, 75 MHz): δ 24.2, 24.5, 25.6, 32.6, 63.4, 78.9, 80.5, 141.4, 150.8, 161.8. ^{51}V NMR ($CDCl_3$, 132 MHz): δ -562.4. Elemental Analysis: Anal. Calcd for $C_{13}H_{16}I_2NO_4V$: C, 28.13; H, 2.91; N, 2.52. Found: C, 28.00; H, 2.79; N, 2.57.

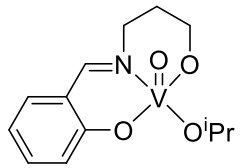

VO(4)(O^{i}Pr). ^1H NMR ($CDCl_3$, 300 MHz): δ 1.37 (d, *J*=6.4 Hz, 3H, CH-C$\underline{H}_3$), 1.43 (d, *J*=6.4 Hz, 3H, CH-C$\underline{H}_3$), 1.82-1.99 (m, 1H, C$\underline{H}_2$), 2.19-2.31 (m, 1H, C$\underline{H}_2$), 3.91 (d, *J*=12.4 Hz, 1H, C$\underline{H}_2$), 4.42 (tt, *J*=12.3, 2.2 Hz, 1H, C$\underline{H}_2$), 4.74-4.90 (m, 1H, C$\underline{H}_2$), 5.40-5.63 (m, 2H, C$\underline{H}_2$, C$\underline{H}$-CH_3), 6.77-6.86 (m, 1H, Ar-$\underline{H}$), 6.89 (d, *J*=8.3 Hz, 1H, Ar-$\underline{H}$), 7.26 (dd, *J*=7.5, 1.9 Hz, 1H, Ar-$\underline{H}$), 7.38 (ddd, *J*=8.6, 7.1, 1.7 Hz, 1H, Ar-$\underline{H}$), 8.29 (br. s., 1H, N-C$\underline{H}$). $^{13}C\{^1H\}$ NMR: ($CDCl_3$, 75 MHz): δ 24.1, 32.7, 63.4, 80.1, 83.0, 118.9, 132.8, 134.9, 163.1. ^{51}V NMR ($CDCl_3$, 105 MHz): δ -556.8. Elemental Analysis: Anal. Calcd for $C_{13}H_{18}NO_4V$: C, 51.49; H, 5.98; N, 4.62. Found: C, 51.32; H, 5.84; N, 4.66.

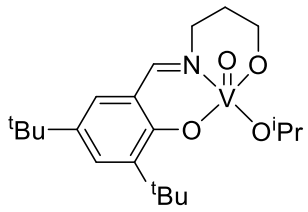

VO(5)(O^{i}Pr). ^1H NMR ($CDCl_3$, 300 MHz): δ 1.25 (s, 9H, C(C$\underline{H}_3$)$_3$), 1.37-1.43 (m, 15H, C(C$\underline{H}_3$)$_3$ (9H), CH(C$\underline{H}_3$)$_2$ (6H)), 1.82-1.91 (m, 1H, C$\underline{H}_2$), 2.13-2.24 (m, 1H, C$\underline{H}_2$), 3.80-3.91 (m, 1H, C$\underline{H}_2$), 4.35 (t, *J*=11.7 Hz, 1H, C$\underline{H}_2$), 4.70-4.85 (m, 1H, C$\underline{H}_2$), 5.43 (t, *J*=12.4 Hz, 1H, C$\underline{H}_2$), 5.63 (spt, *J*=6.0 Hz, 1H, C$\underline{H}$(CH$_3$)$_2$), 7.09 (d, *J*=2.6 Hz, 1H, Ar-$\underline{H}$), 7.46 (d, *J*=2.6 Hz, 1H, Ar-$\underline{H}$), 8.27 (br. s, 1H, N=C$\underline{H}$). $^{13}C\{^1H\}$ NMR ($CDCl_3$, 75 MHz): δ 24.6, 24.9, 25.4, 29.5, 31.5, 32.1, 32.9, 34.2, 35.2, 63.4, 127.0, 129.6, 141.0, 163.8. ^{51}V NMR ($CDCl_3$, 105 MHz): δ -568.8. Elemental Analysis: Anal. Calcd for $C_{21}H_{34}NO_4V$: C, 60.71; H, 8.25; N, 3.37. Found: C, 60.51; H, 8.88; N, 4.10.

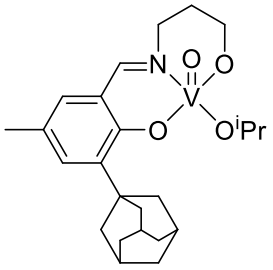

VO(6)(O^{i}Pr). ^{1}H NMR ($CDCl_3$, 300 MHz): δ 1.45 (d, *J*=6.0 Hz, 3H, CH-C$\underline{H}_3$), 1.53 (d, *J*=6.0 Hz, 3H, CH-C$\underline{H}_3$), 1.76 (d, *J*=11.7 Hz, 3H, Ad-$\underline{H}$), 1.86 (d, *J*=11.7 Hz, 3H, Ad-$\underline{H}$), 1.89-2.00 (m, 1H, C$\underline{H}_2$), 2.04-2.11 (m, 3H, Ad-$\underline{H}$), 2.14-2.22 (m, 6H, Ad-$\underline{H}$), 2.22-2.29 (m, 1H, CH_2), 2.32 (s, 3H, C$\underline{H}_3$), 3.92 (dt, *J*=12.3, 3.5 Hz, 1H, CH_2), 4.43 (tt, *J*=12.6, 1.9 Hz, 1H, CH_2), 4.82-4.93 (m, 1H, CH_2), 5.50-5.59 (m, 2H, C$\underline{H}_2$, C$\underline{H}$-CH_3), 6.99 (d, *J*=1.6 Hz, 1H, Ar-$\underline{H}$), 7.23 (d, *J*=2.2 Hz, 1H, Ar-$\underline{H}$), 8.28 (br. s., 1H, N-C$\underline{H}$). ^{13}C{^{1}H} NMR ($CDCl_3$, 125 MHz): δ 19.7, 23.5, 23.9, 28.1, 31.8, 36.0, 39.2, 62.4, 78.7, 84.1, 118.4, 126.9, 129.4, 132.1, 162.3. ^{51}V NMR ($CDCl_3$, 105 MHz): δ -556.4.

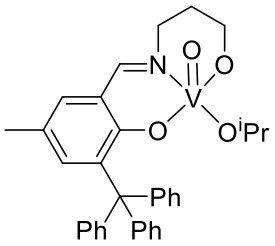

VO(7)(O^{i}Pr). ^{1}H NMR ($CDCl_3$, 500 MHz): δ 1.06 (d, *J*=6.0 Hz, 3H, CH-C$\underline{H}_3$), 1.26 (d, *J*=6.0 Hz, 3H, CH-C$\underline{H}_3$), 1.80-1.93 (m, 1H, C$\underline{H}_2$), 2.17 (d, *J*=13.2 Hz, 1H, C$\underline{H}_2$), 2.27 (s, 3H, C$\underline{H}_3$), 3.86 (d, *J*=11.7 Hz, 1H, C$\underline{H}_2$), 4.33 (t, *J*=12.0 Hz, 1H, C$\underline{H}_2$), 4.66-4.79 (m, 1H, C$\underline{H}$-CH_3), 4.88-4.98 (m, 1H, C$\underline{H}_2$), 5.33 (t, *J*=11.0 Hz, 1H, C$\underline{H}_2$), 7.04-7.40 (m, 17H, Ar-$\underline{H}$), 8.25 (br. s., 1H, N=C$\underline{H}$). ^{13}C{^{1}H} NMR ($CDCl_3$, 75 MHz): δ 20.8, 24.1, 24.4, 32.3, 63.5, 79.1, 84.9, 125.3, 127.1, 127.3, 131.1, 132.1, 136.8, 163.3. ^{51}V NMR ($CDCl_3$, 132 MHz): δ -562.6. Elemental Analysis: Anal. Calcd for $C_{33}H_{34}NO_4V$: C, 70.83; H, 6.12; N, 2.50. Found: C, 70.71; H, 6.24; N, 2.57.

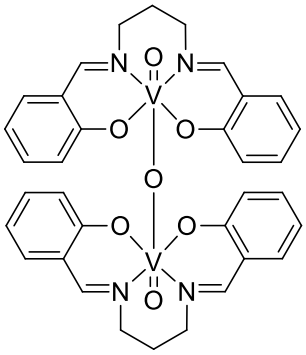

[VO(8)]$_2$O. Recrystallized from toluene. The structure presented was obtained from XRD analysis. ^{1}H NMR spectroscopy indicates the presence of several species in solution which were unable to be isolated. ^{51}V NMR ($CDCl_3$, 105 MHz): δ -498.9 (major), -513.5 (minor). Elemental Analysis: Anal. Calcd for $C_{34}H_{32}N_4O_7V_2$: C, 57.47; H, 4.54; N, 7.89. Found: C, 57.58; H, 4.61; N, 7.70.

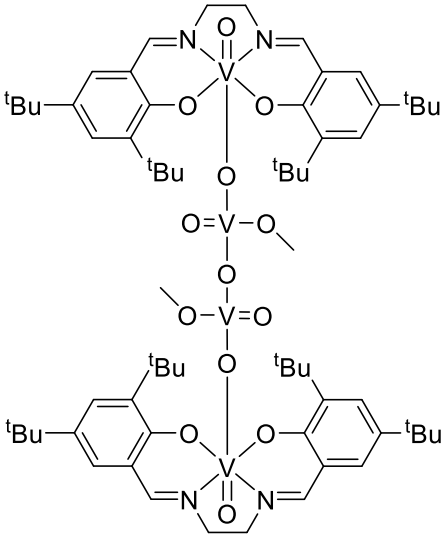

[VO(9)(VO$_2$OMe)]$_2$O. Recrystallized from methanol. The structure presented for this compound was obtained from XRD analysis. ^{1}H NMR ($CDCl_3$, 250 MHz): δ 1.19-1.45 (m, 54H, C(C<u>H</u>$_3$)$_3$), 1.54 (s, 6H, O-C<u>H</u>$_3$), 3.39-3.57 (m, 4H, C<u>H</u>$_2$), 3.70-3.96 (m, 4H, C<u>H</u>$_2$), 7.17 (d, *J*=2.53 Hz, 2H, Ar-<u>H</u>), 7.34 (d, *J*=2.21 Hz, 2H, Ar-<u>H</u>), 7.56 (dd, *J*=4.74, 2.53 Hz, 4H, Ar-<u>H</u>), 8.32 (s, 2H, N=C<u>H</u>), 8.63 (s, 2H, N=C<u>H</u>). ^{51}V NMR ($CDCl_3$, 105 MHz): δ -491.6, -496.9, -577.6, -583.9. Elemental Analysis: Anal. Calcd for $C_{66}H_{98}N_4O_{13}V_4$: C, 58.32; H, 7.27; N, 4.12. Found: C, 59.19; H, 7.29; N, 4.15.

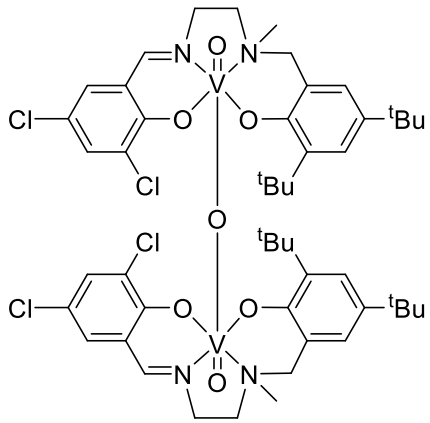

[VO(10)]$_2$O. Recrystallized from benzene. The structure presented for this compound was obtained from XRD analysis. In solution there appeared to be multiple species present and it has not been possible to isolate these. As such, the ^{1}H NMR data presented is for the major species in solution, which appears to match the solid-state structure. ^{1}H NMR ($CDCl_3$, 300 MHz): (major species in solution) δ 1.28 (s, 18H, C(C<u>H</u>$_3$)$_3$), 2.35-2.39 (m, 3H, N-C<u>H</u>$_3$), 2.86 (t, *J*=6.4 Hz, 1H, C<u>H</u>$_2$), 2.96-3.05 (m, 1H, C<u>H</u>$_2$), 3.26-3.36 (m, 1H, C<u>H</u>$_2$), 3.54-3.63 (m, 1H, C<u>H</u>$_2$), 3.82 (t, *J*=6.4 Hz, 1H, C<u>H</u>$_2$), 4.49-4.58 (m, 1H, C<u>H</u>$_2$), 6.55 (d, *J*=2.6 Hz, 1H, Ar-<u>H</u>), 6.93-6.97 (m, 1H, Ar-<u>H</u>), 7.19-7.23 (m, 1H, Ar-<u>H</u>), 7.43 (d, *J*=2.6 Hz, 1H, Ar-<u>H</u>). ^{51}V NMR ($CDCl_3$, 105 MHz): δ -482.1 (broad, major), -530.5 (minor). Elemental Analysis: Anal. Calcd for $C_{50}H_{64}Cl_4N_4O_7V_2$: C, 55.77; H, 5.99; N, 5.20. Found: C, 55.87; H, 6.14; N, 5.28.

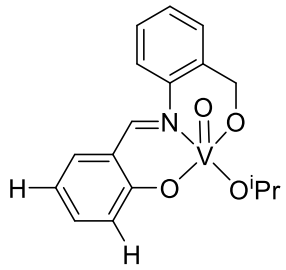

VO(11)(O^{i}Pr). ^{1}H NMR ($CDCl_3$, 500 MHz): δ 1.34 (dd, *J*=13.87, 6.31 Hz, 6H, CH(C<u>H</u>$_3$)$_2$), 5.38 (d, *J*=14.50 Hz, 1H, C<u>H</u>$_2$), 5.63 - 5.72 (m, 2H, C<u>H</u>$_2$), 6.86-6.93 (m, 2H, Ar-<u>H</u>), 7.07 (d, *J*=7.57 Hz, 1H, Ar-<u>H</u>), 7.19-7.32 (m, 3H, Ar-<u>H</u>), 7.38-7.49 (m, 2H, Ar-<u>H</u>), 8.43 (br. s., 1H, N=C<u>H</u>). ^{51}V NMR ($CDCl_3$, 105 MHz) δ -549.1.

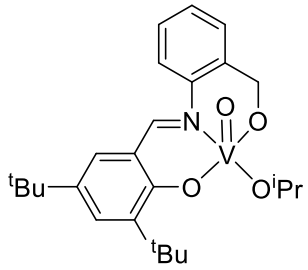

VO(12**)(O^{i}Pr).** ^{1}H NMR ($CDCl_3$, 500 MHz): δ 1.28 (s, 9H, C(C<u>H</u>$_3$)$_3$), 1.39 (d, *J*=6.2 Hz, 3H, CH(C<u>H</u>$_3$)$_2$), 1.41 (s, 9H, C(C<u>H</u>$_3$)$_3$), 1.43 (d, *J*=6.3 Hz, 3H, CH(C<u>H</u>$_3$)$_2$), 5.35 (d, *J*=13.9 Hz, 1H, C<u>H</u>$_2$), 5.59 (d, *J*=14.2 Hz, 1H, C<u>H</u>$_2$), 5.71-5.80 (m, 1H, C<u>H</u>-(CH$_3$)$_2$), 7.10 (d, *J*=7.6 Hz, 1H, Ar-<u>H</u>), 7.22-7.27 (m, 3H, Ar-<u>H</u>), 7.28-7.34 (m, 1H, Ar-<u>H</u>), 7.56 (d, *J*=2.5 Hz, 1H, Ar-<u>H</u>), 8.44 (br. s, 1H, N=C<u>H</u>). ^{51}V NMR ($CDCl_3$, 105 MHz) δ -556.5.

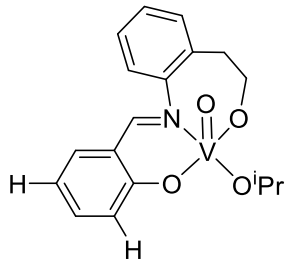

VO(13**)(O^{i}Pr).** ^{1}H NMR ($CDCl_3$, 500 MHz): δ 1.36 (d, *J*=6.0 Hz, 3H, CH(C<u>H</u>$_3$)$_2$), 1.40 (d, *J*=6.0 Hz, 3H, CH(C<u>H</u>$_3$)$_2$), 4.06-4.21 (m, 1H, C<u>H</u>$_2$), 4.46-4.58 (m, 1H, C<u>H</u>$_2$), 4.73-4.82 (m, 1H, C<u>H</u>$_2$), 5.18-5.27 (m, 1H, C<u>H</u>$_2$), 5.44-5.55 (m, 1H, C<u>H</u>-(CH$_3$)$_2$), 6.83-6.88 (m, 2H, Ar-<u>H</u>), 6.96 (d, *J*=8.2 Hz, 2H, Ar-<u>H</u>), 7.33 (dd, *J*=7.7, 1.7 Hz, 2H, Ar-<u>H</u>), 7.44 (ddd, *J*=8.5, 7.1, 1.7 Hz, 2H, Ar-<u>H</u>), 8.31 (s, 1H, N=C<u>H</u>).

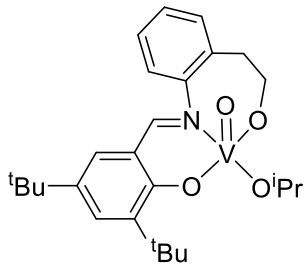

VO(14**)(O^{i}Pr).** ^{1}H NMR ($CDCl_3$, 500 MHz): δ 1.35 (s, 9H, C(C<u>H</u>$_3$)$_3$), 1.44 (d, *J*=6.0 Hz, 3H, CH(C<u>H</u>$_3$)$_2$), 1.47 (d, *J*=6.0 Hz, 3H, CH(C<u>H</u>$_3$)$_2$), 1.53 (s, 9H, C(C<u>H</u>$_3$)$_3$), 4.84-4.92 (m, 1H, C<u>H</u>$_2$), 5.10-5.24 (m, 3H, C<u>H</u>$_2$), 5.60-5.74 (m, 1H, C<u>H</u>-(CH$_3$)$_2$), 7.18-7.21 (m, 1H, Ar-<u>H</u>), 7.24-7.26 (m, 2H, Ar-<u>H</u>), 7.28-7.35 (m, 2H, Ar-<u>H</u>), 7.65 (d, *J*=2.5 Hz, 1H, Ar-<u>H</u>), 8.43 (s, 1H, N=C<u>H</u>).

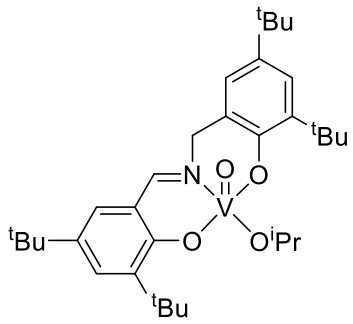

VO(15**)(O^{i}Pr).** Recrystallized from toluene. ^{1}H NMR ($CDCl_3$, 300 MHz): δ 1.24 (s, 9H, C(C$\underline{H}_3$)$_3$), 1.24 (s, 9H, C(C$\underline{H}_3$)$_3$), 1.35 (s, 9H, C(C$\underline{H}_3$)$_3$), 1.38 (s, 9H, C(C$\underline{H}_3$)$_3$), 1.51 (d, *J*=6.0 Hz, 3H, CH(C$\underline{H}_3$)$_2$), 1.58 (d, *J*=6.0 Hz, 3H. CH(C$\underline{H}_3$)$_2$), 4.48 (d, *J*=12.8 Hz, 1H, C$\underline{H}_2$), 5.51 (d, *J*=12.8 Hz, 1H, C$\underline{H}_2$), 5.90-6.05 (m, 1H, C$\underline{H}$(CH$_3$)$_2$), 6.95 (d, *J*=2.3 Hz, 1H, Ar-$\underline{H}$), 7.16 (d, *J*=2.6 Hz, 1H, Ar-$\underline{H}$), 7.20 (d, *J*=2.3 Hz, 1H, Ar-$\underline{H}$), 7.49 (d, *J*=2.6 Hz, 1H, Ar-$\underline{H}$), 8.48 (br. s, 1H, N=C$\underline{H}$). ^{13}C NMR ($CDCl_3$, 75 MHz): δ 24.5, 24.7, 28.5, 28.8, 30.4, 30.7, 34.0, 34.3, 65.0, 120.7, 122.4, 123.1, 125.9, 129.1, 140.9, 141.1, 163.3. ^{51}V NMR ($CDCl_3$, 105 MHz): δ -345.7 (major), -357.9 (minor), -358.7 (minor).

References

1. Department for Transport, Renewable Transport Fuels Obligation, https://www.gov.uk/government/collections/renewable-transport-fuels-obligation-rtfo-orders, (accessed 20th October 2015).
2. United States Environmental Protection Agency, Renewable Energy Production Incentives, http://www3.epa.gov/epawaste/hazard/wastemin/minimize/energyrec/rpsinc.htm, (accessed 25th October 2015).
3. Biomass Energy Centre, UK biomass power stations - current and planned, http://www.biomassenergycentre.org.uk/pls/portal/docs/PAGE/BEC_TECHNICAL/REF_LIB_TECH/EXISTING%20INSTALLATIONS/UK%20BIOMASS%20POWER%20STATIONS%20V1.4%20MARCH%202013.PDF, (accessed 25th November 2015).
4. Energy Saving Trust, Grants and Support England, http://www.energysavingtrust.org.uk/domestic/grants-and-support-england, (accessed 25th October 2015).
5. Biorefinery.nl, Policy and Legislation - The Netherlands, http://www.biorefinery.nl/background-biorefinery/policy-legislation/, (accessed 25th October 2015).
6. N. P. Kutscha and J. R. Gray, *Maine Agricultural Experiment Station Technical Bulletin*, 1970, 1-20.
7. G. Berndes, C. Azar, T. Kåberger and D. Abrahamson, *Biomass Bioenerg.*, 2001, **20**, 371-383.
8. B. Kuznetsov, V. Taraban'ko and S. Kuznetsova, *Kinet. Catal.*, 2008, **49**, 517-526.
9. R.-C. Sun, *Bioresources*, 2009, **4**, 452-455.
10. F. S. Chakar and A. J. Ragauskas, *Ind. Crop. Prod.*, 2004, **20**, 131-141.
11. J. E. Holladay, J. J. Bozell, J. F. White and D. Johnson, Top Value-Added Chemicals from Biomass. Results of Screening for Potential Candidates from Biorefinery Lignin. vol. II, U.S. Department of Energy (DOE) by PNNL, Richland, WA, USA, http://www1.eere.energy.gov/biomass/pdfs/pnnl-16983.pdf, (accessed 20th April 2012).
12. M. Kleinert and T. Barth, *Chem. Eng. Technol.*, 2008, **31**, 736-745.
13. M. P. Pandey and C. S. Kim, *Chem. Eng. Technol.*, 2011, **34**, 29-41.
14. E. Adler, *Wood Sci. Technol.*, 1977, **11**, 169-218.
15. G. Gellerstedt, J. Li, I. Eide, M. Kleinert and T. Barth, *Energy & Fuels*, 2008, **22**, 4240-4244.
16. M. Kleinert and T. Barth, *Energy & Fuels*, 2008, **22**, 1371-1379.
17. M. Kleinert, J. R. Gasson and T. Barth, *J. Anal. Appl. Pyrol.*, 2009, **85**, 108-117.
18. WO/2011/026243, 2011.
19. J. Stephens and C. Halpin, *Improvement of Crop Plants for Industrial End Uses*, Springer Netherlands, 2007.
20. R. J. A. Gosselink, E. de Jong, B. Guran and A. Abacherli, *Ind. Crop. Prod.*, 2004, **20**, 121-129.
21. J. Zakzeski, P. C. A. Bruijnincx, A. L. Jongerius and B. M. Weckhuysen, *Chem. Rev.*, 2010, **110**, 3552-3599.
22. R. ten Have and P. J. M. Teunissen, *Chem. Rev.*, 2001, **101**, 3397-3414.
23. Z. Yuan, S. Cheng, M. Leitch and C. Xu, *Bioresour. Technol.*, 2010, **101**, 9308-9313.
24. H. B. Klinke, B. K. Ahring, A. S. Schmidt and A. B. Thomsen, *Bioresour. Technol.*, 2002, **82**, 15-26.

25. L. d. C. Sousa, S. P. S. Chundawat, V. Balan and B. E. Dale, *Curr. Opin. Biotech.*, 2009, **20**, 339-347.
26. D. C. Dibble, C. L. Li, L. Sun, A. George, A. R. L. Cheng, O. P. Cetinkol, P. Benke, B. M. Holmes, S. Singh and B. A. Simmons, *Green Chem.*, 2011, **13**, 3255-3264.
27. A. George, K. Tran, T. J. Morgan, P. I. Benke, C. Berrueco, E. Lorente, B. C. Wu, J. D. Keasling, B. A. Simmons and B. M. Holmes, *Green Chem.*, 2011, **13**, 3375-3385.
28. R. P. Chandra, R. Bura, W. E. Mabee, A. Berlin, X. Pan and J. N. Saddler, in *Biofuels*, ed. L. Olsson, Springer-Verlag Berlin, Berlin, 2007, vol. 108, pp. 67-93.
29. L. T. Fan, Y. H. Lee and D. R. Beardmore, *Biotech. Bioeng.*, 1981, **23**, 419-424.
30. F. C. Lu and J. Ralph, *Plant J.*, 2003, **35**, 535-544.
31. I. Kilpelainen, H. Xie, A. King, M. Granstrom, S. Heikkinen and D. S. Argyropoulos, *J. Agric. Food Chem.*, 2007, **55**, 9142-9148.
32. P. Sannigrahi, D. H. Kim, S. Jung and A. Ragauskas, *Energ. Environ. Sci.*, 2011, **4**, 1306-1310.
33. M. M. Ksenofontova, A. N. Mitrofanova, N. A. Mamleeva, A. N. Pryakhin and V. V. Lunin, *Ozone-Sci. Eng.*, 2003, **25**, 505-512.
34. N. A. Mamleeva, S. A. Autlov, N. y. G. Bazarnova and V. V. Lunin, *Pure Appl. Chem.*, 2009, **81**, 2081-2091.
35. N. A. Mamleeva, S. A. Autlov, A. V. Fionov, N. G. Bazarnova and V. V. Lunin, *Russ. J. Phys. Chem. A*, 2009, **83**, 745-751.
36. C. J. Chuck, H. J. Parker, R. W. Jenkins and J. Donnelly, *Bioresour. Technol.*, 2013, **143**, 549-554.
37. J. D. Keating, C. Panganiban and S. D. Mansfield, *Biotech. Bioeng.*, 2006, **93**, 1196-1206.
38. F. Garcia Calvo-Flores and J. A. Dobado, *Chemsuschem*, 2010, **3**, 1227-1235.
39. M. M. Hossain and L. Aldous, *Aust. J. Chem.*, 2012, **65**, 1465-1477.
40. D. A. Fort, R. C. Remsing, R. P. Swatloski, P. Moyna, G. Moyna and R. D. Rogers, *Green Chem.*, 2007, **9**, 63-69.
41. A. Brandt, M. J. Ray, T. Q. To, D. J. Leak, R. J. Murphy and T. Welton, *Green Chem.*, 2011, **13**, 2489-2499.
42. A. Brandt, J. Grasvik, J. P. Hallett and T. Welton, *Green Chem.*, 2013, **15**, 550-583.
43. Y. Hamada, K. Yoshida, R. Asai, S. Hayase, T. Nokami, S. Izumi and T. Itoh, *Green Chem.*, 2013, **15**, 1863-1868.
44. N. Sathitsuksanoh, K. M. Holtman, D. J. Yelle, T. Morgan, V. Stavila, J. Pelton, H. Blanch, B. A. Simmons and A. George, *Green Chem.*, 2014, **16**, 1236-1247.
45. N. Sun, R. Parthasarathi, A. M. Socha, J. Shi, S. Zhang, V. Stavila, K. L. Sale, B. A. Simmons and S. Singh, *Green Chem.*, 2014, **16**, 2546-2557.
46. J. Shi, K. Balamurugan, R. Parthasarathi, N. Sathitsuksanoh, S. Zhang, V. Stavila, V. Subramanian, B. A. Simmons and S. Singh, *Green Chem.*, 2014, **16**, 3830-3840.
47. J. L. Espinoza-Acosta, P. I. Torres-Chavez, E. Carvajal-Millan, B. Ramirez-Wong, L. A. Bello-Perez and B. Montano-Leyva, *Bioresources*, 2014, **9**, 3660-3687.
48. K. C. Badgujar and B. M. Bhanage, *Bioresour. Technol.*, 2015, **178**, 2-18.
49. K. Ninomiya, K. Inoue, Y. Aomori, A. Ohnishi, C. Ogino, N. Shimizu and K. Takahashi, *Chem. Eng. J.*, 2015, **259**, 323-329.
50. M. J. Earle and K. R. Seddon, *Pure Appl. Chem.*, 2000, **72**, 1391-1398.
51. R. A. Sheldon, R. M. Lau, M. J. Sorgedrager, F. van Rantwijk and K. R. Seddon, *Green Chem.*, 2002, **4**, 147-151.
52. R. D. Rogers and K. R. Seddon, *Science*, 2003, **302**, 792-793.
53. F. van Rantwijk and R. A. Sheldon, *Chem. Rev.*, 2007, **107**, 2757-2785.
54. R. P. Swatloski, S. K. Spear, J. D. Holbrey and R. D. Rogers, *J. Am. Chem. Soc.*, 2002, **124**, 4974-4975.

55. R. C. Remsing, R. P. Swatloski, R. D. Rogers and G. Moyna, *Chem. Comm.*, 2006, 1271-1273.
56. Y. Q. Pu, N. Jiang and A. J. Ragauskas, *J. Wood Chem. Technol.*, 2007, **27**, 23-33.
57. M. Zavrel, D. Bross, M. Funke, J. Buchs and A. C. Spiess, *Bioresour. Technol.*, 2009, **100**, 2580-2587.
58. J. F. Kennedy, *Cellulose and its derivatives : chemistry, biochemistry and applications*, Chichester : Horwood, 1985.
59. F. O. Licht, *Int. Sugar J.*, 2015, **117**, 182-184.
60. W. Lan, C. F. Liu and R. C. Sun, *J. Agric. Food Chem.*, 2011, **59**, 8691-8701.
61. S. Singh, B. A. Simmons and K. P. Vogel, *Biotech. Bioeng.*, 2009, **104**, 68-75.
62. S. H. Lee, T. V. Doherty, R. J. Linhardt and J. S. Dordick, *Biotech. Bioeng.*, 2009, **102**, 1368-1376.
63. T. V. Doherty, M. Mora-Pale, S. E. Foley, R. J. Linhardt and J. S. Dordick, *Green Chem.*, 2010, **12**, 1967-1975.
64. M. J. Kamlet and R. W. Taft, *J. Am. Chem. Soc.*, 1976, **98**, 377-383.
65. J. L. Anderson, J. Ding, T. Welton and D. W. Armstrong, *J. Am. Chem. Soc.*, 2002, **124**, 14247-14254.
66. G. Cheng, M. S. Kent, L. L. He, P. Varanasi, D. Dibble, R. Arora, K. Deng, K. L. Hong, Y. B. Melnichenko, B. A. Simmons and S. Singh, *Langmuir*, 2012, **28**, 11859-11866.
67. W. E. S. Hart, J. B. Harper and L. Aldous, *Green Chem.*, 2015, **17**, 214-218.
68. W. Y. Ji, Z. D. Ding, J. H. Liu, Q. X. Song, X. L. Xia, H. Y. Gao, H. J. Wang and W. X. Gu, *Energy & Fuels*, 2012, **26**, 6393-6403.
69. J. L. Wen, T. Q. Yuan, S. L. Sun, F. Xu and R. C. Sun, *Green Chem.*, 2014, **16**, 181-190.
70. J. L. Wen, S. L. Sun, B. L. Xue and R. C. Sun, *J. Agric. Food Chem.*, 2013, **61**, 635-645.
71. J. D. Holbrey, W. M. Reichert, M. Nieuwenhuyzen, O. Sheppard, C. Hardacre and R. D. Rogers, *Chem. Comm.*, 2003, 476-477.
72. P. Varanasi, P. Singh, M. Auer, P. D. Adams, B. A. Simmons and S. Singh, *Biotechnology for Biofuels*, 2013, **6**.
73. D. B. Fu, G. Mazza and Y. Tamaki, *J. Agric. Food Chem.*, 2010, **58**, 2915-2922.
74. Q.-P. Liu, X.-D. Hou, N. Li and M.-H. Zong, *Green Chem.*, 2012, **14**, 304-307.
75. C. J. Biermann, *Handbook of Pulping and Papermaking*, San Diego : Academic Press, 2nd Ed. edn., 1996.
76. R. Wang, C. L. Chen and J. S. Gratzl, *Holzforschung*, 2004, **58**, 622-630.
77. S. Shimizu, T. Yokoyama, T. Akiyama and Y. Matsumoto, *J. Agric. Food Chem.*, 2012, **60**, 6471-6476.
78. M. Petkovic, J. L. Ferguson, H. Q. N. Gunaratne, R. Ferreira, M. C. Leitao, K. R. Seddon, L. P. N. Rebelo and C. S. Pereira, *Green Chem.*, 2010, **12**, 643-649.
79. B. G. Janesko, *Phys. Chem. Chem. Phys.*, 2011, **13**, 11393-11401.
80. M. Gericke, T. Liebert, O. A. El Seoud and T. Heinze, *Macromol. Mater. Eng.*, 2011, **296**, 483-493.
81. K. A. Le, C. Rudaz and T. Budtova, *Carbohyd. Polym.*, 2014, **105**, 237-243.
82. A. Radhi, K. A. Le, M. E. Ries and T. Budtova, *J. Phys. Chem. B*, 2015, **119**, 1633-1640.
83. L. E. Ficke and J. F. Brennecke, *J. Phys Chem. B*, 2010, **114**, 10496-10501.
84. S. Zhu, *J. Chem. Technol. Biotechnol.*, 2008, **83**, 777-779.
85. N. Sathitsuksanoh, M. Sawant, Q. Truong, J. Tan, C. G. Canlas, N. Sun, W. Zhang, S. Renneckar, T. Prasomsri, J. Shi, O. Cetinkol, S. Singh, B. A. Simmons and A. George, *Bioenerg. Res.*, 2015, **8**, 973-981.
86. A. G. Cruz, C. Scullin, C. Mu, G. Cheng, V. Stavila, P. Varanasi, D. Xu, J. Mentel, Y.-D. Chuang, B. A. Simmons and S. Singh, *Biotechnology for Biofuels*, 2013, **6**.
87. C. Li, D. Tanjore, W. He, J. Wong, J. L. Gardner, K. L. Sale, B. A. Simmons and S. Singh, *Biotechnology for Biofuels*, 2013, **6**.

88. P. Varanasi, P. Singh, R. Arora, P. D. Adams, M. Auer, B. A. Simmons and S. Singh, *Bioresour. Technol.*, 2012, **126**, 156-161.
89. H. Kim and J. Ralph, *Org.Biomol. Chem.*, 2010, **8**, 576-591.
90. M. Bunzel and J. Ralph, *J. Agric. Food Chem.*, 2006, **54**, 8352-8361.
91. D. J. Yelle, J. Ralph and C. R. Frihart, *Magn. Reson. Chem.*, 2008, **46**, 508-517.
92. S. Y. Jia, B. J. Cox, X. W. Guo, Z. C. Zhang and J. G. Ekerdt, *Chemsuschem*, 2010, **3**, 1078-1084.
93. V. I. Parvulescu and C. Hardacre, *Chem. Rev.*, 2007, **107**, 2615-2665.
94. J. Zakzeski, A. L. Jongerius and B. M. Weckhuysen, *Green Chem.*, 2010, **12**, 1225-1236.
95. J. B. Binder, M. J. Gray, J. F. White, Z. C. Zhang and J. E. Holladay, *Biomass Bioenerg.*, 2009, **33**, 1122-1130.
96. B. J. Cox, S. Y. Jia, Z. C. Zhang and J. G. Ekerdt, *Polym. Degrad. Stab.*, 2011, **96**, 426-431.
97. S. Y. Jia, B. J. Cox, X. W. Guo, Z. C. Zhang and J. G. Ekerdt, *Ind. Eng. Chem. Res.*, 2011, **50**, 849-855.
98. X. P. Ouyang, Z. X. Lin, Y. H. Deng, D. J. Yang and X. Q. Qiu, *Chinese J. Chem. Eng.*, 2010, **18**, 695-702.
99. P. R. Patwardhan, R. C. Brown and B. H. Shanks, *Chemsuschem*, 2011, **4**, 1629-1636.
100. B. Kamm, P. T. Gruber and M. Kamm, eds., *Biorefineries - Industrial Processes and Products*, WILEY-VCH, 2010.
101. J. Hu, D. Shen, R. Xiao, S. Wu and H. Zhang, *Energy Fuels*, 2012.
102. C. O. Kappe, *Angew. Chem. Int. Ed.*, 2004, **43**, 6250-6284.
103. S. K. Badamali, R. Luque, J. H. Clark and S. W. Breeden, *Catal. Comm.*, 2009, **10**, 1010-1013.
104. S. K. Badamali, R. Luque, J. H. Clark and S. W. Breeden, *Catal. Comm.*, 2011, **12**, 993-995.
105. A. Toledano, L. Serrano, J. Labidi, A. Pineda, A. M. Balu and R. Luque, *ChemCatChem*, 2012, ***5***, 997-985.
106. D. J. Macquarrie, J. H. Clark and E. Fitzpatrick, *Biofuels Bioproducts & Biorefining-Biofpr*, 2012, **6**, 549-560.
107. M. E. Alanon, L. Castro-Vazquez, M. C. Diaz-Maroto, M. H. Gordon and M. S. Perez-Coello, *Food Chem.*, 2011, **128**, 997-1002.
108. M. E. Alanon, L. Castro-Vazquez, M. C. Diaz-Maroto, I. Hermosin-Gutierrez, M. H. Gordon and M. S. Perez-Coello, *Food Chem.*, 2011, **129**, 1584-1590.
109. A. Y. Loo, K. Jain and I. Darah, *Food Chem.*, 2008, **107**, 1151-1160.
110. A. G. Sergeev and J. F. Hartwig, *Science*, 2011, **332**, 439-443.
111. J. M. W. Chan, S. Bauer, H. Sorek, S. Sreekumar, K. Wang and F. D. Toste, *ACS Catal.*, 2013, **3**, 1369-1377.
112. S. Kim, S. C. Chmely, M. R. Nimlos, Y. J. Bomble, T. D. Foust, R. S. Paton and G. T. Beckham, *J. Phys. Chem. Lett.*, 2011, **2**, 2846-2852.
113. T. Yoshikawa, T. Yagi, S. Shinohara, T. Fukunaga, Y. Nakasaka, T. Tago and T. Masuda, *Fuel Proc. Technol.*, 2013, **108**, 69-75.
114. A. Toledano, L. Serrano, A. Mariana Balu, R. Luque, A. Pineda and J. Labidi, *Chemsuschem*, 2013, **6**, 529-536.
115. A. Wu, B. O. Patrick, E. Chung and B. R. James, *Dalton Trans.*, 2012, **41**, 11093-11106.
116. J. M. Nichols, L. M. Bishop, R. G. Bergman and J. A. Ellman, *J. Am. Chem. Soc.*, 2010, **132**, 12554-12555.
117. S. K. Hanson, R. T. Baker, J. C. Gordon, B. L. Scott and D. L. Thorn, *Inorg. Chem.*, 2010, **49**, 5611-5618.

118. S. Son and F. D. Toste, *Angew. Chem. Int. Ed.*, 2010, **49**, 3791-3794.
119. S. K. Hanson, R. L. Wu and L. A. Silks, *Angew. Chem. Int. Ed.*, 2012, **51**, 3410-3413.
120. B. Sedai, C. Díaz-Urrutia, R. T. Baker, R. Wu, L. A. P. Silks and S. K. Hanson, *ACS Catal.*, 2011, **1**, 794-804.
121. G. Knothe, *Energy Fuels*, 2008, **22**, 1358-1364.
122. G. J. Van and G. Knothe, *AOCS Monogr. Ser. Oilseeds*, 2008, **2**, 499-538.
123. N. Foidl, G. Foidl, M. Sanchez, M. Mittelbach and S. Hackel, *Bioresour. Technol.*, 1996, **58**, 77-82.
124. R. Huerlimann, R. de Nys and K. Heimann, *Biotech. Bioeng.*, 2010, **107**, 245-257.
125. N. O. Zhila, G. S. Kalacheva and T. G. Volova, *J. Appl. Phycol.*, 2011, **23**, 47-52.
126. F. Santamauro, F. M. Whiffin, R. J. Scott and C. J. Chuck, *Biotechnology for Biofuels*, 2014, **7**.
127. Y. C. Liang, C. Y. May, C. S. Foon, M. A. Ngan, C. H. Chuah and Y. Basiron, *Fuel*, 2006, **85**, 867-870.
128. M. Lapuerta, O. Armas and J. Rodriguez-Fernandez, *Prog. Energ. Combust. Sci.*, 2008, **34**, 198-223.
129. J. Xue, T. E. Grift and A. C. Hansen, *Ren. Sus. Energ. Rev.*, 2011, **15**, 1098-1116.
130. L. Botella, F. Bimbela, L. Martin, J. Arauzo and J. L. Sanchez, *Frontiers in chemistry*, 2014, **2**, 43-43.
131. US Department of Energy Alternative Fuels Data Centre, ASTM Biodiesel Specifications, http://www.afdc.energy.gov/fuels/biodiesel_specifications.html, (accessed 25th November 2015).
132. Biofueltesting.com, Biodiesel Specifications, http://www.biofueltesting.com/specifications.asp, (accessed 25th November 2015).
133. C. D. Bannister, C. J. Chuck, M. Bounds and J. G. Hawley, *Proceedings of the Institution of Mechanical Engineers Part D-Journal of Automobile Engineering*, 2011, **225**, 99-114.
134. B. D. Batts and A. Z. Fathoni, *Energy Fuels*, 1991, **5**, 2-21.
135. M. Meira, P. M. B. Santana, A. S. Araujo, C. L. Silva, J. R. L. Leal Filho and H. T. Ferreira, *Corros. Rev.*, 2014, **32**, 143-161.
136. H. L. Fang, S. D. Whitacre, E. S. Yamaguchi and M. Boons, *SAE technical paper*, 2007, **2007-01-4141**.
137. S. Jain and M. P. Sharma, *Ren. Sus. Energ. Rev.*, 2010, **14**, 667-678.
138. C. E. Frank, *Chem. Rev.*, 1950, **46**, 155-169.
139. J. P. Cosgrove, D. F. Church and W. A. Pryor, *Lipids*, 1987, **22**, 299-304.
140. National Renewable Energy Laboratory, Characterization of biodiesel oxidation and oxidation products, Technical Literature Review, http://www.nrel.gov/docs/fy06osti/39096.pdf, (accessed 24th November 2015).
141. G. Knothe and R. O. Dunn, *J. Am. Oil Chem. Soc.*, 2003, **80**, 1021-1026.
142. E. Christensen and R. L. McCormick, *Fuel Proc. Technol.*, 2014, **128**, 339-348.
143. A. Bouaid, M. Martinez and J. Aracil, *Fuel*, 2007, **86**, 2596-2602.
144. P. Bondioli, A. Gasparoli, L. Della Bella, S. Tagliabue and G. Toso, *Eur. J. Lipid Sci. Technol.*, 2003, **105**, 735-741.
145. G. L. Hasenhuettl and P. J. Wan, *J. Am. Oil Chem. Soc.*, 1992, **69**, 525-527.
146. J. Pahgova, L. u. Jorikova and J. Cvengros, *Energy Fuels*, 2008, **22**, 1991-1996.
147. S. de Goede, C. Wilken, M. Ajam, P. Roets, P. Engelbrecht and C. Woolard, *Journal of Fuels*, 2015, **vol. 2015**, 15 pages.
148. C. J. Chuck, C. D. Bannister, R. W. Jenkins, J. P. Lowe and M. G. Davidson, *Fuel*, 2012, **96**, 426-433.
149. P. Bondioli, A. Gasparoli, A. Lanzani, E. Fedeli, S. Veronese and M. Sala, *J. Am. Oil Chem. Soc.*, 1995, **72**, 699-702.

150. J. C. Thompson, C. L. Peterson, D. L. Reece and S. M. Beck, *Trans. ASAE*, 1998, **41**, 931-939.
151. R. T. Lagemann, *J. Am. Chem. Soc.*, 1945, **67**, 498-499.
152. M. Lapuerta, J. Rodriguez-Fernandez, A. Ramos and B. Alvarez, *Fuel*, 2012, **93**, 391-396.
153. R. O. Dunn, *Energy Fuels*, 2008, **22**, 657-662.
154. D. Y. C. Leung, B. C. P. Koo and Y. Guo, *Bioresour. Technol.*, 2006, **97**, 250-256.
155. K. Yamane, K. Kawasaki, K. Sone, T. Hara and T. Prakoso, *Int. J. Engine Res.*, 2007, **8**, 307-319.
156. I. P. Aquino, R. P. B. Hernandez, D. L. Chicoma, H. P. F. Pinto and I. V. Aoki, *Fuel*, 2012, **102**, 795-807.
157. R. L. McCormick, M. Ratcliff, L. Moens and R. Lawrence, *Fuel Proc. Technol.*, 2007, **88**, 651-657.
158. E. L. Shanina, G. E. Zaikov, L. K. Fazlieva, S. V. Bukharov and N. A. Mukmeneva, *J. Appl. Polym. Sci.*, 2002, **85**, 2239-2243.
159. M. Mittelbach and S. Schober, *J. Am. Oil Chem. Soc.*, 2003, **80**, 817-823.
160. S. Schober and M. Mittellbach, *Eur. J. Lipid Sci. Technol.*, 2004, **106**, 382-389.
161. A. Sarin, N. P. Singh, R. Sarin and R. K. Malhotra, *Energy*, 2010, **35**, 4645-4648.
162. N. Canha, P. Felizardo, J. C. Menezes and M. J. N. Correia, 2012, **97**, 352–357.
163. E. J. Lien, S. J. Ren, H. Y. H. Bui and R. B. Wang, *Free Radical Bio. Med.*, 1999, **26**, 285-294.
164. E. L. Whitelaw, G. Loraine, M. F. Mahon and M. D. Jones, *Dalton Trans.*, 2011, **40**, 11469-11473.
165. T. R. Forder and M. D. Jones, *New Journal of Chemistry*, 2015, **39**, 1974-1978.
166. A. I. Kochnev, I. I. Oleynik, I. V. Oleynik, S. S. Ivanchev and G. A. Tolstikov, *Russ. Chem. Bull.*, 2007, **56**, 1125-1129.
167. W. Priebsch and D. Rehder, *Inorg. Chem.*, 1985, **24**, 3058-3062.
168. P. B. Chatterjee, O. Goncharov-Zapata, L. L. Quinn, G. Hou, H. Hamaed, R. W. Schurko, T. Polenova and D. C. Crans, *Inorg. Chem.*, 2011, **50**, 9794-9803.
169. C. J. Carrano, C. M. Nunn, R. Quan, J. A. Bonadies and V. L. Pecoraro, *Inorg. Chem.*, 1990, **29**, 944-951.
170. P. Adaeo, J. C. Pessoa, R. T. Henriques, M. L. Kuznetsov, F. Avecilla, M. R. Maurya, U. Kumar and I. Correia, *Inorg. Chem.*, 2009, **48**, 3542-3561.
171. R. Evans, Z. Deng, A. K. Rogerson, A. S. McLachlan, J. J. Richards, M. Nilsson and G. A. Morris, *Angew. Chem. Int. Ed.*, 2015, **52**, 3199-3202.
172. A. Butler, M. J. Danzitz and H. Eckert, *J. Am. Chem. Soc.*, 1987, **109**, 1864-1865.
173. U. G. Nielsen, H. J. Jakobsen and J. Skibsted, *J. Phys. Chem. B*, 2001, **105**, 420-429.
174. R. Prado, X. Erdocia and J. Labidi, *J. Chem. Technol. Biotechnol.*, 2013, **88**, 1248-1257.
175. A. Toledano, L. Serrano, A. Pineda, A. A. Romero, R. Luque and J. Labidi, *Appl. Catal B: Environ.*, 2014, **145**, 43-55.
176. H. J. Parker, MRes Thesis, University of Bath, 2012.
177. R. G. LeBel and D. A. I. Goring, *J. Chem. Eng. Data*, 1962, **7**, 100-101.
178. Y. Q. Pu, S. L. Cao and A. J. Ragauskas, *Energ. Environ. Sci.*, 2011, **4**, 3154-3166.
179. Y. Yang, Y. Zhang, S. Hao, J. Guan, H. Ding, F. Shang, P. Qiu and Q. Kan, *Appl. Catal. A: General*, 2010, **381**, 274-281.
180. H. J. Parker, C. J. Chuck, T. Woodman and M. D. Jones, *Catal. Today*, 2015.
181. J. L. Anthony, J. L. Anderson, E. J. Maginn and J. F. Brennecke, *J. Phys. Chem. B*, 2005, **109**, 6366-6374.

182. http://www.gaylordchemical.com, Dimethyl Sulfoxide (DMSO) Solubility Data, http://www.gaylordchemical.com/uploads/images/pdfs/literature/102B_english.pdf (accessed 18th January 2016).
183. S. Kubo, K. Hashida, T. Yamada, S. Hishiyama, K. Magara, M. Kishino, H. Ohno and S. Hosoya, *J. Wood Chem. Technol.*, 2008, **28**, 84-96.
184. J. Shi, J. M. Gladden, N. Sathitsuksanoh, P. Kambam, L. Sandoval, D. Mitra, S. Zhang, A. George, S. W. Singer, B. A. Simmons and S. Singh, *Green Chem.*, 2013, **15**, 2579-2589.
185. G. Papa, P. Varanasi, L. Sun, G. Cheng, V. Stavila, B. Holmes, B. A. Simmons, F. Adani and S. Singh, *Bioresour. Technol.*, 2012, **117**, 352-359.
186. X.-D. Hou, T. J. Smith, N. Li and M.-H. Zong, *Biotech. Bioeng.*, 2012, **109**, 2484-2493.
187. A. M. Socha, R. Parthasarathi, J. Shi, S. Pattathil, D. Whyte, M. Bergeron, A. George, K. Tran, V. Stavila, S. Venkatachalam, M. G. Hahn, B. A. Simmons and S. Singh, *Proceedings of the National Academy of Sciences of the United States of America*, 2014, **111**, E3587-E3595.
188. W. A. Yehye, N. A. Rahman, A. Ariffin, S. B. A. Hamid, A. A. Alhadi, F. A. Kadir and M. Yaeghoobi, *Eur. J. Med. Chem.*, 2015, **101**, 295-312.
189. Marketsandmarkets.com, Fuel Additives Market by Application (Diesel, Gasoline, Aviation & Others), by Type (Deposit Control, Antioxidant, Corrosion, Inhibitor, Lubricity & CETANE Improvers & Others) and by Regions - Global Trends & Forecasts to 2020, http://www.marketsandmarkets.com/Market-Reports/fuel-additives-market-723.html, (accessed 23th November 2015).
190. C. Amen-Chen, H. Pakdel and C. Roy, *Bioresour. Technol.*, 2001, **79**, 277-299.
191. S. Jain and M. P. Sharma, *Ren. Sus. Energ. Rev.*, 2010, **14**, 1937-1947.
192. R. Borges, J. Batista, R. Viana, A. Baetas, E. Orestes, M. Andrade, K. Honório and A. da Silva, *Molecules*, 2013, **18**, 12663-12674.
193. J. A. P. Coutinho and J. L. Daridon, *Pet. Sci. Technol.*, 2005, **23**, 1113-1128.
194. M. V. Kok, J. M. Letoffe, P. Claudy, D. Martin, M. Garcin and J. L. Volle, *Fuel*, 1996, **75**, 787-790.
195. Z. Jiang, J. M. Hutchinson and C. T. Imrie, *Fuel*, 2001, **80**, 367-371.
196. G. Sheldrick, *Acta Crystallogr. A*, 2008, **64**, 112-122.

Appendices

Appendix 1: Crystal data for VO(1)(O^{i}Pr)

Empirical formula	$C_{26}H_{32}Cl_4N_2O_8V_2$	
Formula weight	744.22	
Temperature	150(2) K	
Wavelength	0.71073 Å	
Crystal system, space group	Monoclinic, $P2_1/c$	
Unit cell dimensions	a = 9.6580(5) Å	α = 90°
	b = 17.2520(8) Å	β = 113.179(3)°
	c = 10.1080(5) Å	γ = 90°
Volume	1548.24(13) Å^3	
Z, Calculated density	2, 1.596 Mg.m^{-3}	
Absorption coefficient	0.999 mm^{-1}	
F(000)	760	
Crystal size	0.10 x 0.10 x 0.05 mm	
Theta range for data collection	3.93 to 25.35°	
Limiting indices	-11<=h<=10, -20<=k<=20, -12<=l<=12	
Reflections collected / unique	18309 / 2811 [R(int) = 0.0567]	
Completeness to theta = 25.35	99.1%	
Max. and min. transmission	0.9518 and 0.9067	
Refinement method	Full-matrix least-squares on F^2	
Data / restraints / parameters	2811 / 0 / 192	
Goodness-of-fit on F^2	1.105	
Final R indices [I>2σ(I)]	R1 = 0.0385, wR2 = 0.0922	
R indices (all data)	R1 = 0.0537, wR2 = 0.1025	
Largest diff. peak and hole	0.319 and -0.457 e. Å^{-3}	

Appendix 2: Crystal data for VO(2)(O^iPr)

Empirical formula	$C_{13}H_{16}Br_2NO_4V$	
Formula weight	461.03	
Temperature	150(2) K	
Wavelength	0.71073 Å	
Crystal system, space group	Monoclinic, $P2_1/c$	
Unit cell dimensions	a = 9.6280(2) Å	α = 90°
	b = 17.3200(3) Å	β = 110.6640(10)°
	c = 10.3090(2) Å	γ = 90°
Volume	1608.50(5) $Å^3$	
Z, Calculated density	4, 1.904 $Mg.m^{-3}$	
Absorption coefficient	5.598 mm^{-1}	
F(000)	904	
Crystal size	0.10 x 0.10 x 0.10 mm	
Theta range for data collection	3.79 to 27.48°	
Limiting indices	-12<=h<=12, -22<=k<=22, -13<=l<=13	
Reflections collected / unique	29514 / 3684 [R(int) = 0.0629]	
Completeness to theta = 27.48	99.7%	
Max. and min. transmission	0.6045 and 0.6045	
Refinement method	Full-matrix least-squares on F^2	
Data / restraints / parameters	3684 / 0 / 192	
Goodness-of-fit on F^2	1.072	
Final R indices [I>2σ (I)]	R1 = 0.0325, wR2 = 0.0631	
R indices (all data)	R1 = 0.0523, wR2 = 0.0691	
Largest diff. peak and hole	0.475 and -0.433 e. $Å^{-3}$	

Appendix 3: Crystal data for VO(3)(O^iPr)

Empirical formula	$C_{13}H_{16}I_2NO_4V$	
Formula weight	555.01	
Temperature	150(2) K	
Wavelength	0.71073 Å	
Crystal system, space group	Monoclinic, $P2_1/c$	
Unit cell dimensions	a = 9.7490(2) Å	α = 90°
	b = 16.7460(3) Å	β= 98.9620(10)°
	c = 10.4250(2) Å	γ= 90°
Volume	1681.17(6) $Å^3$	
Z, Calculated density	4, 2.193 $Mg.m^{-3}$	
Absorption coefficient	4.275 mm^{-1}	
F(000)	1048	
Crystal size	0.20 x 0.10 x 0.10 mm	
Theta range for data collection	3.61 to 27.46°	
Limiting indices	-12<=h<=12, -21<=k<=21, -13<=l<=13	
Reflections collected / unique	34595 / 3844 [R(int) = 0.0561]	
Completeness to theta = 27.46	99.7%	
Max. and min. transmission	0.6744 and 0.4818	
Refinement method	Full-matrix least-squares on F^2	
Data / restraints / parameters	3844 / 0 / 192	
Goodness-of-fit on F^2	1.079	
Final R indices [I>2σ(I)]	R1 = 0.0292, wR2 = 0.0602	
R indices (all data)	R1 = 0.0449, wR2 = 0.0653	
Largest diff. peak and hole	0.850 and -0.743 e. $Å^{-3}$	

Appendix 4: Crystal data for VO(4)(O^iPr)

Empirical formula	$C_{33}H_{44}N_2O_8V_2$	
Formula weight	698.58	
Temperature	150(2) K	
Wavelength	0.71073 Å	
Crystal system, space group	Triclinic, *P*-1	
Unit cell dimensions	a = 8.9880(3) Å	α = 93.626(2)°
	b = 10.5310(4) Å	β = 110.130(2)°
	c = 10.7590(5) Å	γ = 113.925(2)°
Volume	849.25(6) $Å^3$	
Z, Calculated density	1, 1.366 $Mg.m^{-3}$	
Absorption coefficient	0.601 mm^{-1}	
F(000)	366	
Crystal size	0.20 x 0.15 x 0.10 mm	
Theta range for data collection	3.89 to 27.47°	
Limiting indices	-11<=h<=11, -13<=k<=13, -13<=l<=13	
Reflections collected / unique	9453 / 3839 [R(int) = 0.0368]	
Completeness to theta = 27.47	98.8%	
Max. and min. transmission	0.9423 and 0.8892	
Refinement method	Full-matrix least-squares on F^2	
Data / restraints / parameters	3839 / 42 / 227	
Goodness-of-fit on F^2	1.034	
Final R indices [$I>2\sigma(I)$]	R1 = 0.0484, wR2 = 0.1233	
R indices (all data)	R1 = 0.0616, wR2 = 0.1333	
Largest diff. peak and hole	0.851 and -0.632 e. $Å^{-3}$	

Appendix 5: Crystal data for VO(5)(O^iPr)

Empirical formula	$C_{21}H_{34}NO_4V$	
Formula weight	415.43	
Temperature	150(2) K	
Wavelength	0.71073 Å	
Crystal system, space group	Triclinic, *P*-1	
Unit cell dimensions	a = 9.2507(3) Å	α = 72.598(3)°
	b = 10.2303(5) Å	β = 76.809(3)°
	c = 12.4817(4) Å	γ = 86.781(3)°
Volume	1097.34(7) $Å^3$	
Z, Calculated density	2, 1.257 $Mg.m^{-3}$	
Absorption coefficient	0.476 mm^{-1}	
F(000)	444	
Crystal size	0.30 x 0.20 x 0.10 mm	
Theta range for data collection	3.51 to 27.48°	
Limiting indices	-11<=h<=12, -8<=k<=13, -16<=l<=15	
Reflections collected / unique	9212 / 5014 [R(int) = 0.0156]	
Completeness to theta = 27.48	99.7%	
Max. and min. transmission	0.9539 and 0.8703	
Refinement method	Full-matrix least-squares on F^2	
Data / restraints / parameters	5014 / 18 / 283	
Goodness-of-fit on F^2	1.047	
Final R indices [I>2σ(I)]	R1 = 0.0333, wR2 = 0.0866	
R indices (all data)	R1 = 0.0385, wR2 = 0.0897	
Largest diff. peak and hole	0.538 and -0.323 e. $Å^{-3}$	

Appendix 6: Crystal data for $[VO(8)]_2O$

Empirical formula	$C_{89}H_{88}N_8O_{14}V_4$	
Formula weight	1697.43	
Temperature	150(2) K	
Wavelength	0.71073 Å	
Crystal system, space group	Triclinic, *P*-1	
Unit cell dimensions	a = 10.5240(6) Å	α = 69.732(3)°
	b = 13.2380(7) Å	β = 87.581(3)°
	c = 15.6000(11) Å	γ = 76.221(3)°
Volume	1978.2(2) $Å^3$	
Z, Calculated density	1, 1.425 $Mg.m^{-3}$	
Absorption coefficient	0.530 mm^{-1}	
F(000)	882	
Crystal size	0.20 x 0.10 x 0.10 mm	
Theta range for data collection	3.93 to 25.13°	
Limiting indices	-12<=h<=12, -15<=k<=15, -16<=l<=18	
Reflections collected / unique	19328 / 6944 [R(int) = 0.1055]	
Completeness to theta = 25.13	98.1%	
Max. and min. transmission	0.9489 and 0.9014	
Refinement method	Full-matrix least-squares on F^2	
Data / restraints / parameters	6944 / 1 / 539	
Goodness-of-fit on F^2	1.015	
Final R indices [I>2σ(I)]	R1 = 0.0538, wR2 = 0.1249	
R indices (all data)	R1 = 0.0912, wR2 = 0.1426	
Largest diff. peak and hole	0.472 and -0.426 $e.Å^{-3}$	

Appendix 7: Crystal data for $[VO(9)(VO_2OMe)]_2O$

Empirical formula	$C_{34.50}H_{54.50}N_2O_8V_2$	
Formula weight	727.18	
Temperature	150(2) K	
Wavelength	0.71073 Å	
Crystal system, space group	Triclinic, *P*-1	
Unit cell dimensions	a = 14.5880(3) Å	α = 71.3060(10)°
	b = 16.1580(3) Å	β = 83.0360(10)°
	c = 17.2860(4) Å	γ = 88.8840(10)°
Volume	3830.29(14) $Å^3$	
Z, Calculated density	4, 1.261 $Mg.m^{-3}$	
Absorption coefficient	0.536 mm^{-1}	
F(000)	1542	
Crystal size	0.20 x 0.20 x 0.15 mm	
Theta range for data collection	3.65 to 27.49°	
Limiting indices	-18<=h<=18, -20<=k<=20, -22<=l<=22	
Reflections collected / unique	77194 / 17430 [R(int) = 0.0679]	
Completeness to theta = 27.49	99.2%	
Max. and min. transmission	0.9240 and 0.9004	
Refinement method	Full-matrix least-squares on F^2	
Data / restraints / parameters	17430 / 3 / 898	
Goodness-of-fit on F^2	1.029	
Final R indices [I>2σ(I)]	R1 = 0.0536, wR2 = 0.1308	
R indices (all data)	R1 = 0.0936, wR2 = 0.1536	
Largest diff. peak and hole	0.814 and -0.831 $e.Å^{-3}$	

Appendix 8: Crystal data for $[VO(10)]_2O$

Empirical formula	$C_{62}H_{76}Cl_4N_4O_7V_2$	
Formula weight	1232.95	
Temperature	150(2) K	
Wavelength	0.71073 Å	
Crystal system, space group	Monoclinic, *C*2/*c*	
Unit cell dimensions	a = 35.639(14) Å	α = 90°
	b = 12.8304(8) Å	β = 95.35(2)°
	c = 13.7300(16) Å	γ = 90°
Volume	6251(3) $Å^3$	
Z, Calculated density	4, 1.310 $Mg.m^{-3}$	
Absorption coefficient	0.523 mm^{-1}	
F(000)	2584	
Crystal size	0.20 x 0.10 x 0.10 mm	
Theta range for data collection	2.86 to 32.80°	
Limiting indices	-53<=h<=51, -19<=k<=18, -20<=l<=20	
Reflections collected / unique	138424 / 11250 [R(int) = 0.0393]	
Completeness to theta = 32.80	97.0%	
Max. and min. transmission	0.9495 and 0.9026	
Refinement method	Full-matrix least-squares on F^2	
Data / restraints / parameters	11250 / 0 / 364	
Goodness-of-fit on F^2	1.074	
Final R indices [I>2σ(I)]	R1 = 0.0332, wR2 = 0.0796	
R indices (all data)	R1 = 0.0460, wR2 = 0.0879	
Largest diff. peak and hole	0.441 and -0.609 $e.Å^{-3}$	